SAPIENZA UNIVERSITÀ DI ROMA

Department of Structural and Geotechnical Engineering

PhD Thesis in Geotechnical Engineering

XXXIII Cycle

Numerical simulations for prediction of seismic ground motion amplification:
2D vs 3D comparison for natural reliefs and earth dams

Candidate	**Supervisor**
Roberto Razzano	Prof. Giuseppe Lanzo
	Co-supervisor
	Dr. Massimiliano Moscatelli Prof. Achilleas G. Papadimitriou

Index

Figure Index

Table Index

Abstract

Local site conditions (i.e., dynamic properties of subsurface and bedrock materials, surface and buried morphology) play an important role on seismic ground motion amplification. Therefore, their effects may become crucial in several geological/geotechnical systems such as earth dams and natural reliefs for selection of ground motion to be used in the analysis of engineering problems. These systems are usually studied based on 2D numerical analyses. However, due to the complexity of geomorphological and geotechnical situations, frequently coupled 3D soil-topography amplification analyses should be conducted to realistically assess the dynamic response.

In this research, large-scale numerical simulations are carried out with the finite difference computer code FLAC3D, that was used for both 2D and 3D analyses. Two case histories have been considered, the Palatino hill, a natural relief in the historical center of Rome, and the Angitola zoned dams in Southern Italy. In both cases visco-elastic linear analyses have been conducted considering models of increasing complexity, from homogeneous to heterogeneous ones with the inclusion of one or more additional layers, in order to distinguish between topographic and stratigraphic/valley amplification. In both cases Chang wavelet was used for input motion for three values of frequency (2Hz, 5Hz and 8Hz).

The comparison between the results of 2D and 3D analyses has been carried out in terms of maximum accelerations and/or displacement in representative points. The numerical analyses have been preceded by a calibration study, comparing the results of 2D and 3D numerical analyses with closed form solutions.

It is shown that 3D behavior can have a pronounced effect on the seismic response of the examined systems in terms of amplitude and shape of the acceleration/displacement profiles. In fact, 3D amplitudes can be much larger than 2D ones depending on the frequency of the input motion. The importance of vertical parasitic component of motion is highlighted, which again is frequency-dependent in that it increases with increasing frequency. For Angitola earth dams, the influence of narrow canyons in which the dams are built significantly contributes to the enhanced amplification of response, which is in agreement with the literature findings.

Acknowledgement

I would like to express my sincere gratitude to my two research supervisors and academic mentors, Prof. Giuseppe Lanzo and Dr. Massimiliano Moscatelli. I am indebted to them, for inspiring me; for continuous support; for patience during my PhD study and for providing me the opportunity to do research. My gratitude extends to the Institute of Environmental Geology and Geoengineering of the Italian National Research Council (CNR-IGAG of Rome) for the excellent computing facilities they provided; and for wholeheartedly welcoming me to their research group; and Department of Structural and Geotechnical Engineering of University La Sapienza of Rome for all academic matters. My gratitude also goes to Professor Achilleas Papadimitriou of the Department of Geotechnical Engineering of the National Technical University of Athens for giving me the opportunity to carry out my research abroad; for inspiring me; and especially for giving me a new point of view on research. My gratitude also goes to the "Consorzio di Bonifica Tirreno-Catanzarese" and in particular to Eng. P. Cimbalo for allowed the use of data relating to the Angitola basin.

Finally, I would like to express my deepest gratitude to my family and the people closest to me: my girlfriend Jessica, my parents, and my sister Elisa.

1 Introduction

1.1 Motivation of the study

It is well known that ground motion at a given site can be significantly enhanced by local soil conditions. This expression indicates different effects related to the propagation of seismic waves in the near-surface earth crust including surface and subsurface irregular geometries, either natural or man-made (e.g., valleys, basins, canyons, ridges, hilltops, dikes, dams, etc.). These effects determine amplification of the intensity and modification of frequency content and duration of ground motion, which has been found to produce uneven damage distribution during destructive earthquakes.

Local site effects are generally taken into account assuming a horizontally layered soil structure (so-called 1D or stratigraphy effects), which ignore the more complex 2D or 3D site effects. The phenomena that 1D soil amplification cannot reproduce are related to the generation of surface waves and the complex wave pattern (associated with the constructive to destructive interference between incident waves, and refracted body and surface waves) and of longer duration.

In the eighties, the extensive damages that struck several large cities (e.g., Mexico City in 1985, San Francisco in 1989, Los Angeles in 1994), have been responsible for drawing worldwide attention on 2D and 3D site effects. Analogously, since the comprehensive studies of Dakoulas and Gazetas in the eighties, it is well established that for dams in narrow canyons the response of the geotechnical structure is of a three-dimensional nature. As an example, many earth and rockfill dams built in narrow canyons experienced strong damages during the Ms 8.0 Wenchuan 2008 earthquake which occurred in Sichuan Province, China. Therefore, reliable and proper analysis of site response as well as dam's seismic response is of great engineering significance in guiding design and construction, and mitigating seismic risk. In particular, it is therefore desirable to know under which conditions 3D behaviour is likely to play an important role in the dynamic response of different geotechnical systems.

In the past 30 years numerical modelling of ground motion during earthquakes made great advances mainly because of increased computer capabilities. Various theoretical and numerical methods were developed which allowed a better understanding of the main factors affecting the dynamic response of these systems under seismic excitations. Different levels of sophistication of the numerical simulations were used, which outlined the importance of complex issues such

as the soil nonlinearity, the development of pore water pressure and real earthquake records. However, the extension from 2D to 3D modeling is not an easy task owing to the difficulties and limitations in describing three-dimensional geometry and material properties, which require a reasonable balance between safety requirements and cost, and because a 3D mesh discretization and the computation is relatively time-consuming. These are the reasons why the comparison between the 2D and 3D analysis has received limited attention so far and is, as yet, not popular in practice.

With the above considerations in mind, the present thesis would focus on the following main items:

1. validation of the finite difference code FLAC3D by using analytical closed-form solutions available in the literature for various surface irregularities and earth dams;
2. comparison between 2D and 3D results of numerical simulations which refer to two well-documented large-scale real case studies: a) the Palatino Hill in Rome, which is a natural hill characterized by a very complex surface and subsurface morphology, and b) the Angitola reservoir in Calabria which is constituted by two earthfill dams separated by a rocky spur.

1.2 Outline of the thesis

In this paragraph, the general contents of the chapters that form the thesis are summarised.

Chapter 2 present an outline of analytical and numerical methods available in literature that describe the parameters that affect 2D and 3D behaviour of surface and subsurface irregularities. Firstly, the closed-form solutions of simple geometric features (canyon, sediment-filled valley, ridge) are examined and the main numerical results are also described. Secondly, the historical development of theoretical and numerical methods for estimating the seismic response of earth dams to earthquake excitation is briefly outlined.

Chapter 3 describes the main features of the finite difference code FLAC3D used for the 2D and 3D numerical simulations. This is followed by the validation studies of the code with some closed-form solutions for simple sediment-filled valley and, especially, for earth dams.

Chapter 4 concerns the comparison between the results of 2D and 3D numerical simulations carried out for investigating the seismic response of surface and subsurface irregularities. Specifically, the simplified geometries selected are the semi-cylindrical sediment-filled valley and the semi-cylindrical hill. For earth dams, a simplified homogeneous trapezoidal dam embedded in a triangular canyon is considered.

Chapter 5 describes the 2D and 3D numerical analyses carried oud to study the seismic response of two well-documented large-scale real cases studies. The first case is the Palatino hill the in historical centre of Rome and its surrounding areas, a complex geological-geotechnical system consisting of topographic reliefs and alluvial valleys. The second case study refers to the Angitola reservoir in Southern Italy (Calabria), which is constituted by two earthfill dams separated by a rocky spur. In both cases the parameters that mostly affect the dynamic response for both 2D and 3D conditions have been investigated. It was followed the same procedure, i.e. the analyses have been carried out with increasing complexity, starting from homogeneous simple models and successively increasing step-by-sep the in-homogeneity characteristics of the subsoil. This procedure allowed to decouple the surface and subsurface amplification from the stratigraphic one.

Chapter 6, finally, summarizes the findings of this study and describes the recommendations for further investigation.

2 Literature review

2.1 Introduction

It is nowadays well known that the expression "local seismic conditions" (or the synonymous "local amplification" or "seismic site effects"), widely used in earthquake engineering, indicate a set of different physical phenomena which arise from the propagation of seismic waves in near-surface geologic materials or in geometrically irregular surface and subsurface configurations, either natural or man-made (e.g., valleys, basins, canyons, ridges, hilltops, dikes, dams, etc.). These phenomena can significantly affect the characteristics of ground motion (amplitude, duration and frequency content) that might occur at a given site. As a matter of fact, experiences from past earthquakes has repeatedly shown that the intensity of ground shaking, as well as the intensity of the damages produced, are strongly affected by local site conditions.

Early studies on seismic site effects date back to late sixties or early seventies (e.g., Idriss and Seed, 1967, 1968; Schnabel et al., 1972; Seed and Idriss, 1973; Seed et al, 1974). In these studies special emphasis was given to the one-dimensional (1D) amplification arising from the flexibility of a soil deposit on a flat formation on rock or very stiff soil. Since then, engineers have traditionally evaluated such influence using simple models based on a 1D soil profile and seismic wave propagation, with reasonable success. However, in the last 25 years, surface and subsurface irregularities have also been identified as a possible source of site effects. One of the most striking examples of topographic effect is represented by the high acceleration recorded on top of the abutment of Pacoima dam in 1971 during the San Fernando earthquake (ML=6.4) in Southern California. A PGA as high as 1.25g was recorded, this value being much larger than the values expected for an earthquake of similar magnitude. Site effects due to surface topography can similarly de-amplify ground shaking in canyons or near the base of slope (e.g., Ashford et al., 1997; Ashford and Sitar, 1997). Another example is the 1995 Hyogoken Nanbu (Japan) earthquake with its narrow "intensified damage" belt crossing the city of Kobe. In this case a remarkable complexity in seismic amplification patterns was disclosed, mainly due to the mechanism of generation of the basin-induced diffracted Rayleigh waves at the basin edge (Kawase, 1996). Many other examples worldwide can be made in which the more complex 2D/3D phenomena (e.g. focusing and defocusing of seismic waves, generation of surface waves at valley edges, constructive interference between direct body

waves and generated surface waves, etc.) are responsible for significant damages occurred during earthquakes (e.g., Yegian et al., 1994; Lanzo and Pagliaroli, 2009; Assimaki et al., 2005; Assimaki and Jeong, 2010; Garini et al. 2020). However, these 2D/3D effects have received much less attention than 1D site effects because of the lack of instrumental data from damaging earthquakes on one side and because these effects are frequently overshadowed by the soil amplification on the other side.

In the first part of this chapter a very brief overview of the 1D amplification is carried out. The second part, which forms the main body of the literature review, deals with the seismic response of surface and subsurface irregularities, as derived from both analytical and numerical studies. In particular, emphasis is given to the site effects arising in sediment-filled alluvial valleys, canyons and earth dams.

2.2 "Stratigraphic" or one-dimensional amplification

The so-called "stratigraphic" or one-dimensional (1D) local seismic response is based on the assumption that ground surface and the underlying bedrock surface are practically horizontal and have an infinite lateral extent. Thus the response is dominated by shear waves vertically propagating and horizontally polarized. As already said, even if based on overly simplistic assumption of shear wave propagation, the 1D model was proved to be effective in explaining the prominent causes of damages in many case studies of engineering interest worldwide.

The basic underlying mechanism of 1D amplification phenomena can be illustrated by considering the dynamic response of a damped elastic surface layer resting on deformable (elastic) bedrock. The main physical phenomenon responsible for the amplification of motion is the trapping of seismic waves due to the impedance contrast between the soil deposit underlying bedrock (Pitilakis, 2004). For the simple case illustrated in Figure 2.1, this trapping affects only body waves travelling up and down in the soil deposit and the interference between these waves would lead to "resonance". The resonance pattern can be visualized by the amplification function in Figure 2.2 where the natural frequencies occur at well-defined peaks related to the geometry of the soil deposit and its mechanical characteristics, according to the following expression:

$$f_n = (2n+1)\frac{V_s}{4H} \qquad n = 0,1,2 \ldots .. \tag{2.1}$$

The amplification at the fundamental resonant frequency (f0) is given by:

$$A\,(f_0) = \frac{IR}{1 + 0.5\pi \cdot D \cdot IR} \tag{2.2}$$

where the parameters D and IR control the extent of the amplification phenomena. D is the soil damping ratio and IR is the impedance ratio IR defined as:

$$IR = \frac{\rho_{rV_r}}{\rho_{sV_s}} \tag{2.3}$$

For configurations having a marked 2D or 3D geometry other complex site effects arise as compared to the 1D dynamic response. The main characteristics of 2D/3D site response will be analysed in the subsequent paragraphs with reference to different surface and subsurface geometries such as sediment-filled valleys, canyons, hills and earth dams.

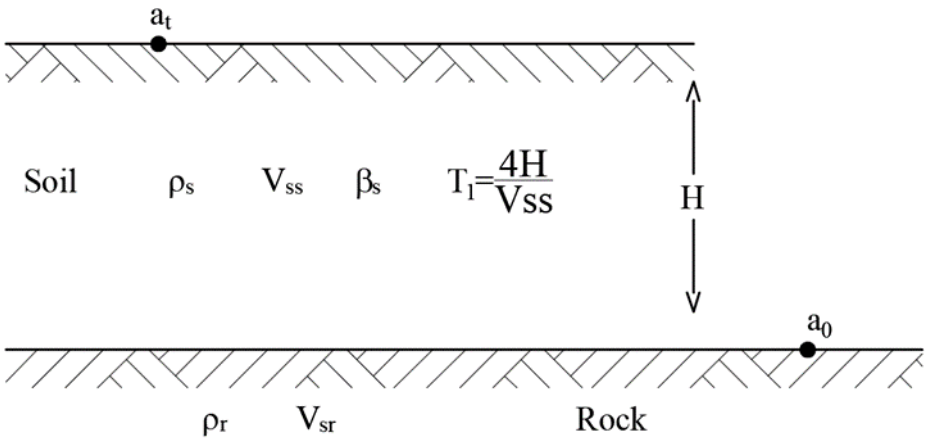

Figure 2.1: 1D model for soil amplification: elastic damped layer over deformable bedrock

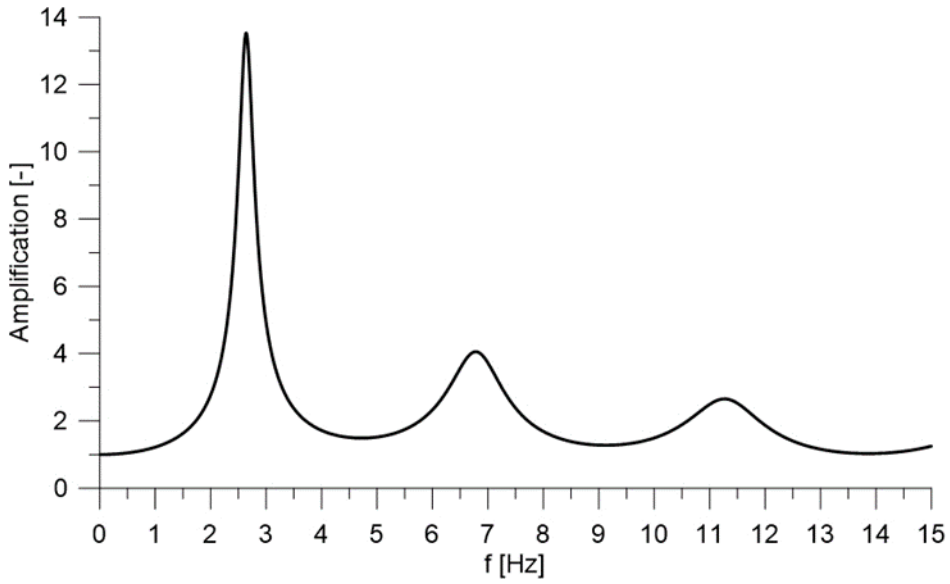

Figure 2.2: amplification function of elastic damped layer over deformable bedrock

2.3 Seismic response of surface and subsurface irregularities

2.3.1 Introduction

Figure 2.3 illustrates some possible surface and subsurface irregularities that can lead to different effects in terms of ground motion generated during an earthquake (Faccioli et al., 2002). Both types of irregularities tend to produce an increase in amplitude, and often also in the duration, of the surface ground motion. Depending on the 2D/3D irregularity, the fundamental frequency can remain sustained at substantial levels over broad frequency ranges. An interesting comparison between 1D, 2D and 3D amplification function is presented in Figure 2.4 (Bard and Riepl-Thomas, 1999). The differences between 1D and 2D spectral peaks of amplification resonance are much more pronounced than between 2D and 3D cases. The consideration of the second and third lateral dimension in the wave propagation phenomena, in case of 2D and 3D resonance, leads to an increase in ground motion amplification and a shift towards higher values of the peak frequencies. From the engineering point of view, the previous distinctions are significant because the severity and the spatial extent of the site effect can vary substantially in terms of expected damage to man-made construction, depending on the kind of phenomenon at play (Faccioli et al., 1992).

The scattering and diffraction of waves by surface and subsurface irregularities has always been an important research topic in the field of wave motion. A remarkable amount of work has been

conducted since seventies on the scattering problem of various types of waves (SH, SV, P) from irregularities of different shapes.

In this paragraph closed-form solutions available in literature for some geometric configurations are first examined. Then, the main results from numerical modelling for solving the scattering problem of waves in various situations for even more complex geometries, using different numerical techniques are presented. Finally, closed-form solutions and numerical modelling results are described for earth-dams.

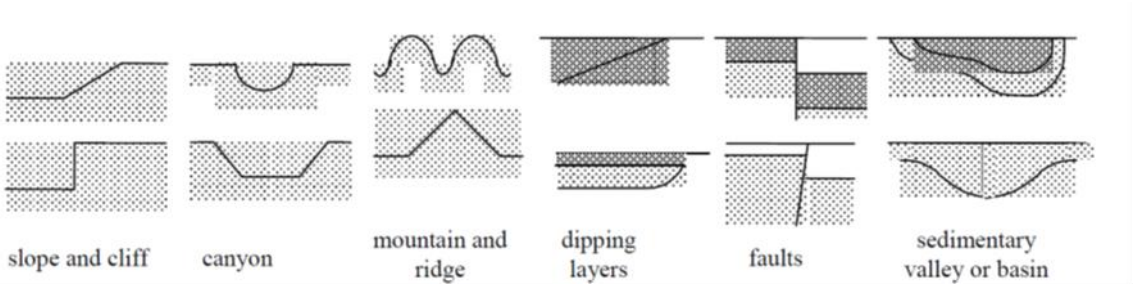

Figure 2.3: Idealized examples of surface (left) and subsurface (right) irregularities (Naganoh et al., 1993; Faccioli et al., 2002

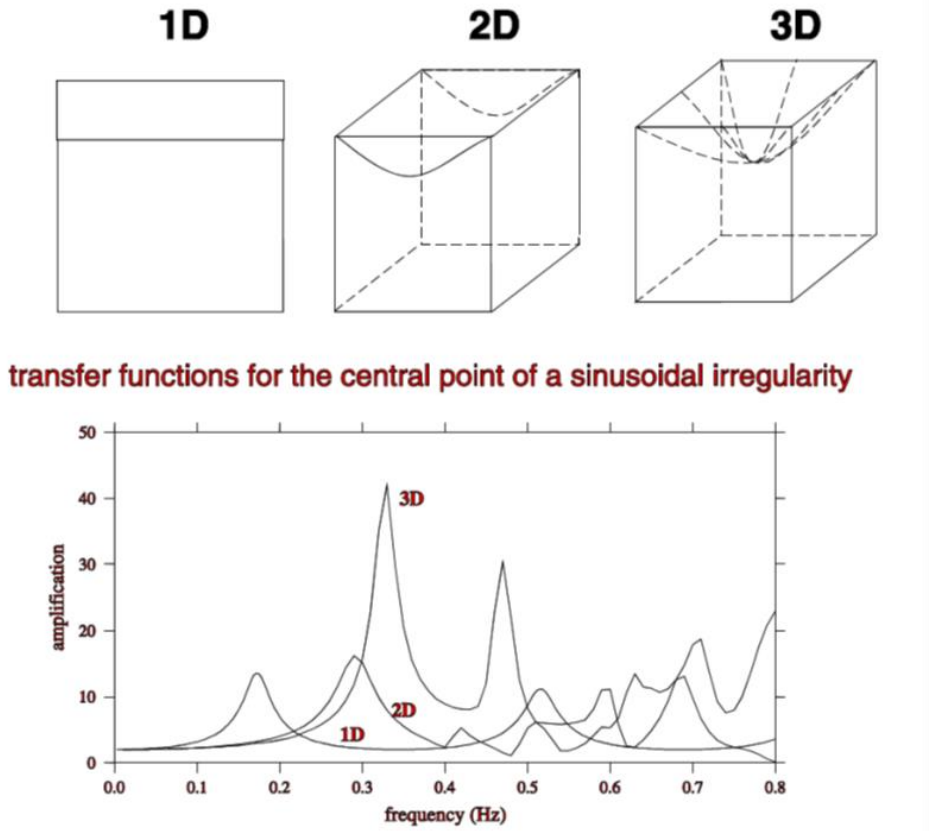

Figure 2.4: Comparison of spectral responses of 1D, 2D and 3D models for a cosine-shaped basin. For 2D and 3D models, the motion is computed at basin center (from Bard and Riepl-Thomas, 1999).

2.3.2 Analytical studies

As mentioned before, the problem of the interaction between seismic wave propagation and surface and subsurface irregularities on ground motion has been extensively investigated since seventies. Much of the earliest research work was conducted on simple geometric configurations and was essentially analytical such as it could be solved exactly in closed form. This fact may be of special value for different approximate numerical techniques (e.g., finite differences, finite element, etc.) since the analytical solutions can be used to test the accuracy of the approximate methods.

The two-dimensional diffraction of SH-wave represents the simplest problem in elastic wave propagation in the presence of geometric irregularities because SH waves can be analysed separately from other body waves (Sanchez-Sesma, 1987).

The first closed-form solutions were provided by Trifunac and his co-workers for valleys and canyons. In particular, Trifunac (1971) studied the characteristics of surface motion in and around a semi-cylindrical alluvial valley (Figure 2.5) for incident SH waves and showed that it depends both on the impedance ratio (IR) between half-space and sediment-filled valley and the dimensionless parameter η defined as the ratio between one characteristic dimension of the system (e.g., the radius of the valley) and the wavelength 'λ' of input motion.

$$\eta = \frac{2a}{\lambda} \tag{2.4}$$

In Figure 2.6 the effects of dimensionless parameter (η=0.25, 0.75, 2.00) and incidence angle (γ=0°, 30°, 60°, 90°) of SH waves on surface displacements are shown. It can be observed that the displacement amplification on the surface of the alluvium may change rapidly over short distances, by as much as one order of magnitude; for fixed material and geometric properties, the degree of complexity of the amplification pattern increases as frequency of incident waves increases. Analogously, in Figure 2.7 the effect of impedance ratio by assuming vertical incident SH waves (Trifunac, 1971) is illustrated. Large amplification can be obtained if the shear wave velocity of the alluvial material decreases, other model properties being fixed. Overall analytical results show that the pattern and amplitudes of surface displacements can be extremely complicated because of the interference wave phenomena depending significantly on η, γ and IR. The Author also emphasizes the different amplification pattern obtained comparing 1D soil model with the semi-cylindrical 2D model.

Bard & Bouchon (1985) provided an analytical solution for the SH resonance frequencies of a rectangular shape sediment-filled valley on rigid half-space (Figure 2.8). As shown in Figure

2.9, the formula derived can predict very accurately the resonance frequencies of a sine-shaped valley provided that the equivalent width (2w) is chosen equal to the valley half-width l. Todorovska and Lee (1991a) use an approximate analytical method based on Bessel-Fourier series representation of the scattered waves to calculate the steady-state response of two-dimensional shallow circular valleys for incidence plane SH waves. The advantage of this method over the other exact available methods is that the shape of valleys to which it is applicable are closer to the shape of natural alluvial valleys. Sherif and Lee (1996) studied the wave propagation behaviour in an elastic wedge-shaped medium, with a circular alluvial valley at its vertex. Specifically, an analytic closed-form solution was obtained for the case of plane SH waves. The analysis demonstrates that the incident plane SH-waves travelling through this geometry will lead to total displacement fields to be dependent upon several parameters, such as the wedge angle of the space, the angle of incidence, the frequency of the incident wave train, and the material properties of the wedge medium and the alluvial valley.

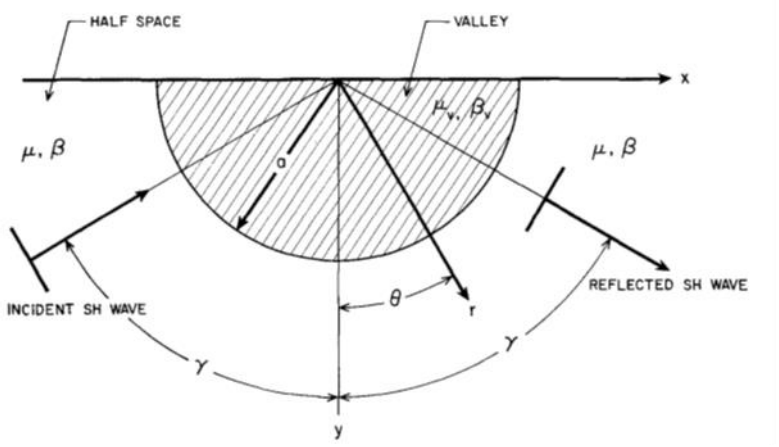

Figure 2.5: Semi-cylindrical filled valley studied by Trifunac (1971)

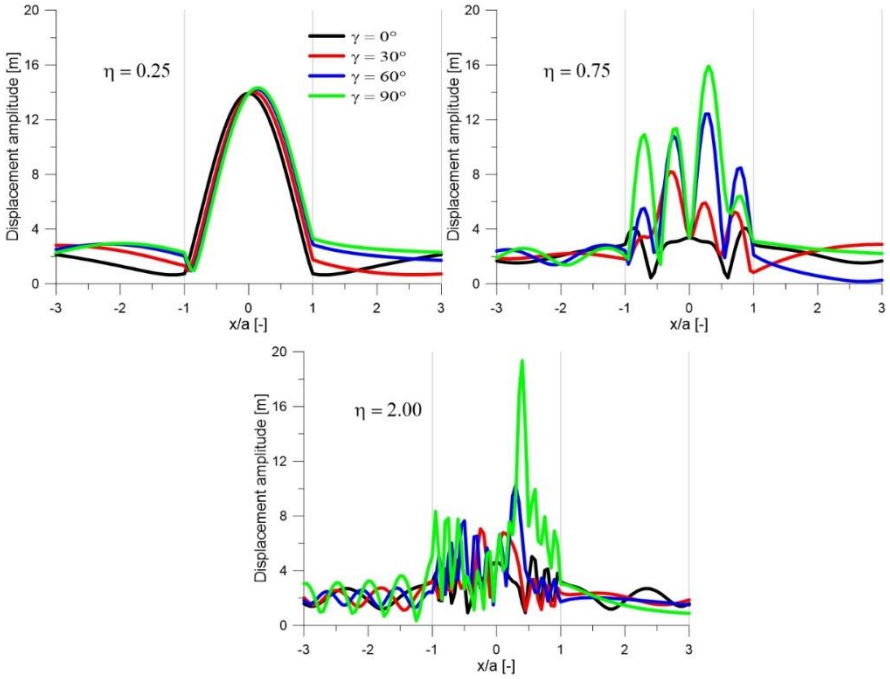

Figure 2.6: Effect of incidence angle (γ) for different η in terms of surface displacement of semi-cylindrical sediment-filled valley, (Trifunac, 1971, modified)

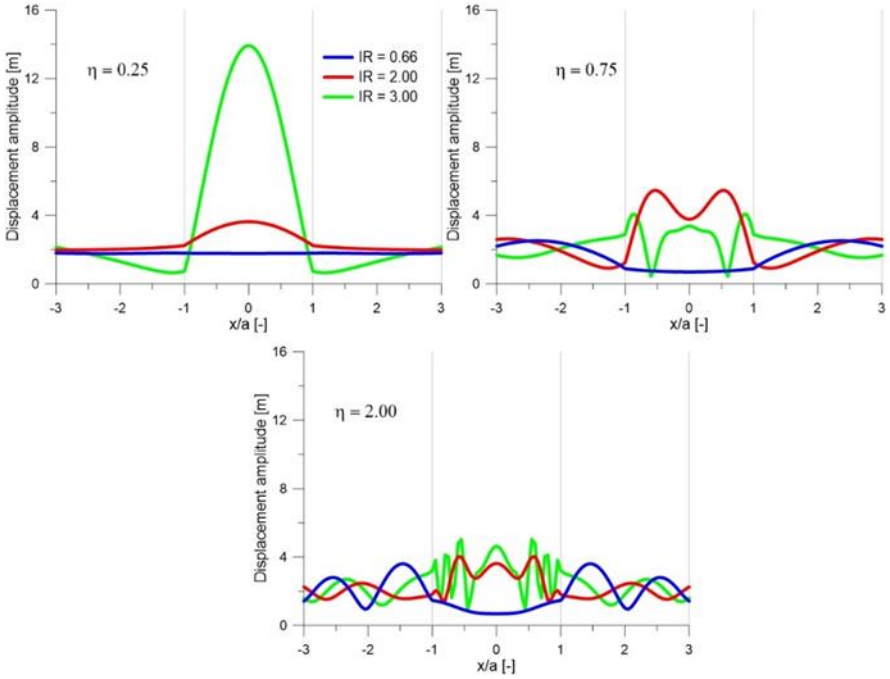

Figure 2.7: Effect of impedance ratio (IR) in terms of surface displacement of semi-cylindrical sediment-filled valley, by assuming vertical incident SH waves for different η (Trifunac, 1971, modified).

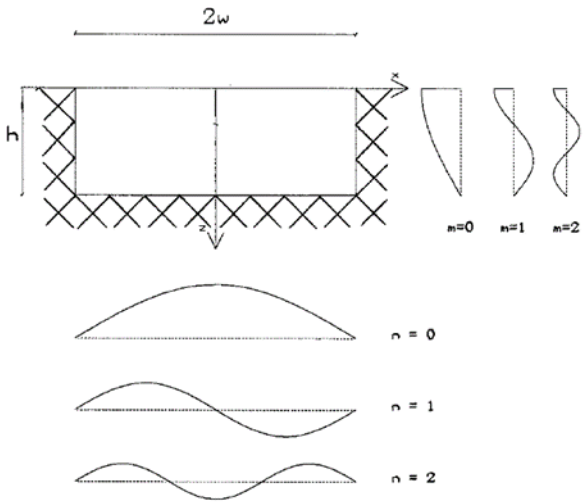

Figure 2.8: Antiplane vibration modes of an elastic rectangular inclusion embedded in a rigid half-space. The curves on the bottom represent the admissible variations of motion amplitude along the x axis, and the curves on the right represent the admissible variations of motion amplitude along the z axis. The n and m indexes correspond to the harmonics order (Bard & Bouchon, 1985)

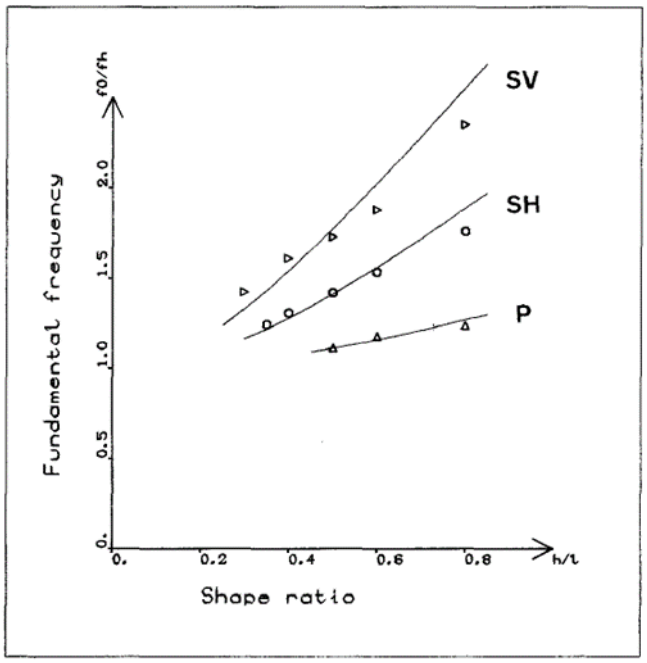

Figure 2.9: Dependence of the dimensionless frequency f0/fh (fh=Vs/4h) on the shape ratio h/L for the SH, SV, and P fundamental modes. The symbols represent the results of the Aki-Larner computations while the continuous lines correspond to the formulas (Bard & Bouchon, 1985)

The research on the 2D elastic wave diffraction and scattering by canyons has also been of interest for many decades. The closed-form solution for a semi-cylindrical canyon in a half-space (Figure 2.10) under SH waves was first provided by Trifunac (1972). It was found that

the seismic motion could be amplified by the geometry and the surface displacement depended significantly on the direction of incident waves as well as the dimensionless frequency η (i.e. the ratio of radius of the canyon and one-half wavelength of incident waves). This is illustrated in Figure 2.11 where the surface displacement amplitudes with different incident angles (γ=0°, 30°, 60°, 90°) and η values (0.25, 0.75, 1.25, 2.00) are plotted. The surface amplification of displacement in the canyon and around it, changes rapidly from one point to another and it is always lower than 2. The overall pattern of amplification is strongly influenced by the dimensionless frequency parameter: the higher η (i.e., for wavelength of incident motion shorter than the radius of the canyon), the greater the complexity surface motion displacement. The incident angle mainly determines the overall trends of displacement amplitudes. Their results show that for incident angles forming an angle γ with the vertical and travelling form the left to the right of the canyon, there occurs scattering and diffraction of waves essentially on the left side, while the right edge of the canyon is in a shadow zone. As a consequence, the left side of the canyon experiences amplification while a shadow zone is developed in the right edge of canyon leading to a uniform de-amplification (Trifunac, 1972). Wong and Trifunac (1974) analysed the 2D scattering and diffraction of plane SH waves by a semi-elliptical canyon and examined the dependence of surface amplifications inside and near the canyon. Sanchez-Sesma (1985) calculated the displacement field at the surface of a wedge-shaped medium for incidence of SH waves. The solution was given for various values of the internal angle of the wedge ν. It was found that the motion amplitude at the vertex, normalized to the free space amplitude, is simply given by 2/ν, where np is the internal wedge angle ($0<\nu\leq 2$). It can be noted that normalized amplitude would be 2 at the surface of a half-space for which ν=1. Results for a valley-like wedge (ν =3/2) indicate that reductions of motion amplitude can be important in the side in the shadow zone, thus leading to large differential motion near the vertex (Figure 2.12).

Lee (1978) investigated the three-dimensional (3D) scattering of plane waves by a hemispherical canyon in an elastic half-space. It was found that for incident SV, P and SH waves the pattern and amplitude of surface displacement depend significantly on the direction of incident waves. For acute angles of incidence, amplification and shadow zones are observed around the canyon. The extent to which these effects are evidenced is largely affected by the dimensionless parameter η.

Subsequently, several studies were also conducted for investigating the scattering of SH waves with different concave topographies. Cao and Lee (1989) solved the problem of 2D scattering

and diffraction of plane SH waves by half-space with semi-circular canyon of different depth-to-width ratio. In particular, it was shown in accordance with previous studies, that that for long waves the canyon is not "seen' by the waves, whereas for short waves the canyon effects on the resulting wave amplitudes become prominent. The ratio of the canyon depth h to its half width affects the wavefield around the canyon so that a deeper canyon results in larger amplification and more complex motion around it. Lee (1990) solved the problem of the diffraction of plane SH waves by a semi-parabolic canyon. Recent research by Tsaur and Chang (2008) and Tsaur et al. (2010), based on the region mapping technique (RMT), gave respectively the analytical solution of the scattering of SH waves by a shallow and deep symmetrical V-shaped canyon. Other analytical studies were provided in the last decade for valley irregularities with more complex shapes (e.g., Gao et al., 2012; Zhang et al., 2012).

For incidence of P, SV, and Rayleigh waves, the analytic solution is more complicated because of the coupling of boundary conditions (Sanchez-Sesma, 1987). Lee and Cao (1989) and Cao and Lee (1990) presented, respectively for incident P and S waves, solutions for scattering and diffraction for shallow semi-circular canyons (depth-to-half width ratio ≤ 1). Todorovska and Lee (1991b) used an approximate analytical method to calculate the response of two-dimensional shallow circular valleys to incident Rayleigh waves. Lee (1984) calculated the exact solutions for the mixed boundary value problem of diffraction of P, SV and SH plane waves by a hemispherical alluvial valley embedded in homogeneous elastic half space (Figure 2.13). It was found that the ground motion surface displacements on or near the valley show significant departure from the half space motions, greatly depending on the elastic properties of the valley relative to the half-space and on the incidence angle of the arrival waves. The principal role of the ratio of the diameter of the canyon to the wavelength of the incident plane waves is that it determines the extent to which the above-mentioned effects are developed (Lee, 1984).

The analytical study of hill topography is characterized by a much higher degree of uncertainties as compared to concave morphologies. As a consequence, simple closed-form analytical solutions are limited in the scientific literature. From a physical viewpoint it would be reasonably to imagine more complicated wave patterns caused by the hill rather than by the canyon morphology because of the multiple reflections of the waves within the hill. This would lead to more remarkable amplifications of surface ground motion displacements. Yuan and Men (1992) have developed an analytical method for solving the scattering problem of SH waves by a semi-cylindrical hill (Figure 2.14). The result show that: (1) the hill has quite considerable

effects on ground motions for both the points on the hill and its environs, (2) these effects depend mainly on the frequency, the angle of wave incidence and the ratio of radius of hill to one-half the wave length of incident waves, and (3) prominent and depression topographies having equal form and radius for the same incident waves would cause quite different mechanisms of wave propagation in both response performance and magnitude (Yuan and Men, 1992). The results are only applicable to low-frequency SH waves. An improvement to the method of Yuan and Men (1992) was provide by Lee et al. (2006) which derived accurate closed-form wave function analytic solution of two-dimensional scattering and diffraction of anti-plane SH waves by a semi-circular cylindrical hill on an elastic half space by using Analytical Wave Series Solution method (Figure 2.15). The calculations extend to higher dimensionless frequency η ($\eta > 10$ and beyond) which plays an important role in determining the surface displacement patterns. Higher η values result in higher complexity of displacements and in higher amplifications. More recently Lee and Amornwongpaibun (2013) presents an exact analytical solution to the boundary-value problem of the two-dimensional scattering of anti-plane (SH) waves by a shallow, semi-elliptical hill on an elastic half-space. Complicated effects on ground motion due to the existence of an elliptical hill at various aspect ratios and angles of wave incidence are illustrated. More recently, analytic studies investigating more complex topographies (i.e., hill with slopes) in addition to hill with circular and elliptical boundaries, have also been considered. Pioneering work in analytical studies on the wave scattering by isosceles hill, which results in complicated boundary conditions, was done in the beginning of this century. Hayir et al. (2001) solved antiplane response of a dike with flexible soil-structure interface to incident SH waves (Figure 2.16). However comparing the result obtained by Hayir et al. (2001) by using the analytical method with that by Sanchez-Sesma et al. (1982) by using numerical method for the same case, an obvious difference can be found. Therefore, antiplane response of isosceles triangular hill to incident SH waves was studied again by Qiu and Liu (2005) obtaining correct results under very low-frequency incidence waves for the case of shallow hill.

In Table 2.1 some of the closed-form solutions provided by several Authors for different geometric configurations (i.e. sediment-filled valley, canyon and hill) subject to inclined plane SH, SV or P waves are summarized. These solutions will be used in the paragraph 3 in order to make comparison with the numerical results calculated by using the finite difference code FLAC3D.

Table 2.1: Selected closed-form solutions for sediment-filled valley, hill and canyon geometries

Geometry	Authors	Notes
Sediment-filled valley	Trifunac (1971)	Semi-cylindrical valley subject to SH inclined waves
	Lee (1984)	Hemi-spherical valley subject to inclined SH, SV and P waves
	Todorovska & Lee (1991)	Shallow circular alluvial valleys for incident plane SH
Canyon	Trifunac (1973)	Semi-cylindrical canyon subject to SH inclined waves
	Wong & Trifunac (1974)	Semi-elliptical canyon subject to SH inclined waves
	Lee (1978)	Hemi-spherical canyon subject to inclined SH, SV and P waves
	Cao & Lee (1989, 1990)	Semi-cylindrical canyon subject to inclined SH, SV and P waves
Hill	Lee, Luo, Liang (2006)	Semi-cylindrical hill subject to inclined SH waves

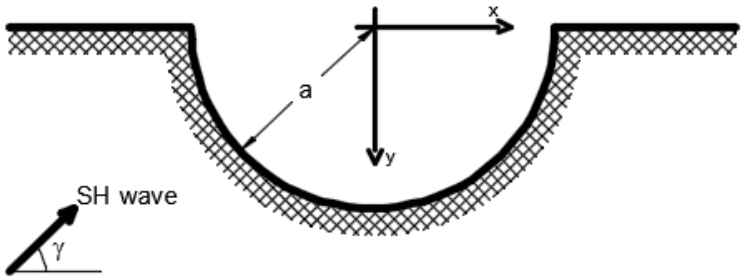

Figure 2.10: Half-space with semi-cylindrical canyon under inclined SH waves (Trifunac, 1973)

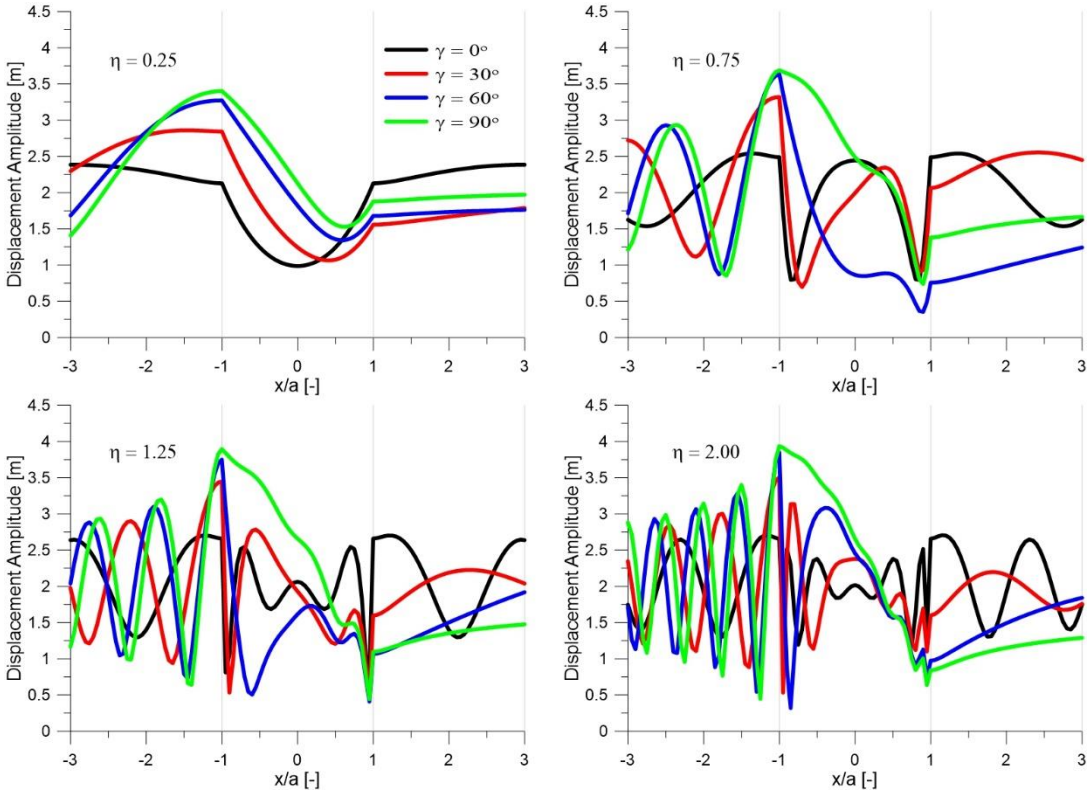

Figure 2.11: Surface displacement of semi-cylindrical canyon, effect of incidence angle 'γ' for different η (Trifunac, 1973, modified)

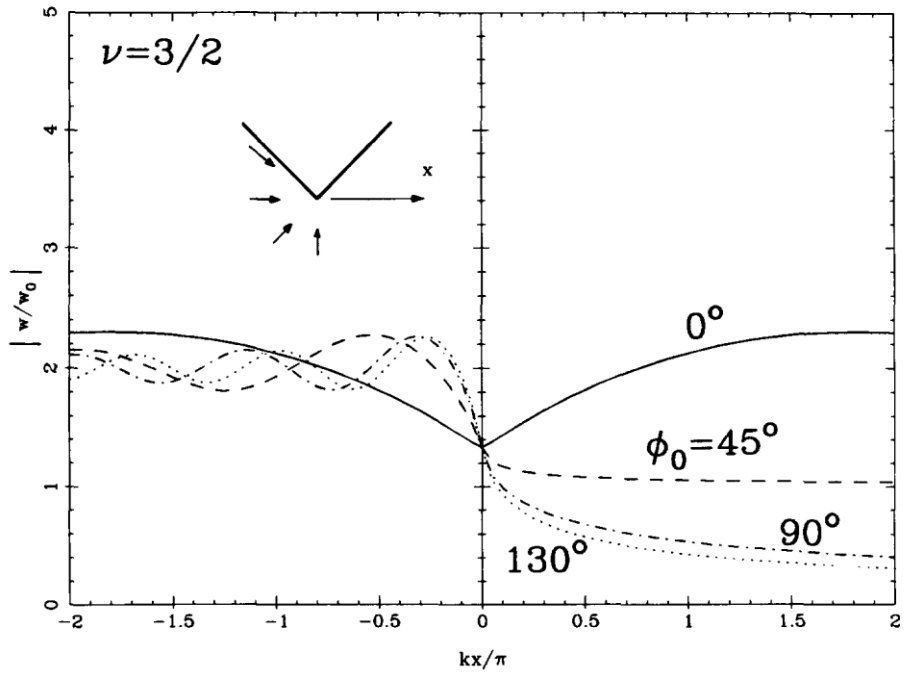

Figure 2.12: Normalized surface amplitudes versus a normalized horizontal coordinate (kx/π) for incidence of plane SH waves upon a valley-like wedge with internal angle of 3π/2. Results are provided for different incidence angles (0 °, 45 °, 90 °, and l30°). Sanchez-Sesma (1985).

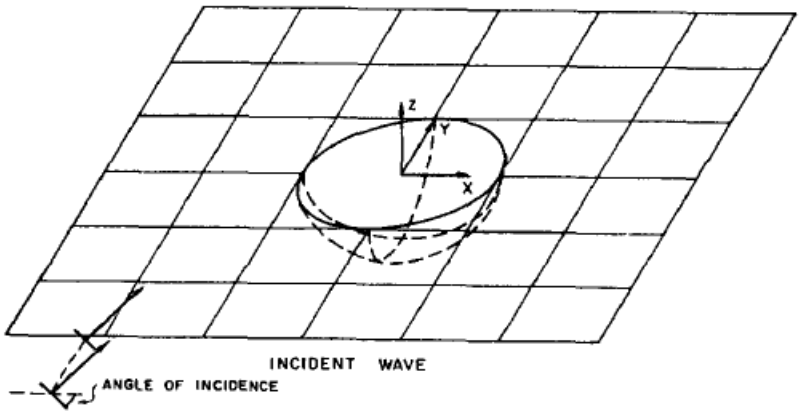

Figure 2.13: Model of the hemispherical valley studied by Lee (1984)

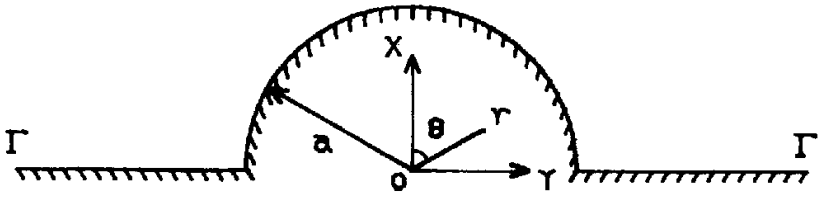

Figure 2.14: Model of the hill topography (Yuan and Men, 1992)

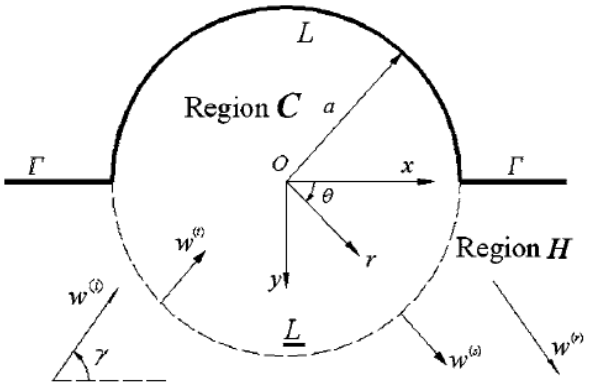

Figure 2.15: Semi-cylindrical hill subject at incident SH waves (Lee et al, 2006).

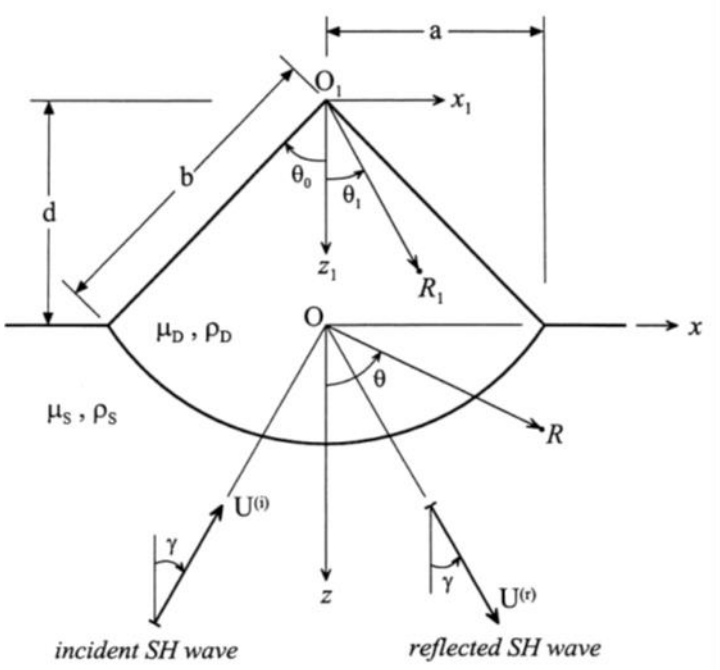

Figure 2.16: Cross-section of a two-dimensional circular wedge ('structure') welded to an elastic homogeneous half-space (Hayir et al 2001).

2.3.3 Numerical studies

The first Authors that considered the wavefield due to incident plane waves in a shallow elastic layer on elastic half-space separated by an irregular interface were Aki and Larner (1970), which used the discrete wavenumber method (hereinafter referred to as the A-L method). In this method, the scattered wavefield is represented as a linear combination of plane waves with discrete horizontal wavenumbers where the coefficient are determined in such a way that boundary condition is approximately satisfied (Figure 2.17). The A-L method is the basis of numerical studies both for alluvial valleys (e.g., Bard & Bouchon, 1980a, 1980b 1985) and for topographic effects (e.g., Bouchon, 1973; Geli et al. 1988; Bard, 1982).

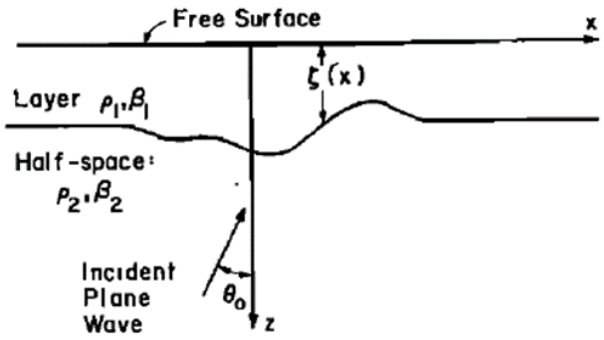

Figure 2.17: Elastic layer on stiffness half-space separate by irregular interface studied by Aki & Larner (1970).

Aki and Larner (1970) applied the method to calculate the response at the surface of a soft basin on elastic half-space. In Figure 2.18 and Figure 2.19 the comparisons between the A-L method and one-dimensional Haskell-Thompson method in the cases of vertical and obliquely incident SH waves are shown. It is found that the effect of lateral interference becomes more important as the interface becomes more irregular and the direction of incident waves becomes closer to the horizontal.

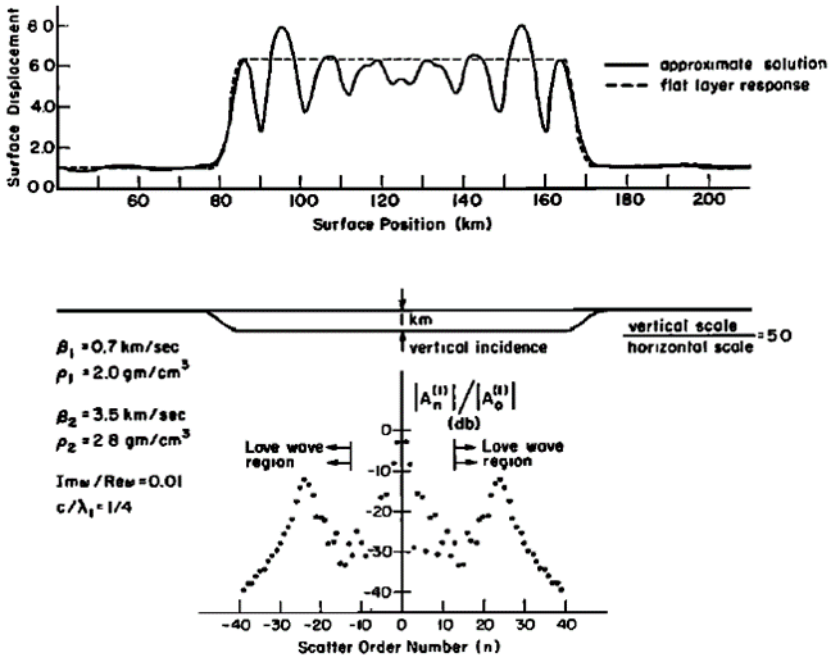

Figure 2.18: Top: Normalized displacement amplitude at the free surface of a flat soft basin which is 1km deep and 80km wide (maximum depth is 1/4 wavelength in the layer). The dots are amplitudes computed by the flat-layer theory assuming at each point that the basin structure is a horizontal layer having a constant thickness equal to that directly beneath the point. Bottom: Wavenumber spectrum of spectral-amplitude ratio versus scatter-order number. (Aki & Larner, 1970)

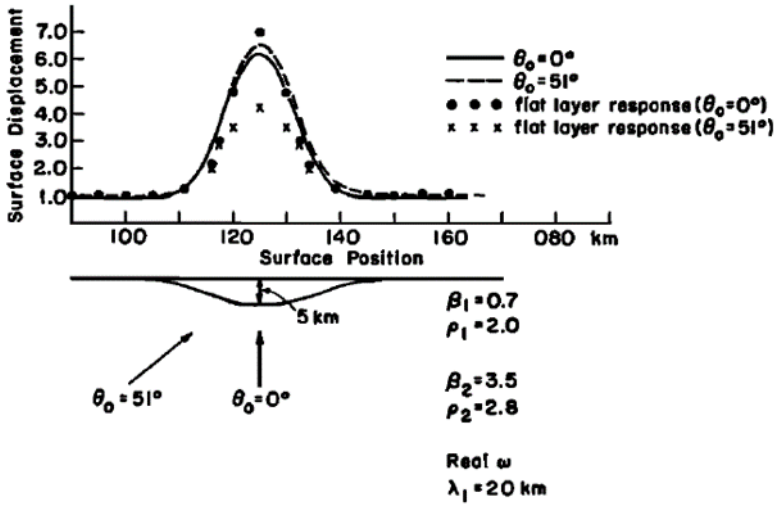

Figure 2.19: Normalized displacement amplitude at the free surface of a soft basin for two directions of incidence of long wavelength waves. The dots are amplitudes computed by the flat-layer theory assuming at each point that the basin structure is a horizontal layer having a constant thickness equal to that directly beneath the point. (Aki and Larner, 1970).

As this method does not consider the outgoing waves, it cannot be applied in presence of high-slope irregularity. Bard & Bouchon (1980a, 1980b) extended the A-L method in time domain

to calculate the response to SH, SV and P waves of relatively shallow sediment-filled valley, such the type 1 and Type 2 illustrated in Figure 2.20. The study showed the important role played by the nonplanar interface, which, when the incident wavelengths are comparable to the depth of the valley, results in the generation of surface waves (Love waves for incident SH waves and Rayleigh waves for incident P-SV waves) which may have much larger amplitude than the incident signal. These surfaces can propagate back and forth within the soil deposit and this can lead to an amplification of the surface motion, an elongation of duration and, finally, a significant differential motion. The computed displacement at the surface of type 2 valley is shown for SH and SV vertical incident Ricker wavelet in Figure 2.21 and Figure 2.22, respectively.

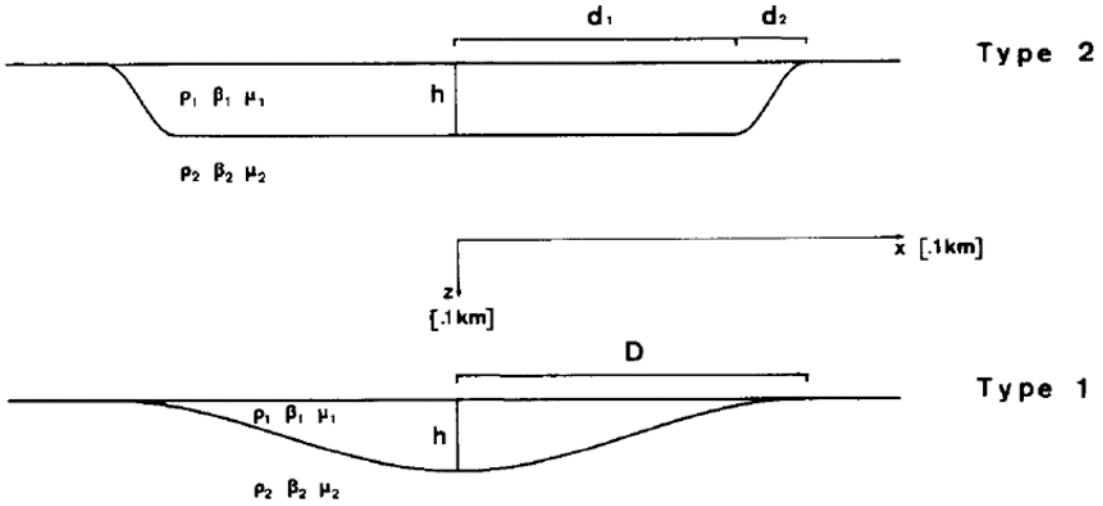

Figure 2.20: Configuration of the valleys studied by Bard & Bouchon (1980a and 1980b), where r b and μ are density, shear wave velocity and rigidity respectively.

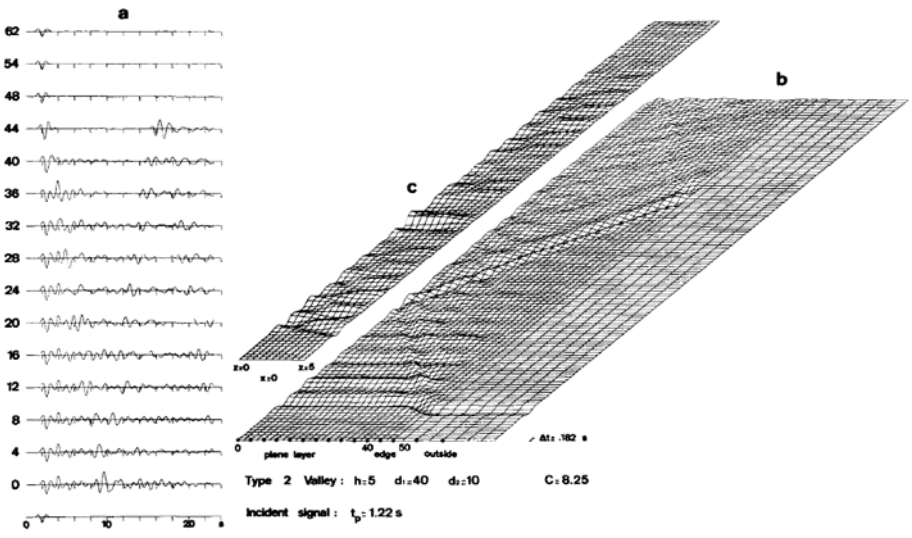

Figure 2.21: Response of valley type 2 subject at vertical incident SV Ricker wavelet of characteristic period tp=1.22 s; the traces represent the horizontal {bottom, u) and vertical (upper, w) displacements at surface receivers, spaced from 0 to 6.0 km from the valley center. The bottom trace would be the surface (vertical) displacement signal without the valley. Right: Diagrams showing the spatial (x) and temporal (t) evolution of the surface displacement components in the valley and in its immediate proximity. The dots indicate the location of the sites where the seismograms (leftpart) are computed. In both figures, the length unit is 100 m, the time unit is 1 sec, and we represent only one side of the valley because of the symmetry of the problem. The vertical scale is the same for the two components (Bard and Bouchon, 1980a)

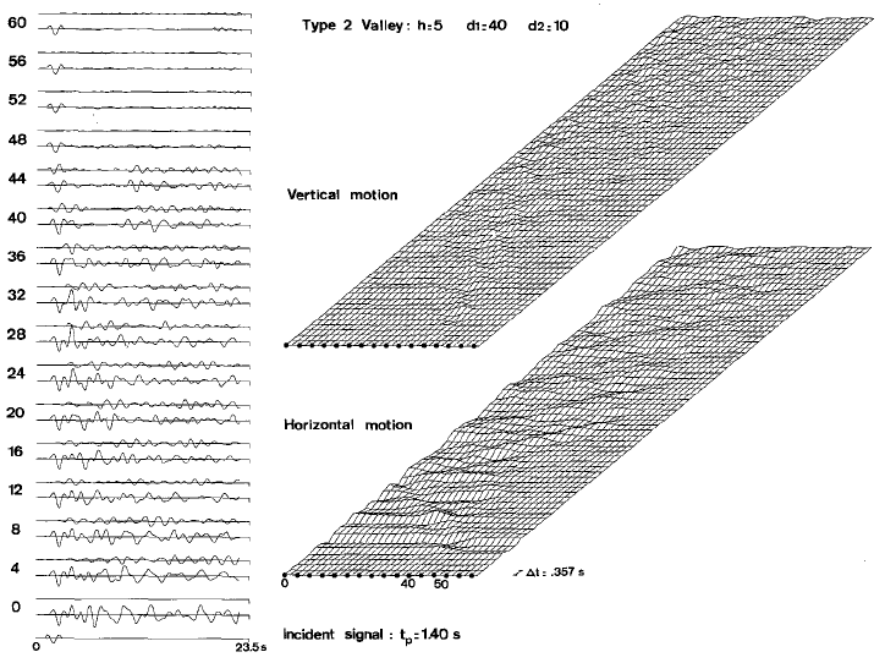

Figure 2.22: Response of valley type 2 subject at vertical incident SV Ricker wavelet of characteristic period tp=1.40 s; see figure above for further explanations (Bard and Bouchon, 1980b)

Bard and Bouchon (1985) further extended the A-L method both to steep and deep valleys. They showed that in shallow valleys, the wavefield is dominated by laterally propagating surface waves generated at the valley edges. In deeper valleys, the interference of these surface waves with vertically propagating waves gives rise to a 2-D resonance pattern. More specifically, using the A-L technique to simulate the seismic behavior of a sine shaped valley on incident SH, SV and P-waves, the Authors showed the existence of three fundamental modes. This is better illustrated in Figure 2.23 and Figure 2.24 by Roten et al. (2006) in which the Authors used of the terms perpendicular and axial for horizontal motion perpendicular and parallel to the valley, respectively. Only the axial component is excited in the SH-mode, while the SV- and P-mode excite both the perpendicular and vertical component (Figure 2.24). In the fundamental mode SH0, the amplification reaches its maximum in the valley center. The SV0 fundamental mode is characterized by a maximum amplification in the center for the perpendicular component and a central node and two maxima for the vertical component. The P fundamental mode shows and opposite behavior (Roten et al., 2006).

The transition between the behavior of shallow and deep valleys is dictated by a critical shape ratio, which is defined as the ratio of the maximum sediment thickness to the valley half-width. The critical shape ratio depends on the velocity contrast between bedrock and fill material, as illustrated in Figure 2.25 (Bard and Bouchon, 1985). If the shape ratio of a valley is above the critical value, it's seismic behavior at low frequencies will be characterized by 2-D resonance, by 1D resonance plus lateral propagation otherwise. The critical shape ratio depends also on the wave type; its value is higher for P-waves than for SH- and SV-waves. According to Bard and Bouchon (1985), the equation of the critical shape ratio is given by the following formula:

$$\left(\frac{h}{l}\right)_{crit} = \frac{0.65}{\sqrt{C_v - 1}} \qquad 2.5)$$

where Cv is the velocity contrast. Bard and Bouchon (1985) also compared the results of numerical analyses with those obtained by the corresponding 1D analyses and concluded that a completely wrong estimate can be obtained in terms of both spectral amplification and resonant frequencies if 2D effects are disregarded (Figure 2.26). The frequencies of 2-D resonance modes are higher than the 1-D resonance frequency fn calculated at the valley center. The frequency of fundamental mode SH00 is slightly above fn for shallow valleys and increases

with increasing valley depth. The frequencies observed in the case of 2-D resonance can, therefore, not be explained with 1-D analysis of the sediment.

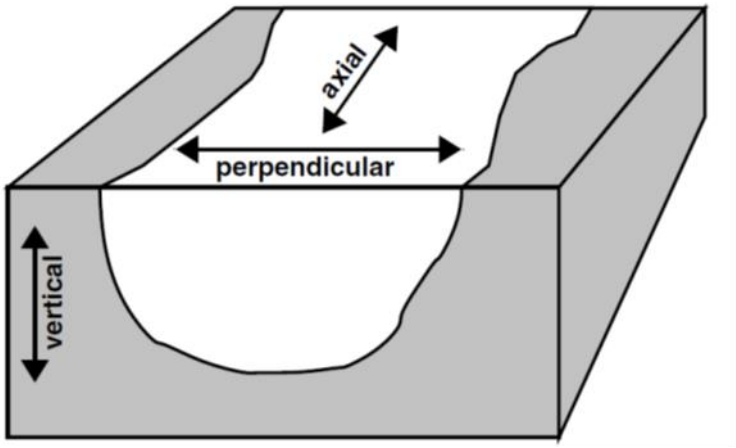

Figure 2.23: Naming convention for directions used in the paper by Roten et al. (2006)

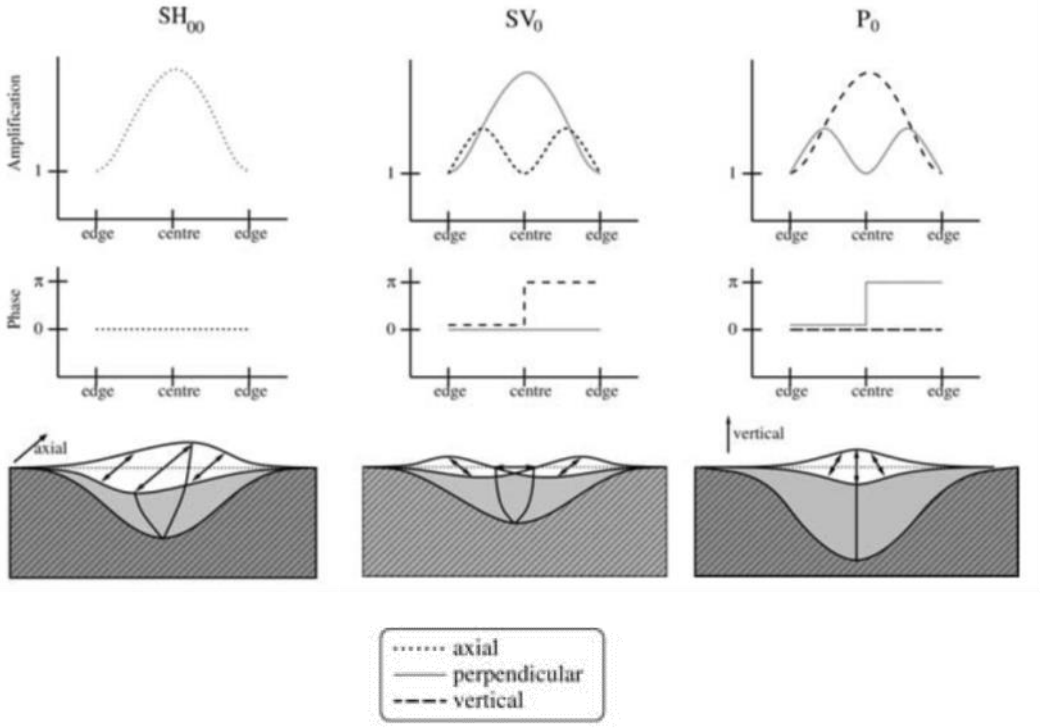

Figure 2.24: Amplification and particle motion of the three fundamental modes of a sine shaped valley for the corresponding critical shape ratio (modified from Roten et al., 2006)

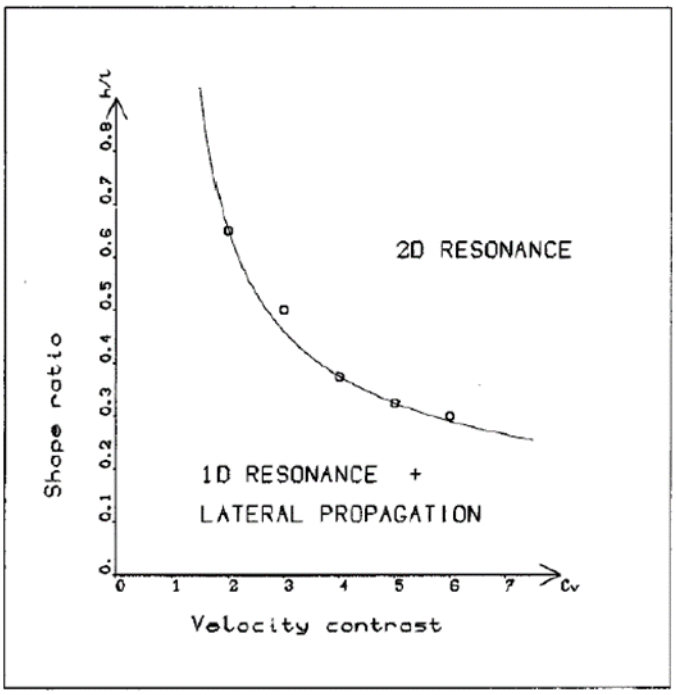

Figure 2.25: Type of valley response for sine-shaped valleys subjected to SH waves, according to valley shape ratio (h/l) vs sediment-bedrock velocity contrast (Bard and Bouchon, 1985)

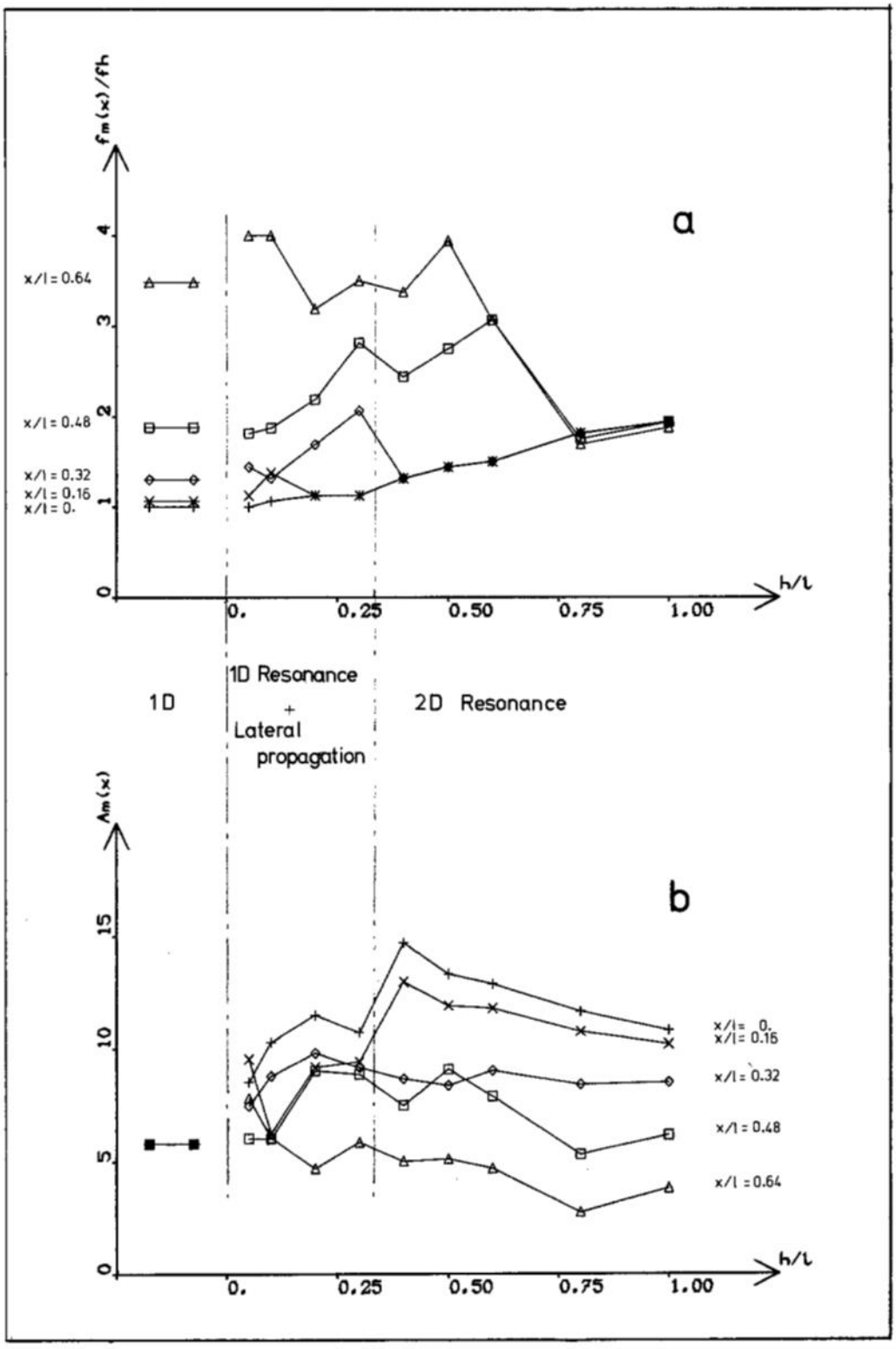

Figure 2.26: Dependence of (b) maximum spectral amplification, and (a) the corresponding frequency on the shape ratio h/l of the valley for five surface sites (from x/l=0, center, to x/l=0.64, edge) and comparison with the corresponding 1D values displayed on the left (Bard and Bouchon, 1985)

Papadimitriou et al. (2010) studied 2D symmetrical trapezoidal valleys subjected to vertically incident SV waves by the FLAC finite difference code in terms of aggravation of the horizontal

acceleration, as compared to 1D conditions, and development of a parasitic vertical component at the surface. They found that the most important dimensionless parameters governing the seismic response are λ/H and B/λ ratios, where B and H are the width and the thickness of the valley, and λ is the predominant wavelength of S wave, and the soil-to-bedrock impedance ratio. In particular, aggravation generally decreases with increasing of the dimensionless parameters λ/H, B/λ and impedance ratio. This means that amplification under 2D condition is larger for narrow and thick valleys, especially for soils much softer than the underlying bedrock. The same 2D code FLAC was used by Iyisan and Khanbabazadeh (2013) and Khanbabazadeh and Iyisan (2014) to investigate the effects of the valley edge on the dynamic behavior of trapezoidal valleys with various side bedrock inclinations, ranging from slighter 10-20 to steeper 30°-40°. Using several different real earthquake motions, the assessment of the site response to the variation of the motion intensity was also studied. The analyses results were presented in the form of the acceleration and spectral acceleration amplification curves. Also, by conducting 1D analyses along the valley, the aggravation curve for every case were evaluated and discussed. It was seen that variation of the bedrock inclination not only affects the peaks of the spectral amplification curves, but also the position of the maximums of the curves on the valley surface are changed. Also, the frequency domain results show that different parts of the valleys are sensitive to different periods. While the lateral parts are sensitive to lower periods, the maximum amplification of the inner parts takes place at higher periods. It was also found that the use of the 1D analyses for the estimation of the 2D behaviour remains insufficient. Finally, the results of this research show the important effect of the motion intensity on the 2D behaviour of the valley, especially on the increase of the resonance period at higher period.

Worth to mention are also the numerical studies conducted on the Ohba valley, a shallow soft alluvial valley located in Japan (Psarropoulos et al., 2007; Gelagoti et al., 2010, Gelagoti et al., 2012) via finite elements codes (Abaqus and Quad4m). Psarropoulos et al. (2007), used Ricker wavelets of different central frequency as input motion and compared linear and nonlinear soil behaviour for a given central frequency. It was found (Figure 2.27) that the valley response is governed by surface Rayleigh waves generated at the edges of the valley which propagate back and forth within the valley; the main effect of soil nonlinearity consists in reducing the amplitude of ground motion amplification. Utilizing the same valley as a test case, Gelagoti et al. (2010) conducted a numerical study to highlight the role of frequency content of input motion and soil nonlinearity. The following conclusions have emerged: 1) the aggravation of

seismic motion is due to the trapping of obliquely incident body waves close to the valley edges for high-frequency excitations whereas it is due to surface waves generated at the corners of the valley and propagating towards the center for low-frequency excitations; 2) soil nonlinearity may modify the 2-D valley response to a substantial extent, mainly at the center of the valley (where the role of surface waves is dominant); 3) the 2-D geometry of the valley (excited by exclusively-horizontal waves) generates a "parasitic" vertical component; in contrast to the natural vertical component of an earthquake, which is the result of P-waves and is usually of very high frequency content to pose a serious threat to structures, this valley-generated parasitic vertical component may be detrimental for overlying structures being of practically the same dominant period as the horizontal component.

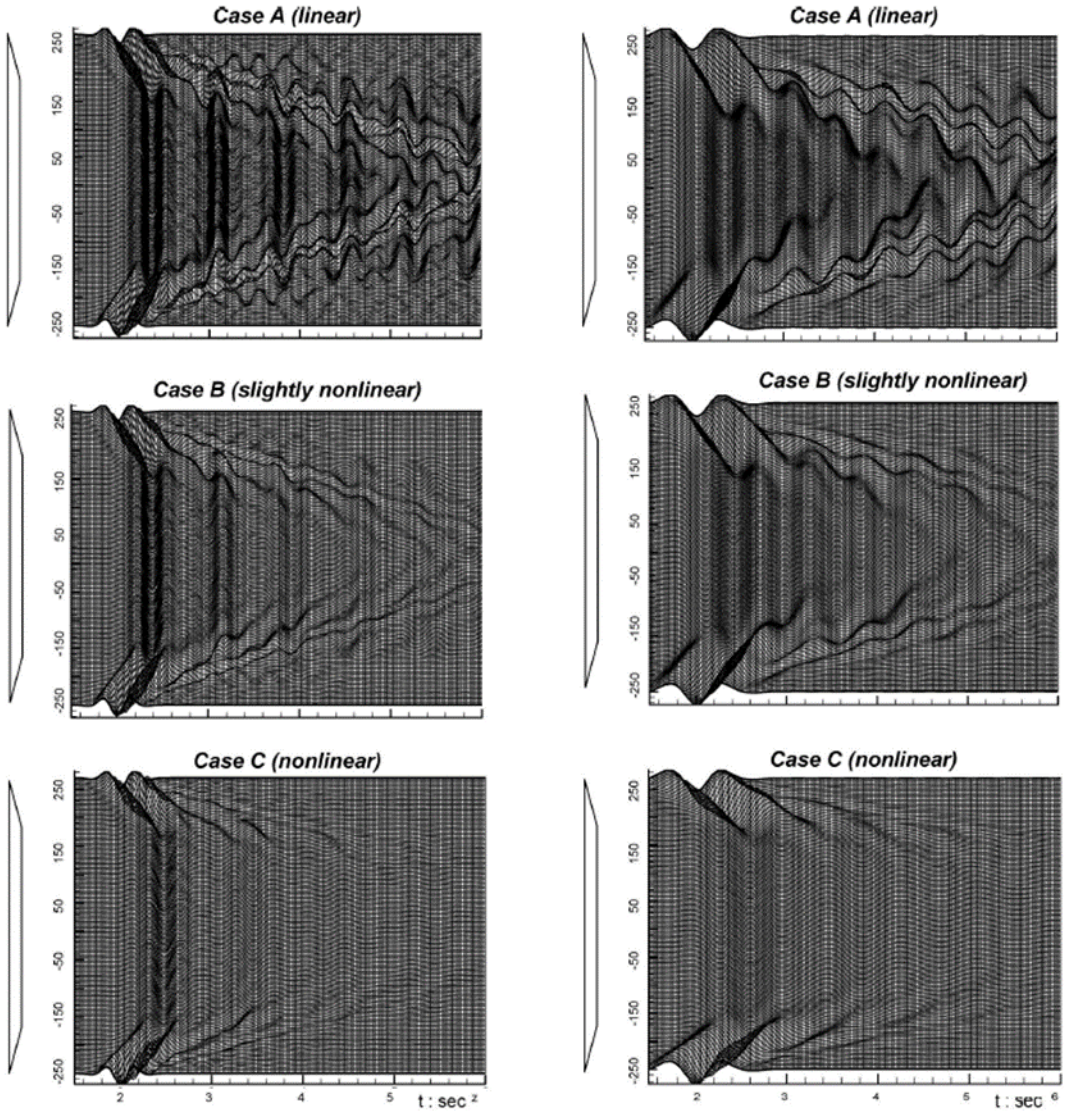

Figure 2.27: Synthetics of horizontal acceleration calculated along the surface of the Ohba valley for two Ricker pulses (f0=1 Hz and f0=2 Hz) and for linear, slightly nonlinear and nonlinear soil behavior (Psarropoulos et al., 2007)

Riga et al. (2016) carried out extensive numerical analyses of the linear viscoelastic response of trapezoidal valleys to investigate the sensitivity of their 2D response to parameters related to the valley geometry (width, thickness and inclination angle of lateral boundaries) and the dynamic soil properties (shear and compressional wave velocity, soil density, soil damping). The results are expressed in terms of peak aggravation factor, defined as the ratio between 2D and 1D response spectra, as well as their spatial distribution calculated at the ground surface. The Authors show that above the sloping edge of the basin, peak values of aggravation factors less than one may occur, that is 2D response is attenuated as compared to 1D response, particularly for steep slopes. At the nearly constant-depth part of the basin, peak aggravation factor strongly depends on the shape ratio of the valley (h/L), and it increases as shape ratio increases, especially in the central part of the valley, where for high shape ratio (i.e. deep and narrow valleys) the computed mean values are as high as 1.8 and 84th percentile around 2.3.

Recently, Papadimitriou (2019) studied the valley effects considering an idealized scheme depicted in Figure 2.28. Specifically, trapezoidal valleys of maximum thickness H, width B at the ground surface subject at vertical SV waves (therefore vertical acceleration is parasitic); the bedrock outcrops with inclination angles iL and iR at the left and right bedrock slopes and creates a step-like slope of height HL and HR above the left and right sides of the horizontal ground surface of the alluvial deposits. However, in most of the analyses it was assumed iL = iR = i and HL = HR. 2D parametric numerical analyses were carried out with the finite difference code FLAC, using simplified seismic excitations (vertically impinging SV waves, harmonic and non-harmonic). The results are presented in the form of elastic response spectra for the horizontal Sah and parasitic vertical accelerations Sav at each ground surface location compared to the elastic response spectrum for the 1D outcropping bedrock horizontal acceleration Sah,b far from the valley edges. In other words, the aggravation factors ASah,b and ASav,b (functions of structural period T) were defined as:

$$AS_{ah,b}(T) = \frac{S_{ah}(T)}{S_{ah,b}(T)} \quad , \quad AS_{av,b}(T) = \frac{S_{av}(T)}{S_{ah,b}(T)} \tag{2.6}$$

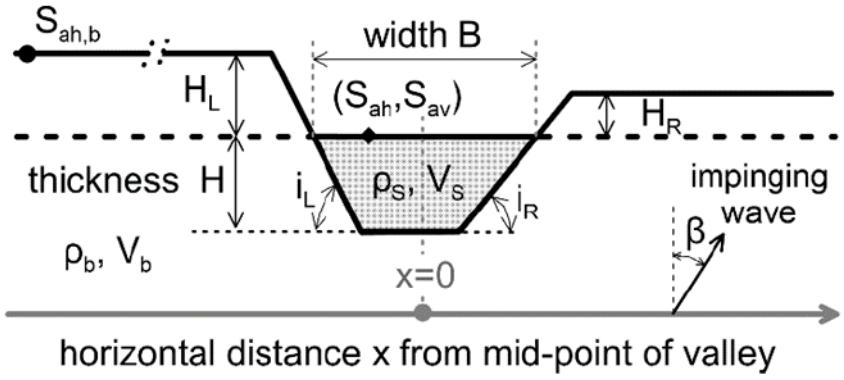

Figure 2.28: Definition of parameters for valley effects (Papadimitriou, 2019)

Parametric seismic ground response analyses were performed for 2D symmetric trapezoidal valleys (iL=iR=i=30° and HL=HR=0; B = 90–1215 m, impedance ratios a = 0.08–0.125, seismic excitations predominant periods Te = 0.15–0.4 s), from very narrow up to quite wide ones. The three valley-excitation combinations have the same normalized valley width B/λ = 6, where λ is the predominant shear wavelength in the soil layer (λ = VSTe), and the same low impedance ratio a = 0.125 making them directly comparable. They differ in the value of the normalized valley thickness λ/H, since they correspond to valleys with relatively large (λ/H = 0.75 – 1.15) to medium normalized thickness (λ/H = 2.6). Figure 2.29 presents the spatial variability of the aggravation factors ASah,b and ASav,b for T=0 s for 3 different valley-excitation combinations. This figure shows a very intense variability of the peak horizontal acceleration, where the maxima may be very large (up to 2.6 times the horizontal acceleration at the outcropping bedrock) and appear at different locations, due to the difference in the λ/H value. For comparison, the figure also includes the code-proposed value of F=1.35 for ground type D as per EC8. In addition, it can be seen that F=1.35 can no longer be considered over-conservative, especially along the center of the valleys, and that a unique F factor all along such valleys is an over-simplistic code provision. In the same figure (bottom plot) the apparition of intense parasitic vertical accelerations along such valleys can be shown, where locally it may even reach 2.0 times the horizontal acceleration at the outcropping bedrock.

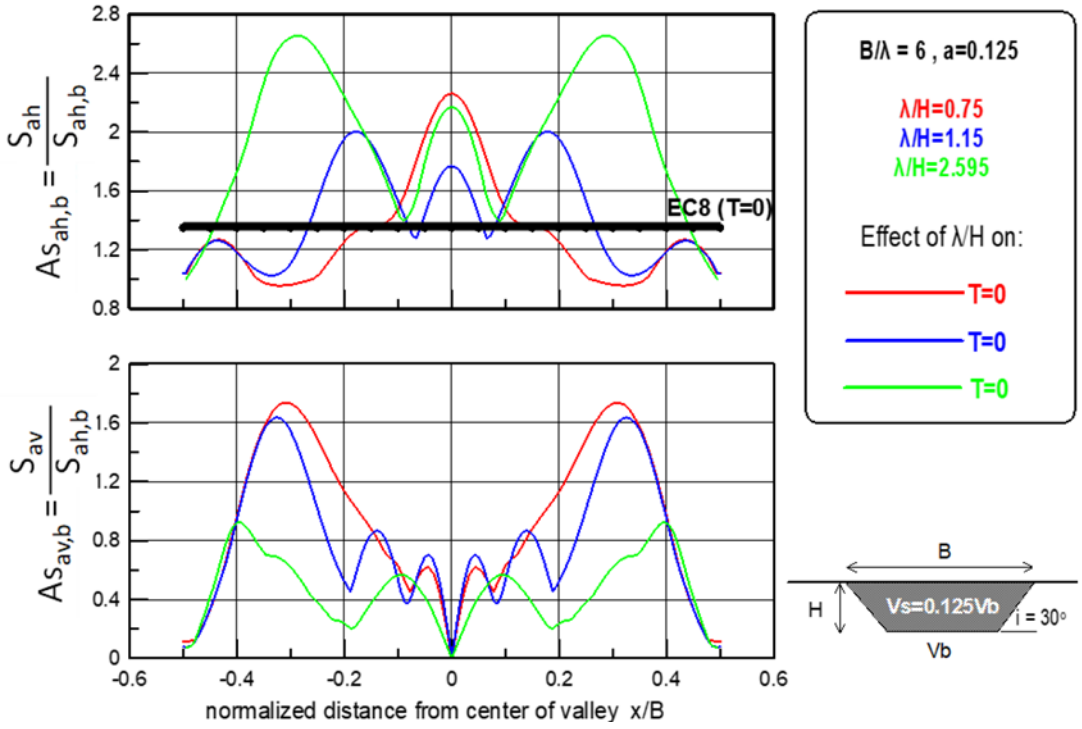

Figure 2.29: Spatial variability of ASah,b and ASav,b (for T = 0 s) along the surface of trapezoidal valleys with ground stype D conditions and the same normalized width B/λ and comparison with EC8 soil factor value (Papadimitriou, 2019)

Papadimitriou (2019) further examined the effect of frequency content and soil inhomogeneity on valley response. Figure 2.30 presents the spatial variation of aggravation factors ASah and ASav for various values of structural period along a 2D symmetrical trapezoidal valley (B/H=4, impedance ratio soil-to-bedrock a=0.5 and steep bedrock inclination angle i=45°). On the left-hand side the results correspond to the valley response for high-frequency excitation (Te=0.18 s) while the right-hand side results to the response of the same valley for low-frequency excitation (Te=0.42 s). The results are presented along the valley (from x/B=-0.5 to 0.5) but also on either side of the horizontal outcropping bedrock. Some general conclusions are: i) valley effects are more intense for high-frequency excitations; ii) valleys effects are more intense for low structural periods while for large periods (T>1.0 s) they essentially disappear; iii) the existence of the valley affects primarily the seismic ground motion within it, however it also affects the outcropping bedrock motion, including local amplification that may reach 20% in the close vicinity of the valley; iv) valley effects can be quite significant with values ASah=2.0 and ASav=0.8 for low structural periods; even higher values may appear for narrow valleys where the peak aggravation factors appear at the valley centre while lower values are expected for wide valleys where the peak aggravation appear at the valley edges. The influence

of the degree of inhomogeneity is illustrated in Figure 2.30 where the aggravation factor is plotted for different various of the parameter d (d=0 for homogenous soil and values of 0.5 to 1.5 correspond to lightly up to strong inhomogeneous soil). The figure shows that in comparison to the outcropping bedrock, the valley exhibits completely different ground response, the higher the values of d the more intense the aggravation of peal horizontal and peak parasitic vertical acceleration along the valley. Therefore, considering valley effects with homogeneous soil is more or less conservative, provided that the average shear wave velocity is properly accounted.

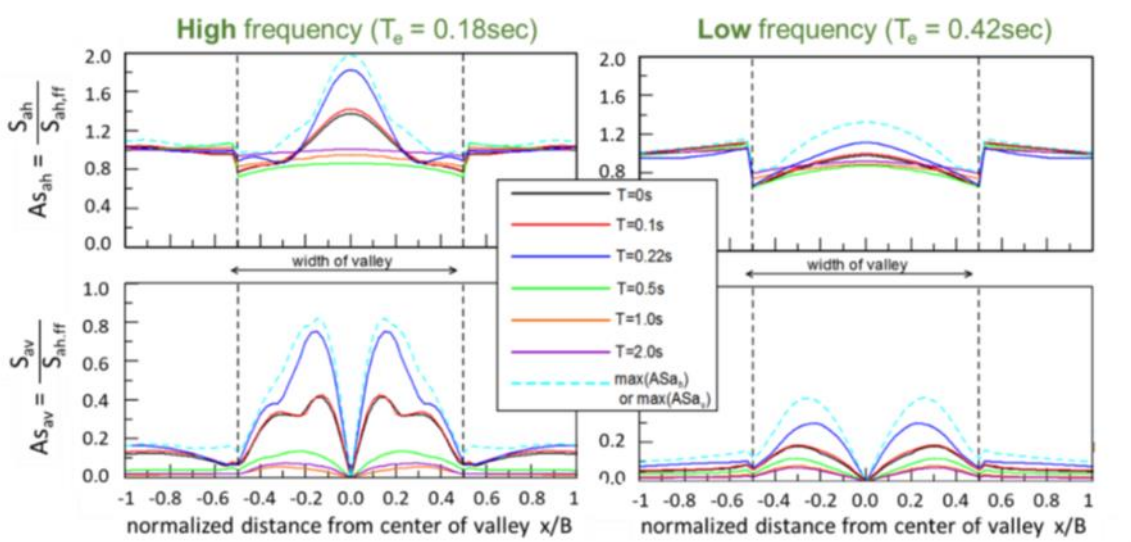

Figure 2.30: Spatial variation of ASah,b and ASav,b for various structural periods T along a 2D symmetrical valley (B/H=4, a=0.5, i=45°) under excitation with different predominant period Te (Papadimitriou, 2019)

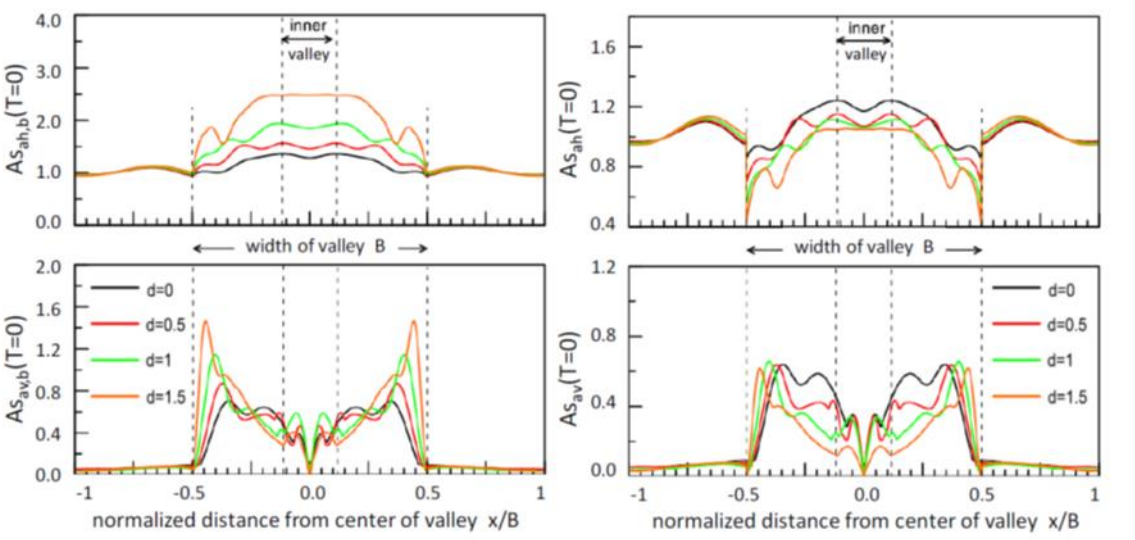

Figure 2.31: Spatial variation of ASah,b and ASav,b for for T = 0 s (left) and ASah and ASav for T = 0 s (right) along 2D symmetric valleys (B/H = 4.5, i = 30°) over bedrock Vb = 800 m/s and soil with VS,ave = 360 m/s having 4 different degrees of inhomogeneity d under a high frequency excitation (Te = 0.20 s) (Papadimitriou, 2019)

Bielak et al. (2000) studied via numerical examples the major differences existing between 1D and 2D, 3D conditions. It was found that 1D simulations tend in general to exhibit lower peaks and the motion is of lower duration as compared to 2D/3D response, as 1D assumption cannot incorporate edge effects. On the other hand, because of the destructive interference of waves, there are sites where the response can be much smaller than predicted by 1D models. In fact, under 2D/3D conditions the surface motion can vary significantly over short distances even with little or no change in soil properties, whereas in 1D case only abrupt changes of material properties in the lateral direction can lead to strong modifications of response. Chavez-Garcia (2003) computed ground surface motion in Parkway Valley, a small alluvial valley in New Zealand, and compared numerical results with observational studies. A 3-D, finite difference code for the vertical incidence of plane waves, P and S, was used. The results of the simulations confirm the observation that ground motion in Parkway Basin is dominated by locally generated surface waves and suggest that the 3-D shape of the basin may be more important than a detailed knowledge of the subsoil mechanical properties in predicting ground response. Another numerical technique used for investigating the seismic response of 3D alluvial basins is the spectral method (Faccioli et al., 1997). The 3D version of the code GeoElse, which is an implementation of GeoElse2D (Stupazzini et al., 2004), was used for the numerical simulation of the Grenoble basin (Stupazzini et al., 2009a). The same code was also used (Stupazzini et al., 2009a, Paolucci and Smerzini, 2011, Smerzini et al., 2011) to study the seismic response of the Gubbio plain, an intra-mountain alluvial basin in Central Italy, which evidenced long period

ground motion during the 1997 Umbria-Marche earthquake sequence. The comparison of 1D, 2D, and 3D numerical results with observations show that 1D and 2D simulations fail to capture the long period amplification due to the generation of surface waves at the southern edge of the basin.

Recently, Makra and Chavez-Garcia (2016), compared simulation with observations for the Mygdonian basin in Northern Greece (Euroseistest), using different approximation for the basin, that is 1D, 2D and 3D. As expected, it was found that the use of 2D or 3D model can significantly modify the amplification computed using 1D model at some sites. The amplifications function appear more complex, with large amplification at frequencies that do not correspond to the resonance frequencies of the soil deposit. In general, ground motion simulated using 2D models is very similar to that computed from a full 3D model of the basin. However, it has to be remembered that the development of a reliable 3D model requires significantly more information than a 2D model, and therefore a lot of uncertainties may be associated to the 3D model, especially for a large basin.

Numerical research into the influence of surface morphology (hill, ridge, cliff, slope, etc.) has also received increasing attention in the last decades. 1D, 2D and more recently 3D numerical simulations, for various surface morphologies, have been carried out in order to model and predict the topographic effects on seismic ground motions, and to compare the theoretical amplifications with observations. Early numerical studies on the topographic irregularities on ground motion amplification were carried out for simple configurations by means of different methods (finite elements, finite differences, boundary and discrete wavenumber methods, etc.). In 1973, Bouchon carried out a parametric study using the A-L method to investigate the effect of topographic for SH, P and SV waves (Bouchon, 1973). It was shown that surface topography, incident angle of input motion and wavelength greatly affect the numerical results. Successively, Bard (1985) applied the A-L technique both in time and frequency domain to study the scattered wave field considered a simplified topographic configuration (Figure 2.32). The topographic effects strongly depend on the characteristics of incident waves. For wavelength of the incident motion similar o slightly shorter than the irregularity width, amplification of ground motion occurred systematically. It was also found that the wave scattering is frequency-dependent. Finally, crest amplification is greater for incident S than P waves. Sanchez-Sesma et al. (1984) used boundary method for solving the scattering and diffraction of elastic waves by three-dimensional irregularities of a half-space (Figure 2.33). Figure 2.34 and Figure 2.35 show the normalized amplitude of displacement for incident P and

SV waves, respectively. The results shows that the amplifications are about 200 and 250% for P and SV waves, respectively. Large amplification is evident at the top of irregularities and for incident SV waves.

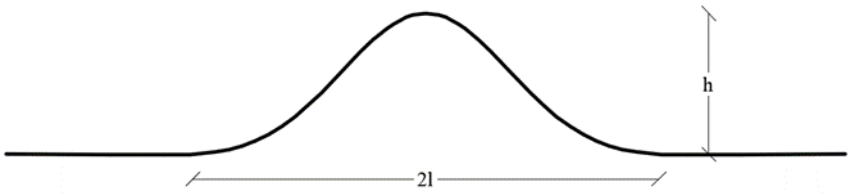

Figure 2.32: Topographic relief considered by Bard (1985)

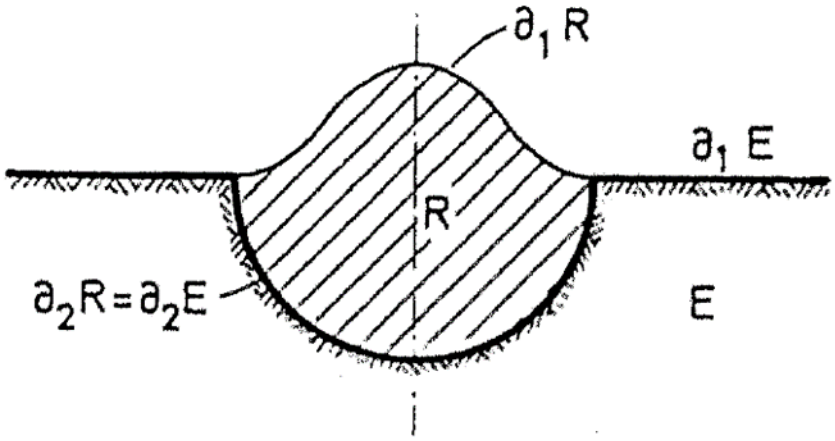

Figure 2.33: Three-dimensional irregularities of a half-space considered by Sanchez-Sesma et al., (1984)

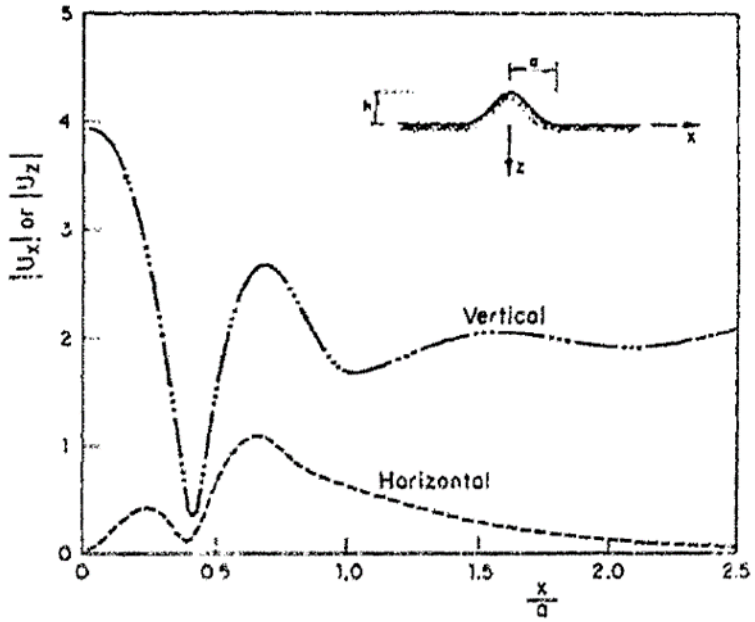

Figure 2.34: Surface amplitude of vertical and horizontal displacement, with normalized frequency η =1, Sanchez-Sesma et al., (1984)

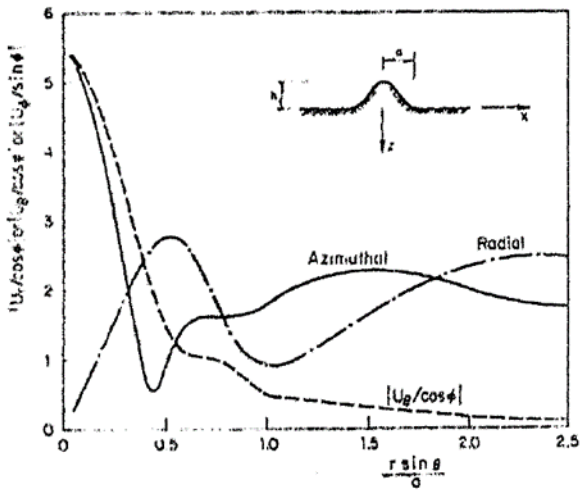

Figure 2.35: Surface amplitude of spherical displacement (Sanchez-Sesma, Chavez-Perez & Aviles)

A comprehensive review of numerical studies on ridges and hills was presented by Geli et al. (1988). They found that most of the studies gave consistent results, which can be summarized hereafter: (i) the time-domain crest-to-base acceleration amplification ratios are below two; (ii) the frequency-domain crest-to-base amplification peaks occur when wavelength is about equal to the ridge width; (iii) amplification and attenuation occur along the surface of the slope from the crest to the base; (iv) the amplification is lower for incident P waves than for incident S waves; (v) the amplification is slightly larger for horizontal SV waves than for SH waves.

One of the first systematic parametric studies on the topographic effects was conducted by Ashford et al. (1997) and Ashford and Sitar (2002). With reference to steep coastal bluffs, they consider topographic amplification as the amplification at the crest relative to the free-field behind the crest, rather than comparing the ground motion at the crest to the motion at the base. Parametric analyses were conducted considering different parameters (slope inclination, wave type, wavelength, angle of incidence) and it was found that peak amplification of motion at the slope crest occurs at a normalized frequency $H/\lambda=0.2$.

Bouckovalas and Papadimitriou (2004) examined the seismic response of step-like ground slopes in uniform visco-elastic soil, under vertically propagating SV seismic waves (Figure 2.36) by using the FLAC code. The Authors provide qualitative as well as quantitative insights to the phenomenon in terms of topography aggravation factors both for horizontal, Ah = ah/ah,ff, and vertical parasitic motion Av = av/ah,ff where ah, av and ah,ff are the peak horizontal acceleration, vertical parasitic and input horizontal acceleration in the free-field behind the crest, respectively. Their results show that: i) reflection of incoming SV waves on the inclined free-surface forms reflected P, SV and Rayleigh waves with significant parasitic

vertical acceleration; the superposition of these waves with incoming SV waves can lead to intense amplification or attenuation of motion with consequent variability at neighbouring points behind the crest within a few tens of metres (i.e. H/2); ii) attenuation near the toe of the slope indicates that topographic effects can be overestimated when comparing crest-toe ground motions, therefore an adequate free-field site has to be identified in order to reliable quantify site effects; iii) slope angle (i) and normalized height (H/λ) significantly affects horizontal and vertical amplification as well as the distance to the free-field in front and behind the slope; free-field conditions behind the crest are usually encountered at a distance Dff=(2-8H). In Figure 2.37 and Figure 2.38 the effect of slope inclination (i) and normalized height ratio (H/λ, respectively, are shown. The topography effects become important for H/λ > 0.16 and i > 17°. In these conditions, the peak values of topography aggravation factors for the horizontal and the vertical ground acceleration behind the crest usually vary between Ah,max = 1.20–1.50 and Av,max = 0.10–1.10. Moreover, the Authors provide simplified relations for topography aggravation factors:

$$A_{h,max} = 1 + \frac{0.225(H/\lambda)^{0.4}\left(\frac{I^2 + 2I^6}{I^{0.3} + 0.02}\right)}{1 + 0.9\xi} \quad (2.7)$$

$$A_{v,max} = \frac{0.75(H/\lambda)^{0.8}(I^{0.5} + 1.5I^5)}{1 + 0.15\xi^{0.5}} \quad (2.8)$$

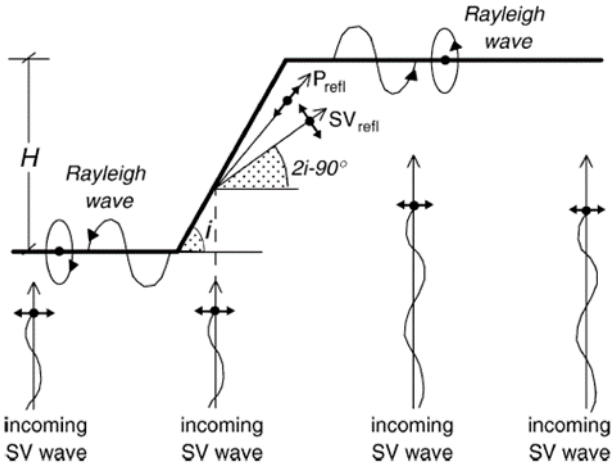

Figure 2.36: Schematic illustration of incoming SV waves and induced Prefl, SVrefl and Rayleigh waves in the case of step-like slopes (i ≥ 45). (Bouckovalas and Papadimitriou, 2004)

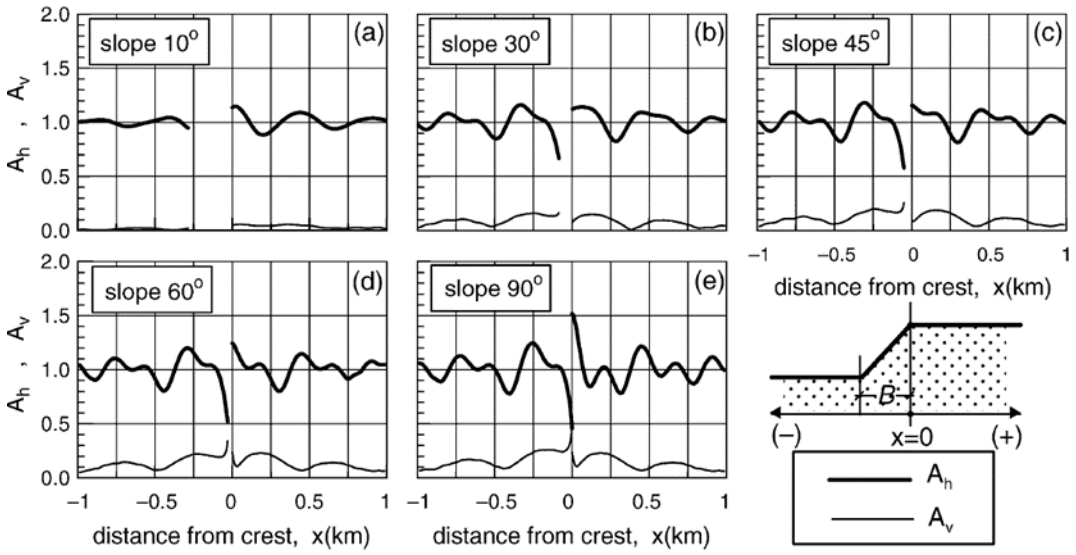

Figure 2.37: Effect of slope inclination (i) on the amplification of peak horizontal acceleration Ah and of parasitic vertical acceleration Av, as a function of horizontal distance x from the crest of a step-like slope (H/λ=0.2, harmonic motion (Bouckovalas and Papadimitriou, 2004)

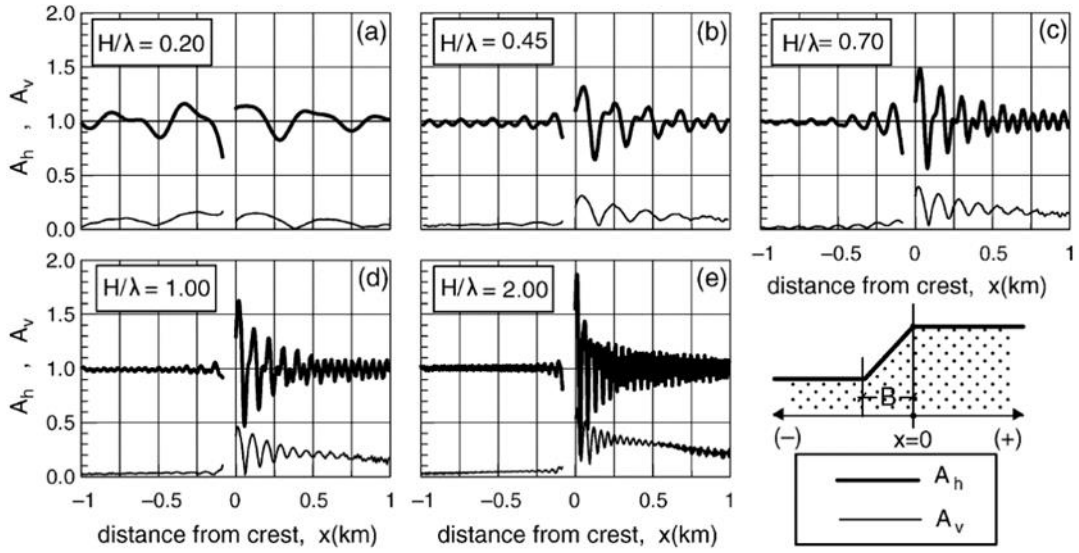

Figure 2.38: Effect of normalized height (H/λ on the amplification of peak horizontal acceleration Ah and of parasitic vertical acceleration Av, as a function of horizontal distance x from the crest of a step-like slope (i>30°, harmonic motion (Bouckovalas and Papadimitriou, 2004)

Papadimitriou and Chaloulos (2010) recognize that the problem is multi-parametric and make an effort to analyses within a common framework the fundamental similarities and differences of the seismic response of different topographic features such as 2D uniform slopes, trapezoidal canyons and hills under vertically impinging harmonic SV waves. Based on the results of 2D

finite difference numerical simulations, they examined the influence of different parameters on topographic aggravation factors, which are: i) slope inclination i; ii) wavelength λ; iii) height H and width B of 2D geometries; iv) normalized height H/λ (Figure 2.39). They concluded that trapezoidal canyons and slopes with the same H/λ and i produce similar aggravation of horizontal and vertical accelerations in front of their toe and behind their crest. Canyons show larger amplification of the parasitic vertical acceleration compared to the respective slope. On the other hand, trapezoidal hill show higher aggravation of the horizontal acceleration at their top, compared with the slope with the same H/λ and i, on average by 30% or more. In parallel, in front of their toe, hills show larger or equal aggravation of the horizontal and vertical acceleration, again compared to the respective slope. In Figure 2.40 and Figure 2.41 the numerical results for trapezoidal canyon and hills, respectively, are shown both for horizontal and parasitic vertical components by assuming i = 45° and H/λ = 0.45 for various B (Papadimitriou and Chaloulos, 2010). As mentioned before, the analyses show the increased parasitic vertical accelerations at the crest of canyon as compared to the respective slopes (with the same ι and H/λ), while the aggravation of the horizontal acceleration is similar. Trapezoidal hills produce much higher aggravation of the horizontal acceleration at their top, as compared to slopes with the same i and H/λ. The Authors conclude highlighting that one of the limitation of their research is that it pertains to 2D trapezoidal hills and canyons and that the consideration of the third dimension can lead to more intense amplifications.

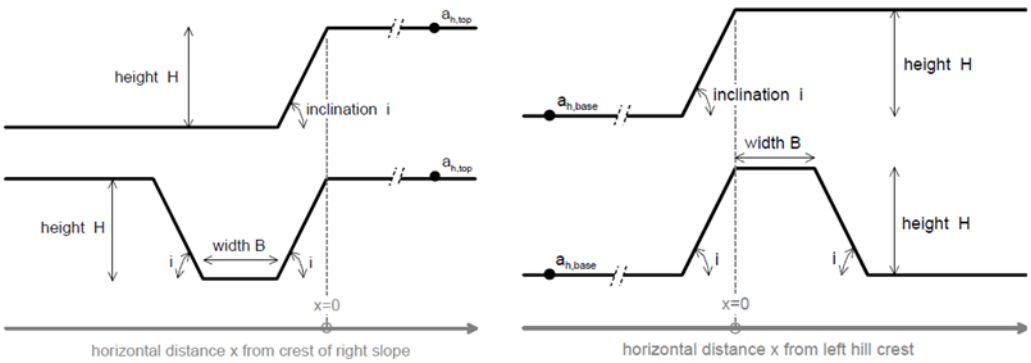

Figure 2.39: Schematic illustration of (left) 2D slope (inclination I and height H) and respective 2D trapezoidal canyon of width B part the base and (right) slope with (inclination i, height H) and respective 2D trapezoidal symmetrical hill of width B at the crest; location of ah,base used in the estimation of topographic aggravation (Papadimitriou and Chaloulos, 2010)

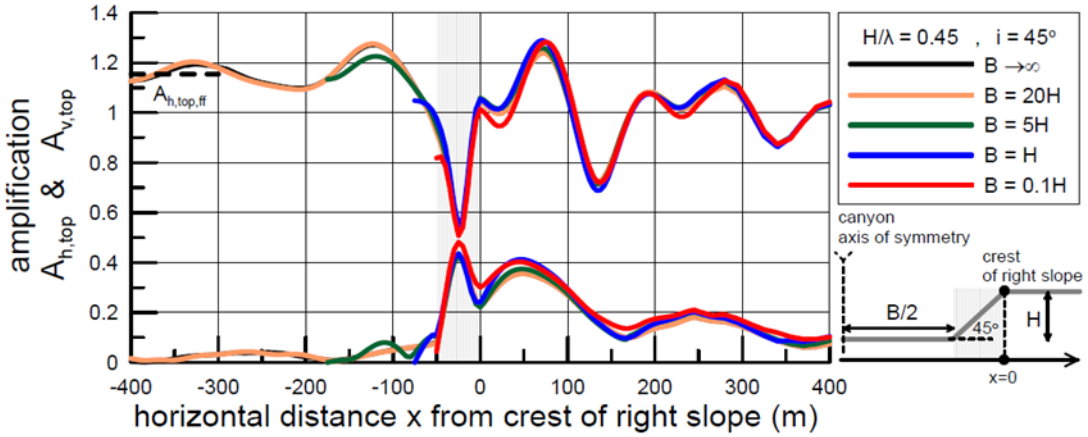

Figure 2.40: Spatial variability of topographic aggravation factors Ah,top and Av,top in the vicinity of symmetric trapezoidal canyons with slope inclination i=45°, normalized height H/λ=0.45 and various widths B = 0.1H, H, 5H, 20H and B→∞. Results are shown from the axis of symmetry of the canyon up to x=8H=400m behind the crest of the right slope.

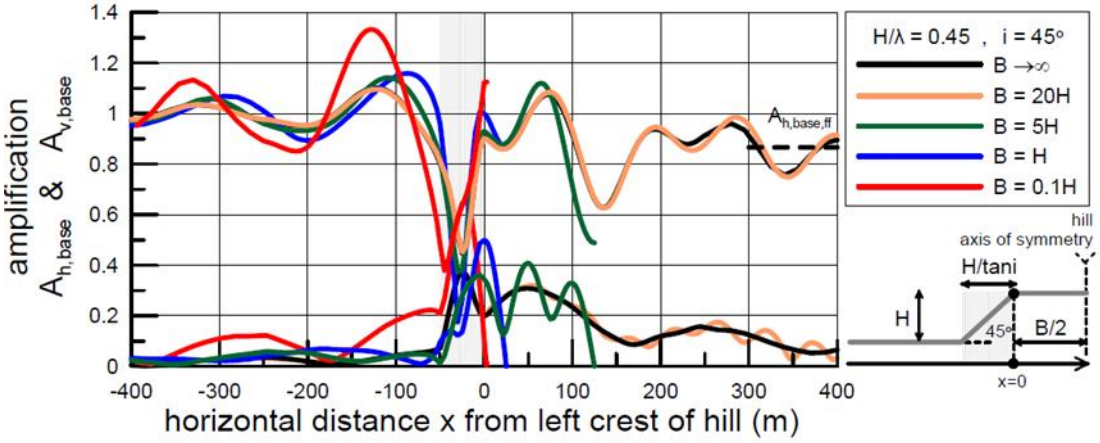

Figure 2.41: Spatial variability of topographic aggravation factors Ah,base and Av,base in the vicinity of symmetric trapezoidal hills with slope inclination i=45°, normalized height H/λ=0.45 and various widths B = 0.1H, H, 5H, 20H and B→∞. Results are shown from x=-8H=-400m in front of the toe of the left slope and reach the axis of symmetry of the hill.

In summary, the effects of surface irregularities on seismic ground motion have been studied by many researchers using theoretical as well as numerical modelling. For these studies, carried out using different analytical or numerical techniques, similar parameter were highlighted that are of importance for studying the site effects of these features.

Lastly, a comment on the instrumental observations which are much more limited than analytical/numerical studies because they have to face with two objective difficulties: i) the monitoring for a long period of time; ii) the coupling between 1D and 2D effects, i.e. the interaction between stratigraphic amplification and topographic amplification; in fact it has to

be considered that stratigraphy effects tend to overwhelm the 2D ones. In general, literature studies show that numerical predictions always underestimate the field observations. In this respect 3D numerical models could be more efficient than 1D and 2D ones for studying wave propagation for topographic features.

2.4 Seismic response of earth dams

2.4.1 Introduction

A considerable amount of earth dams were built in Italy during the last century, most of them without considering the seismic actions, even in areas of medium to large seismicity. Taking into account the important role played by these geotechnical systems for water supply, irrigation and hydroelectric energy production, their stability when subjected to seismic actions is of paramount importance for service operations and especially for the public safety. In fact, the sudden collapse of a large dam with uncontrolled release of water can results in major consequences for loss of life and socio-economic losses. The need to reliably assess the dynamic response of earth dams and the main influencing factors is therefore important in order to avoid the aforementioned problems and to provide possible remedial measures.

Earth dams are complex 3D geotechnical systems and therefore their dynamic response during earthquakes is rather complicated problem to deal with. This response is controlled by many factors spanning from the geometric configuration and the material properties of the dams, the characteristics of foundations soils as well as those of the input motion (intensity, frequency content and duration). Since sixties, the dynamic response of dams has traditionally been estimated using an analytical technique (the so-called shear-beam approach) for determining the natural modes and frequencies of vibration of an earth dam (e.g., Ambraseys, 1960). In the eighties-nineties, a number of closed-form solutions were developed for simplified dam geometries embedded in canyons of various shapes, mostly under the assumption of linear elastic dam behaviour. A comprehensive review was given by Gazetas (1987), Dakoulas and Gazetas (1991) and Gazetas and Dakoulas (1992), who outlined the main features of the theoretical methods, their benefits and limitations. At the same time, improvements in the numerical procedures and increasing efficiency of computational tools have resulted in widespread use of these methods to study the dynamic behaviour of earth dams. The use of 3D models has revealed various aspects of dam response to seismic shaking and has shed some light on the capability of 2D analyses procedures to predict the 3D response of earth dams (e.g., Mejia and Seed, 1984).

In the following, closed-form solutions available in literature are examined first. These solutions are useful for understanding the parameters that influence the response under dynamic conditions but are defined for simplified models in terms of geometries (rectangular, semi-cylindrical and semi-elliptical), mechanical behaviour (visco-elastic linear) and input motion (stationary SH waves). Then, the main results from numerical modelling using different

numerical techniques are presented and the comparison with real earthquake records to check their reliability is also discussed.

2.4.2 Analytical studies

The first attempts to study the vibrations of earth dams were addresses by Hatanaka (1952) and Ambreseys (1960), which showed that bending-type deformations are negligible compared to those in simple shear when the parameter α, defined as the ratio between height and base of dam (Figure 2.42), is larger than 3. They introduced the 'shear-wedge' or 'shear-beam' (SB) model. This model is the basis of all closed-form solutions for seismic behaviour of earth dams (e.g., Gazetas, 1987; Dakoulas, 1991; Gazetas & Dakoulas, 1992; Dakoulas and Hasmini, 1992; Dakuolas and Hsu, 1993).

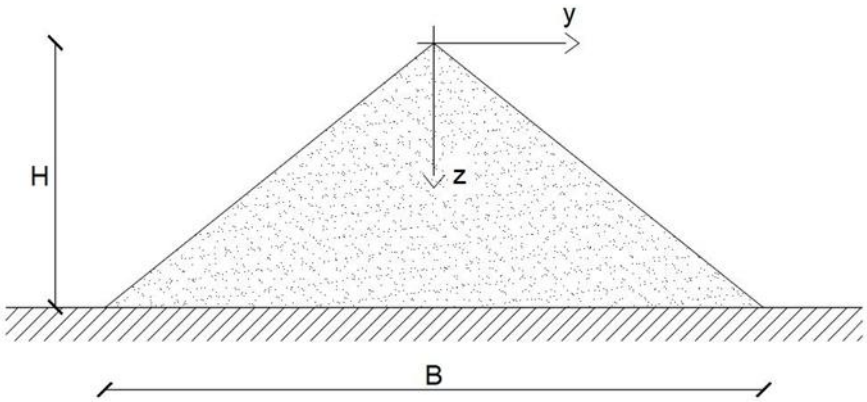

Figure 2.42: Triangular system considerer by Hatanaka (1952)

In Figure 2.43 and Figure 2.44 are illustrated the fundamental periods and the first modal shape obtained (Hatanaka, 1952) by assuming: 1) only bending-type deformation (TB, blue lines); 2) only shear type deformation (TS, green lines); and 3) both bending and shear type (TBS, red lines) by varying the parameter α. The analytical results show that the bending-type deformation can be neglected when $\alpha \geq 3$ (typical values of earth dams). This approach does not take into account vertical and transversal input motion.

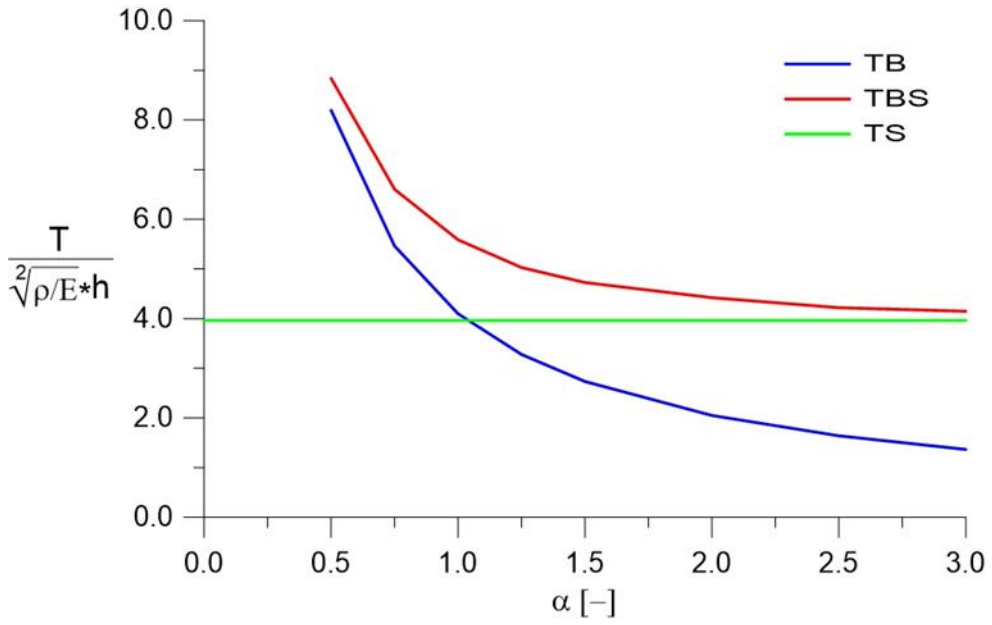

Figure 2.43: Relation between fundamental period and the parameter α for bending, shear and complete system conditions (redrawn from Hatanaka, 1952)

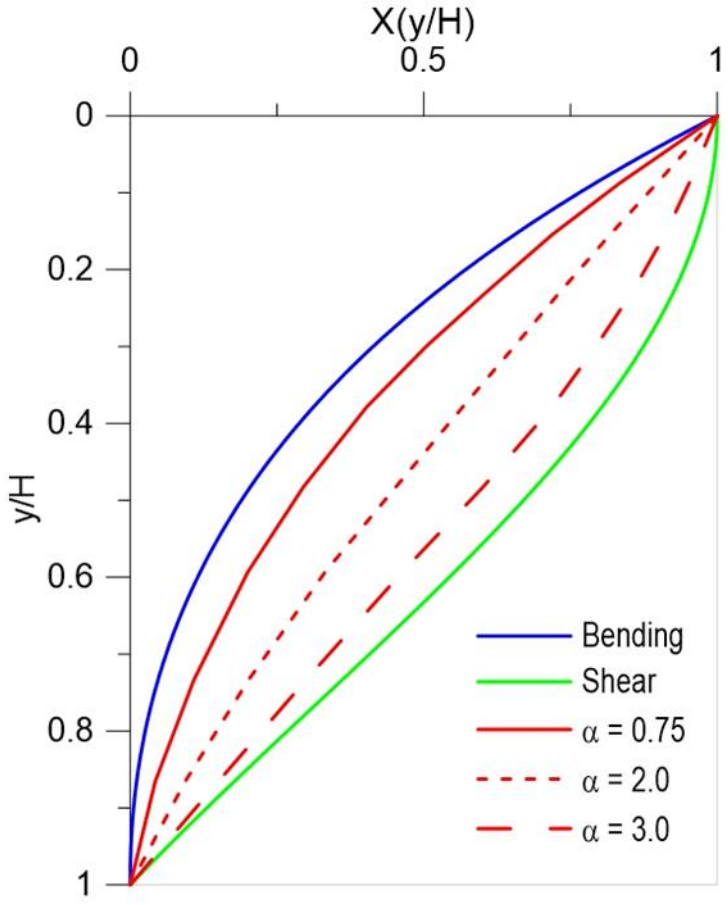

Figure 2.44: Comparison between modal shape of bending, shear and complete system as a function of parameter α (redrawn from Hatanaka, 1952)

In the scheme adopted by Ambraseys (1960), the dam is represented by a truncated wedge with plane inclined faces, constructed in a rectangular canyon (Figure 2.45). This model was employed to estimate the lateral vibrations of earth dams built in relatively wide canyons. Based on the assumption of uniform horizontal lateral shear strain, shear stress and displacements, this model leads to values of natural frequencies and mode shapes which are quite reliable and have been largely used over the years to estimate the dynamic response of earth and rockfill dams and embankments (Dakoulas and Gazetas, 1985). Successively, the SB model was used extensively for developing analytical closed-form solutions for several idealized canyon shapes such as rectangular, semi-cylindrical, trapezoidal and triangular. In Table 2.2 the main studies based on the SB model (therefore the dam responds primarily in horizontal shear mode) are summarized. In all studies the behaviour is visco-elastic linear and the seismic input is a stationary train of waves SH, generally inclined at an angle γ with respect to the vertical direction. In the following a brief review of the most representative studies is given, with emphasis on main aspects that affect the dynamic response such as inhomogeneity of dam material, 3D effect due to canyon geometry, impedance ratio between dam and supporting canyon, angle of incidence of waves and the presence of a foundation alluvial layer.

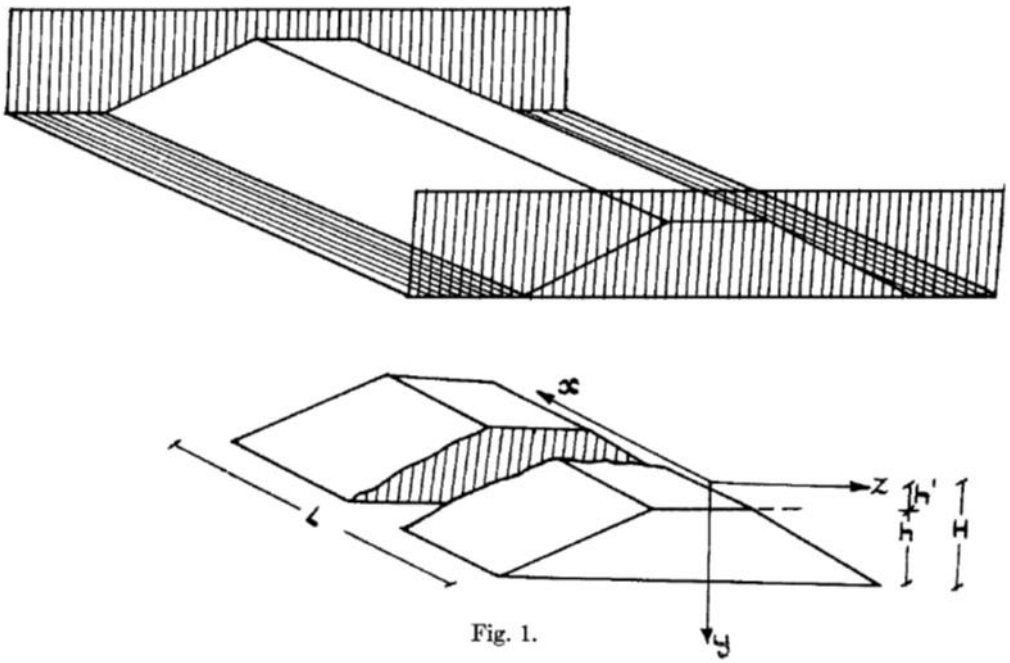

Figure 2.45: Geometry of the dam according to Ambraseys (1960)

Table 2.2: Closed-form solutions for earth dams embedded in canyons of different geometry

Authors	System
Ambraseys (1960)	Rectangular canyon on rigid halfspace
Dakoulas & Gazetas (1985)	Plane strain inhomogeneous dam
Dakoulas & Gazetas (1986)	Semi-cylindrical rigid canyon
Dakoulas & Gazetas (1987)	Rectangular canyon on foundation alluvial layer
Dakoulas (1990)	Rectangular canyon on foundation alluvial layer
Dakoulas & Hashmi (1991)	Rectangular canyon on deformable bedrock
Dakoulas (1993a, b)	Semi-cylindrical canyon on deformable bedrock
Dakoulas & Hsu (1993)	Semi-elliptical rigid canyon
Dakoulas & Hsu (1995)	Semi-elliptical deformable canyon

2.4.2.1 Inhomogeneity of dam materials

An unrealistic simplification of the model is based on the assumption that soil properties are constant throughout the dam. It is well known that the soil stiffness is indeed a function of effective mean stress, which in earth dams vary from point to point, it is very small near the crest and very large near the centre of the base of the dam. To account for the dependence of soil stiffness on confining pressure, an improved version of the SB model has been proposed by Dakoulas and Gazetas (1985) in which the average shear modulus G increases as the 2/3 power of the depth, according to the following expression:

$$G(z) = G_b \left(\frac{z}{H}\right)^m \tag{2.9}$$

where z and H are the vertical distance from the crest of the dam and the height of the dam, respectively, Gb is the shear modulus at base of dam and m is the exponent of the stiffness which govern its variation with depth (see Figure 2.46).

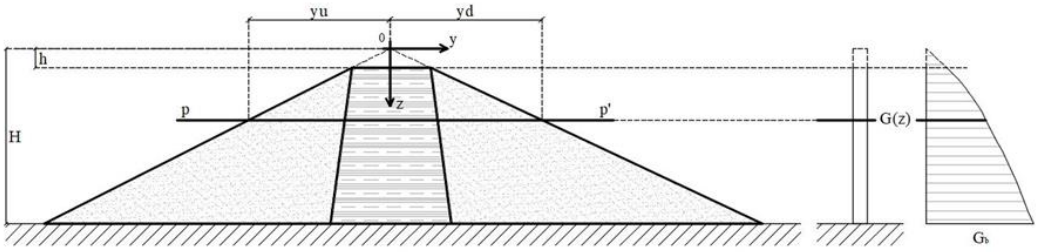

Figure 2.46: Dam cross-section and distribution of shear modulus with depth (Dakoulas & Gazetas, 1985).

Figure 2.47 show the ratio of the n-th natural period of inhomogeneous dam Tn(m), which corresponds to the n-th mode of vibration for a given value of m, over the period of a homogeneous dam Tn(0) (m=0). The degree of inhomogeneity varies from m=0 (constant stiffness) to m=1 (linear variation of stiffness with depth). Results are shown for two values of the truncation ratio λ = h/H, that is λ=0 (untruncated dam) and λ=0.5. It can be seen that for λ=0 the degree of inhomogeneity has a negligible effect on the first mode while it is appreciable at higher modes; on the contrary, for λ=0.5 the effect of m on the natural periods appears negligible, regardless of the value of m (Dakoulas and Gazetas, 1985). Therefore, it can be concluded that the fundamental period of the dam seems to be constant, regardless of m and l. The effect of inhomogeneity on the first four displacement modal shapes for five different values of the parameter m is illustrated in Figure 2.48 for λ=0. The inhomogeneity results in a concentration of the displacements near the crest of the dam as compared to the homogeneous case. This behaviour is slightly dependent of the value of m, especially for the range of values usually expected in practice (n=0.40-0.75).

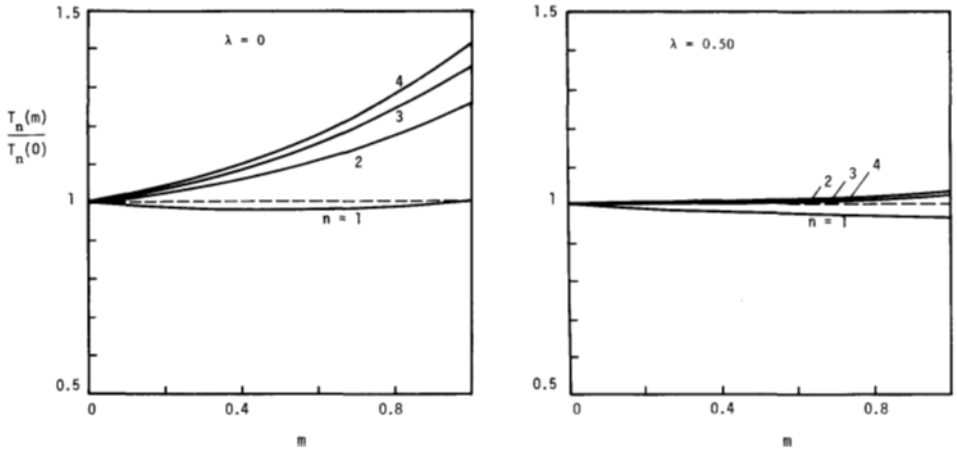

Figure 2.47: Effect of inhomogeneity on the ratio of the natural periods of the inhomogeneous and homogeneous dams for: (upper) λ=0 and (bottom) λ=0.50. (Dakoulas & Gazetas, 1985)

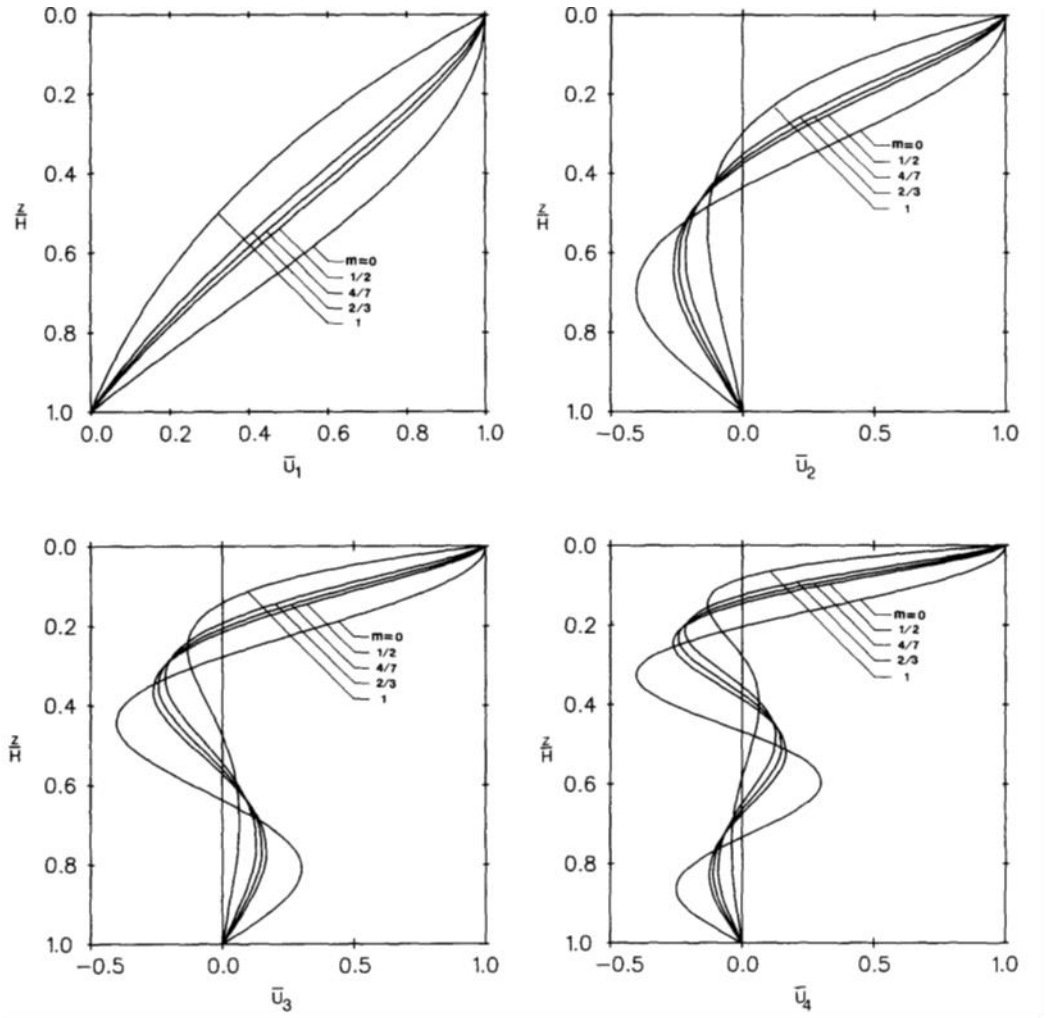

Figure 2.48: Crest amplifications of inhomogeneous and homogenous dams for a) λ=0 and b) λ=0.50 (Dakoulas & Gazetas, 1985)

In Figure 2.49 the amplification functions calculated at the crest are also plotted for λ=0 and λ=0.5 as a function of the dimensionless frequency $\omega H/V_s$ is the average shear wave velocity. It can be observed that increasing the degree of inhomogeneity m results in larger amplitudes of the fundamental frequency as well as of higher frequencies. However, for higher values of λ=0.5 (embankment), the crest amplification is quite insensitive to variation of parameter m.

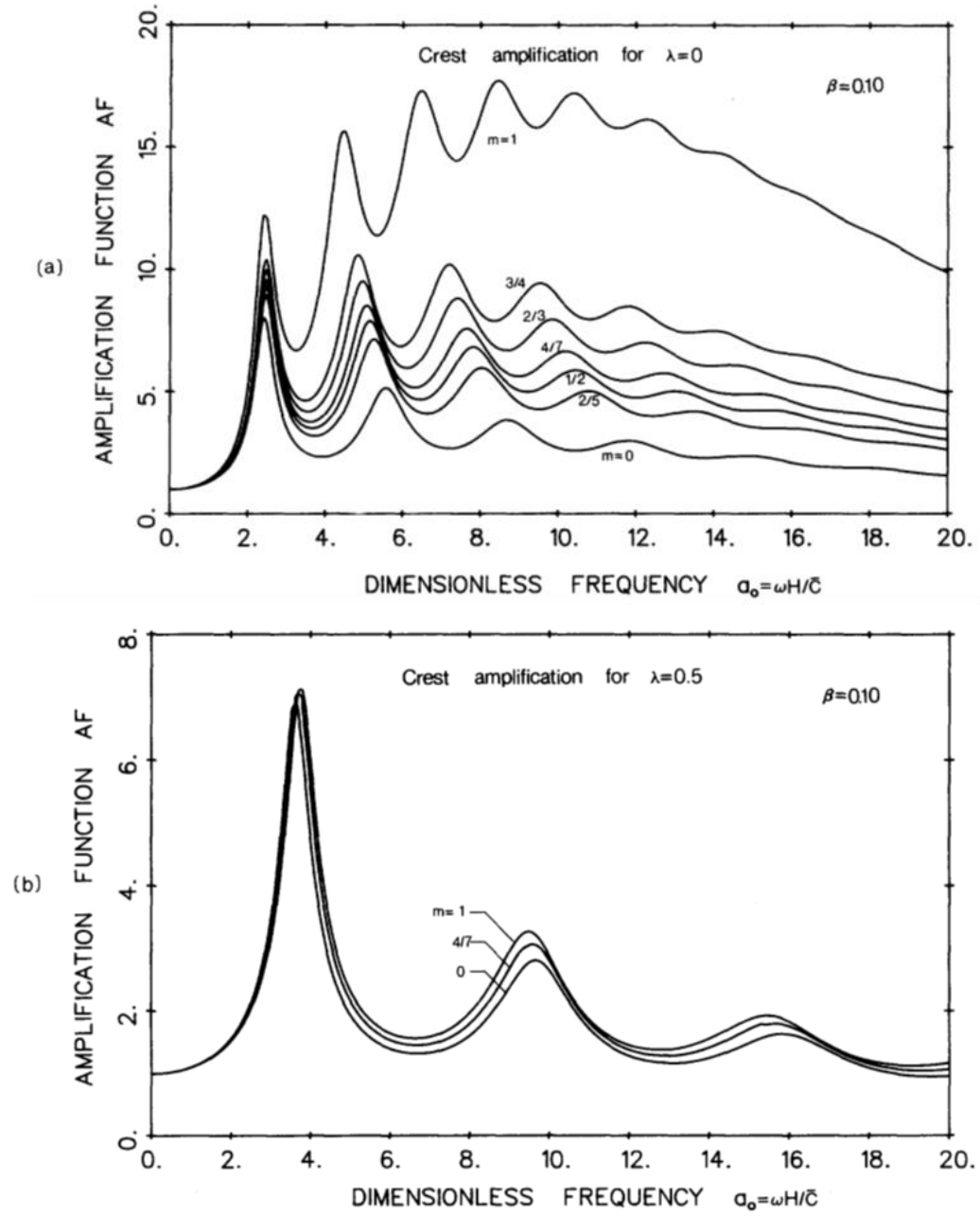

Figure 2.49: Effect of inhomogeneity on amplification functions of the inhomogeneous and homogeneous dams for: (upper) λ=0 and (bottom) λ=0.50 (Dakoulas & Gazetas, 1985)

The effect of inhomogeneity on profile of maximum acceleration with depth is discussed by Gazetas (1987) and illustrated in Figure 2.50; in this figure the effect of nonlinearity is also investigated. It can be observed that peak acceleration in inhomogeneous dams is particularly pronounced close to the crest of the dam, but this effect diminishes as soil nonlinearity increases.

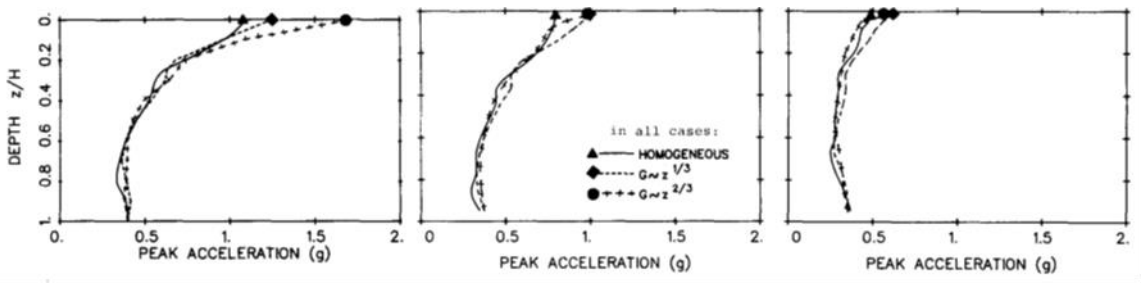

Figure 2.50: Effect of inhomogeneity on the profile of maximum horizontal acceleration: linear elastic analysis (left), moderately nonlinear analysis (centre), strongly nonlinear analysis (right) (Gazetas, 1987)

In conclusion, based on the discussed results from literature review, it appears that the degree of inhomogeneity, expressed by the parameter m, has significant effects on modal shapes, magnitude of amplification function, especially in correspondence of the fundamental frequency, and profile of maximum horizontal acceleration with depth but this effect reduce with increasing truncation ratio and nonlinearity. However, the effect on the values of the natural periods of the dam is negligible.

2.4.2.2 3D effects due to canyon geometry

The assumption of plane-strain conditions, which is the basis for the 2D analyses, is strictly valid only for infinitely long dams subjected to a synchronous base excitation (that is identical motion of all points along the base). However, it has been observed (Gazetas, 1987; Gazetas and Dakoulas, 1992) that dams built in narrow canyons exhibit a stiffer response compared to dams in wide canyons. This geometric constraint creates a 3D stiffening effect, which results in an increase of natural frequencies (smaller natural periods) and sharpness of modal displacement shapes as the canyon becomes narrower (Gazetas, 1987).

There are several factors that influence the fundamental period of a dam T1, that is its height H, the average value and spatial distribution of shear modulus, the inclination of the two sloping faces, the stiffness characteristics of the foundation soils, and the geometry of the canyon. This latter is expressed in terms of the canyon shape and its aspect ratio L/H (length over height) as illustrated in Figure 2.51.

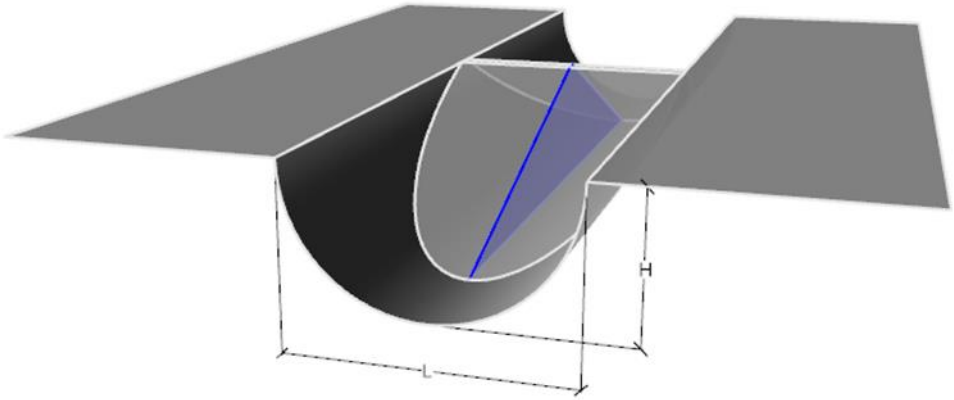

Figure 2.51: Dam in a narrow canyon, where L and H are length and height respectively.

In Figure 2.52 the increase of T1 with increasing L/H ratio is shown for five idealized canyon shapes: rectangular, wide-trapezoidal, semicylindrical, narrow-trapezoidal, and triangular; the period T1 is normalized with respect to the natural period of an infinitely long dam ($T_{1,\infty}$). These results are based on both SB and finite element analyses (Dakoulas and Gazetas, 1987), refer essentially to linear analyses and are applicable to both homogeneous and inhomogeneous dams. The scatter, shown only for the triangular and rectangular shapes, is related to the range of surface slopes (1:1.5 to 1:1.3) used as well as the differences in the methods of analyses. It can be observed that the fundamental period of a dam in a narrow canyon can reduce to a fifth of the corresponding dam in a wide canyon for triangular dams with small ratio H/L. This phenomenon is known in the literature as stiffening effect. However, the canyon effects decrease as the L/H increase. For higher natural periods Tn ($n \geq 2$) results are available only for semicylindrical and rectangular shapes and suggest that the ratio $T_n/T_{n,\infty}$ is essentially independent on the canyon shape.

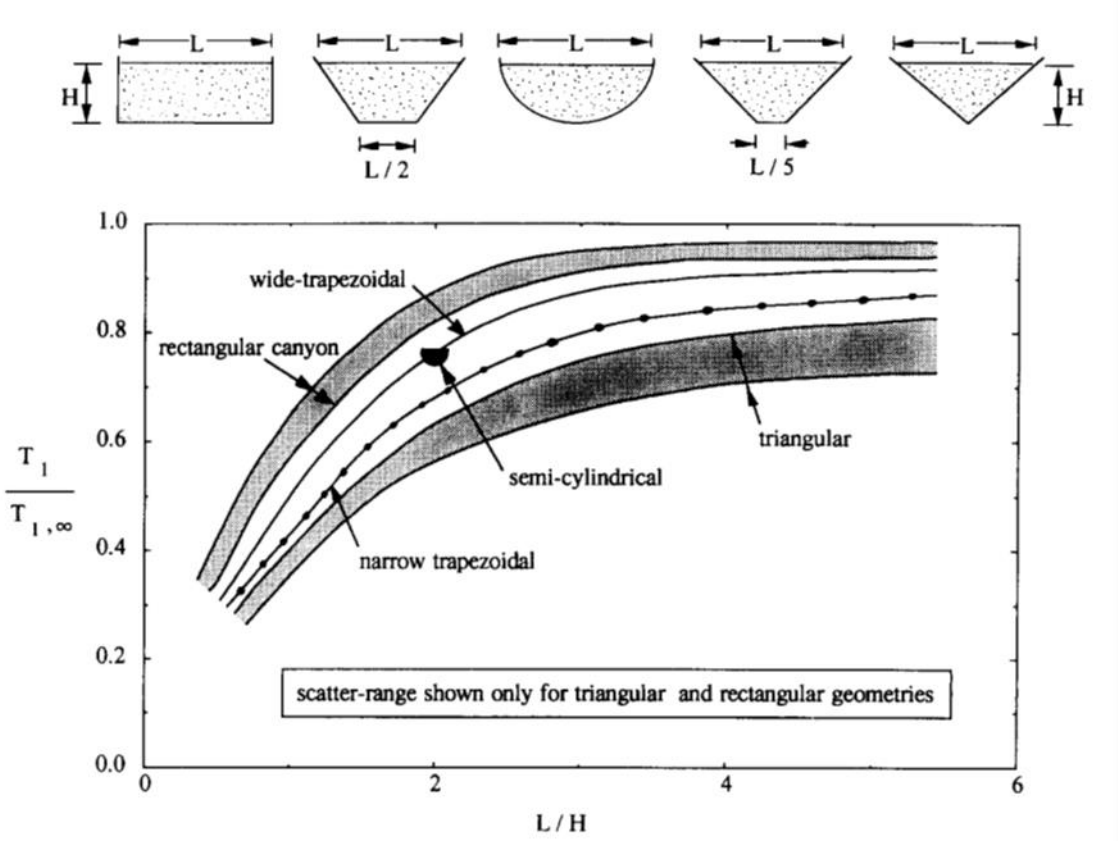

Figure 2.52: Effect of canyon geometry on the fundamental natural period T1 of a dam (Gazetas and Dakoulas, 1985).

2.4.2.3 The effect of canyon shape

In order to study the effect of canyon shape, 2D plane strain condition are compared with 3D semi-cylindrical, rectangular and trapezoidal canyons with the same shape ratio L/H = 2 (Figure 2.53); for semi-cylindrical and rectangular canyons, the closed-form solutions are provided by Dakoulas and Gazetas (1986) and Dakoulas and Hashmi, (1991), respectively. The comparison is caried out in terms of rigid-rock amplification functions AF (Figure 2.54), defined as the ratio of the absolute mid-crest acceleration over the base acceleration, as a function of the frequency factor a0=ωH/Vs, where Vs is the shear wave velocity of the dam; a constant value of internal soil damping D=10% is assumed. It can be observed a change in the fundamental frequency of the dam, which increases as compared to 2D conditions, even if the magnitude of amplification function is essentially independent on the canyon shape. The most striking difference between 2D and 3D results concern the higher modes of vibrations, which for rectangular and semi-cylindrical canyons are significantly higher for 3D modelling. Therefore, 2D plane strain analyses would underpredict the amplification at the fundamental frequency and the amplification at higher resonances.

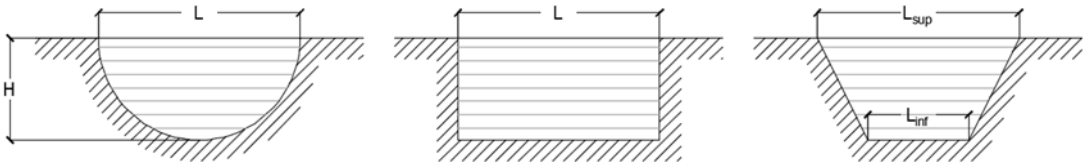

Figure 2.53: Simplified shape of canyons with the same shape ratio (L/H = 2), from left to right semi-cylindrical, rectangular and trapezoidal.

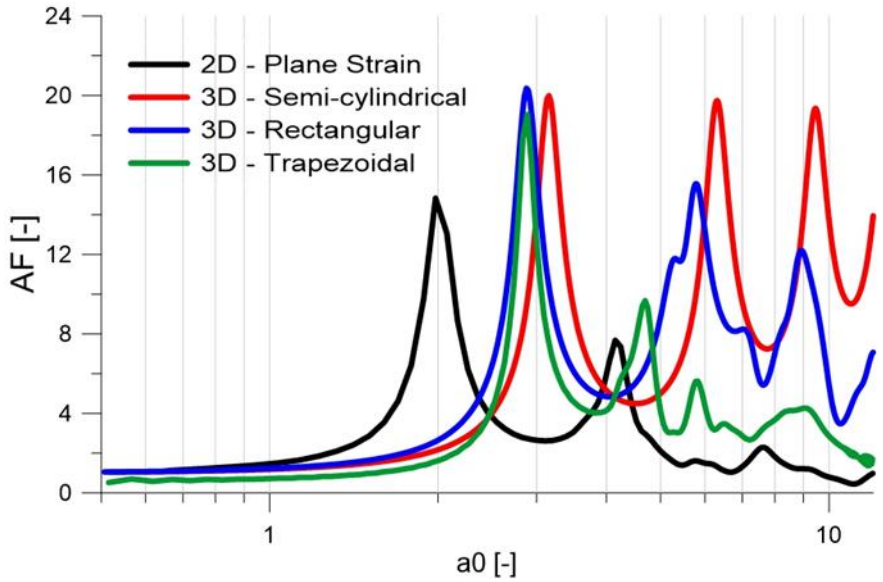

Figure 2.54: Comparison between 2D plane strain and 3D canyons of simplified shapes in term of amplification functions.

In Figure 2.55 are shown the comparisons for the first four displacements modal shapes, normalized to a unit amplitude at the base. Shown are the distributions along the crest (z=0) and along the depth from middle-crest (x=0), for semi-cylindrical (red line) and rectangular (blue line) canyon. The first mode is essentially independent on the canyon-shape for both horizontal and vertical distributions. Notice further that cylindrical canyon leads to a sharper attenuation of displacements with depth from the crest and along the surface.

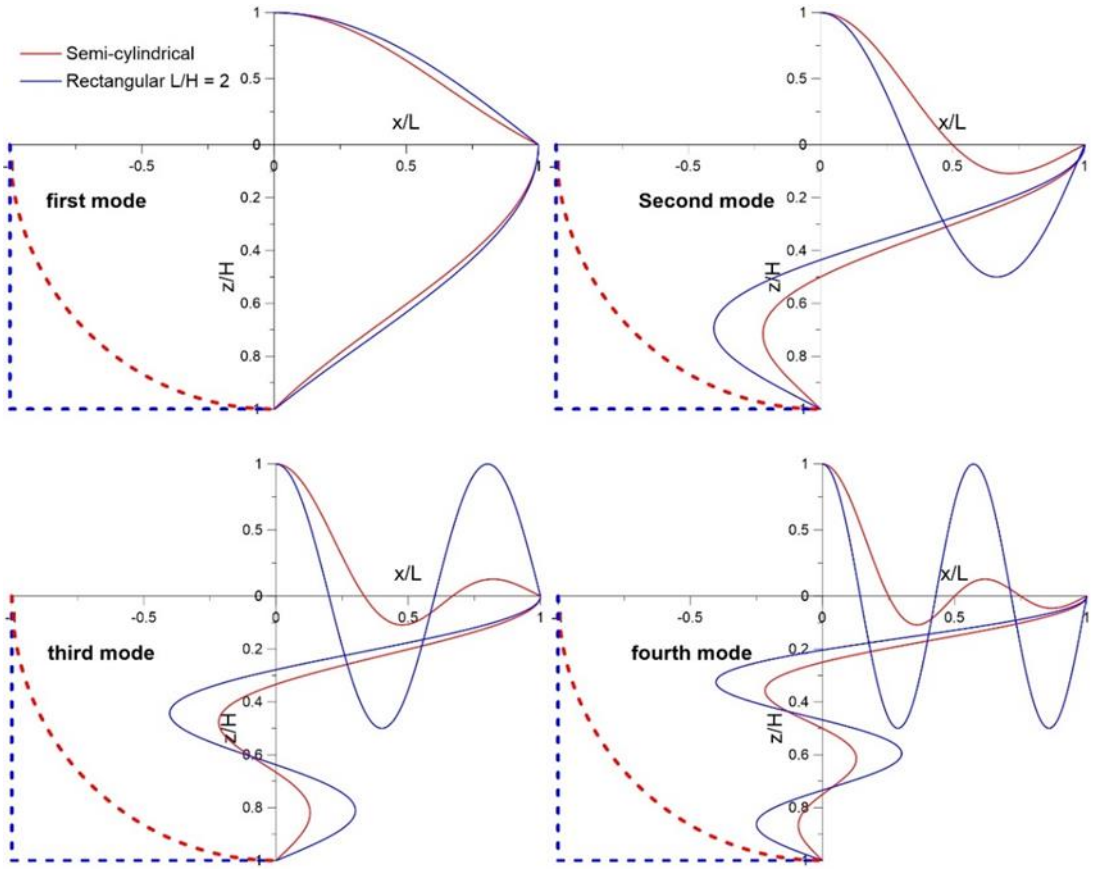

Figure 2.55: First four displacement modal shapes for a semi-cylindrical and a rectangular canyon with L/H=2 (Dakoulas & Gazetas, 1986).

Dakoulas and Hsu (1995) presented a closed-form analytical solution for the dynamic response of earth dams embedded in semi-elliptical canyon. This canyon shape (Figure 2.56) offers more flexibility in better approximating the geometry of several actual canyons. The results can be compared with those of the closed-form solutions of rectangular canyon with the same shape-ratio L/H, obtained by Dakoulas and Hashmi (1991) and plane-strain conditions. These comparisons are plotted in Figure 2.57 in terms of rigid-rock amplification functions AF, defined as the ratio of the absolute mid-crest acceleration over the base acceleration, versus frequency factor a0=ωH/Vs; again, a constant value of internal soil damping D=10% is assumed and two values of shape ratio L/H are considered, L/H=3 and L/H=5. It can be noted substantial amplification for L/H=3 as compared to the rectangular canyon, which is probably due to the difference in the narrowness of the two canyon shapes, with the semi-elliptical canyon being "narrower" than the rectangular one (Dakoulas and Hsu, 1995). For L/H=5, however, the mid-crest amplification for both dams tends to become comparable to the 2D amplification.

Figure 2.58 and Figure 2.59 show transversal (z axis) modal shapes assuming L/H=3 and L/H=5, respectively, and plane strain conditions (2D). Figure 2.60 and Figure 2.61 the longitudinal (x axis) modal shapes for the first fourth mode are plotted. There are no appreciable differences for transversal mode shapes between 3D and 2D conditions; however significant differences can be observed for longitudinal ones.

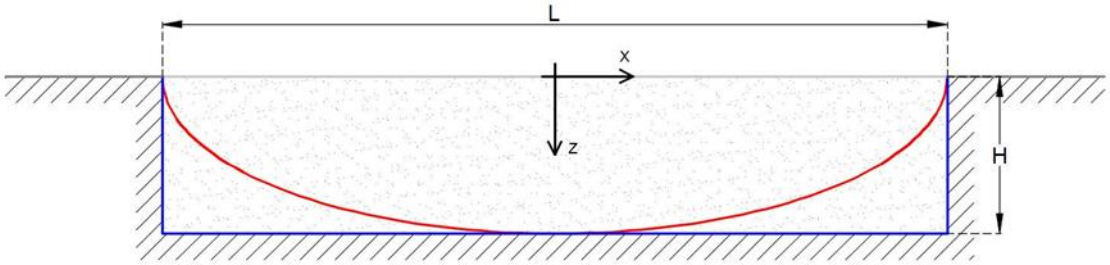

Figure 2.56: Semi-elliptical canyon (red line) and rectangular one with same shape ratio L/H.

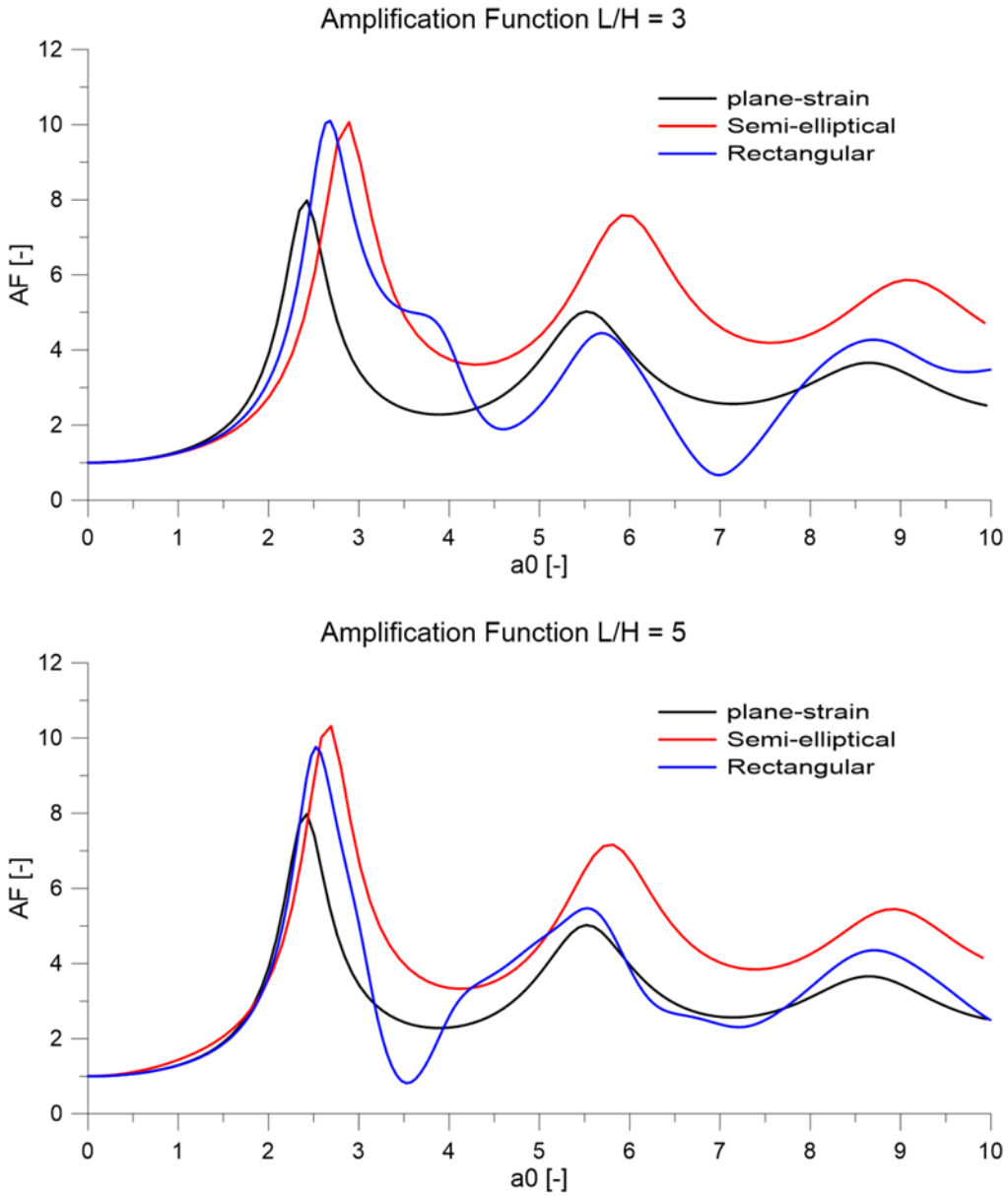

Figure 2.57: Comparison between transfer functions for plane strain conditions (black lines), semi-elliptical (red lines) and rectangular (blue lines) canyons for shape ratio L/H = 3 (upper plot) and L/H = 5 (bottom plot).

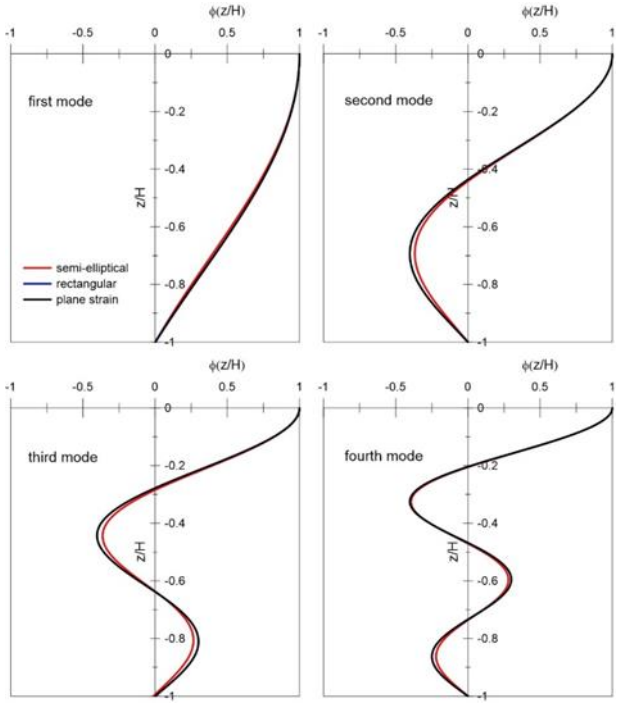

Figure 2.58: Comparison between displacement transversal modal shape for semi-elliptical (red line), rectangular (blue line) shape canyon with L/H = 3 and plane strain conditions (black line)

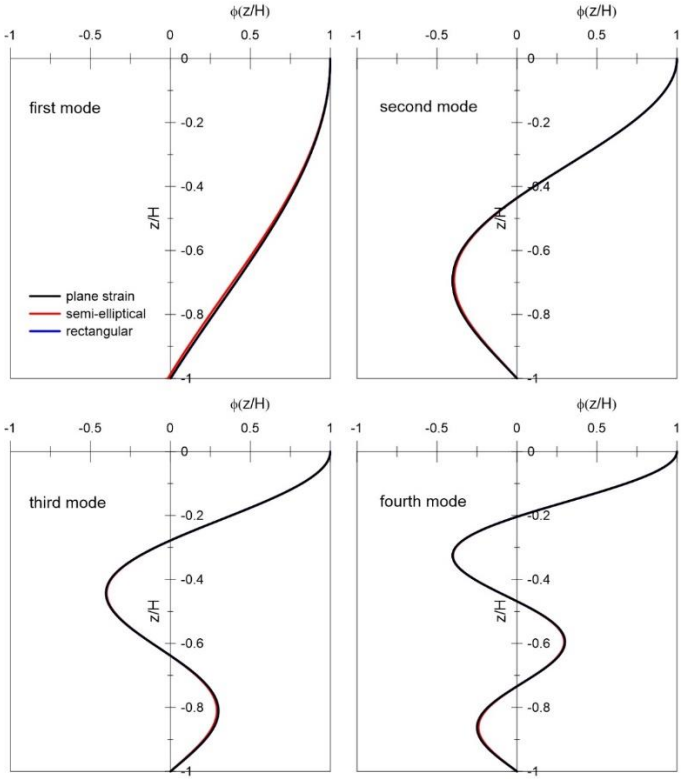

Figure 2.59: Comparison between displacement transversal modal shape for semi-elliptical (red line), rectangular (blue line) shape canyon with L/H = 5 and plane strain conditions (black line)

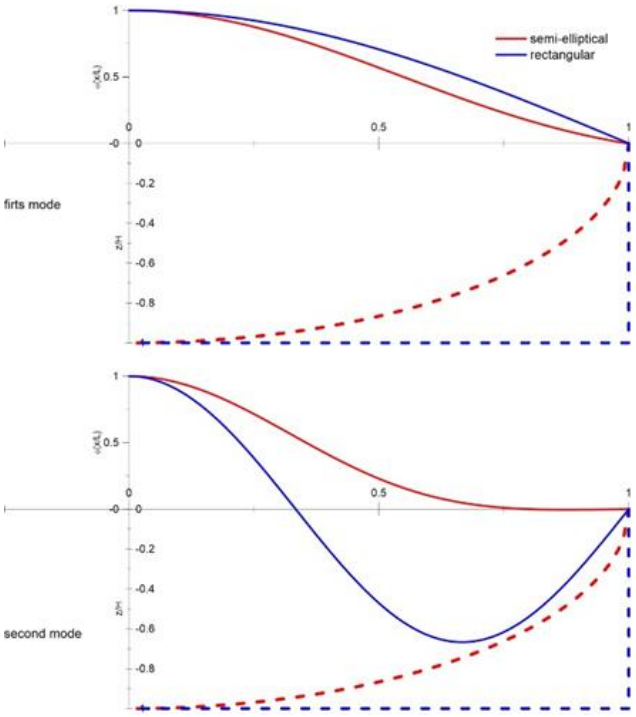

Figure 2.60: Comparison between first (upper) and second (bottom) longitudinal modal shape for semi-elliptical (red line) and rectangular (blue line) shape canyon with L/H = 5 (dashed lines represent the shape of canyon)

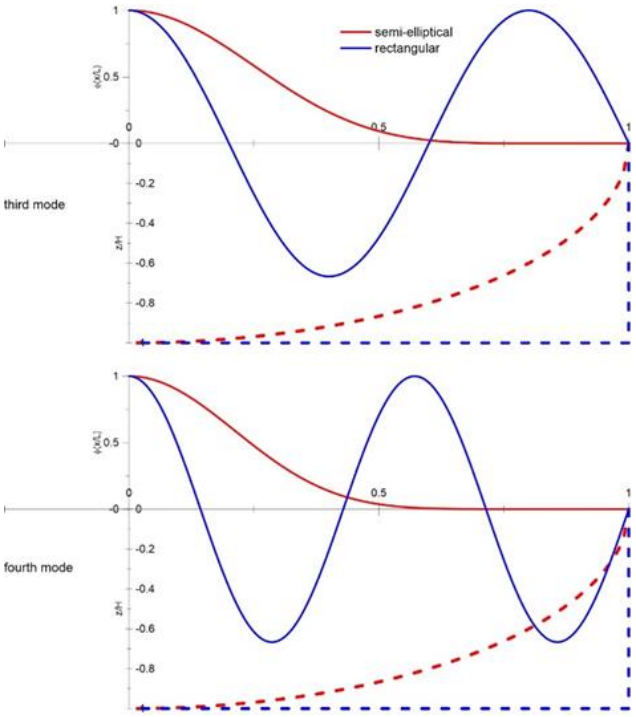

Figure 2.61: Comparison between third (above) and fourth (below) longitudinal modal shape for semi-elliptical (red line) and rectangular (blue line) shape canyon with L/H = 5 (dashed lines represent the shape of canyon)

2.4.2.4 The effect of impedance ratio

To account for the amount of wave energy radiated back into the half-space (canyon), the amplification function referring to deformable (elastic) bedrock can be determined as a function of impedance ratio IR. This amplification function is defined as the ratio of the absolute mid-crest acceleration to the free-field, rock-outcrop acceleration. Closed-form expressions are available for the semi-cylindrical and plane-strain case. Figure 2.62 shows the comparison in term of amplification functions both for 3D and 2D conditions for various IR (2,5, 15, ∞); soil damping is D=10%. The results indicate consistently a drastic effect of the impedance ratio on the response, which results in the highest amplification of acceleration for the rigid canyon (IR=∞) (Dakoulas, 1993).

In Figure 2.63 the amplitude at fundamental resonance of semi-cylindrical 3D dam is plotted as a function of the impedance ratio IR; for comparison the amplitude of fundamental resonance for the plane strain condition is also plotted. This plot clearly demonstrate that the simplifying assumption of a rigid base may be overly conservative.

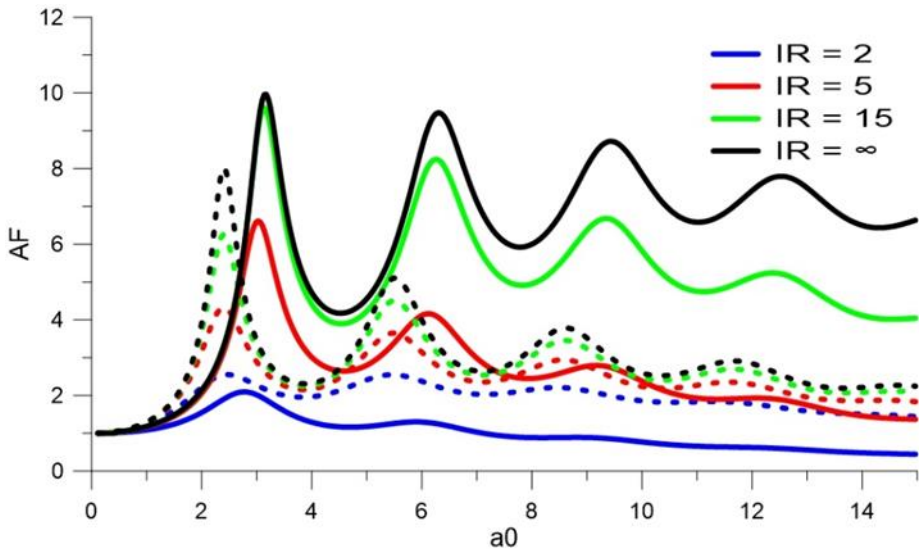

Figure 2.62: Comparison between 3D (solid lines) and 2D (dashed lines) the impedance ratio.

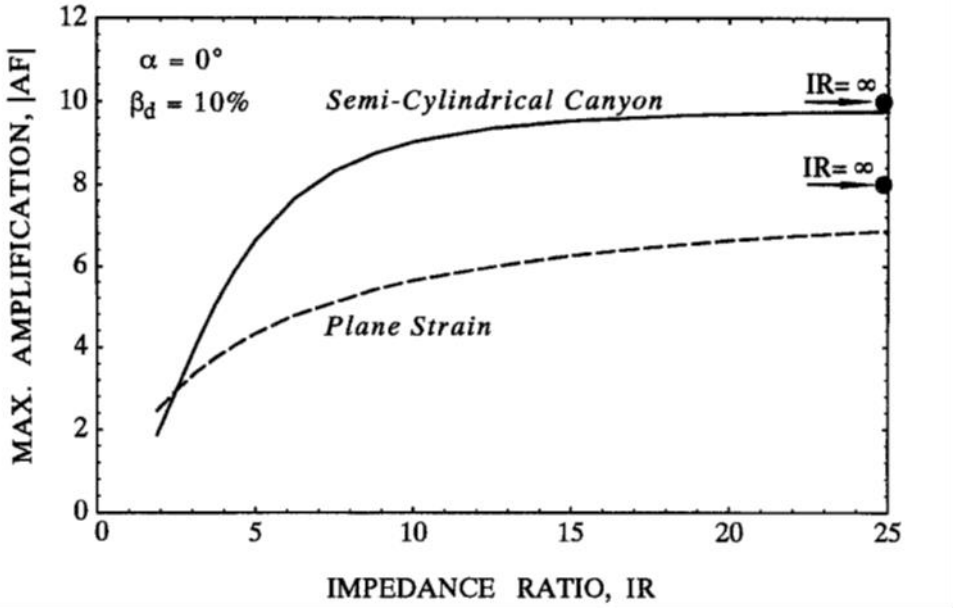

Figure 2.63: Mid-crest amplification at the fundamental resonance as a function of impedance ratio for plane strain condition and semi-cylindrical canyon shape (Dakoulas, 1993)

2.4.2.5 The effect of angle of incidence of seismic waves

For near-field conditions, the usual assumption of vertical propagation of seismic waves is not strictly valid. Dakoulas and Hashimi (1991) showed that the angle of incidence of seismic waves has a significant effect on the amplification. For a dam of height H = 120 m, shear wave velocity Vs,dam=350 m/s and impedance ratio IR=5, in Figure 2.64 the amplification function for semi-cylindrical dam is plotted. Figure 2.65 shows the effect of incidence angle α in terms of maximum amplification along the crest of the dam ($-1 \leq x/H \leq 1$) and along the surface of half-space versus a dimensionless distance x/H, for different dimensionless frequency $a0 = \omega H/Vs$ and four different angles of incidence (α=0, 30°, 60° and 90°). The response of the dam corresponds to $-1 < x/H < 1$, while the response of the half-space surface to $x/H < -1$ and $x/H > 1$. The results show that for a0 = 3.09 and a0=1.5, corresponding to the first natural frequency and the minimum of amplification function, respectively, the amplitude at surface is essentially independent on the incidence angle. For a0=6.13 and a0=4.58, corresponding to the second natural frequency and the minimum value between the first and second natural frequency, respectively, the amplitude increases as α increases. Note that the amplification at mid-crest (x/H = 0) is independent on the angle of incidence α.

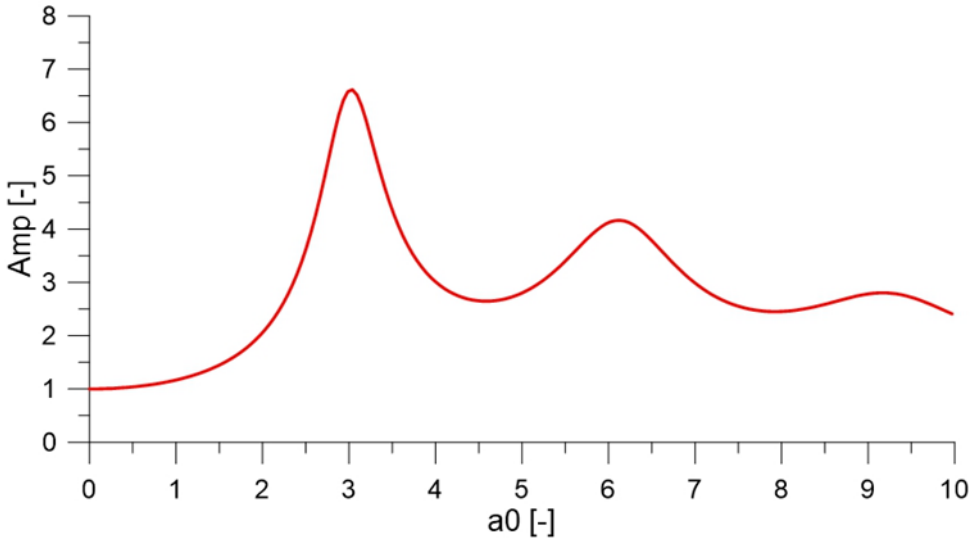

Figure 2.64: Amplification function of semi-cylindrical dam at mid crest.

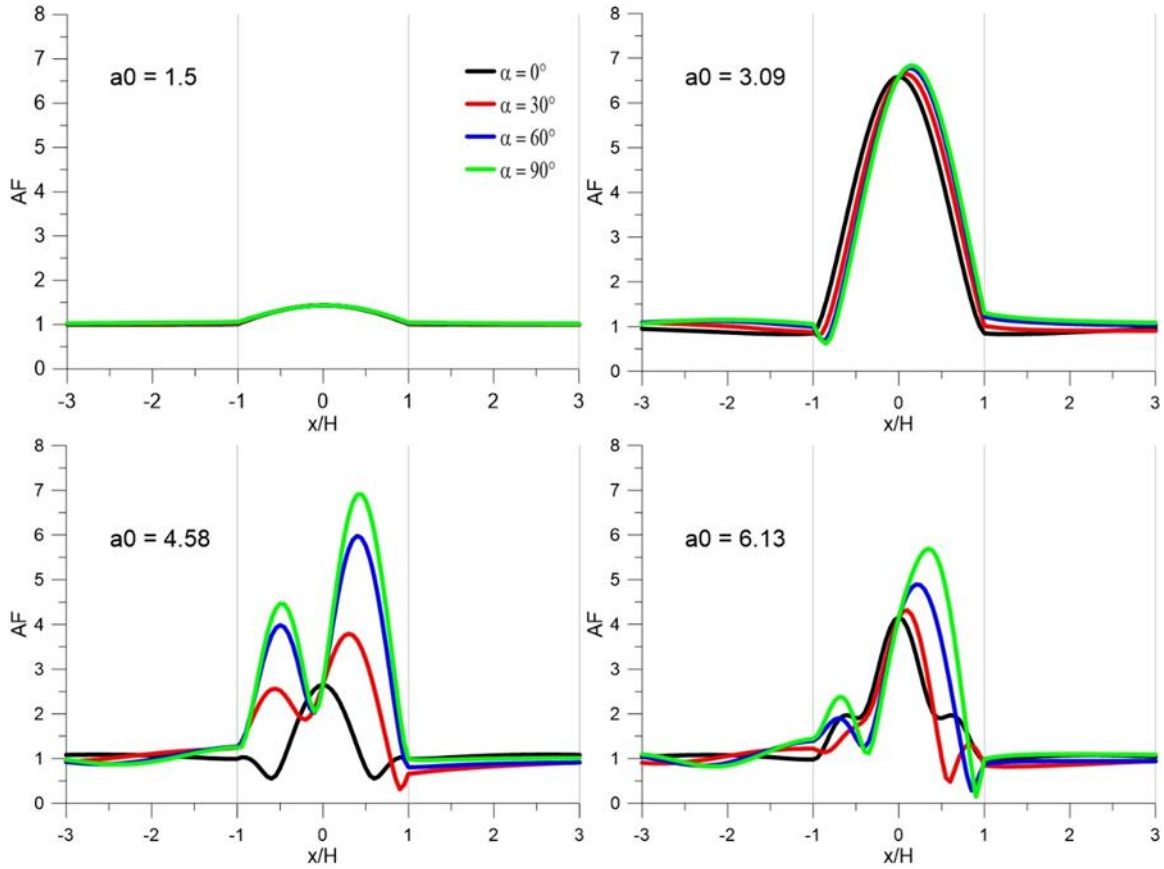

Figure 2.65: Amplification function along the crest of dam and along the surface of half-space for different values of dimensionless frequency a0 and four angles of incidence for semi-cylindrical dam (Dakoulas, 1993).

2.4.2.6 The effect of foundation alluvial layer

Many existing dams have been constructed on alluvial deposits typically overlying the base of the canyons. The presence of a foundation layer can have a significant effect on the natural period of the dam. The interaction between the dam and its foundation layer is called dam-foundation interaction. Analytical closed-form solutions are available allowing to quantify the effect of a deformable foundation layer on dams in narrow canyons (Figure 2.66) in terms of natural periods and modal shapes of the system dam-foundation layer. It is worth mentioning the studies carried out for rectangular (Dakoulas and Gazetas, 1987; Dakoulas, 1990), semi-cylindrical (Dakoulas, 1993a, b) and semi-elliptical (Dakoulas, 1993, 1995) canyons.

A comprehensive study was carried out by Dakoulas (1990) who studied the effect of the presence of an alluvial layer on the natural period of a dam for the case of rectangular rigid canyon. According to Figure 2.67, the system studied consist of a triangular dam with shear wave velocity, Vs,dam, thickness, Hdam and inhomogeneity parameter m; the foundation layer is characterized by Vs,layer and Hlayer, and lies on top of the canyon of width L. The Author shows that the behaviour of the system dam-foundation layer depends on: i) velocity ratio c= VS,dam/VS,layer; ii) thickness ratio t = Hdam/Hlayer; iii) shape ratio L/Hdam; iv) inhomogeneity parameter m in the dam.

In Figure 2.68 the results are plotted in terms of ratio of the period $\tilde{T}11$ of the dam-foundation layer system over the period of the dam founded directly on rock, T11, as a function of the thickness ratio, t. Three values of the velocity ratio c=Vs,dam/Vs,layer, were considered (c = 0.5, 1.0 and 1.5), and five different values of the shape ratio L/H (L/H=2,3 5, 10 and ∞); the inhomogeneity parameter m was assumed equal to 0.5. It can be observed that the fundamental period of the dam-foundation layer system increases as the height of the foundation layer increases, in comparison with the height of the dam. This effect is more significant as the velocity ratio c increases (that is for softer alluvial soils, as compared to the stiffness of the dam) and for longer dam (L/Hlayer increases).

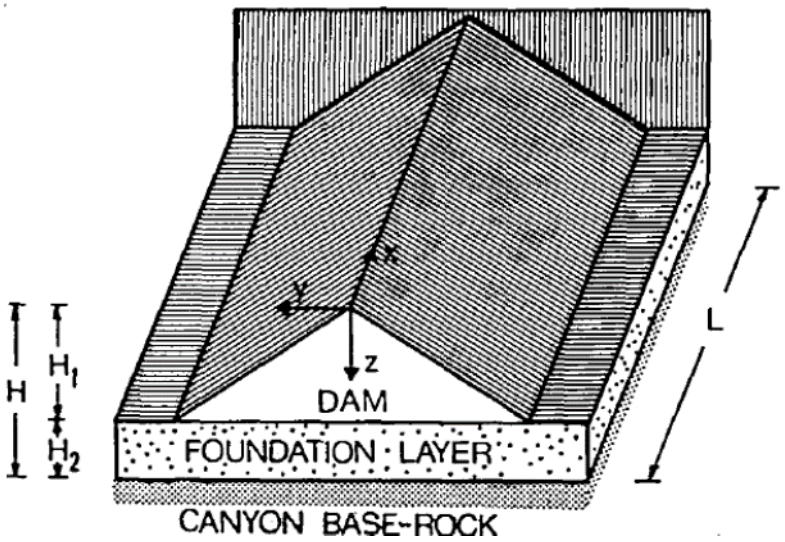

Figure 2.66: Dam and foundation layer in a rectangular canyon (Dakoulas, 1990)

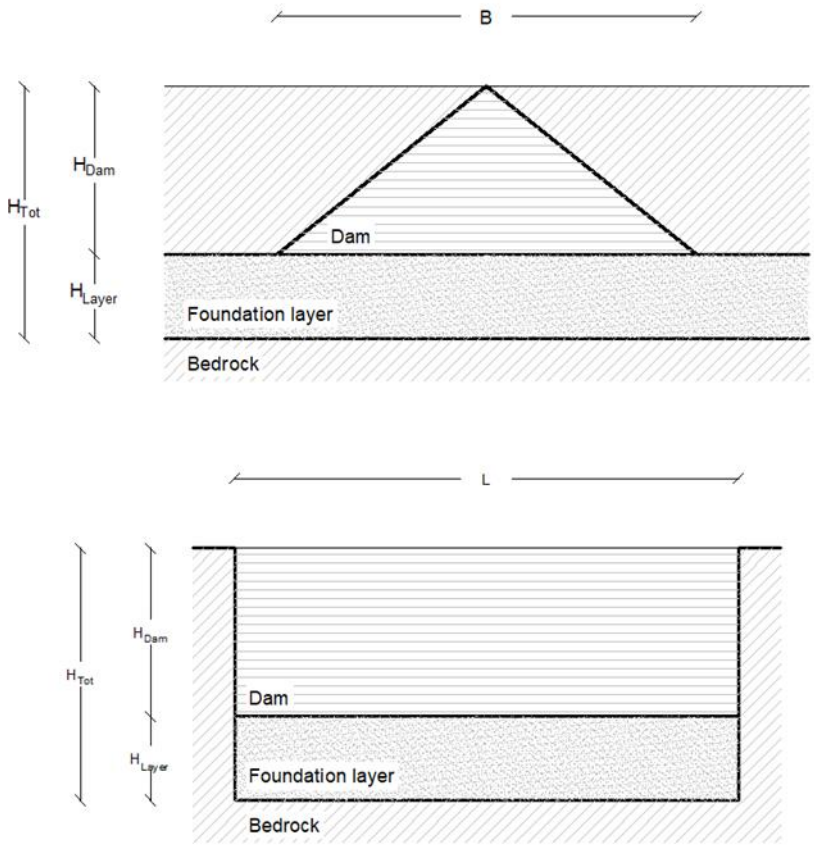

Figure 2.67: Dam and foundation layer in rectangular rigid canyon (Dakoulas, 1990)

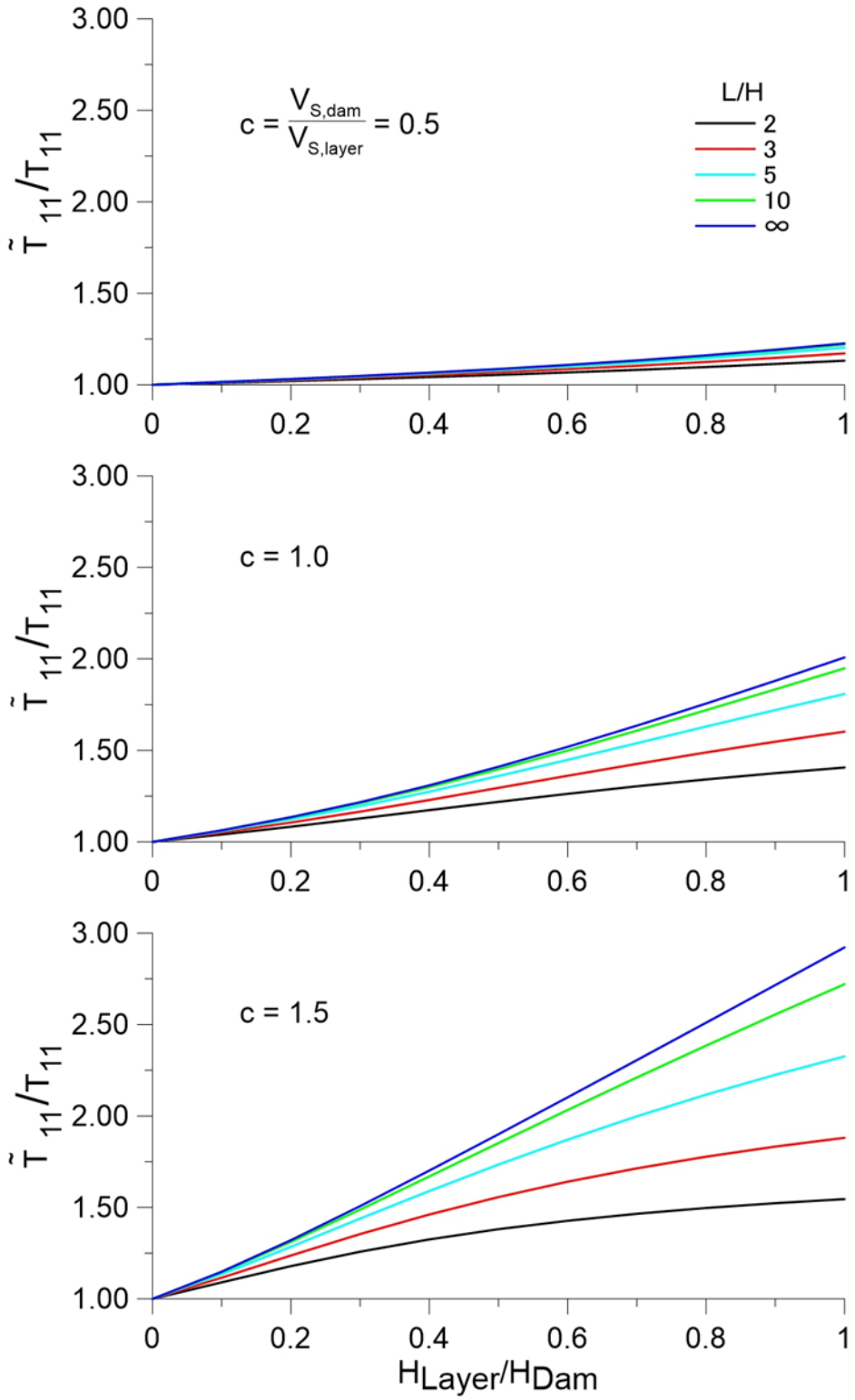

Figure 2.68: Effect of the foundation layer thickness HLayer and canyon width L on the fundamental period $\tilde{T}_{11}$ of the dam for three velocity ratios, VS,dam/VS,layer. T11 is the fundamental period of a dam in a rectangular canyon with no underlying layer (Dakoulas 1990)

2.4.3 Numerical methods

As already mentioned, the theoretical studies discussed in the preceding section are particularly useful because the closed-form solutions available allow to obtain indications on the main parameters affecting the dynamic response of earth dams, even if simplified assumptions regarding geometries involved, material properties and input motion are considered. Generally, a more thorough analysis of the seismic response of earth dams can be obtained using numerical techniques, which is widely used in current engineering practice. Issues such as complex geological and morphological conditions (e.g., asymmetrical shape of the valley), soil nonlinearity, development of pore pressures during seismic shaking, 3D conditions especially for dams built in narrow canyons, the use of real earthquake records, can be more easily simulated and investigated. In the following, some numerical studies will be reviewed from literature, with special attention to the comparison between the results of 3D and 2D numerical analyses for earth dams embedded in narrow canyons.

Early numerical methods taking into account the effect of canyon shape were developed by several researchers (e.g., Martinez and Bielak, 1980; Makdisi et al., 1982; Ohmachi, 1981). These studies confirm the importance of canyon geometry on the natural frequencies and displacement mode shapes. Narrow canyons have restraining effects on vibration motion of earth dams and this is reflected in natural frequencies increase (or natural period decrease), thus leading to the stiffening effect, as compared to those for 2D dams. Makdisi et al. (1982) performed comparison between the results obtained with 2D and 3D models of dams in triangular canyons. They reported considerable differences between acceleration and stresses between 2D and 3D results, even if the coarse degree of discretization of the finite element mesh used limits in some way the reliability of the results.

Mejia and Seed (1983) compared the results of 2D and 3D dynamic response of earth dams in triangular and rectangular canyons by means of finite element analyses. They confirm the stiffening effect, as shown in Figure 2.69 where the ratio of 3D to 2D fundamental natural frequency of the dam increases as the L/H ratio decreases. A value of 2.5 can be obtained for triangular dams, which means that the fundamental period of a 2D dam can be ¼ of the period of 2D dam. As the ratio L/H increases, the ratio f3D/f2D decreases, so that at a value of L/H=6 its magnitude is about 1.3. In the figure is also shown the ratio f3D/f2D for dams in rectangular and triangular canyons reported by Ambraseys (1960) and Makdisi et al. (1982) as well as the ratio computed from the shear wedge solution in triangular canyons. The computed results were

also compared in terms shear stress and accelerations. Acceleration were found to be more sensitive to the boundary conditions and therefore less accurately computed form a 2D analysis.

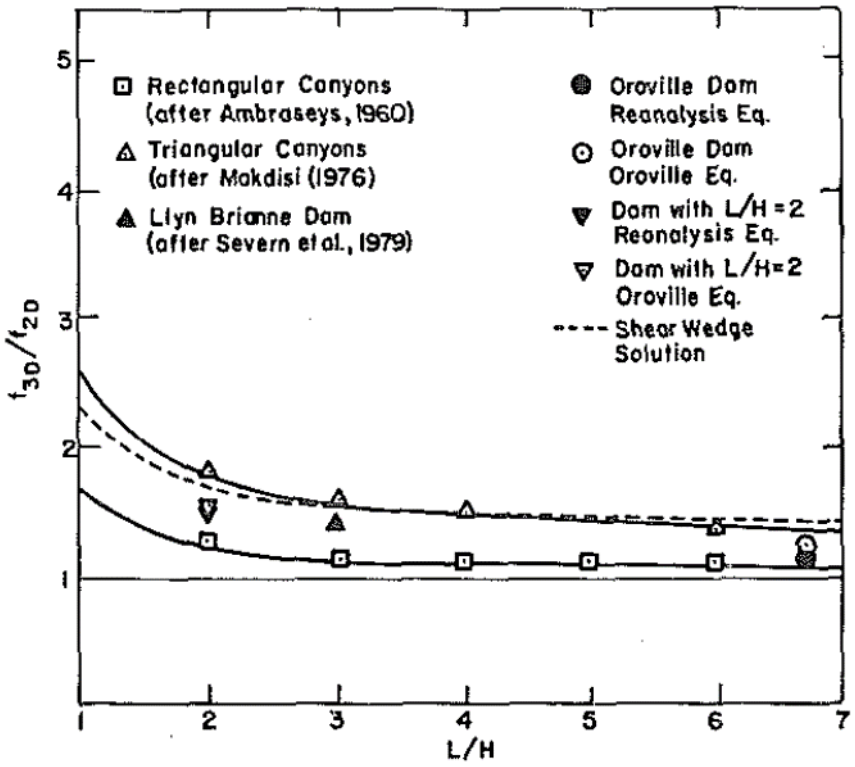

Figure 2.69: Comparison between natural frequencies computed from 2D and 3D analyses of dams in triangular and rectangular canyons (Mejia and Seed, 1983)

3D dynamic analyses of earth dams have been available in the last decades (e.g., Griffiths and Prevost, 1988; Roth et al., 2004; Meja and Dawson, 2010). Generally, in agreement with previous indications, the 3D behaviour can result in significantly larger accelerations at the dam crest than might otherwise be expected based on 2-D analysis procedures. This is especially true for narrow and asymmetrical shapes of valleys. Thus, for such types of dams, 3-D analysis procedures may be required to adequately evaluate their acceleration response and potential for seismic deformations. However, additional case histories are needed to assess whether such procedures are capable of simulating the seismic response of dams in narrow canyons, and to further evaluating the capability of 2D numerical procedures in determining the dynamic response of dams.

3 The finite difference code FLAC3D

In this research study, 2D and 3D finite difference analyses were carried out to investigate the seismic response of natural reliefs and earth dams, using the finite difference computer code FLAC3D Version 7.0 (ITASCA, 2017). In the following, an overview on the software FLAC will be given first in which the basic concepts are summarized. Then, a closer look will be taken on the required procedures for the dynamic analysis related to the assessment of site effects. Finally, the calibration of the code with some closed-form solutions for simple sediment-filled valley and, especially, for earth dams are presented.

3.1 Overview of the code

In the finite difference FLAC3D code, the domain of interest can be discretized by a grid (or mesh) constituted by elements. An element consisting of a tetrahedron whose vertices there are four nodes is illustrated in Figure 3.1. Each element can have its particular properties and behaves according to assigned constitutive laws when subjected to forces and boundary conditions. The discretization of the mesh results in a finite number of grid points (or nodes) that define zones to which stresses and strains apply. The principle on which the code is based, is to regenerate the finite difference equations relative to the grid points with each computation cycle (or step), as illustrated in Figure 3.2. For the first cycle the code makes use of the initial equilibrium equation and stress/strain-state to calculate velocities and displacements for all grid points. These velocities are then used by the constitutive equations to obtain strain rates and stresses. In return, these latter ones are re-used by the equilibrium equation to launch the next cycle. This way of stepwise state calculation, in which the new state is only a function of the previous one, is called explicit.

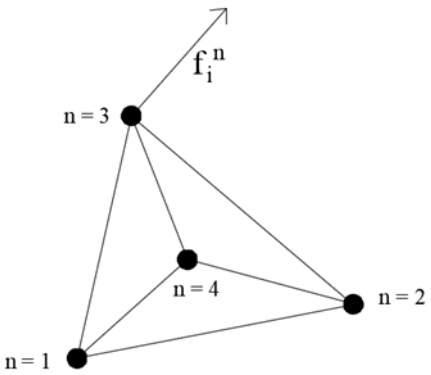

Figure 3.1: Generic tetrahedron of a numerical grid and equivalent nodal force f_i^n

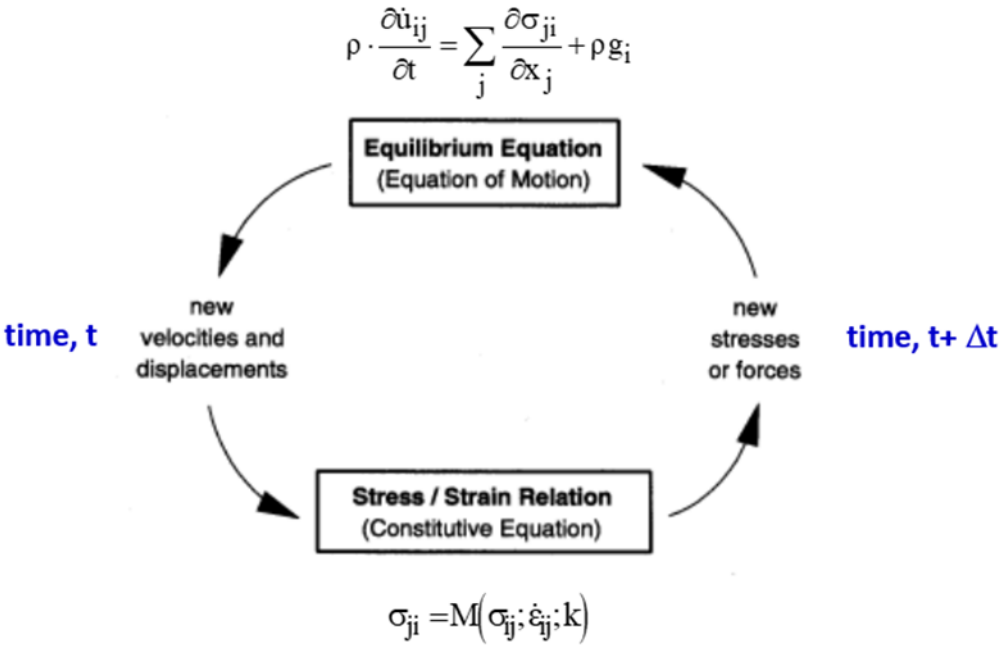

Figure 3.2: One calculation cycle used by the finite difference code FLAC3D

The equivalent nodal force fin applied at node n in local system (hereafter "n" and "l" are the notations in local and global system, respectively), and the subscript i is the component in global system (i = 1,2,3). This force depends on the stress state tensor [T], volumetric force and the inertial contribute and it is expressed as:

$$-f_i^n = \frac{T_i^n}{3} + \frac{\rho b_i V}{4} - m^n \left(\frac{dv_i}{dt}\right)^n \tag{3.1}$$

Applying the 3.2 Newton law and considering all the tetrahedrons that have in common the node n, the global force (called unbalanced force) is expresses as:

$$F_i^{<l>} = M^{<l>} \left(\frac{dv_i}{dt}\right)^{<l>} \tag{3.3.2}$$

where M is the total nodal mass, the symbol <l> indicate the sum of the contributions at global node l of all tetrahedra at that node. Equation 3.2(5) can be expressed as a system of differential equation of this type:

$$\left(\frac{dv_i}{dt}\right)^{<l>} = \frac{1}{M^{<l>}} F_i^{<l>}(t, \{v^{<1>}, v^{<2>}, v^{<3>}, \ldots\ldots, v^{<p>}\}, k) \tag{3.4}$$

In FLAC3D this system of equation is solved numerically by using the explicit finite difference scheme in time domain with a large number of calculation steps. In each calculation step there is a progressive redistribution of unbalanced force caused by changes to stress or displacement boundaries through the mesh. The unbalanced force is the algebraic sum of the net nodal-force vectors for all of the nodes within the mesh. The model is considered to be in equilibrium when the maximum unbalanced force is small compared with the total applied forces within the problem. If the unbalanced force approaches a constant non-zero value, this normally indicates that failure and plastic flow are occurring within the model. By default the model is assumed to be in equilibrium when the maximum unbalanced force ratio (i.e. the ratio between the magnitude of the maximum unbalanced force and the magnitude of the average applied mechanical force within the mesh) falls below 1×10-5 (Itasca, 2006). The mechanical timestep for numerical stability is to impose a unit timestep $\Delta t = 1$ and assume the nodal mass M<l> in equation as variables in static condition.

To account for damping ratio at low levels of deformations, two methods are implemented in FLAC3D: local damping and Rayleigh damping formulation. The first method is frequency-independent and provides a constant value of damping applied in grid points. However, there is some evidence suggesting that, for real earthquakes, local damping underdamps the high frequency components, and may introduce high frequency noise. The Rayleigh damping formulation is frequency-dependent and it is widely used to model internal damping in dynamic analyses due to its convenience of being defined as linear combination of the mass matrix [M] and the stiffness matrix [K] according to the following expression:

$$[C] = \alpha[M] + \beta[K] \tag{3.5}$$

where α and β are the Rayleigh damping coefficients depending by the target damping and the control frequencies. Rayleigh-Damping represents a form of viscous damping. The Rayleigh-Damping function as well as its two components – the mass-proportional part ($\alpha \cdot M$) and the stiffness-proportional part ($\beta \cdot K$) – are shown in Figure 3.3.

FLAC3D implement a single control frequency formulation. A drawback of this formulation is that it results in damping values very variable over frequency, and thus only the very small section around the lowest damping ratio (ξmin) at its associated damping frequency can be considered as constant.

The frequency-dependent Rayleigh damping formulation was used in this work for numerical simulations.

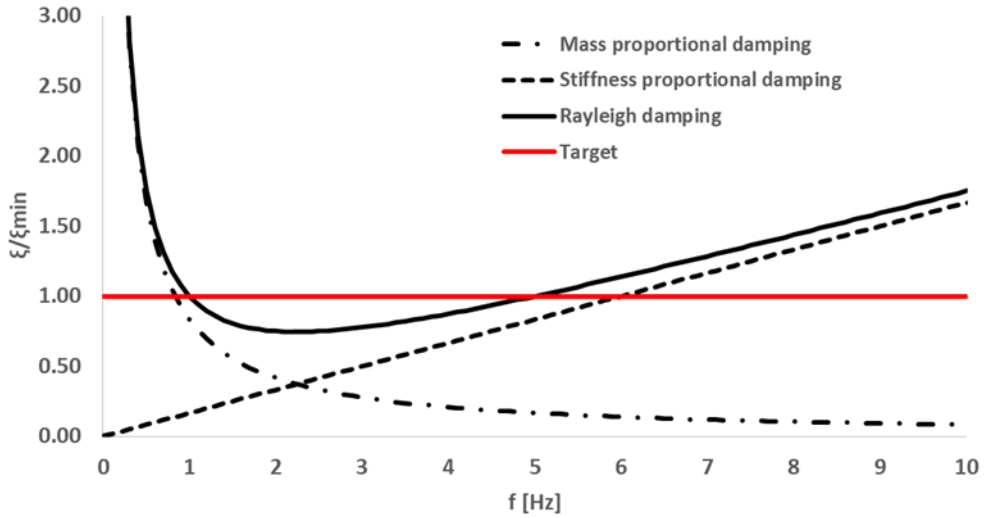

Figure 3.3: Rayleigh damping formulation in solid black line, mass matrix proportional term and stiffness ones in black dashed-point line and dashed line respectively and target damping in red line

Boundary conditions have to be set up for static and dynamic analyses. In static analyses, elementary boundaries (zero displacement) can be realistically placed at some distance from the region of interest. Dynamic analysis requires adequate modelling of the model boundary (both verticals and horizontal base). Such boundary conditions cause reflections of propagating waves back into the model. Energy is thus accumulated in the model what does not correspond to wave propagation patterns in reality. To obtain the necessary radiation of the waves generated in the model, the use of a larger model can minimize the problem, since material damping will absorb most of the energy in the waves reflected from distant boundaries; the alternative is to use quiet (absorbing) boundaries and free field boundaries must be applied in order to ensure energy absorption (Figure 3.4).

The viscous boundary developed by Lysmer and Kuhlemeyer (1969) is used in FLAC3D. It is based on the use of independent dashpots in the normal and shear directions at the model boundaries. The method is almost completely effective at absorbing body waves approaching the boundary at angles of incidence greater than 30°. For lower angles of incidence, or for surface waves, there is still energy absorption, but it is not perfect. For vertical boundaries FLAC3D implement the free-field boundaries condition to ensure the mono-dimensional propagation. The input motion is applied as time history of acceleration, velocity or displacement.

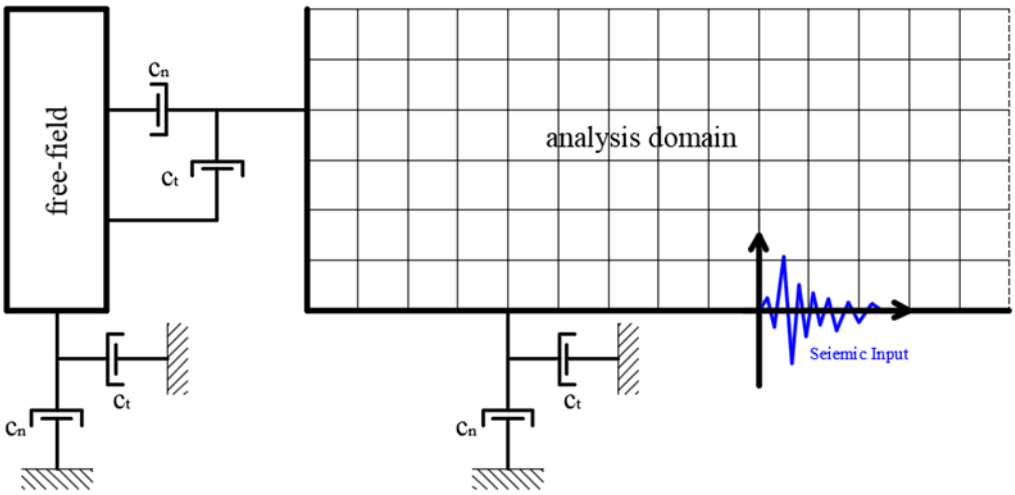

Figure 3.4: Boundary conditions of FLAC3D dynamic analysis

3.2 Comparison between closed-form solutions and FLAC3D numerical results

In this section the comparison between closed-form solutions available in literature for simple surface and subsurface features (as illustrated in chapter 2) and the results of numerical simulations obtained with FLAC3D, was carried out in terms of amplification functions. These comparisons allowed to calibrate the code in terms of boundary conditions implemented in FLAC3D (free-field at vertical sides and quiet-bases at bottom of model) and Raileigh damping formulation with one control frequency. Table 3.1 show the closed-form solutions used for comparisons. All solutions assume vertically incident SH waves. The first one in the table refers to 2D sediment-filled valley whereas the other five cases considered refer to earth dams resting on rigid or deformable bedrock. The earth dams are assumed visco-elastic linear and the solution is based on shear-beam approach. These cases will be detailed in the following paragraphs.

Table 3.1: Closed form solutions used for comparison with FLAC3D numerical results

System	Authors
Semi-cylindrical filled valley on deformable bedrock	Trifunac (1971)
Plane strain homogenous earth dam on rigid bedrock	Dakoulas & Gazetas (1985)
Plane strain in-homogenous earth dam on rigid bedrock	Dakoulas & Gazetas (1985)
Plane strain earth dam on deformable bedrock	Dakoulas (1993)
Semi-cylindrical earth dam on deformable bedrock	Dakoulas (1993)
Rectangular earth dam on rigid bedrock	Dakoulas & Hashimi (1991)

3.2.1 Semi-cylindrical alluvial valley on flexible bedrock (Trifunac, 1971)

The analytical solution is based on wave propagations theory and it is obtained under the assumption of linear elastic soil. Figure 3.5 show the geometry used by Trifunac (1971), with the points taken for comparison between closed-form solutions and numerical results, whereas Figure 3.6 show FLAC3D numerical grid. The linear properties adopted for the sediment-filled material and half-space are shown in Table 3.2. The results are presented in terms of amplification function AF versus the frequency factor a0 (defined as ωh/Vs), in Figure 3.7 for different values of the ratio r/h, where h= radius of the valley and r=cylindrical coordinate. It can be shown that in all cases a very good agreement is found, either in terms of amplitude and frequency of the amplification function.

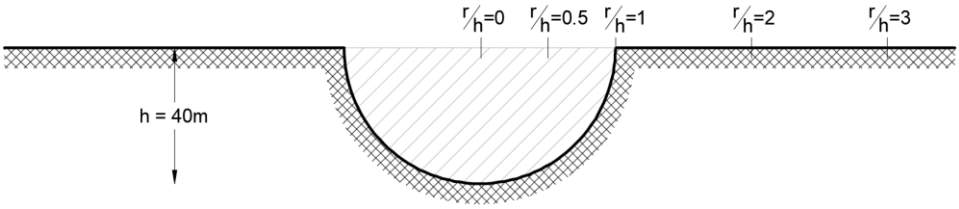

Figure 3.5: Semi-cylindrical sediment-filled valley considered by Trifunac (1971)
h: radius of valley; r: cylindrical coordinate.

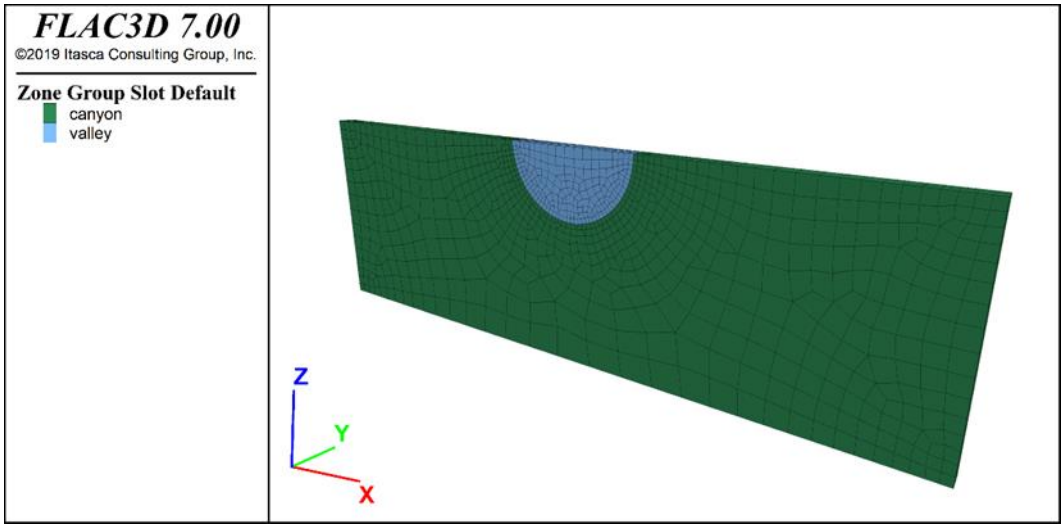

Figure 3.6: FLAC3D numerical grid for semi-cylindrical sediment-filled valley.

Table 3.2: Linear properties adopted for semi-cylindrical filled valley

Material	γ	Vs	ν
[-]	[kg/m3]	[m/s]	[-]
valley	1800	300	0.33
half-space	2700	900	0.33

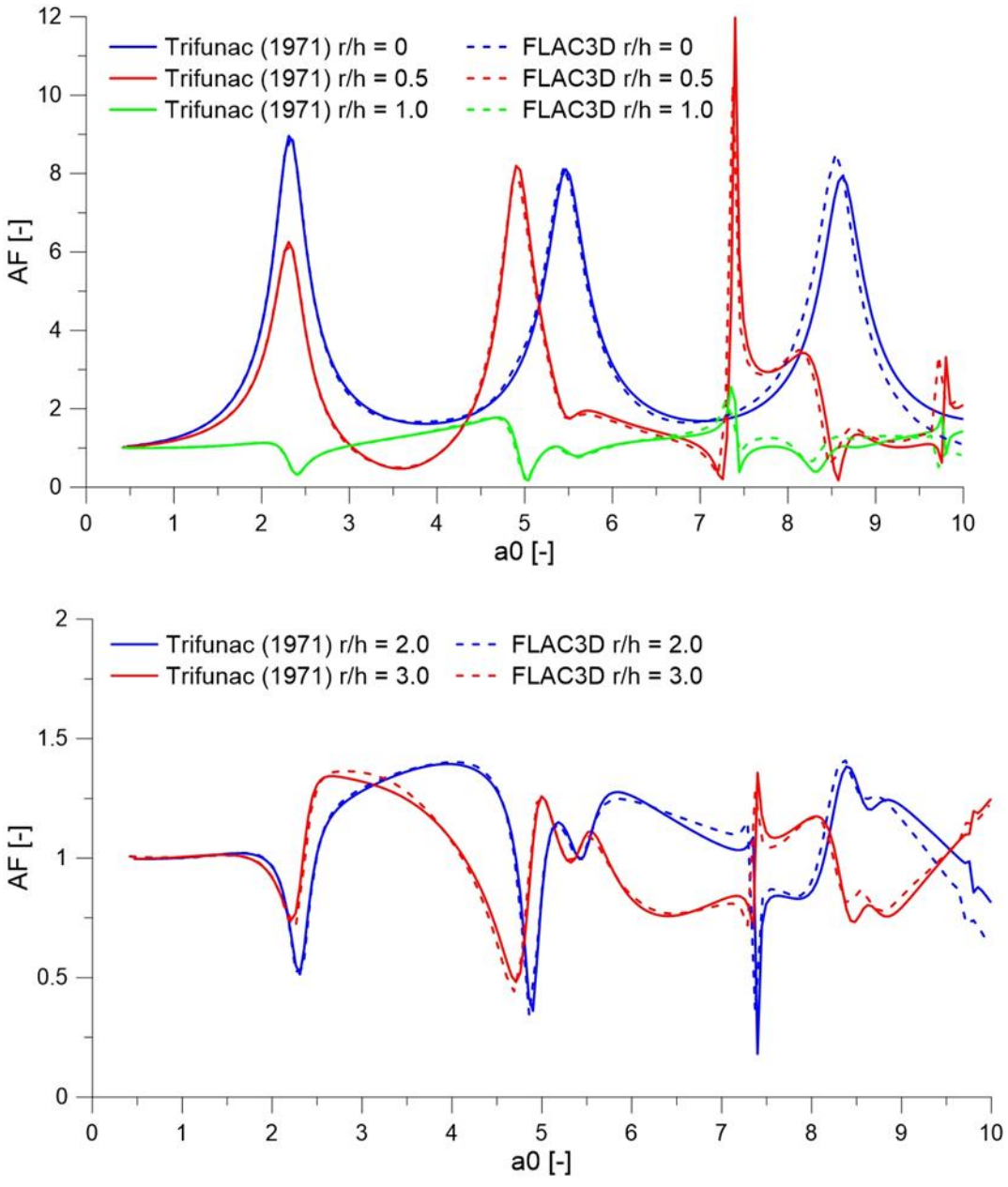

Figure 3.7: Comparison between closed-form solution (solid lines) and FLAC3D numerical results (dashed lines)

3.2.2 Plane strain earth dam on rigid bedrock (Dakoulas and Gazetas, 1985)

In Figure 3.8 the cross-section of the earth-dam with the locations of the four points taken for comparison between the closed-form solutions and the results of FLAC3D simulations are shown. The numerical grid of the model developed in FLAC3D is illustrated in Figure 3.9. The linear properties adopted are shown in Table 3.3. In Figure 3.10 and Figure 3.11 the comparisons in terms of transfer functions are portrayed for two in-homogeneity parameter m: 1) homogeneous dam (m=0); 2) in-homogeneous dam (m = 2/3), respectively. The comparisons result satisfactory for first mode both in terms of amplitude and frequency, while the discrepancy for the higher modes it is presumably due to vertical displacement (not considered in the shear-beam approach).

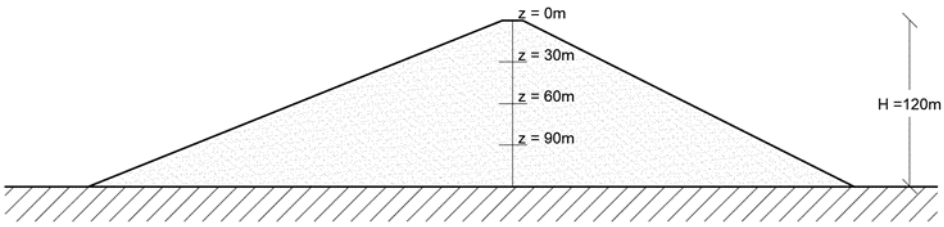

Figure 3.8: Cross-section of the dam and locations of points for comparisons between FLAC3D numerical results and closed-form solution

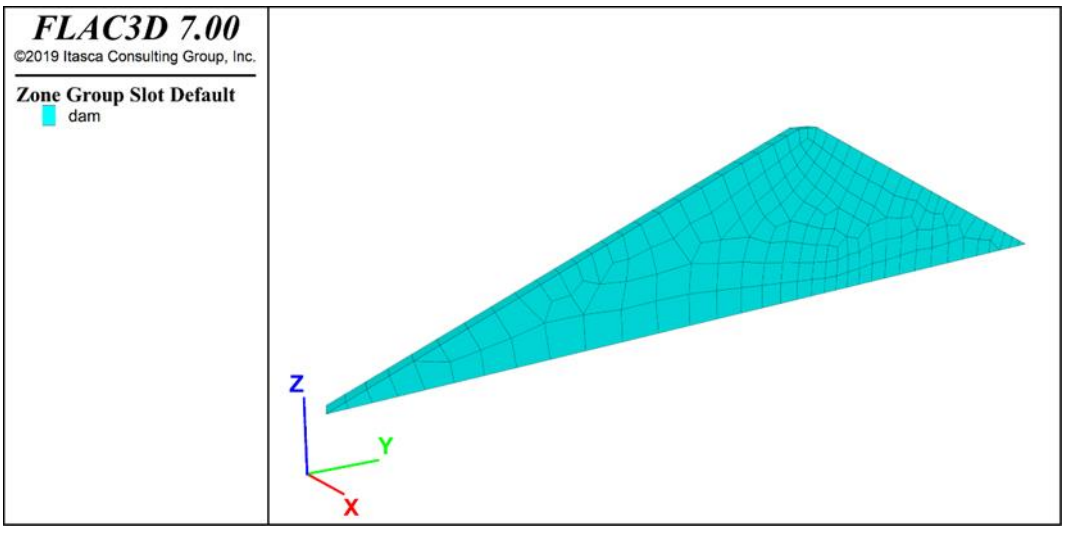

Figure 3.9: FLAC3D numerical grid for plane-strain earth dam on rigid bedrock

Table 3.3: Linear properties adopted for plane-strain earth dams

Dam	γ	Vs	m	ν
[-]	[kN/m3]	[m/s]	[-]	[-]
1	18.0	280	0.0	0.35
2	18.0	280	2/3	0.35

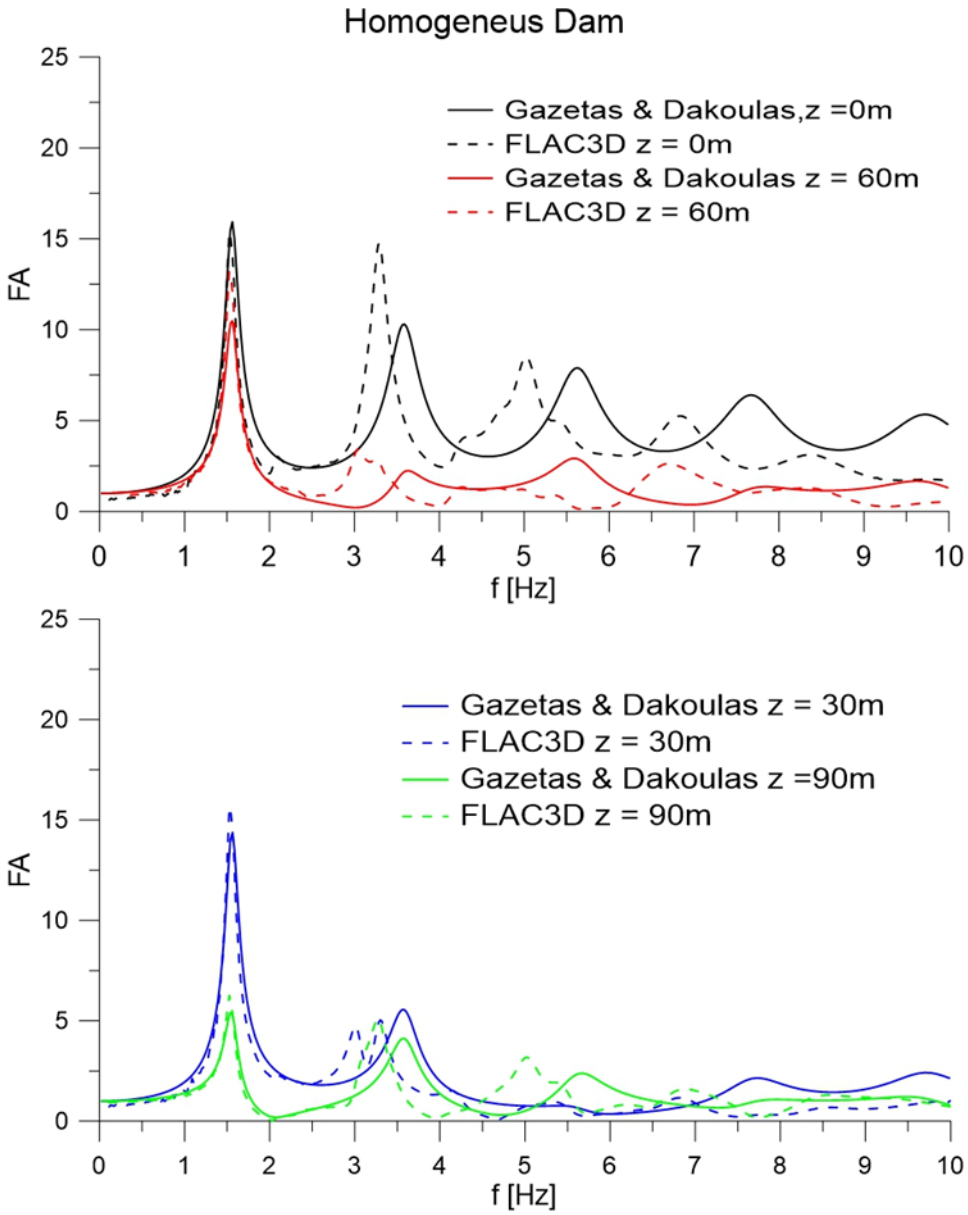

Figure 3.10: Comparison between closed-form solutions (solid lines) and FLAC3D numerical simulation (dashed lines) for plane-strain homogenous earth dam on rigid bedrock.

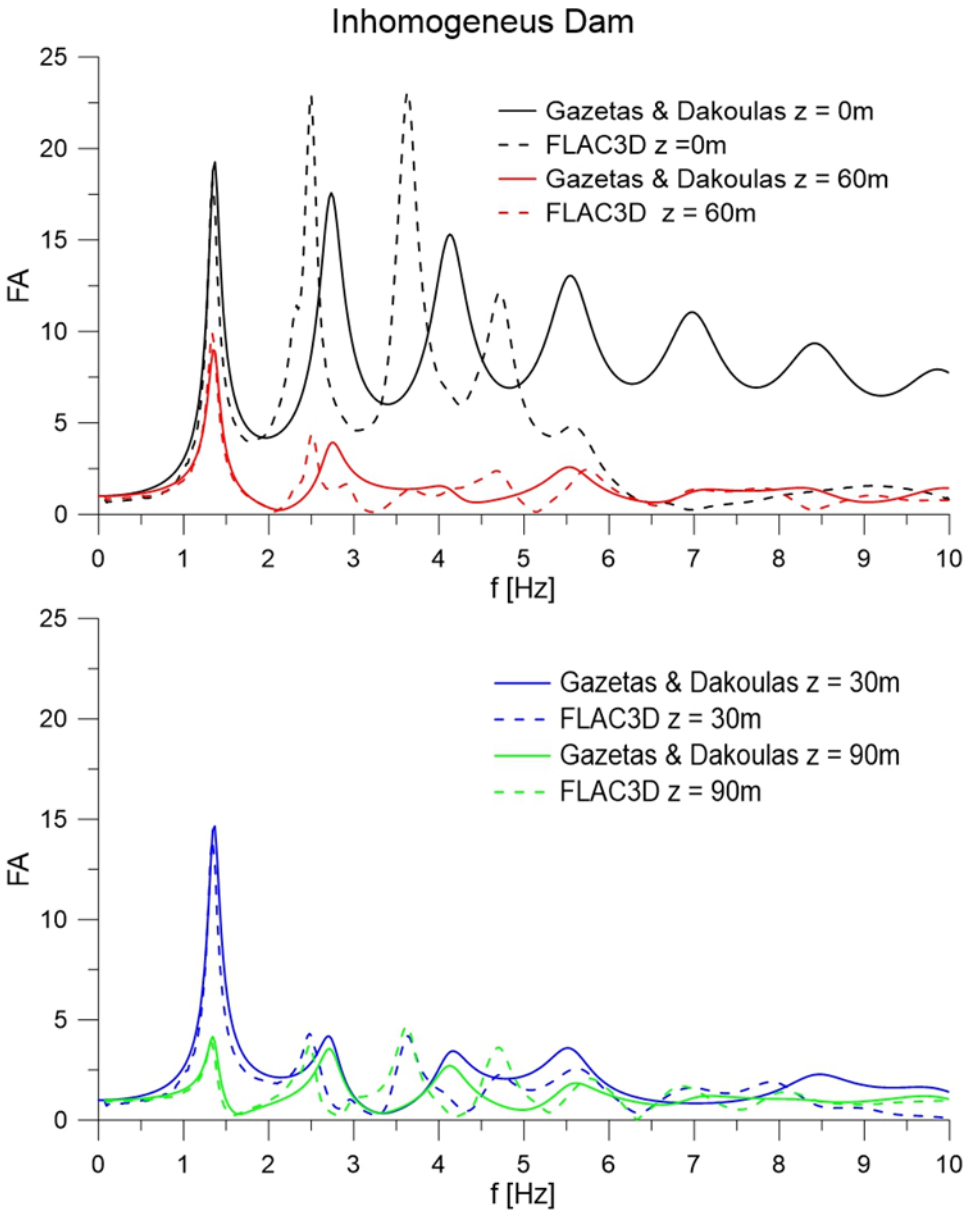

Figure 3.11: Comparison between closed-form solution (solid lines) and FLAC3D numerical simulation (dashed lines) for plane-strain in-homogenous earth dam on rigid bedrock.

3.2.3 Plane strain earth dam on flexible bedrock (Dakoulas, 1993)

The model assumed is the same as the previous case (see Table 3.3), with the only exception of deformable bedrock instead of rigid one. The impedance ratio half-space-dam IR= 7. Numerical grid is show in Figure 3.12. Figure 3.13 shows the comparison between analytical solutions and numerical results in terms of transfer functions, that is AF versus the frequency factor a0 again, it can be noted a good correspondence for the fundamental peak in terms of amplitude and frequency while the higher modes the agreement is less satisfactory.

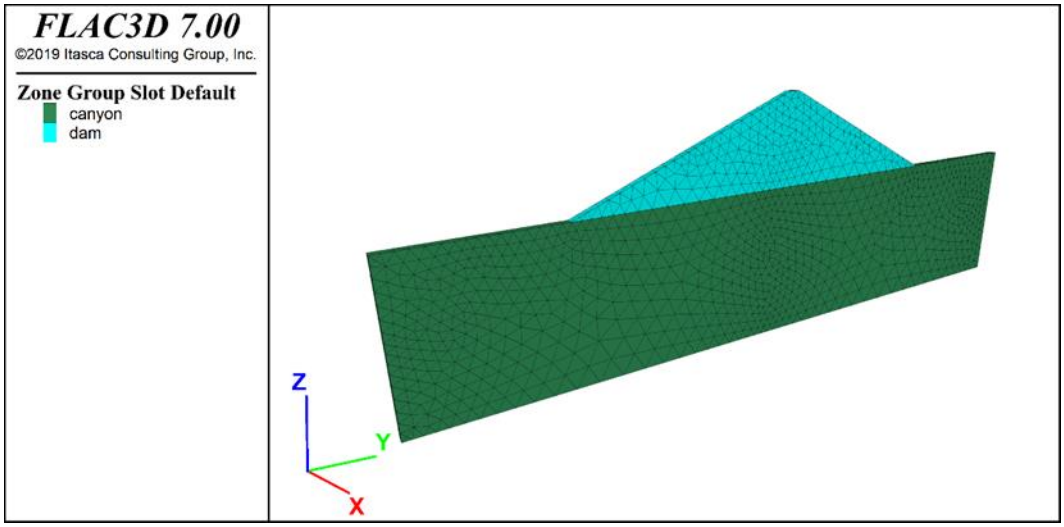

Figure 3.12: FLAC3D numerical grid for plane strain earth dam on flexible bedrock.

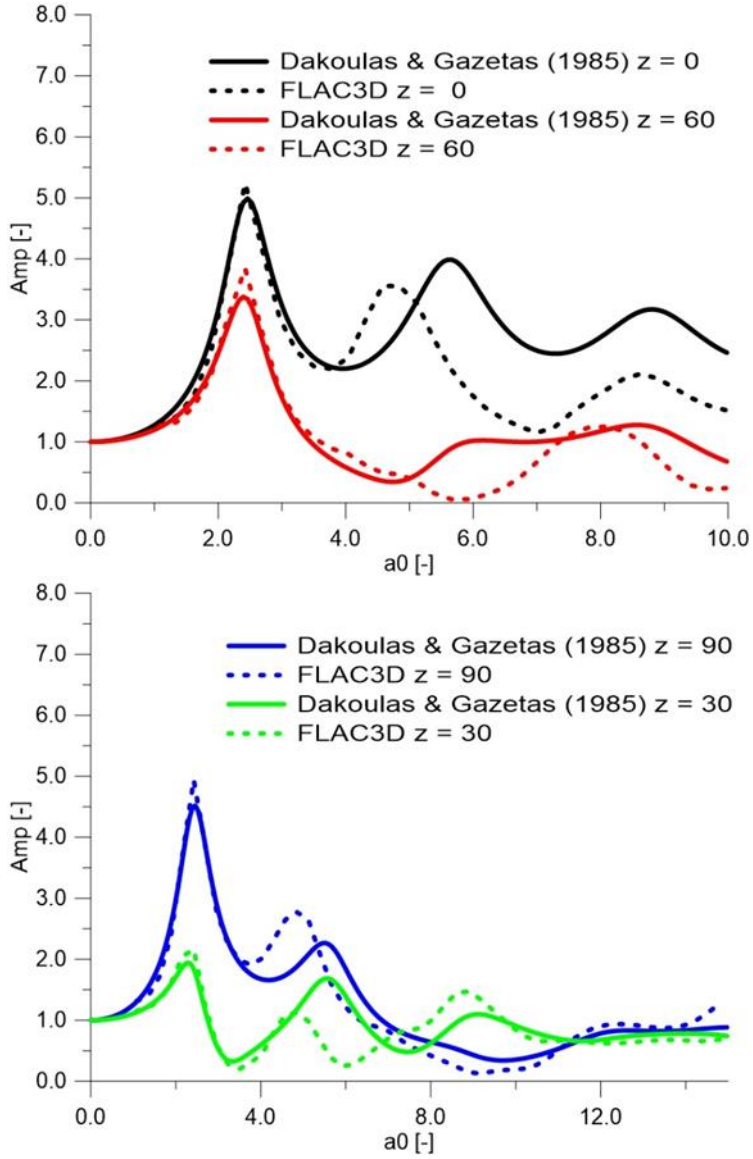

Figure 3.13: Comparison between closed-form solution (solid lines) and FLAC3D numerical simulation (dashed lines) for plane-strain homogenous earth dam.

3.2.4 Semi-cylindrical earth dam on deformable bedrock (Dakoulas, 1993)

Dakoulas (1993) provide closed-form solution for 3D homogeneous semi-cylindrical shape earth dam on flexible bedrock. In Figure 3.14 are shown the cross- and longitudinal sections with the locations of nodes for comparison between closed-form and FLAC3D numerical results (red points). Figure 3.15 shows the FLAC3D numerical grid. The linear properties adopted are shown in Table 3.4.

In Figure 3.16 and Figure 3.17 the comparison in terms of transfer functions for the selected points along cross- and longitudinal-sections are shown, respectively.

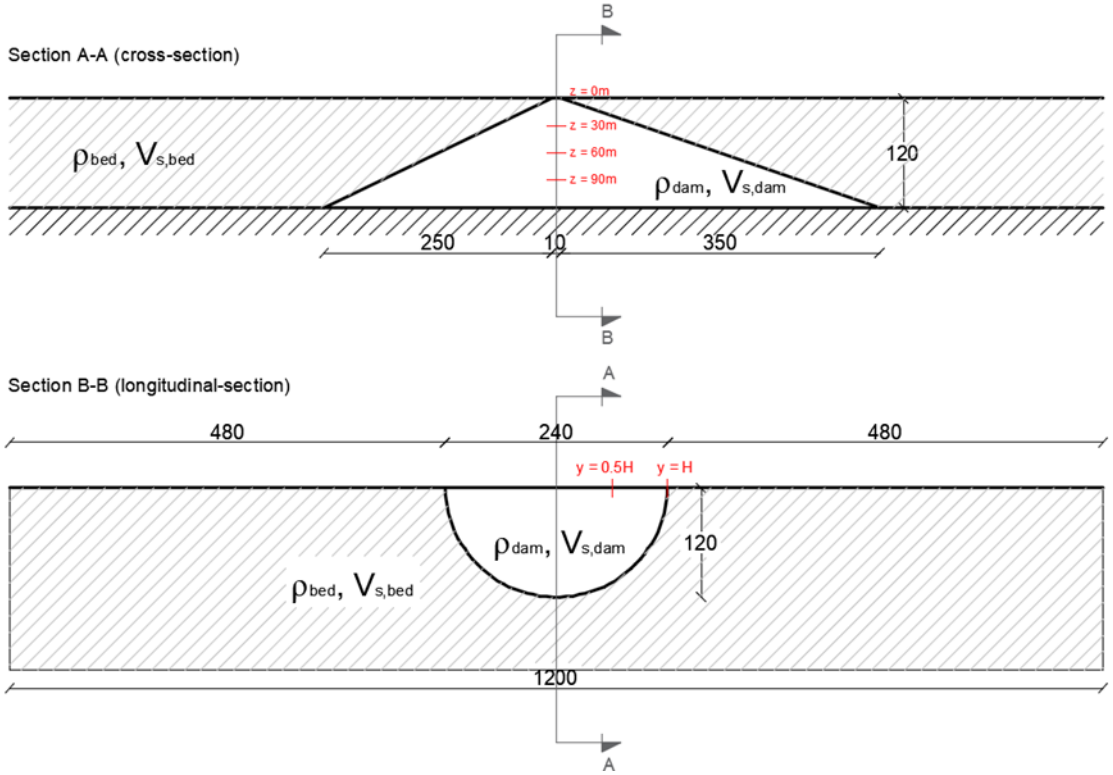

Figure 3.14: Semi-cylindrical earth dam. Above: cross-section; below: longitudinal section.

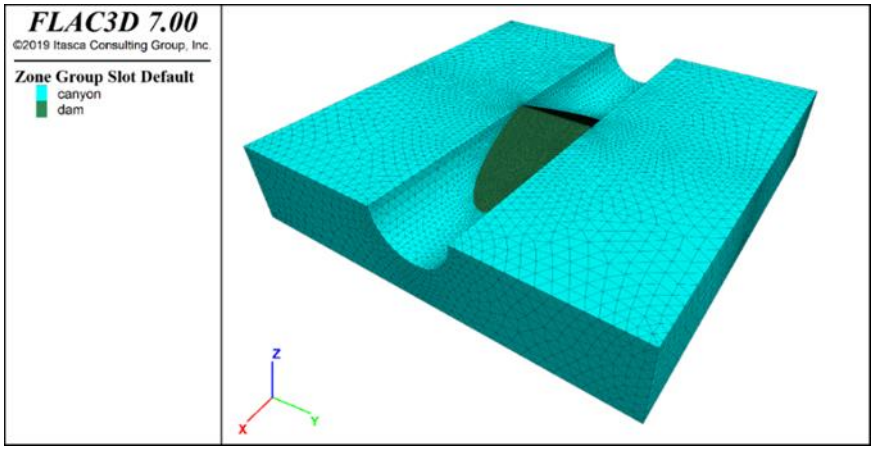

Figure 3.15: FLAC3D numerical grid for semi-cylindrical shape earth dam.

Table 3.4: Linear properties adopted for semi-cylindrical shape earth dams

Material	γ	Vs	D	ν
[-]	[kg/m3]	[m/s]	[%]	[-]
Dam	1800	280	10	0.3
Canyon	2250	1120	10	0.3

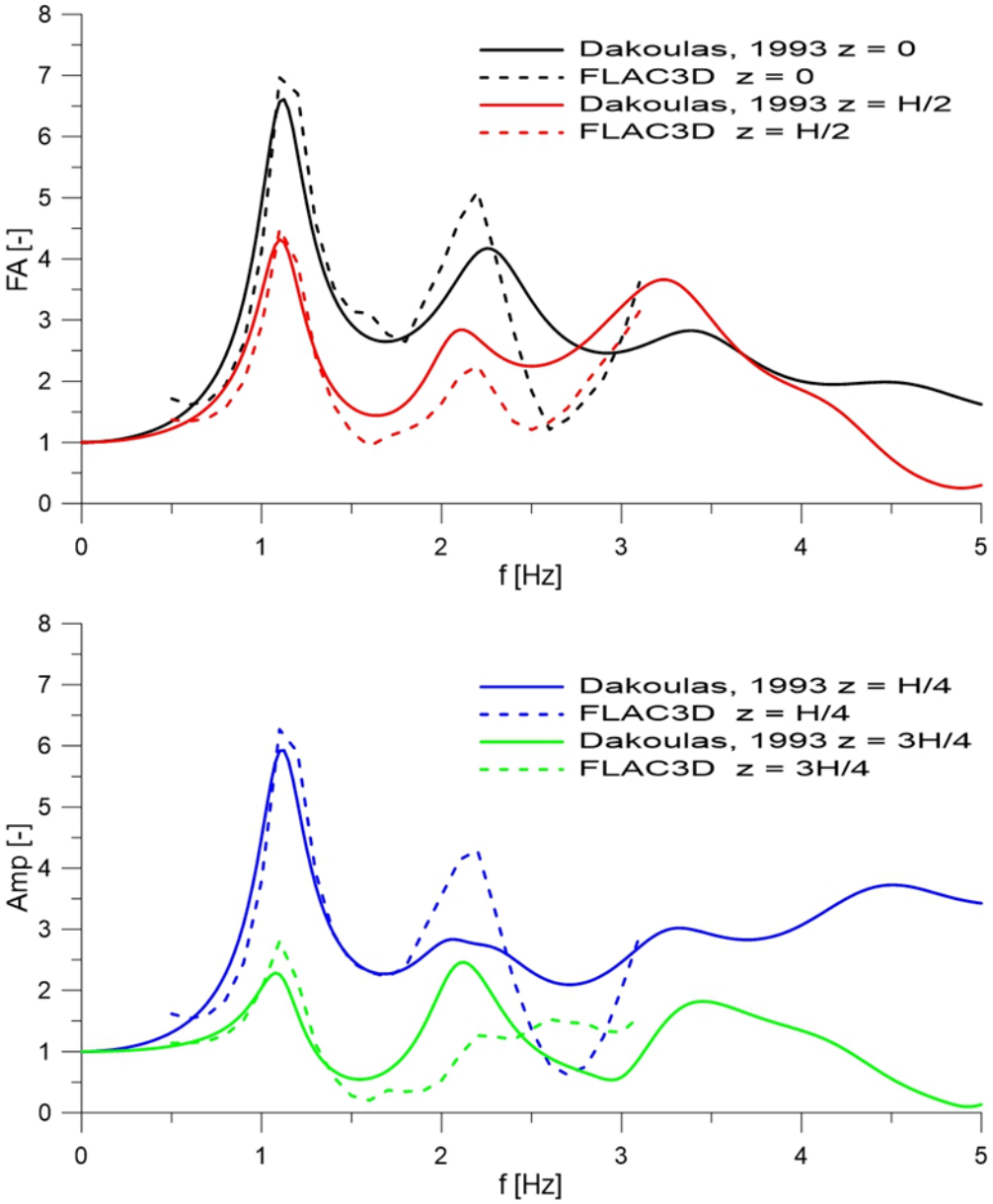

Figure 3.16: Comparison between closed-form solutions (solid lines) and FLAC3D numerical results (dashed lines) for semi-cylindrical earth dam on deformable bedrock.

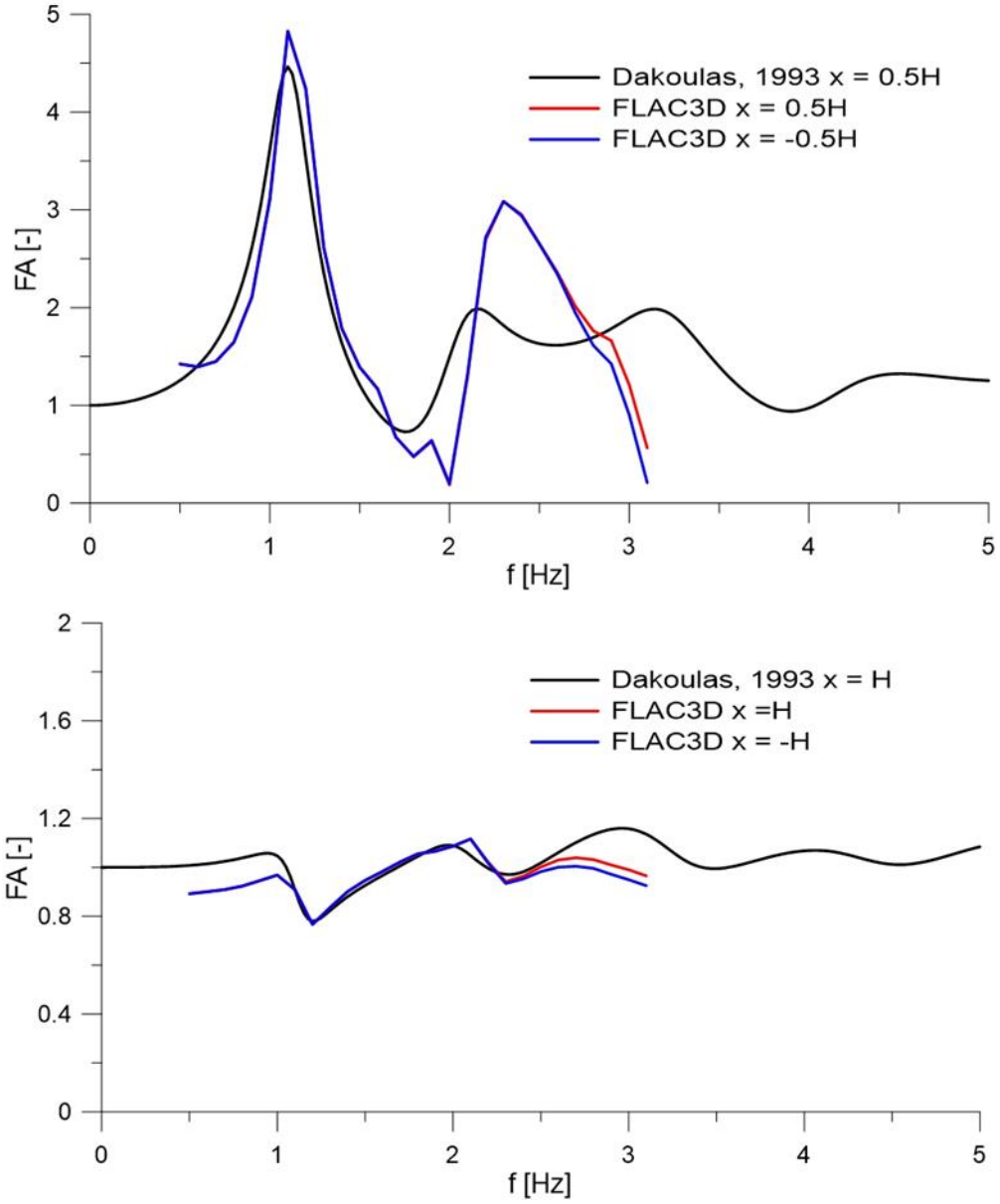

Figure 3.17: Comparison between closed form solution (black lines) and FLAC3D numerical results (red and blue lines) for semi-cylindrical earth dam on deformable bedrock.

3.2.5 Rectangular earth dam on rigid bedrock (Dakoulas and Hashimi, 1991)

In Figure 3.18 the transversal and longitudinal sections of a rectangular shape dam on rigid bedrock with shape-ratio L/H = 2 are shown. FLAC3D numerical grid is show in Figure 3.19. The comparison in terms of amplification function is shown in Figure 3.20 and Figure 3.21. Similar conclusions made for the other case studied can be made. The linear properties adopted are shown in Table 3.5.

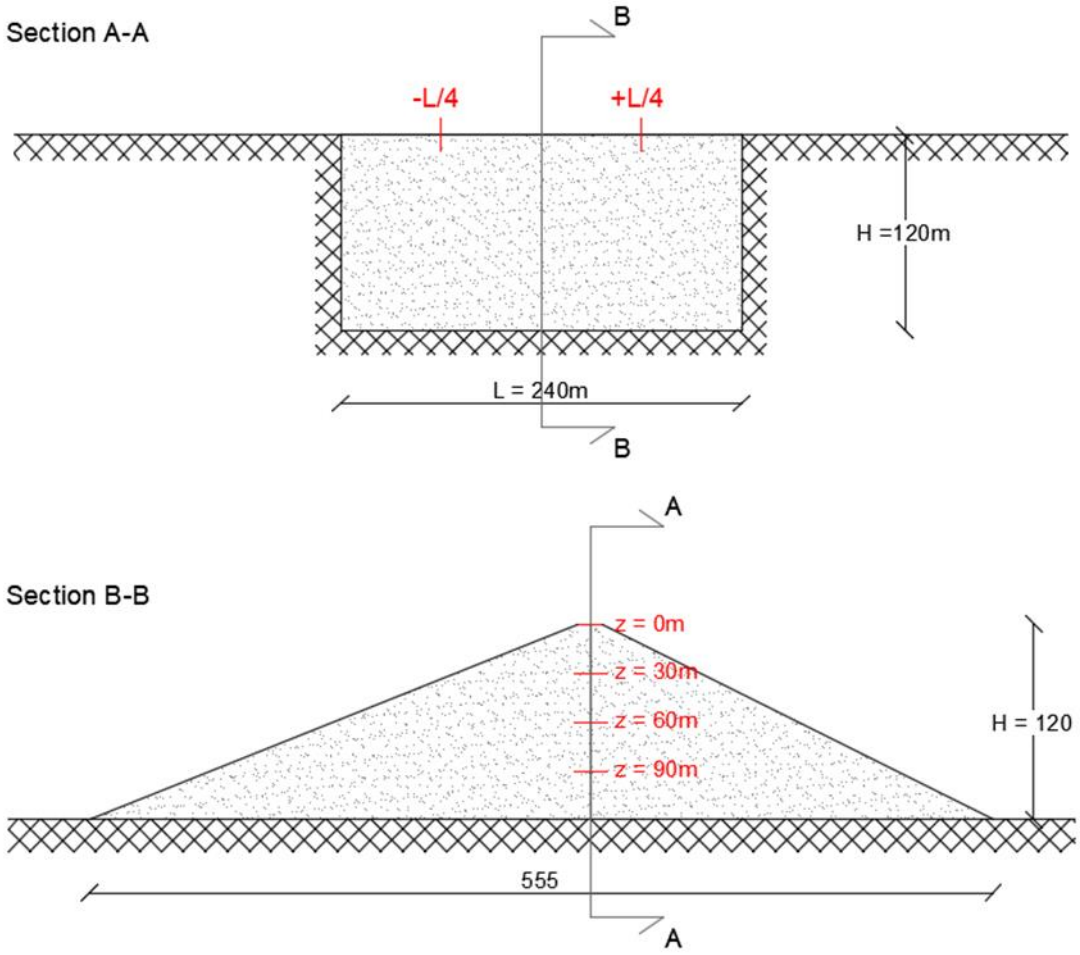

Figure 3.18: Longitudinal (above) and transversal (below) of rectangular shape dam with L/H =2

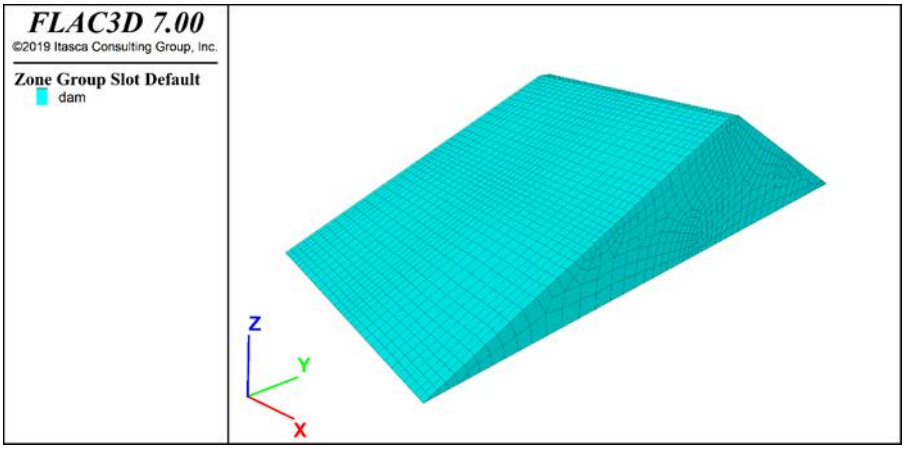

Figure 3.19: FLAC3D numerical grid for rectangular shape earth dam on rigid bedrock.

Table 3.5: Linear properties adopted for rectangular-shape earth dam

Material	γ	Vs	ν	D
[-]	[kg/m3]	[m/s]	[-]	[%]
Dam	1800	350	0.35	10
Canyon	2250	700	0.35	10

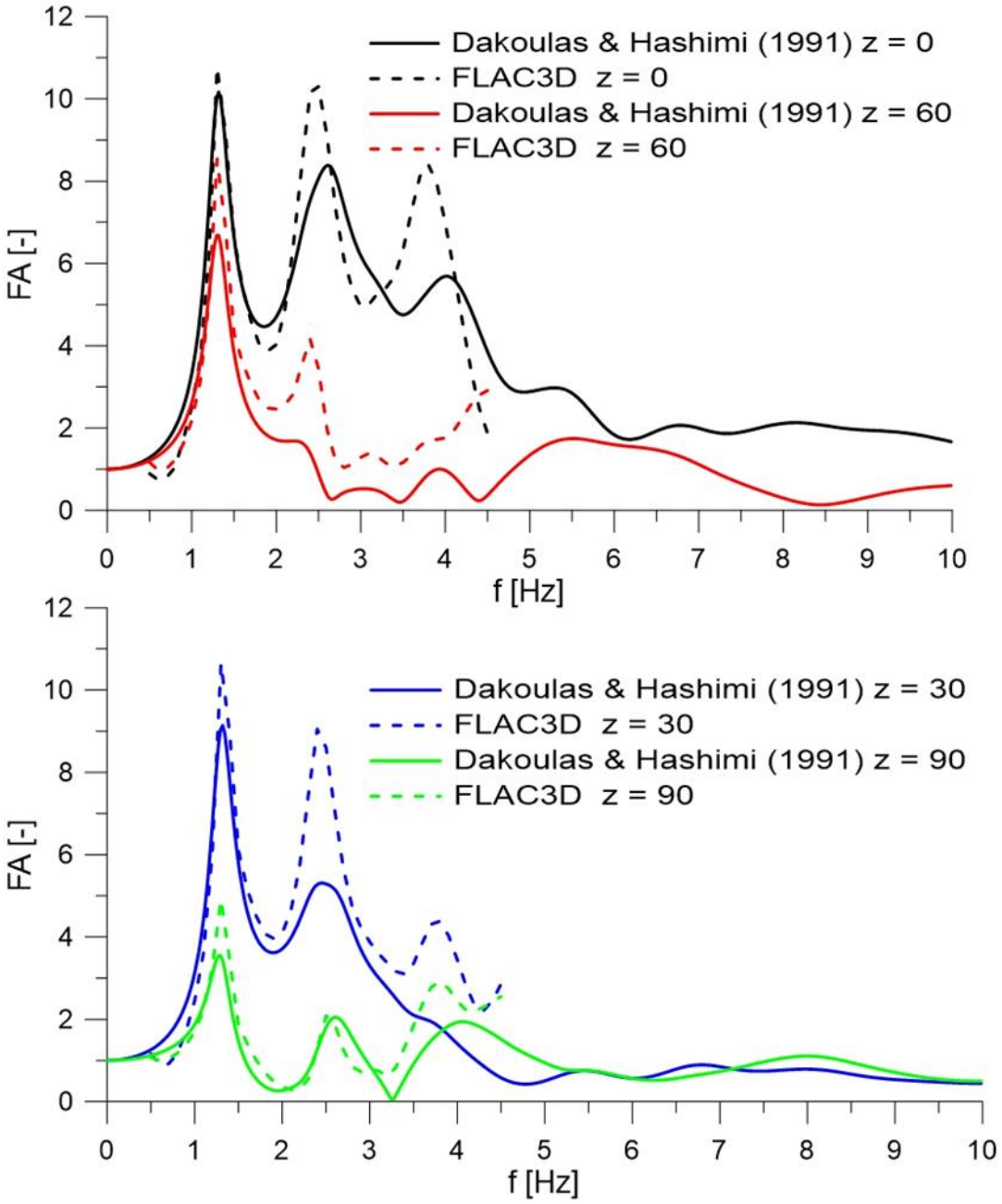

Figure 3.20: Comparison between closed form solution (solid lines) and FLAC3D numerical results (dashed lines) for semi-cylindrical shape earth dam.

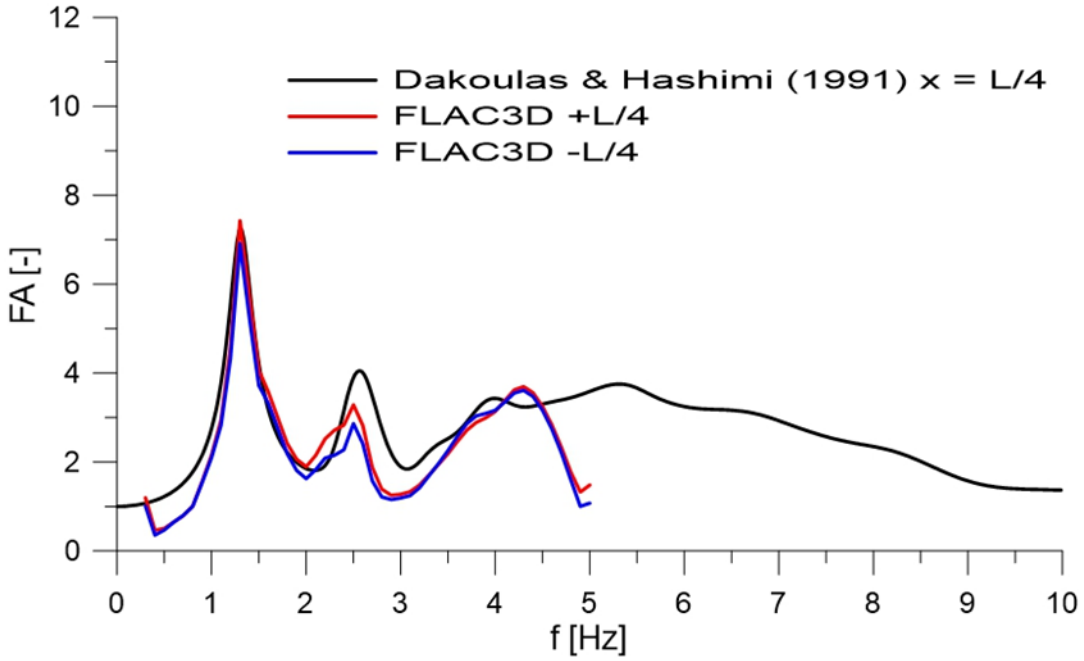

Figure 3.21: Comparison between closed form solution (black lines) and FLAC3D numerical results (blue and red lines) for semi-cylindrical shape earth dam.

4 Comparison between 2D and 3D numerical simulations for simple irregularities

In this chapter the comparison between the results of numerical simulations for 2D and 3D models of simplified surface and subsurface irregularities are presented.

4.1 Simple geometries of alluvial valleys and topographic irregularities

A semi-cylindrical alluvial valley with maximum thickness h = 60 m was studied with 2D and 3D analyses. The cross-section of the valley and the FLAC3D numerical grid are shown in Figure 4.1 and Figure 4.2, respectively. The linear properties adopted for visco-elastic analyses are shown in Table 4.1. The impedance ratio between valley and half-space is 3. The comparisons between 2D and 3D numerical results are carried out in terms of horizontal and vertical acceleration ratio, defined as the ratio of peak acceleration at the ground surface (PGAoutput) to the outcrop acceleration (PGAoutcrop). Two input motions have been considered: 1) only horizontal motion (X and Y); 2) both horizontal and vertical one (X, Y and Z).

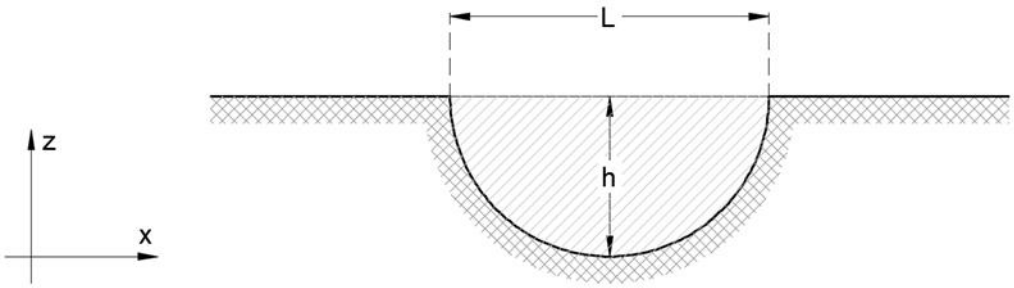

Figure 4.1: Cross-section for semi-cylindrical alluvial valley.

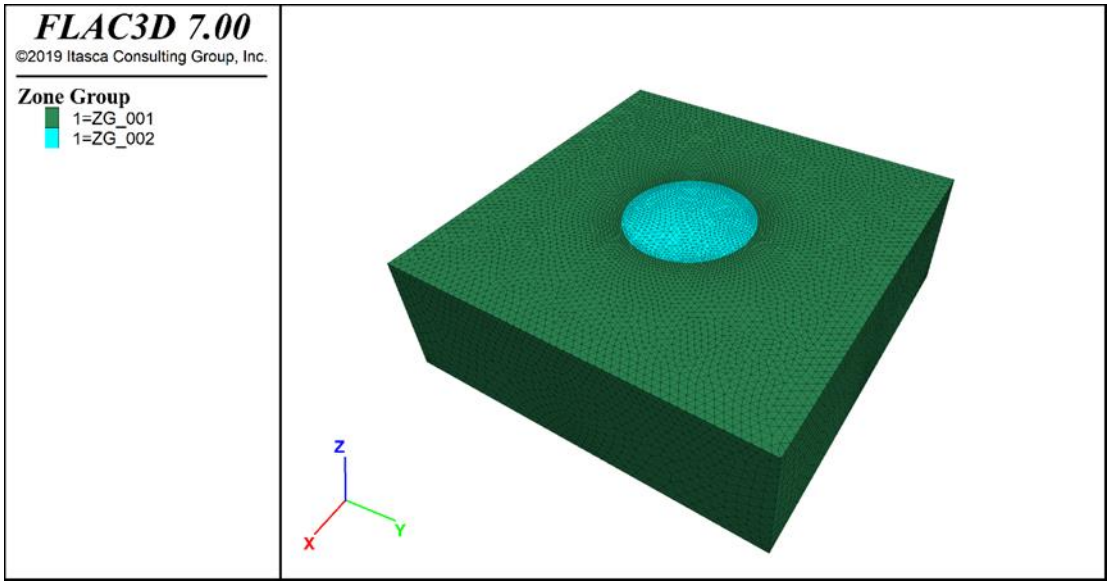

Figure 4.2: FLAC3D numerical grid for semi-cylindrical valley.

Table 4.1: Linear properties adopted for semi-cylindrical hill

Unit	γ	Vs	Vp	D
	[kN/m3]	[m/s]	[m/s]	[%]
valley	16	131.3	273	1
half-space	18	350.0	729	1

In Table 4.2 the corresponding wavelengths λs and λp and dimensionless frequencies λs and λp (Trifunac 1971) for shear and compression wave velocity, respectively, are shown.

Table 4.2: Wavelengths (λs, λp) and dimensionless frequencies (λs, λp) for semi-cylindrical alluvial valley

Horizontal			Vertical		
f	ls	ls	f	lp	lp
[Hz]	[m]	[-]	[Hz]	[m]	[-]
2	65.7	1.828	2.9	94.2	1.274
5	26.3	4.570	7.25	37.7	3.184
8	16.4	7.312	11.6	23.6	5.095

In Figure 4.3 the comparisons between 2D and 3D numerical results obtained applying only horizontal motion (vertical component is parasitic) are shown. The following considerations

can be made: i) 3D model provides greater amplification of horizontal motion as compared to 2D model at medium and high frequencies (f=5 and 8Hz) corresponding to wavelength ηs less than the radius of the valley (h=60m); ii) for the horizontal component, no appreciable difference between 3D and 2D can be noted for wavelength ηs similar at the radius (f=2Hz); iii) 2D model provides, for both horizontal and vertical parasitic components, negligible amplification at high frequency (f = 8Hz); iv) vertical parasitic component depend on frequency of input motion, both 3D and 2D models provide negligible amplification in the centre of valley (x/h = 0); v) the pattern of displacement become more complex with increasing frequency.

The introduction of vertical input motion (Figure 4.4) provides significant amplifications on vertical component regardless of the frequency, especially at f = 2.9 Hz that corresponds to wavelengths greater than the radius of valley (λp = 94.3m).

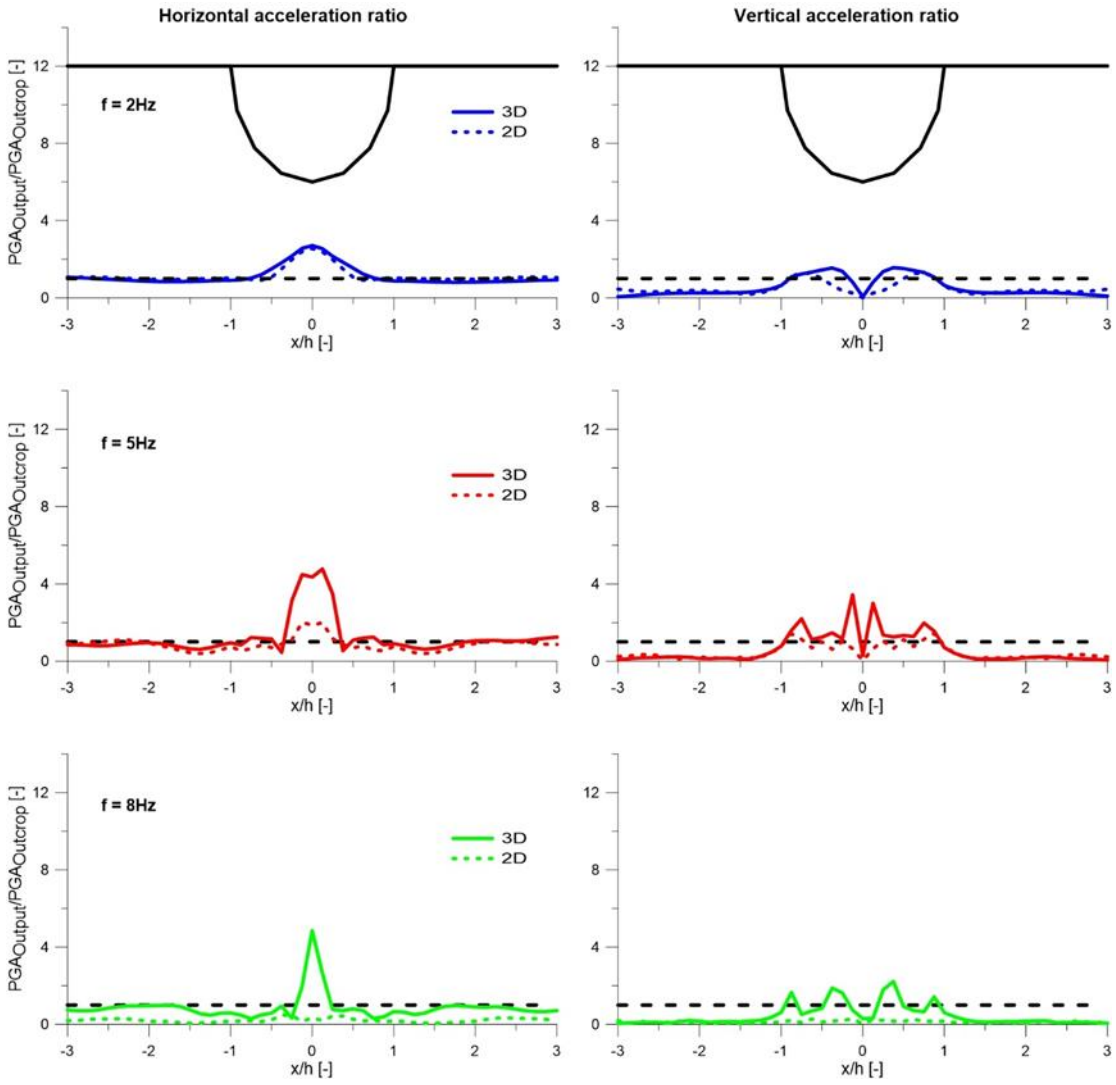

Figure 4.3: Comparison between 2D (dashed lines) and 3D (solid lines) acceleration ratio, obtained applying only horizontal motion, for semi-cylindrical valley.

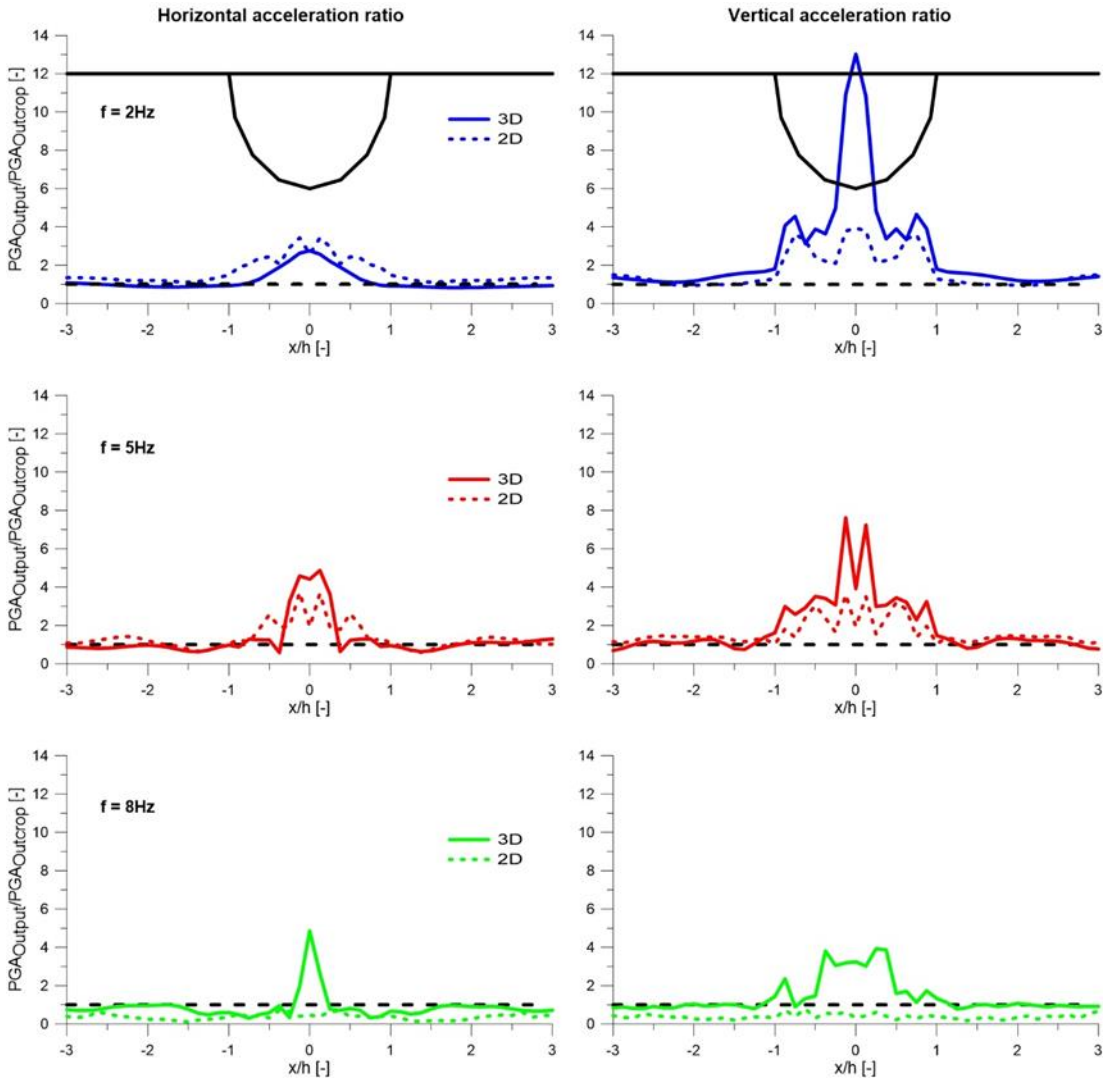

Figure 4.4: Comparison between 2D (dashed lines) and 3D (solid lines) acceleration ratio, obtained applied both horizontal and vertical motion, for semi-cylindrical valley.

As discussed in paragraph 2.3, the most important parameters that affect the dynamic response of alluvial valleys are the impedance ratio IR and the shape-ratio L/h. In Figure 4.5 two semi-circular shape valleys, with L/h = 2 and 3, respectively, are shown.

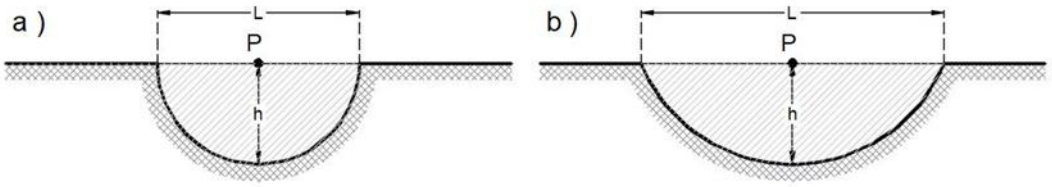

Figure 4.5: Simplified geometry for alluvial valley effects. a: L/H = 2; b: L/H = 3. P: comparison point

In Figure 4.6 and Figure 4.7 the horizontal and vertical transfer functions both for 2D and 3D conditions, evaluate in the center of valley (point P), are illustrated. Two values of impedance

ratio, i.e. IR = 2 and IR=3, for each valley, have been considered. The following considerations can be made: i) 3D models provides greater amplifications at all frequencies; ii) the peak of fundamental frequency increases in 3D model as compared to 2D one; iii) the increase of IR provides significant amplifications both in 2D and 3D conditions.

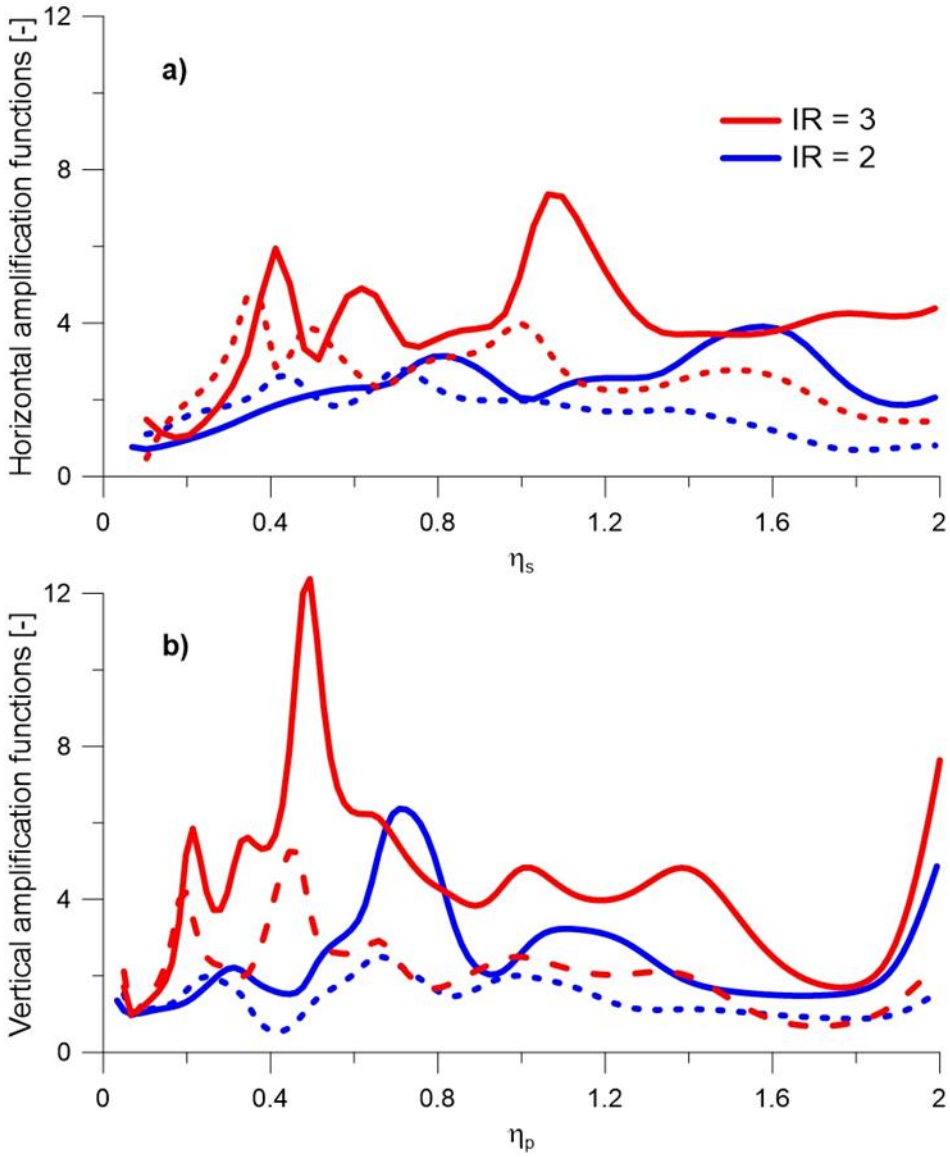

Figure 4.6: Figure 4.6: Comparison between 3D (solid lines) and 2D (dashed lines) amplification functions for semi-cylindrical valley. Red lines: IR = 3; blue lines: IR = 2 a): horizontal component by applying incident S waves; b): vertical component by applying incident P waves.

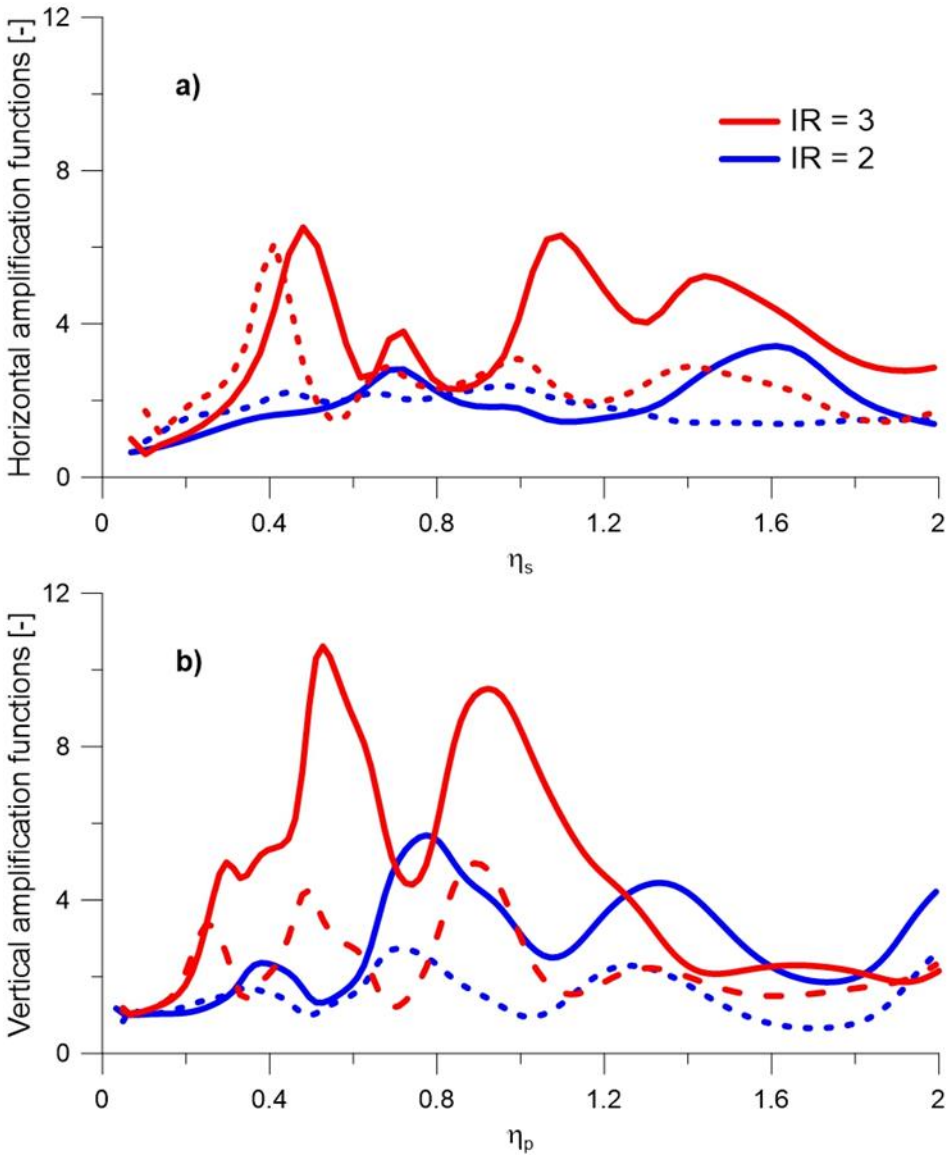

Figure 4.7: Comparison between three-dimensional (solid lines) and bidimensional (dashed lines) amplification functions for semi-cylindrical valley with L/H = 3. Red lines: IR = 3; blue lines: IR = 2 a): horizontal component by applying incident S waves; b): vertical component by applying incident P waves.

The evaluation of topographic effects on dynamic response for 2D and 3D, semi-cylindrical hill with height h = 60 m was also studied. The cross-section of the hill and the FLAC3D numerical grid are shown in and Figure 4.8 and Figure 4.9, respectively. Analyses are visco-elastic, and the linear properties adopted are shown in Table 4.3. The comparisons between 2D and 3D numerical results are carried out in terms of horizontal and vertical acceleration ratio at the top of profile. Two seismic conditions were considered: 1) only horizontal motion (X and Y); 2) both horizontal and vertical one (X, Y and Z).

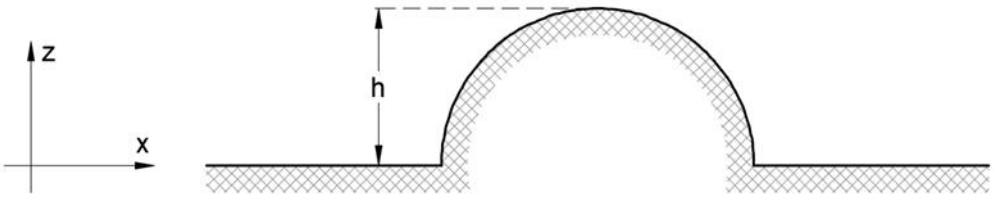

Figure 4.8: Cross-section for semi-cylindrical hill.

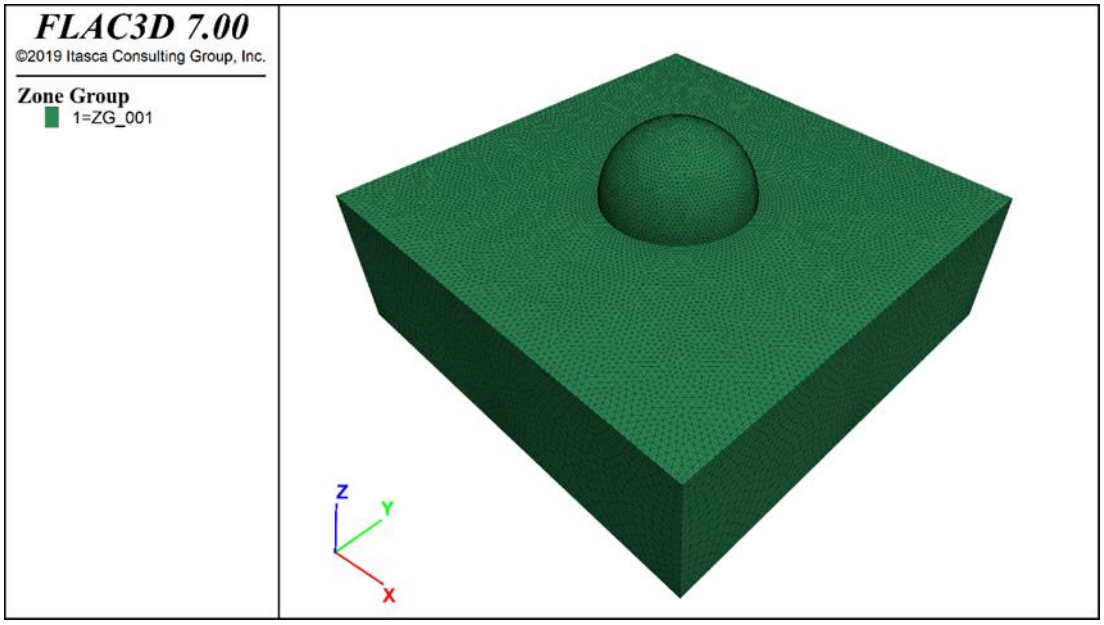

Figure 4.9: FLAC3D numerical grid for semi-cylindrical hill.

Table 4.3: Linear properties adopted for semi-cylindrical hill

γ	Vs	Vp	D
[kN/m3]	[m/s]	[m/s]	[%]
18	350	728	1.0

The input motion is a Chang wavelet with predominant frequencies f = 2, 5 and 8 Hz for horizontal motion, vertical one was assumed equal to half horizontal amplitude and frequency 45% larger than horizontal (f = 2.9, 7.25 and 11.6 Hz). In Table 4.4 the corresponding wavelengths λs and λp and dimensionless frequencies λs and λp (Trifunac 1971) for shear and compression wave velocity propagation, respectively, are shown.

Table 4.4: Wavelengths (λs, λp) and dimensionless frequencies (ηs,ηp) for semi-cylindrical hill

Horizontal			Vertical		
f	λs	ηs	f	λp	ηp
[Hz]	[m]	[-]	[Hz]	[m]	[-]
2	175.00	0.686	2.9	364.29	0.329
5	70.00	1.714	7.25	145.72	0.824
8	43.75	2.743	11.6	91.07	1.318

In Figure 4.10 the comparisons for first seismic scenario (only horizontal motion as input, vertical component is parasitic) are shown. The following considerations can be made: i) 3D model provides greater amplifications of horizontal component as compared to 2D one at low and medium frequency (f=2 and 5Hz) that correspond at wavelength λs greater than radius (h=60m) of hill; ii) no appreciable difference between 3D and 2D, on horizontal component, for wavelength less that radius (f=8Hz); iii) vertical parasitic component increases with frequency, but negligible values at top of hill (x/h = 0); 4) the pattern of displacement become more complex with increasing frequency. The introduction of vertical input motion (Figure 4.11) provides significant amplifications on vertical accelerations regardless of the frequency.

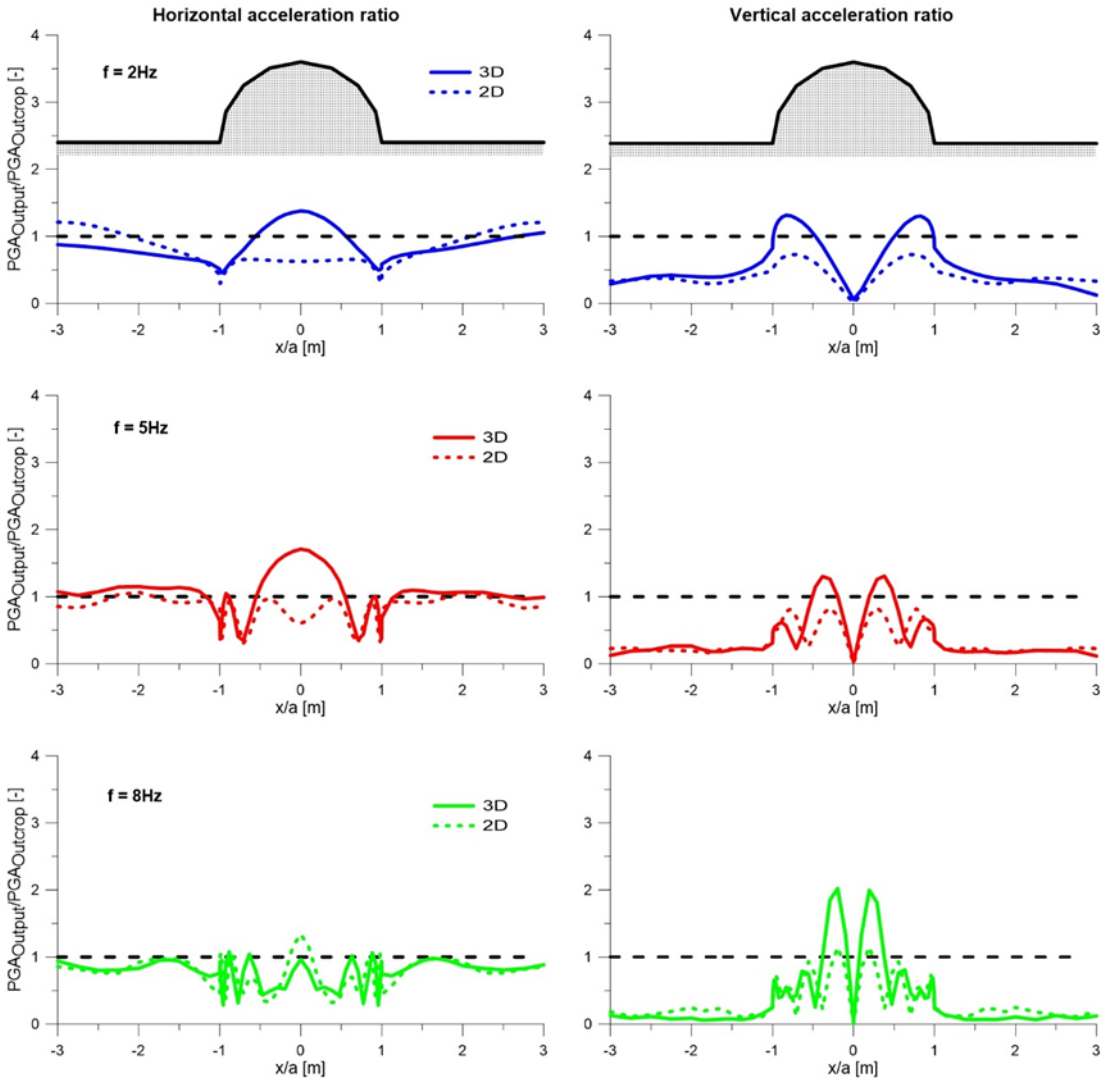

Figure 4.10: Comparison between 2D (dashed lines) and 3D (solid lines) acceleration ratio, obtained applied only horizontal motion, for semi-cylindrical hill.

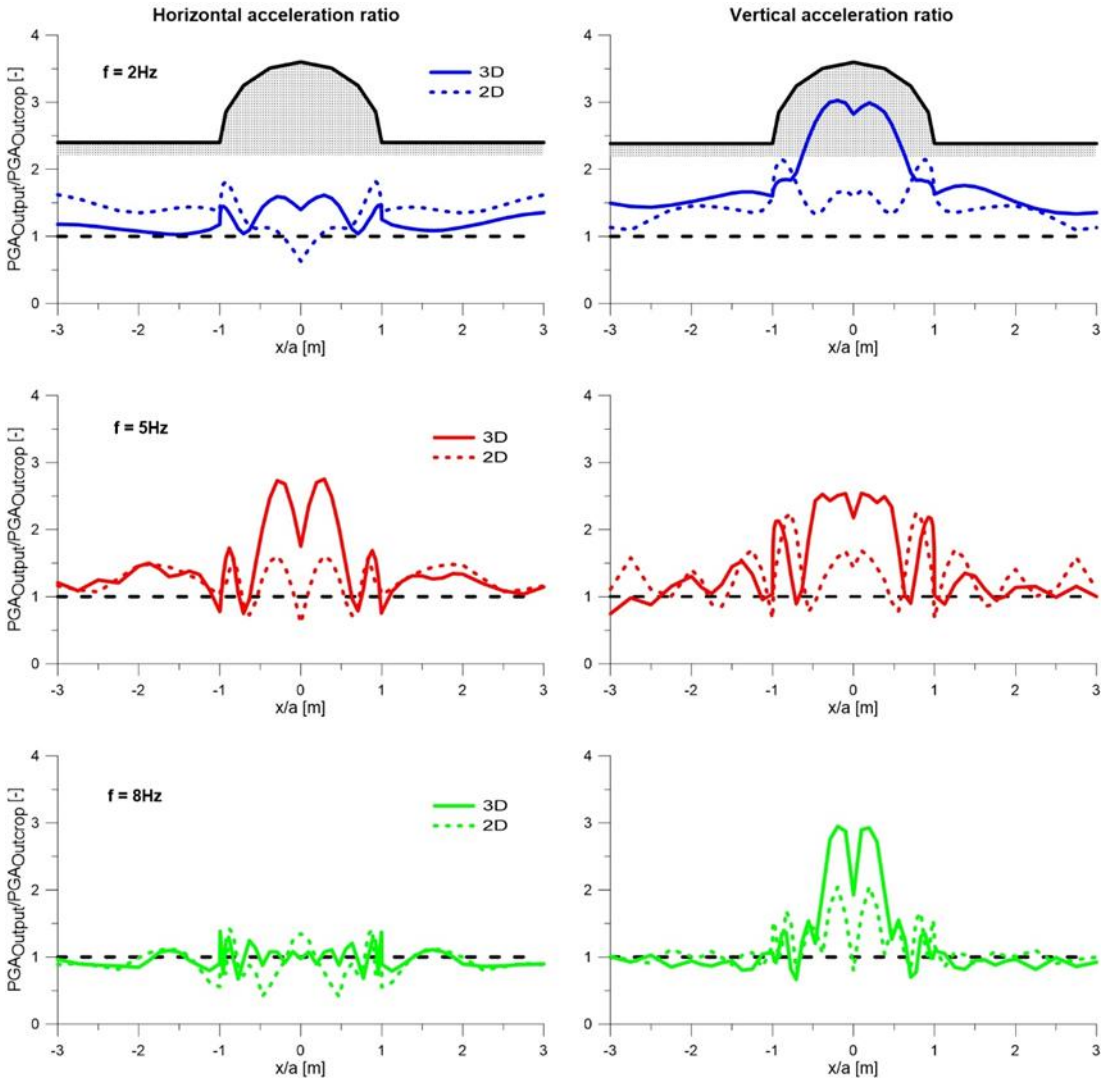

Figure 4.11: Comparison between 2D (dashed lines) and 3D (solid lines) acceleration ratio, obtained applied both horizontal and vertical motion, for semi-cylindrical hill.

Furthermore, to evaluate the effect of the shape of the topographic irregularity, four simplified shapes shown in Figure 4.12, that is semi-cylindrical canyon (a); semi-cylindrical hill (b); ridge (c) and cliff (d), have been studied. The comparisons have been conducted in terms of transfer functions at selected points P1 (top or crest) and P2 (bottom or toe) of the irregularity.

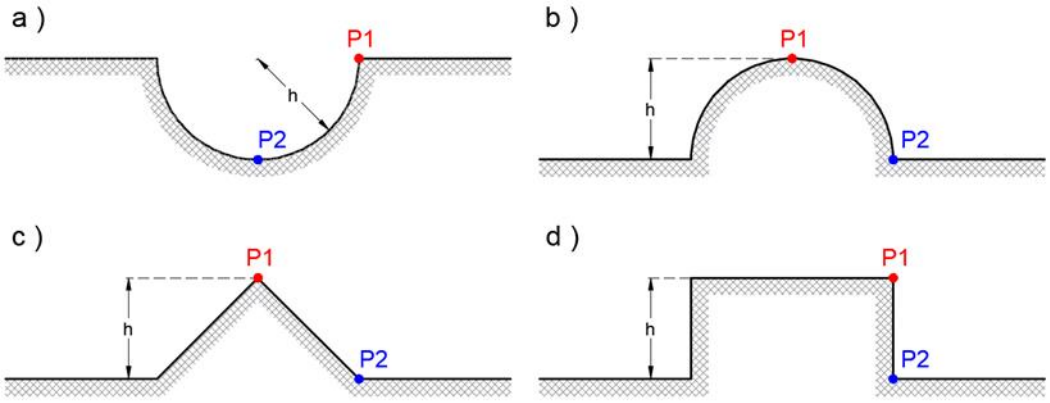

Figure 4.12: Simplified geometries selected for investigating the topographic effects. a) semi-cylindrical canyon; b) semi-cylindrical hill; c) ridge and d) cliff. P1 and P2: comparison points.

From Figure 4.13 to Figure 4.16 2D and 3D transfer functions are illustrated. For each figure: a) horizontal component, obtained by applying S waves, by varying the dimensionless parameter ηs; b) vertical component applying P waves, by varying ηp. The following considerations can be made: i) generally, 3D features exhibit greater amplitude than 2D at the top of each system (P1); ii) at the bottom or toe point (P2) there are no appreciable difference between 3D and 2D both for horizontal and vertical components; 3) horizontal transfer functions, generally, shown greater amplification than vertical ones; 4) the difference between 2D and 3D results strongly depend on the shape of the irregularity, especially for higher mode.

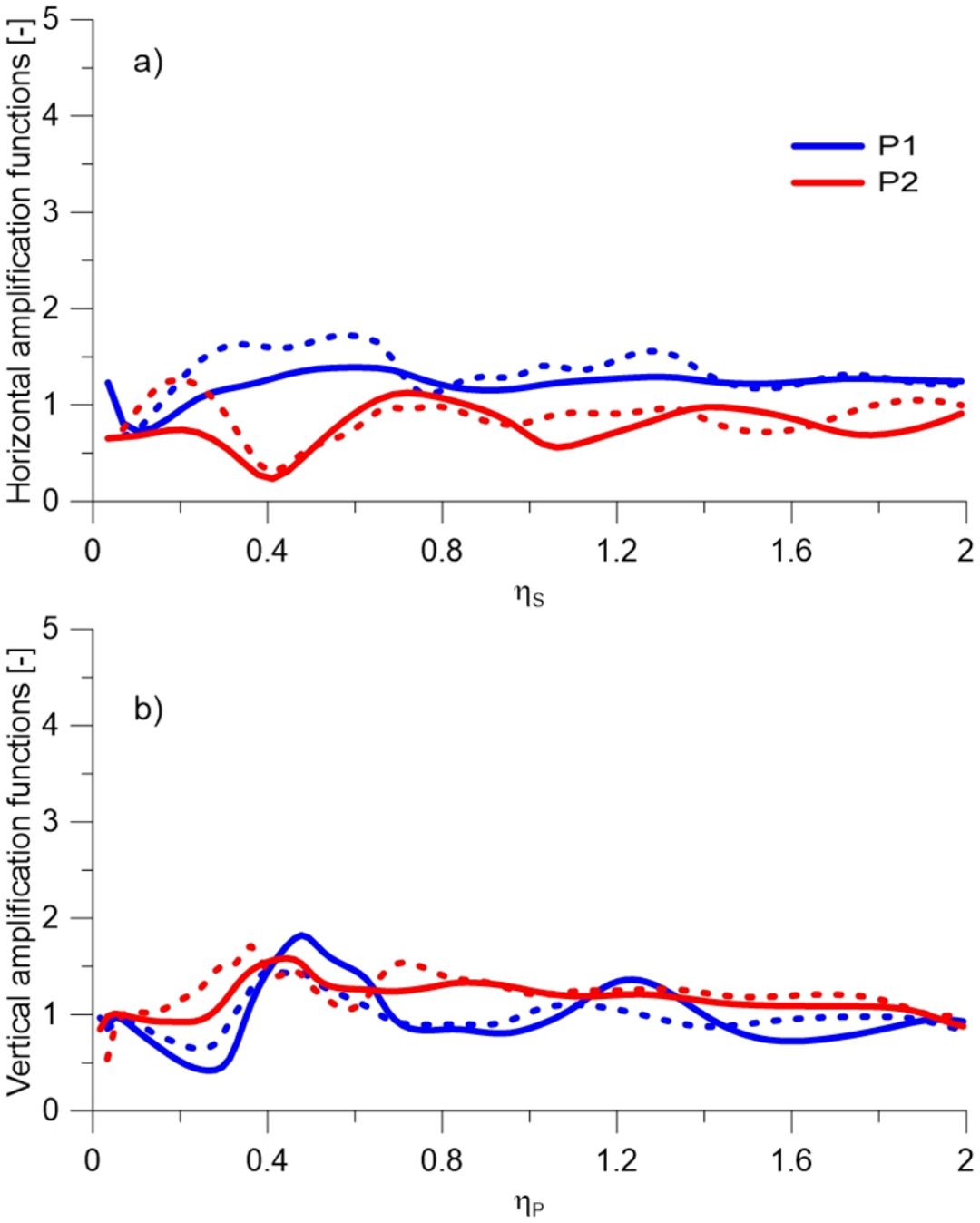

Figure 4.13: Comparison between 3D (solid lines) and 2D (dashed lines) amplification functions for semi-cylindrical canyon. a): horizontal component by applying incident S waves; b): vertical component by applying incident P waves

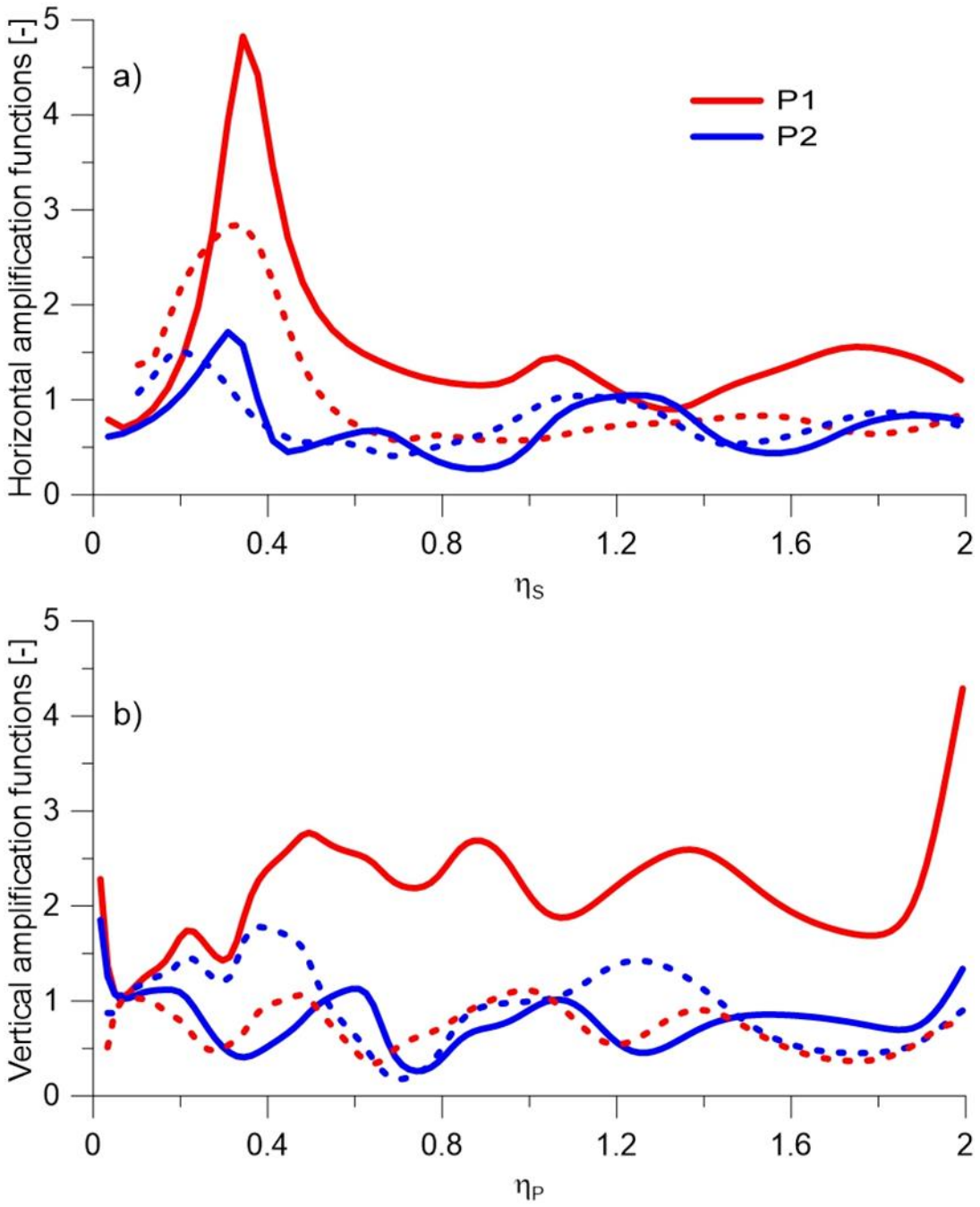

Figure 4.14: Comparison between 3D (solid lines) and 2D (dashed lines) amplification functions for semi-cylindrical hill. a): horizontal component by applying incident S waves; b): vertical component by applying incident P waves

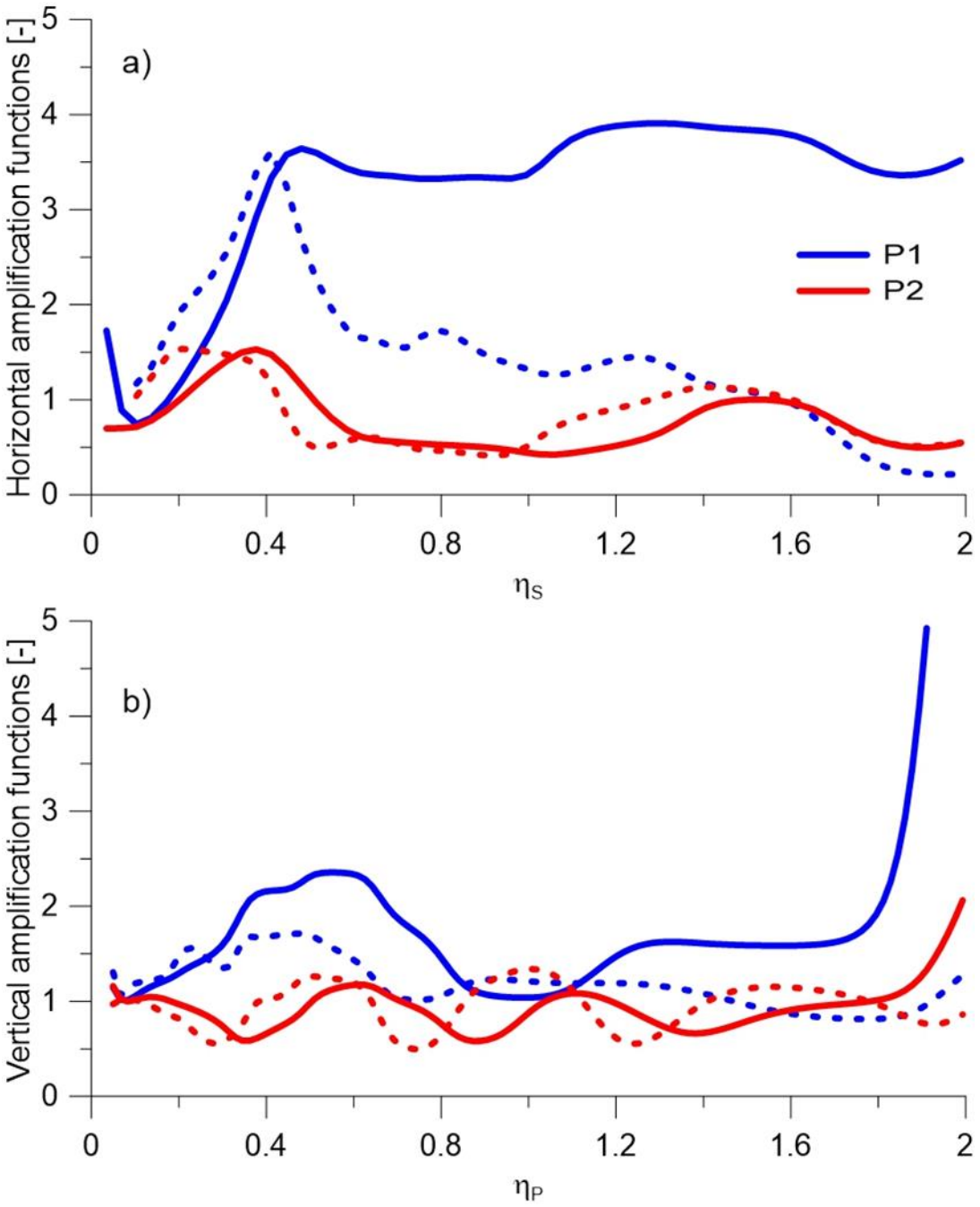

Figure 4.15: Comparison between 3D (solid lines) and 2D (dashed lines) amplification functions for cone. a): horizontal component by applying incident S waves; b): vertical component by applying incident P waves

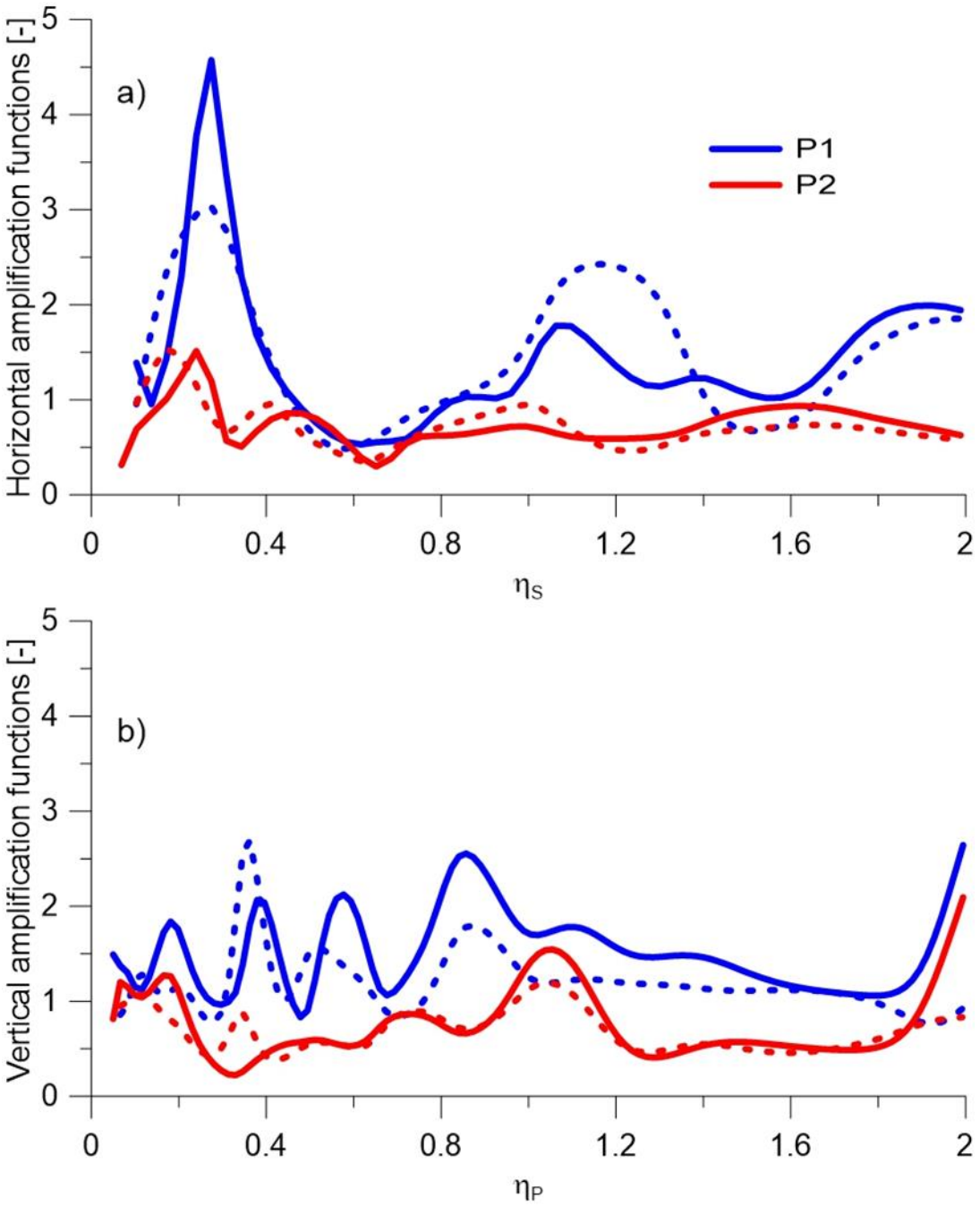

Figure 4.16: Comparison between 3D (solid lines) and 2D (dashed lines) amplification functions for cliff. a): horizontal component by applying incident S waves; b): vertical component by applying incident P waves

4.2 Earth dam of simple geometry

To evaluate the 2D and 3D dynamic response of earth dam, a trapezoidal shape was considered with shape-ratio L/H ≈ 2.0 (Figure 4.17). Figure 4.18 the 3D numerical grid, the transversal (red points) and longitudinal (yellow points) axes for comparison with bidimensional model are shown. In Table 4.5 the linear properties adopted for body dam and subsoil are reported.

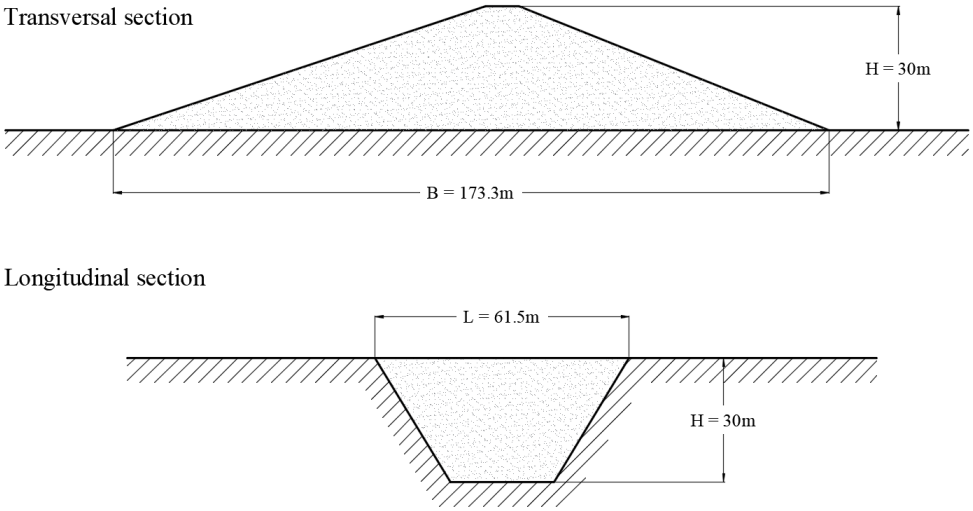

Figure 4.17: Simplified homogeneous trapezoidal earth dam; above: transversal section and below: longitudinal section.

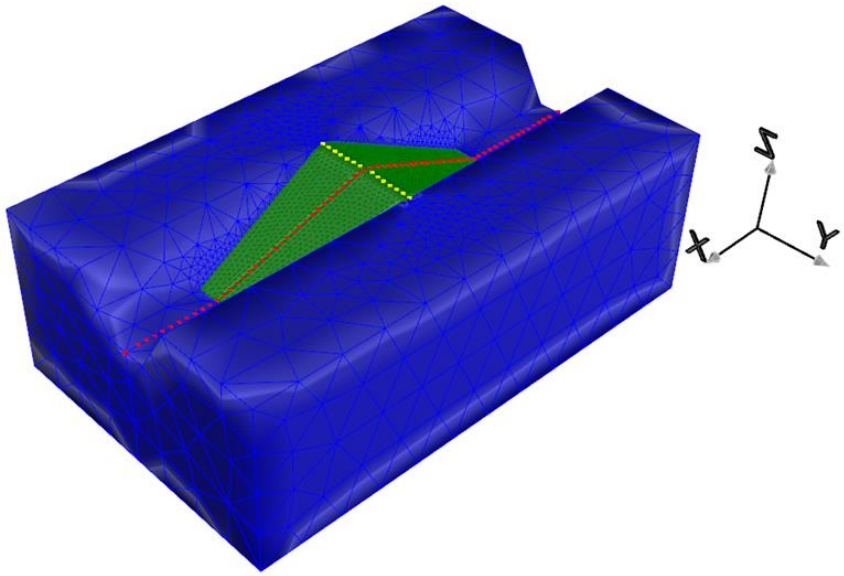

Figure 4.18: Simplified homogeneous trapezoidal earth dam; red points transversal axis and yellow points longitudinal one.

Table 4.5: Linear properties adopted for the model

Unit	γ	Vs	Vp	ν	D
[-]	[kg/m3]	[m/s]	[m/s]	[-]	[%]
dam	1600	200	416	0.35	1
subsoil	2200	1455	3028	0.35	1

The comparisons between 2D (dashed lines) and 3D (solid lines) numerical results, in terms of displacement ratio, along the transversal and longitudinal axes, are illustrated in Figure 4.19 and Figure 4.20, respectively. Three different load combinations has been considered: 1) Mod 1 (green lines) applying only horizontal motion along the axes X and Y; 2) Mod 2 (blue lines) as Mod 1 by adding the vertical component; 3) Mod 3 (red lines) applying the motion along the direction of the section. For Mod 1 and Mod 3 numerical results show: i) greater 2D amplification at low frequency compared to 3D (frequency shift presumably due to stiffening effect); ii) greater 3D amplification as compared to 2D, especially at medium frequency (f=5Hz); iii) the vertical parasitic component increases with frequency of input motion, in agreement with literature studies; iv) for Mod 2 the introduction of vertical input motion provide high amplifications especially at medium and high frequencies.

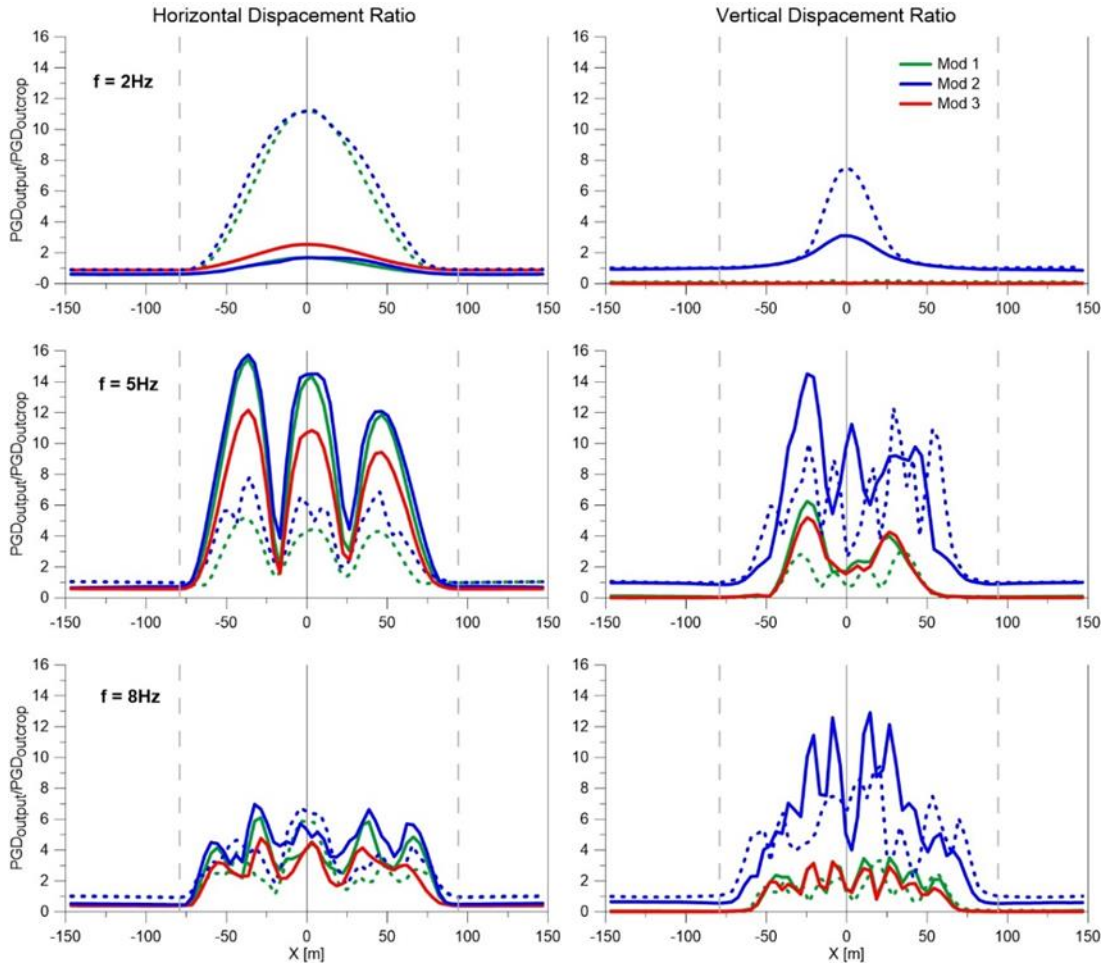

Figure 4.19: Comparison between displacement ratio at top of dam for transversal axis. Green lines (Mod 1) applying only horizontal motion along the axes X and Y; Blue lines (Mod 2) as Mod 1 with adding the vertical component; Red lines (Mod 3) applying the motion along the direction of the section. Solid lines 3D numerical results and dashed lines 2D numerical results.

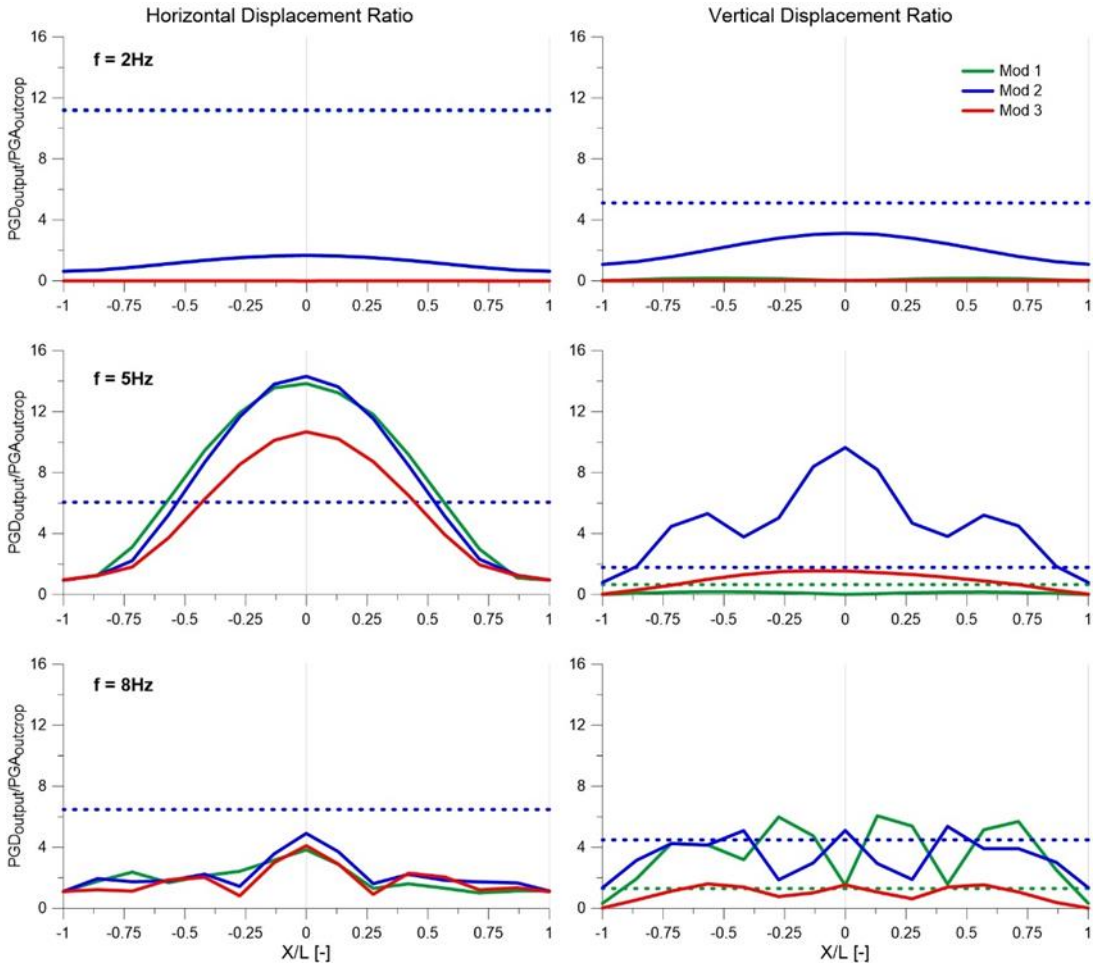

Figure 4.20: Comparison between displacement ratio at top of dam for longitudinal axis. Green lines (Mod 1) applying only horizontal motion along the axes X and Y; Blue lines (Mod 2) as Mod 1 with adding the vertical component; Red lines (Mod 3) applying the motion along the direction of the section. Solid lines 3D numerical results and dashed lines 2D numerical results

5 Cases Studies

5.1 Introduction

This chapter describes the numerical analyses carried oud to study the seismic response of two cases studies. The first refers to two earth dams constituting the Angitola reservoir in Southern Italy (Calabria) and the second concerns the Palatino hill the in historical center of Rome, a complex geological-geotechnical system comprehensive of alluvial valleys and topographic reliefs.

The principal aim of this work is to investigate the parameters that mostly affect the dynamic response for both 2D and 3D conditions. Therefore, detailed large scale 2D and 3D numerical grids were built. The analyses have been carried out with increasing complexity, starting from homogeneous simple models and successively increasing step-by-step the in-homogeneity characteristics of the subsoil. This procedure allowed to decouple the topographic amplification from the stratigraphic one.

The effect of the frequency input motion and its direction (horizontal and vertical components) has also been investigated. Two seismic scenarios were considered:

1. motion applied along the two principal horizontal directions (EW and NS) by using three input frequencies (f = 2, 5 and 8 Hz);
2. as above, adding the vertical component; this was assumed equal to half horizontal amplitude and frequency 45% larger than horizontal one.

The first scenario allows to study the far field condition and the vertical parasitic component in the frequencies range 1-10Hz (considered significant from engineering point of view), the second one the effects of vertical component, typically of near field conditions.

The choice of the input motion for parametric studies is dictated by the need to use a synthetic signal characterized by a low impulsive Fourier spectrum around the predominant frequency. In all cases a Chang wavelet was applied at base of the models as outcrop motion (Figure 5.1).

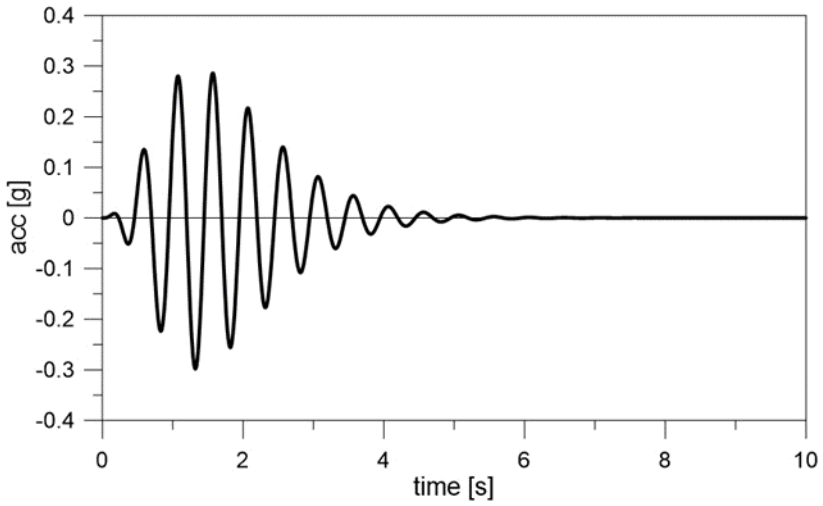

Figure 5.1: Chang wavelet used for numerical simulations

The three-dimensional numerical simulations were performed by applied each component along the principals directions of models (North-South, East-West and Up-Down) separately. The total motion for each frequency were obtained applying the superposition effects; the motion was rotated along appropriate sections for comparisons with bidimensional ones. The comparisons are in terms of ratio between a synthetic motion parameter at the top of the models and the corresponding input outcrop. The parameter considered is acceleration ratio for Palatino hill (PGAoutput/PGAoutccrop) and displacement ratio for Angitola lake embankment (PGDoutput/PGDoutccrop). Dynamic analyses are linear visco-elastic (using Rayleigh formulation), by using the finite difference code FLAC3D. In choosing the element size, the standard rule suggested by Kuhlemeyer and Lysmer (1973) was adopted to achieve a satisfactory level of solution accuracy. These authors define hmax = Vs/(8fmax), where Vs = material shear wave velocity value selected accordingly to the shear strain level, hmax=maximum element height, and fmax = maximum frequency to be transmitted (assumed equal to 10 Hz).

5.2 The Palatino Hill in the Historical center of Rome

5.2.1 Background

The Palatino hill, Roman Forum and archaeological Colosseum area are a reasonably well documented case study because of the availability of data and information on geological characteristics of the area, geophysical and geotechnical properties of soil and rock materials as well as 1D and 2D seismic response analyses that can be derived from a previous extensive research investigation (Moscatelli et al 2013, Pagliaroli et al 2014). Figure 5.2 shows the study area and the two cross sections A (red line) and B (blue lines) used for comparison between 2D and 3D numerical results.

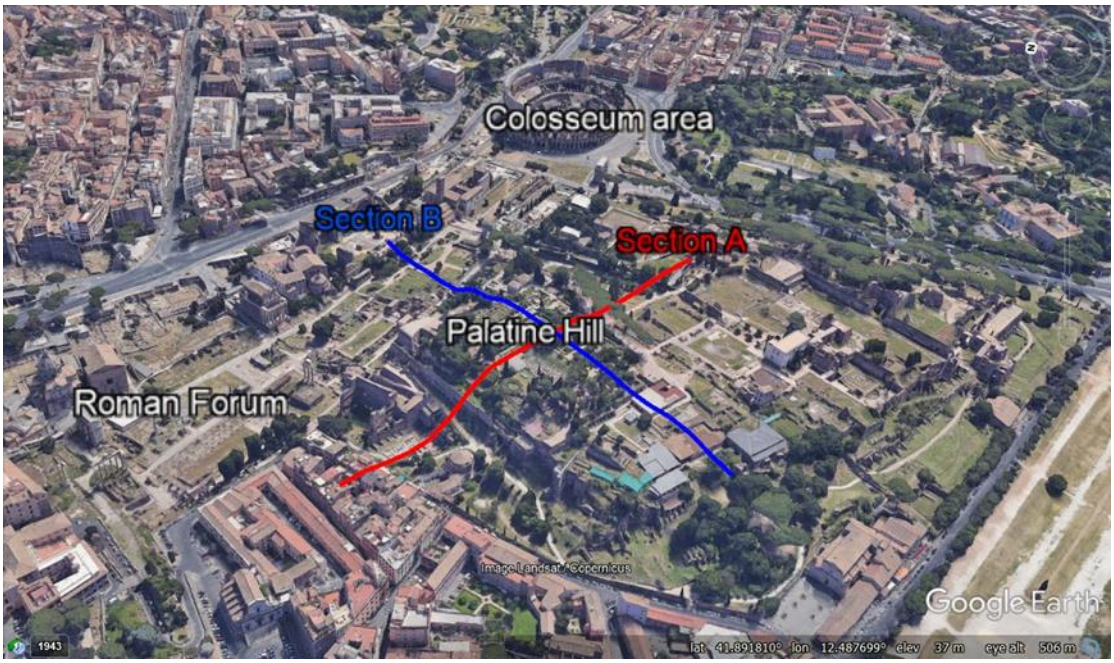

Figure 5.2: Palatino hill, Roman forum and archaeological area of Rome and two cross section considered in the analyses, Section A (Red line) and section B (Blue line)

In the next sections are shown: i) the geological setting and FLAC3D numerical grid; and ii) 2D and 3D numerical results obtained by considering three simplified models of increasing complexity to study the main parameters affecting the seismic response.

5.2.2 Integrated subsoil model and geological setting

5.2.2.1 Stratigraphic setting of Palatine hill and surrounding area

The Palatine area is presently covered by a thick blanket of anthropic origin. As a matter of fact, the original environment of the hill and surroundings is completely lost because of the anthropic reworking during the last 3000 years. Nevertheless, the original topography of the hill should have resembled that of the present day rises in the Latium region, north of Rome:

almost flat plateaus bordered by steep slopes and surrounded by narrow and elongated alluvial valleys. A thick section of alternating sedimentary and volcanic continental deposits of Quaternary age constitute the framework of the Palatine, and locally crops out along the north-western slope of the hill.

The geological bedrock of Palatine hill and surrounding areas is constituted by a Pliocene sandy-clayey unit of marine origin, the Monte Vaticano Formation (Funiciello and Giordano 2008), that was drilled just south of the Palatine hill by the Circo Massimo exploration borehole in the 1930s (Signorini 1939), for a total thickness of about 900 meters. The Quaternary complex covering the Monte Vaticano Formation is constituted by fluvial-palustrine and distal volcanic deposits belonging to six superimposed formations12, which are mainly middle Pleistocene in age: 1) Santa Cecilia (CIL) and Valle Giulia (VGU) Formations; 2) Palatine Unit (PTI); 3) Prima Porta Unit (PPT); 4) Fosso del Torrino Formation (FTR); 5) Villa Senni Formation (VSN); 6) Aurelia Formation (AEL). These formations show a sub-horizontal multilayer vertical arrangement except for the Fosso del Torrino Formation (FTR), filling a paleo-valley deeply cutting the previous Quaternary units in the eastern portion of the Palatine hill.

Finally, all the previous units were curved by local tributaries of the Tiber River during the last Late Quaternary sea-level fall, giving rise to deep (up to 70-80 meters) and narrow alluvial valleys confined by steep slopes joining the hilltop plateaus (Marra and Rosa 1995a,b): the Velabro, Labicano, and Murcia valleys to the west, east, and south of the Palatine hill, respectively. These valleys were filled during the Holocene see level rise mainly by clayey deposits (SFTa), and are presently buried by anthropogenic deposits (RPI) locally reaching the thickness of 20 m.

5.2.2.2 Subsoil model for site-response analysis

This case study combines all the most important aspects that can determine the presence of amplification phenomena. In fact, modification of the characteristics of the incoming ground motion can arise from the presence of layers of different physical and mechanical properties and thickness, the presence of two valleys filled with recent alluvial sediments, the various buried morphology of the seismic bedrock as well as the occurrence of a non-flat topographic surface. All these conditions can lead to complex two or three-dimensional effects.

To define the subsoil model of the Palatine hill, two aspects are highlighted in the following of this section: i) definition of subsoil stratigraphy, and ii) identification of the seismic bedrock.

5.2.2.3 Definition of the lithotype scheme and FLAC3D numerical grid

All the different formations recognized in the study area have been interpreted in terms of lithofacies mainly based on their sedimentological features (Mancini et al. 2014; Moscatelli et al. 2014). In relation to the results of in situ and laboratory geotechnical tests (in terms of unit weight γ, shear wave velocity VS, and Poisson ratio ν), for each formation the lithofacies have been then grouped in lithotypes, in Figure 5.3 and Figure 5.4 are shown the two cross-sections and the 3D model, respectively. Each lithotypes are characterized by homogeneous physical properties (i.e., grain size distribution, unit weight, plasticity index), and by a quite similar behavior under static loading conditions. The linear properties adopted are summarized in Table 5.1 (modified after Pagliaroli et al. 2013). Nine main units were defined to perform numerical modelling. With respect to the lithostratigraphic divisions recognized in the Palatine area, it is important to underline the following peculiarities of the lithotype scheme:

- CIL and VGU are homogeneous in terms of physical and mechanical properties; so, for sake of simplicity, they were grouped in the same unit (CIL) and differentiated in terms of texture: sandy pebbly (CIL1) and silty sand (CIL1_2);
- PTI and PPT tuffs, due to their lithological and geometric features, are difficult to distinguish in terms of their contribute to the site-response; they were consequently unified in the PTI_PPT unit;
- VSN tuffs were differentiated in terms of degree of welding, by distinguishing a massive lithotype (VSN1a) and a pozzolanaceous lithotype (VSN1b);
- AEL, because of its reduced thickness (1 to 3 meters), was grouped with the anthropogenic deposits, RPI.

The MVA overconsolidated clays, geological bedrock of the whole Roman area, are characterized by an average shear wave velocity of about 500 m/s in the upper tens of meters, directly investigated by geophysical tests. This value is lower than 800 m/s usually assumed for the seismic bedrock where the seismic input motion is applied in the site response analyses.

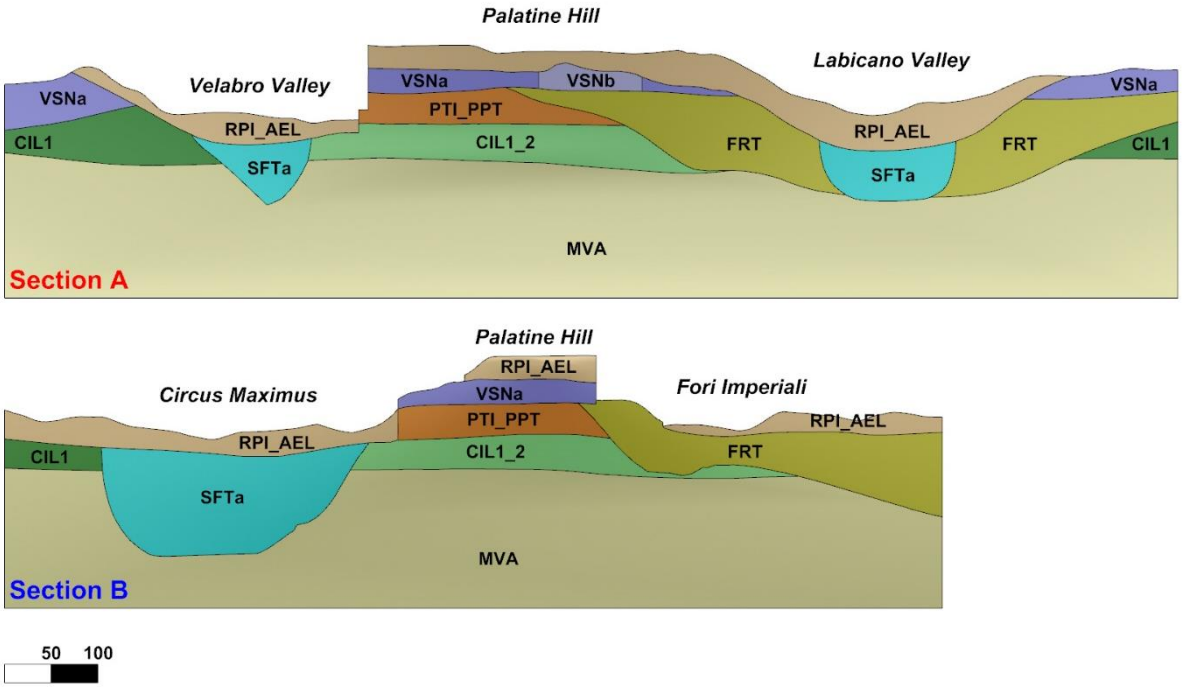

Figure 5.3: Cross sections A (upper plot) and B (bottom plot).

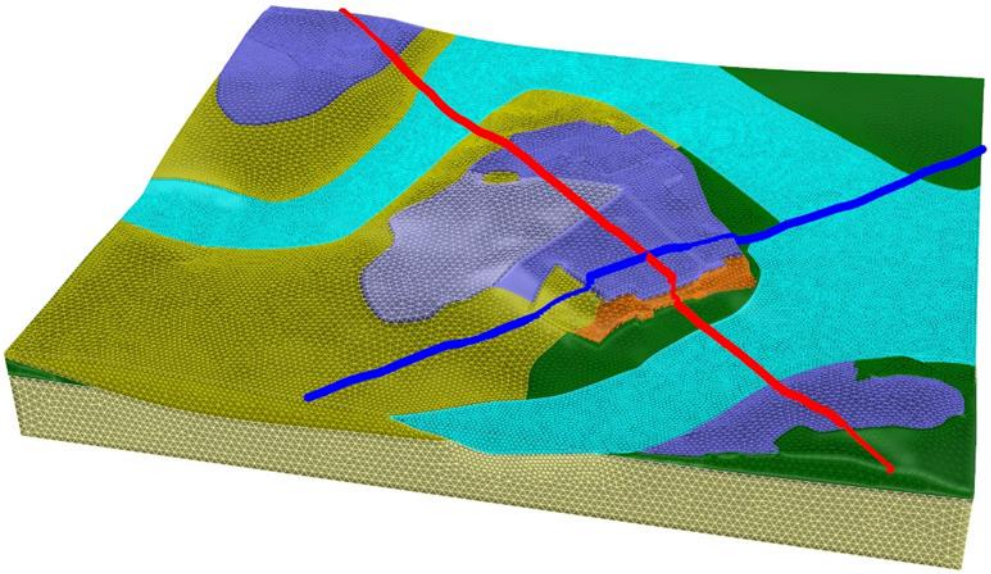

Figure 5.4: Three-dimensional model of Palatino hill, Roman Forum and archaeological area of Colosseum. Red line section A and blue line section B.

Table 5.1: Linear properties of geotechnical units

Lithotype	Symbol	γ	VS	ν
	[-]	(kN/m3)	(m/s)	(–)
Brick walls and conglomeratic	RPI_AEL	18.0	350	0.42
Clayey-silty fluvial deposit	SFTa	18.5	270	0.49
Massive lithoid tuff	VSN1a	16.0	600	0.4
Pozzolanaceus tuff	VSN1b	19.7	340	0.48
Tuff	PTI_PPT	16.0	650	0.39
Silty, sandy silty	FTR	20.1	510	0.465
Silty sand	CIL1_2	20.1	480	0.435
Sandy pebbly	CIL1	20.5	620	0.39
OC marine clay	MVA	20.5	550	0.48

In Figure 5.5 and Figure 5.6 are shown the FLAC3D numerical grids for 3D numerical results.

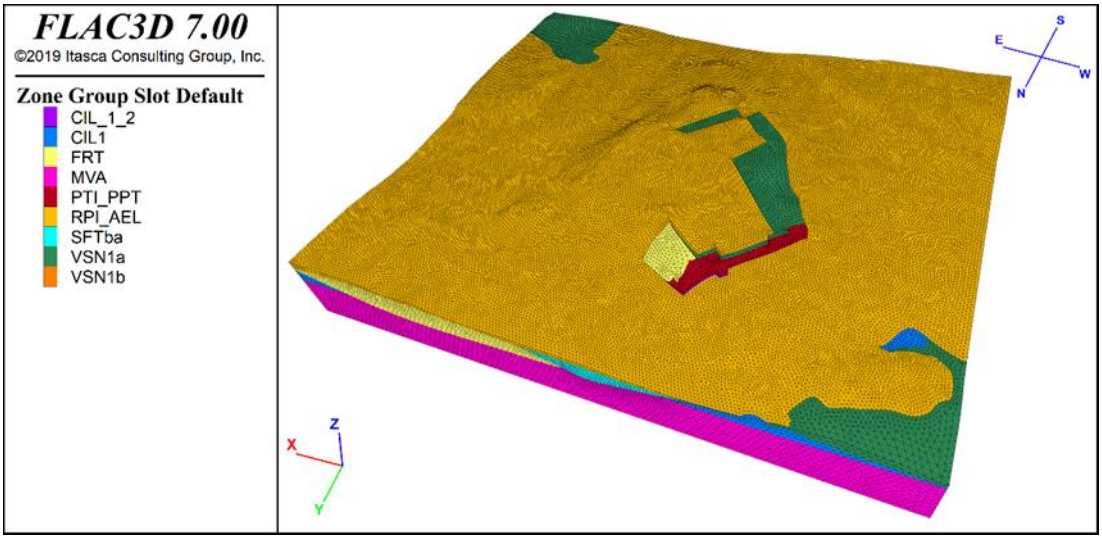

Figure 5.5: FLAC3D numerical grid for Palatino hill and surrounding areas.

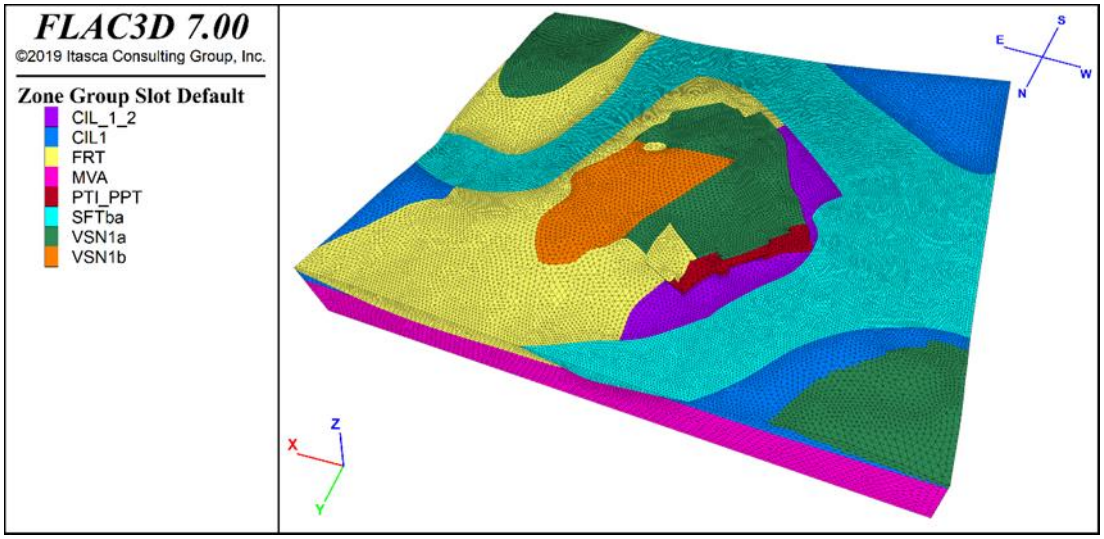

Figure 5.6: FLAC3D numerical grid for Palatino hill and surrounding areas without cover layer RPI-AEL.

Three simplified models with increasing complexity, obtained by merging some units, were considered in order to study some of the parameters that affect the dynamic response:

- Homogeneous model, obtained by merging all units, that take into account the topographic effects;
- Bi-Layer model, obtained by merging all units except the cover layer (RPI_AEL), that take in to account its effect on dynamic response;
- Bi-Layer + sediment-filled valleys model, obtained by merging all units except the cover layer (RPI_AEL) and the valley bordering the Palatino hill (SFTa), to study the effect of soft incises valleys.

The simplified models studied are shown in Figure 5.7 and Figure 5.8 for section A and B respectively.

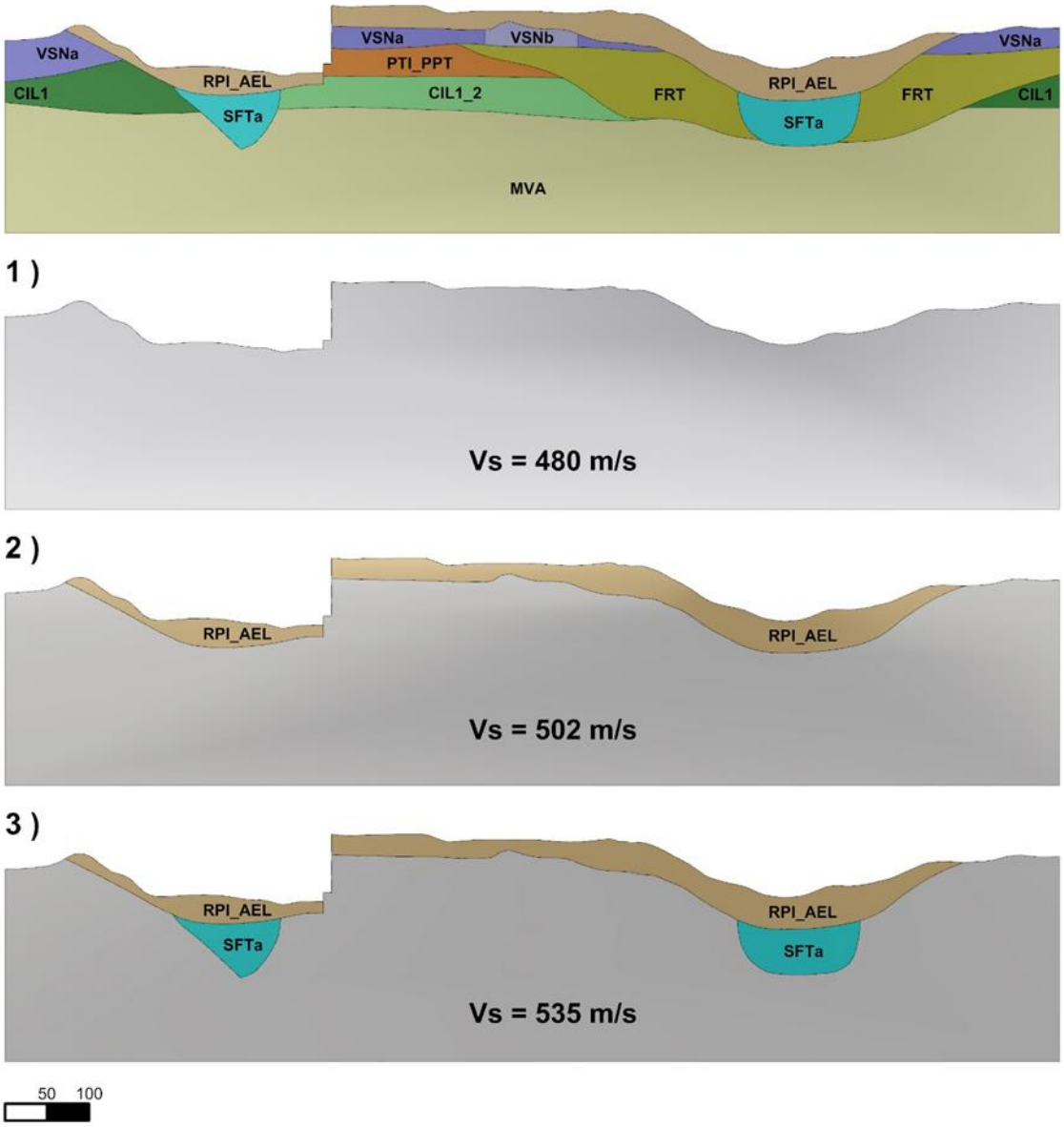

Figure 5.7: Simplified models of section A (upper plot); 1) Homogeneous model; 2) Bi-Layer model and 3) Bi-Layer + sediment-filled valley model

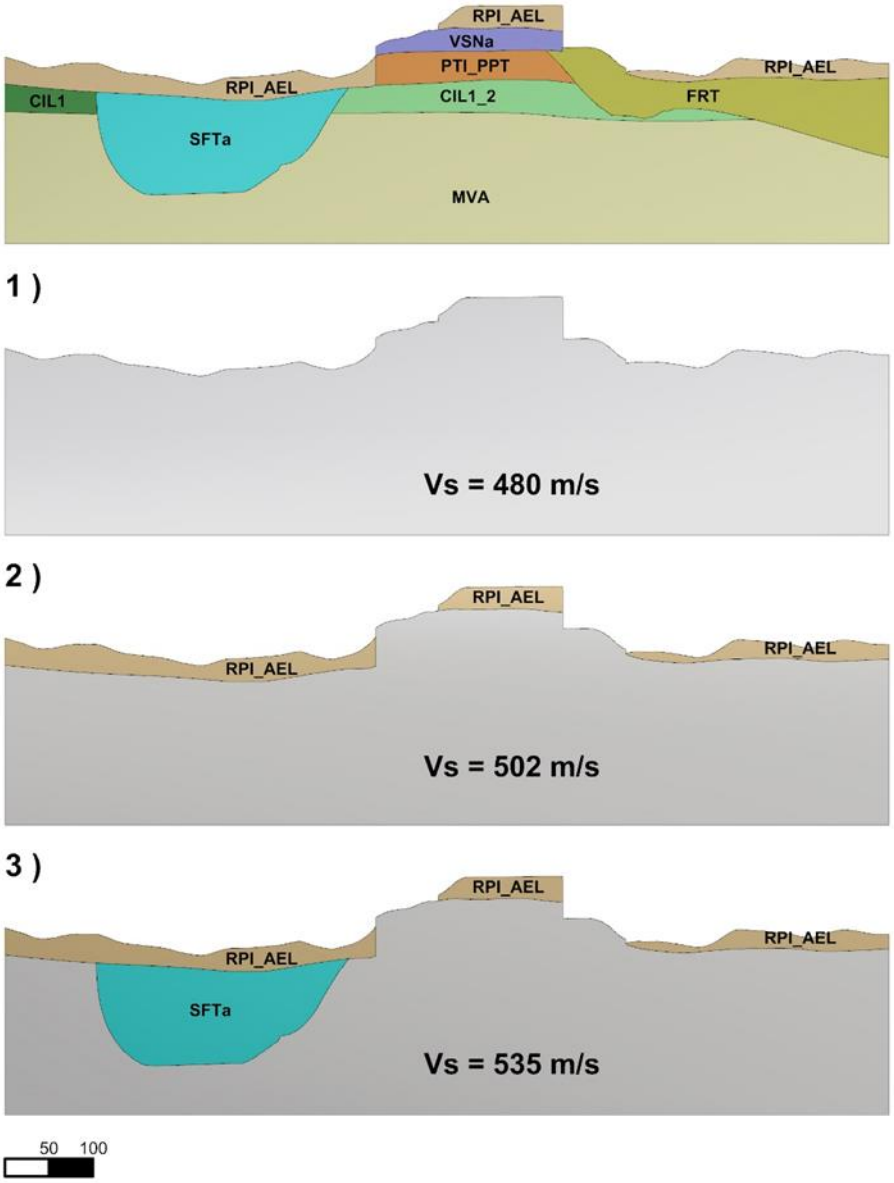

Figure 5.8: Simplified models of section B (upper plot); 1) Homogeneous model; 2) Bi-Layer model and 3) Bi-Layer + sediment-filled valley model

5.2.3 Homogeneous model

The Homogeneous model was obtained by merging all units and assigning the model an average the average shear wave velocity Vs=480 m/s (Figure 5.9). This model was studied to take into account only topographic effects.

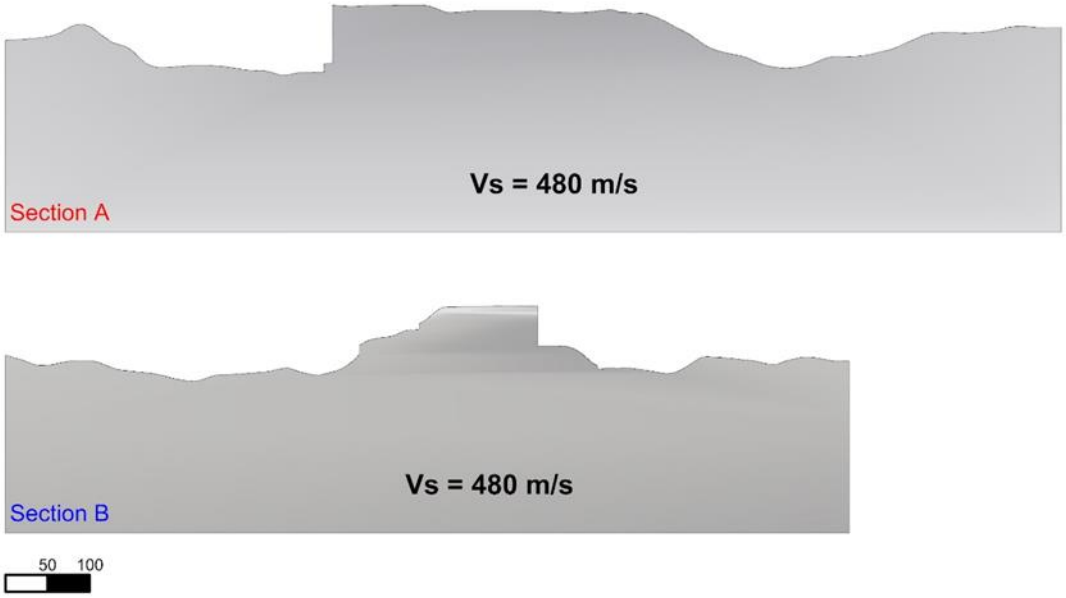

Figure 5.9: Homogeneous model, section A (upper plot) and section B (bottom plot).

Two seismic scenarios were considered: 1) only EW and NS components; 2) application of a motion parallel to the sections. The comparisons between 2D and 3D numerical results are in terms of ratio between maximum accelerations at top of model (PGA_{OUTPUT}) and the corresponding input outcrop ($PGA_{OUTCROP}$). In Figure 5.10 and Figure 5.11 are shown, for section A and B respectively, the numerical results both for 2D and 3D models as dashed and solid lines, respectively. The comparisons shown that:

- 3D results are greater than 2D ones regardless of frequency;
- the vertical (parasitic) component increases with frequency especially for 3D in correspondence of Palatino slope; it is generally less than one except for section B at f = 8Hz.

By applying the motion parallel to the sections, the comparisons shown that there are no appreciable differences between 3D and 2D analyses. Table 5.2 show the maximum amplification ratios, as high as 2 for three-dimensional model and 1.2-1.4 for bi-dimensional ones.

Table 5.2: Maximum amplification ratio for homogeneous model

	Section A			Section B		
	2D	3D	3D/2D	2D	3D	3D/2D
2Hz	1.19	1.79	1.499	1.38	2.08	1.511
5Hz	1.38	2.00	1.447	1.41	2.00	1.418
8Hz	1.36	1.73	1.280	1.35	2.12	1.574

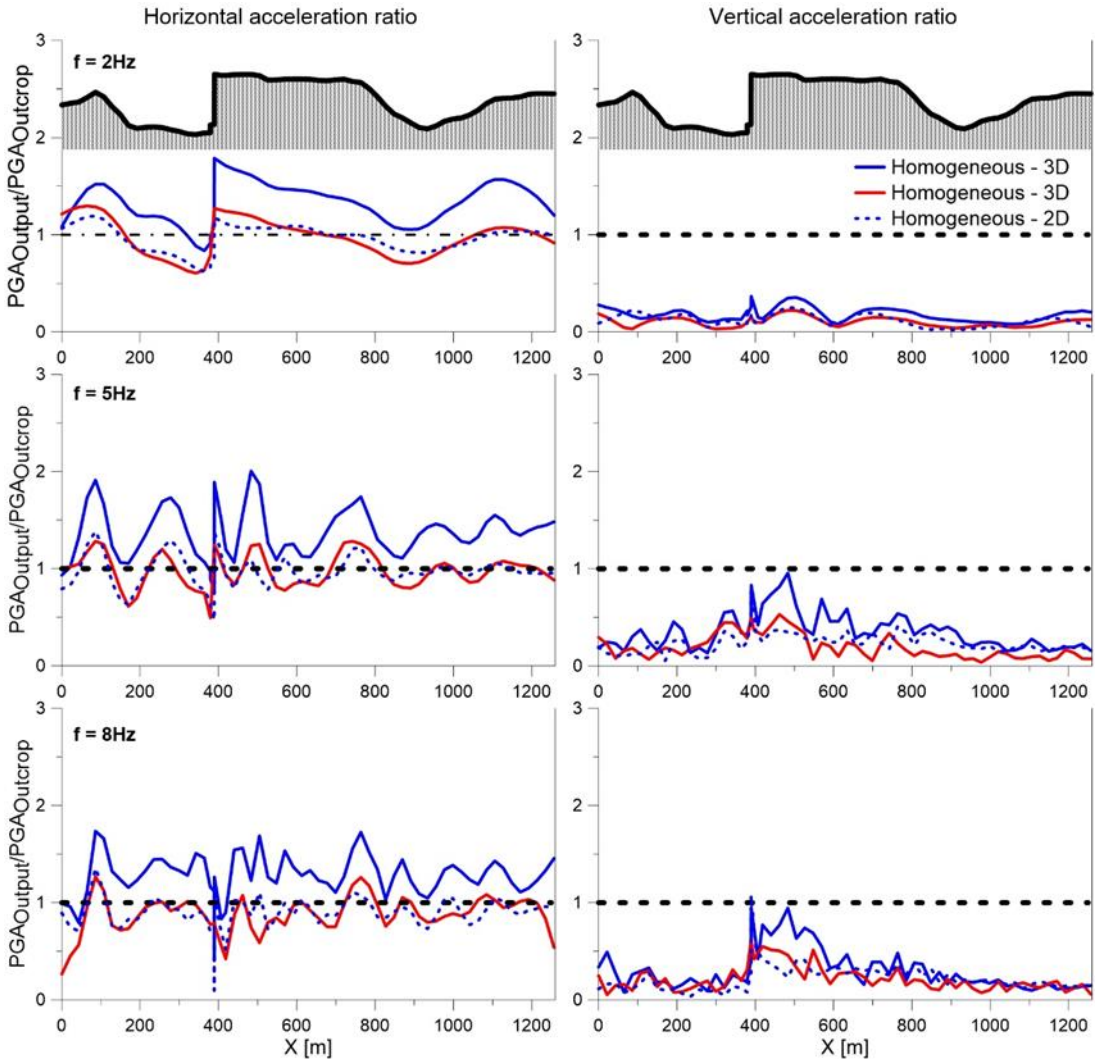

Figure 5.10: Comparison between 3D (solid lines) and 2D (dashed lines) acceleration ratio at top of model for section A. Blue lines: numerical results obtained applied the motion in E-W and N-S directions; red lines: applied the motion parallel to the section.

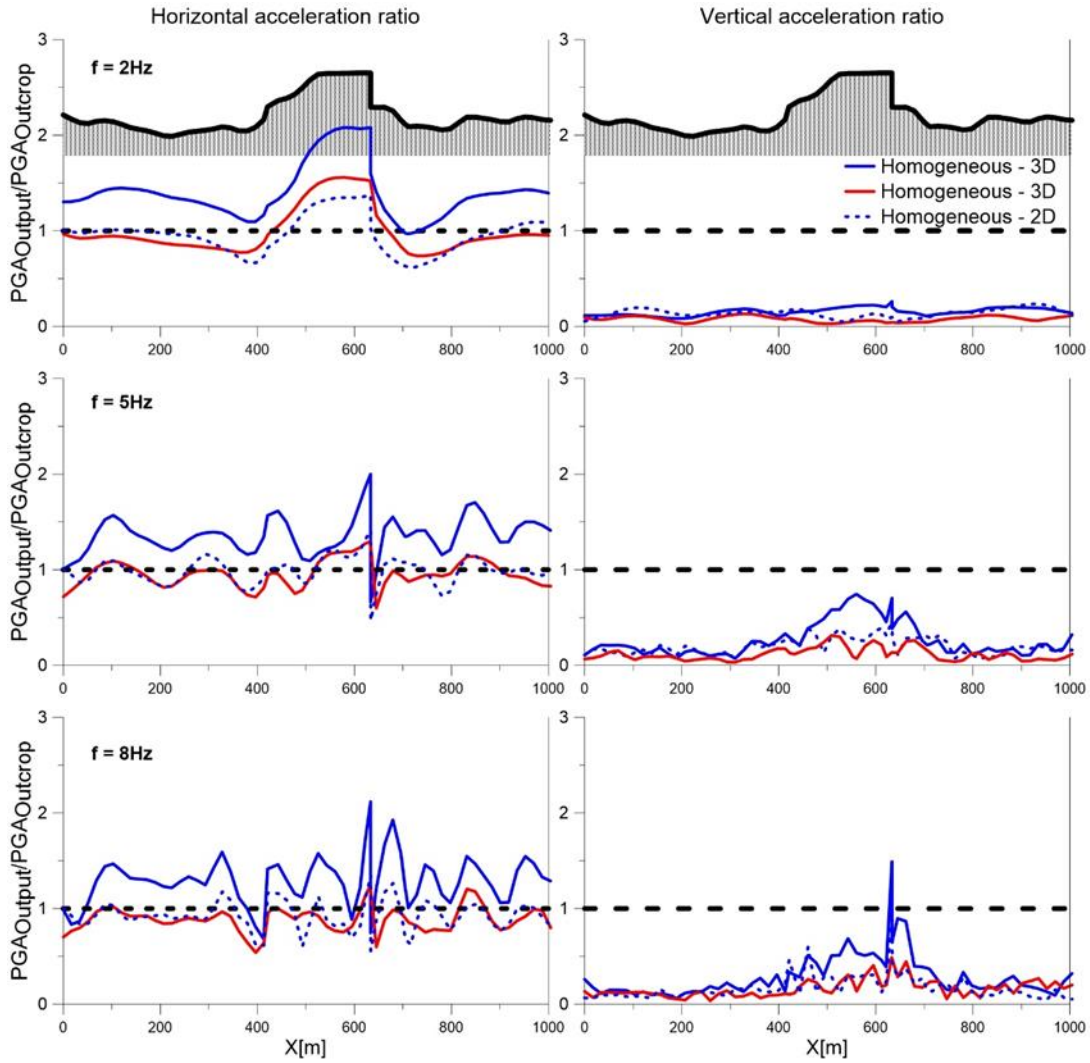

Figure 5.11: Comparison between 3D (solid lines) and 2D (dashed lines) acceleration ratio at top of model for section B. Blue lines: numerical results obtained applied the motion in E-W and N-S directions; red lines: applied the motion parallel to the section.

5.2.4 Bi-Layer model

In order to evaluate the effect of surficial layers on dynamic response, a Bi-Layer model has been studied (Figure 5.12). This model was obtained by merging all units except the cover layer RPI_AEL with shear wave velocity Vs,RPI_AEL=350m/s and maximum thickness hRPI_AEL≈10m. Its first natural frequency is fRPI-AEL = Vs,RPI_AEL/(4*hRPI_AEL) = 8.75 Hz.

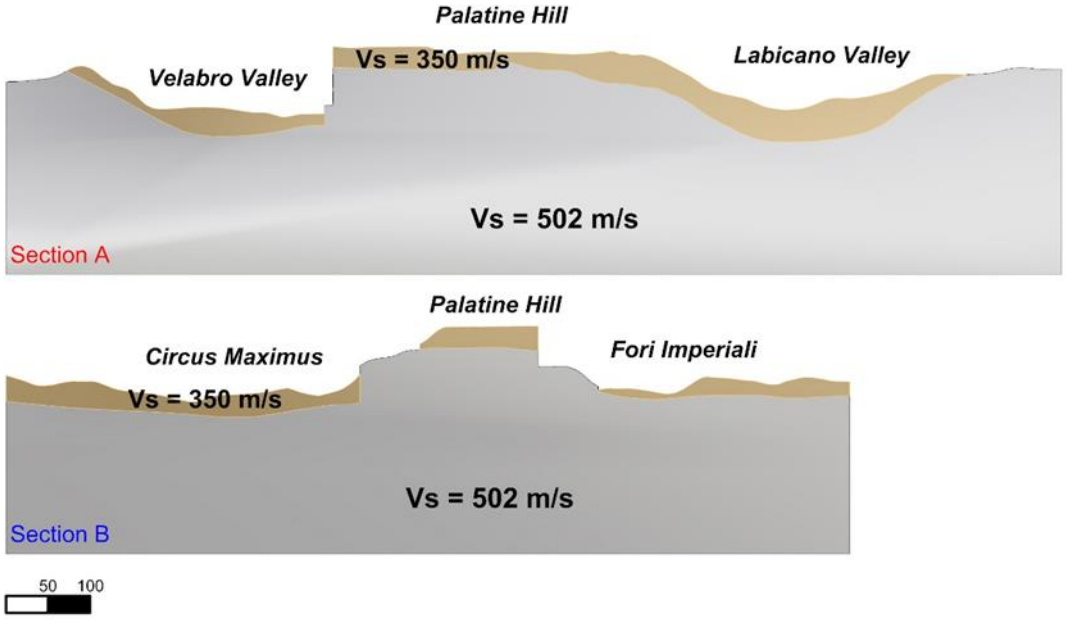

Figure 5.12: Bi-Layer model, above section A and below section B

In Figure 5.13 and Figure 5.14 are shown the bi- and three-dimensional numerical results for Bi-Layer model (brown lines) and the comparison with homogeneous one (blue lines) for section A and B respectively. The 3D Bi-Layer model provides: 1) greater amplitudes as compared to 2D ones, the maximum horizontal component amplification is as high as 5.0 for f = 8Hz (near the first natural frequency of the cover layer $f_{RPI\text{-}AEL}$ = 8.75Hz); 2) the vertical parasitic component amplitudes are two- to three times the amplitude of input motion for f = 5Hz and 8Hz, respectively in correspondence of the Palatino slope.

The comparison with homogeneous model shows that there are no appreciable differences at low frequency (f = 2Hz) both for 2D and 3D models, but for f = 5 and 8 Hz three-dimensional amplitudes are greater than those of the Homogeneous model, especially at high frequencies.

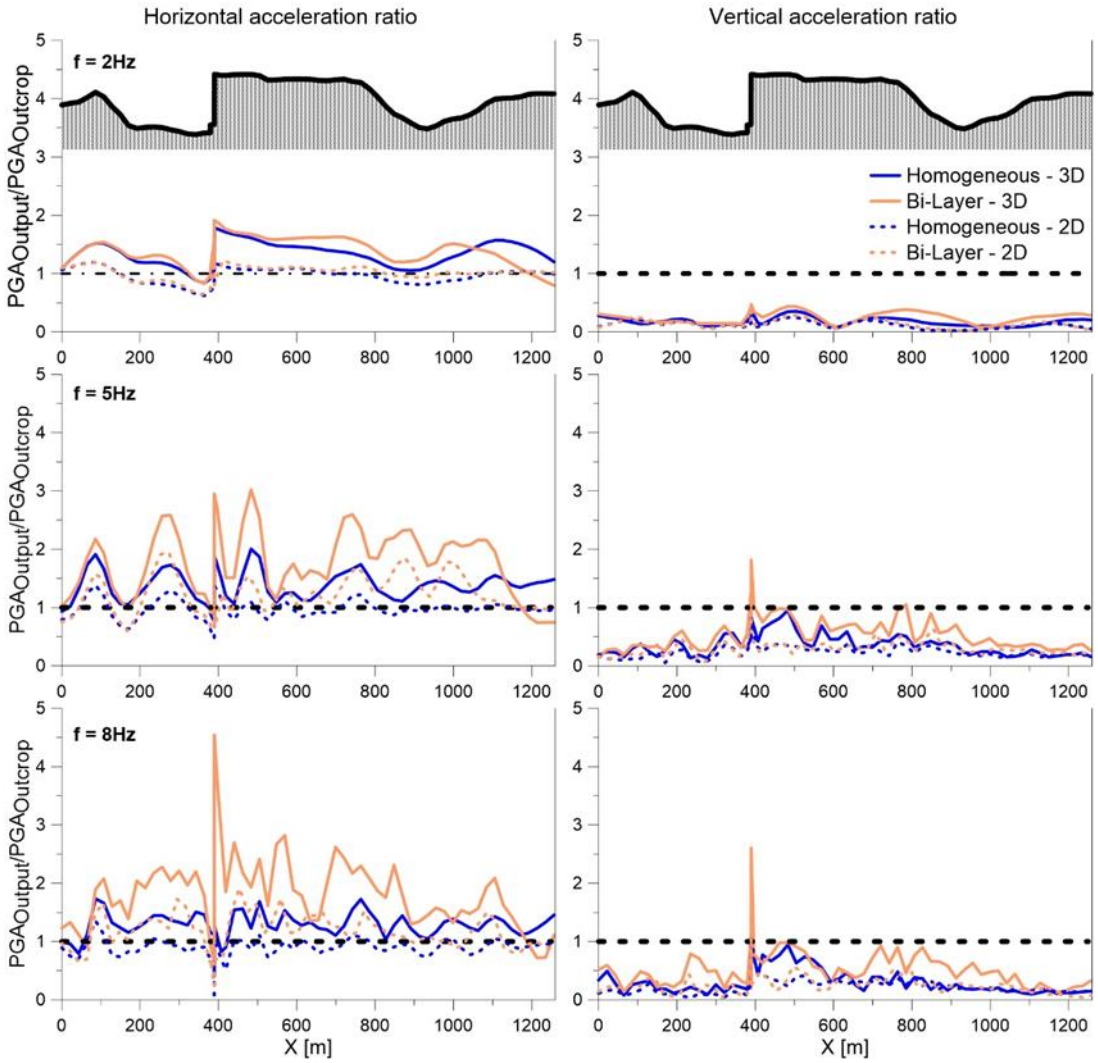

Figure 5.13: Comparison between Homogeneous model (blue lines) and Bi-Layer model (brown lines) for section A. Solid lines 3D numerical results and dashed lines 2D ones.

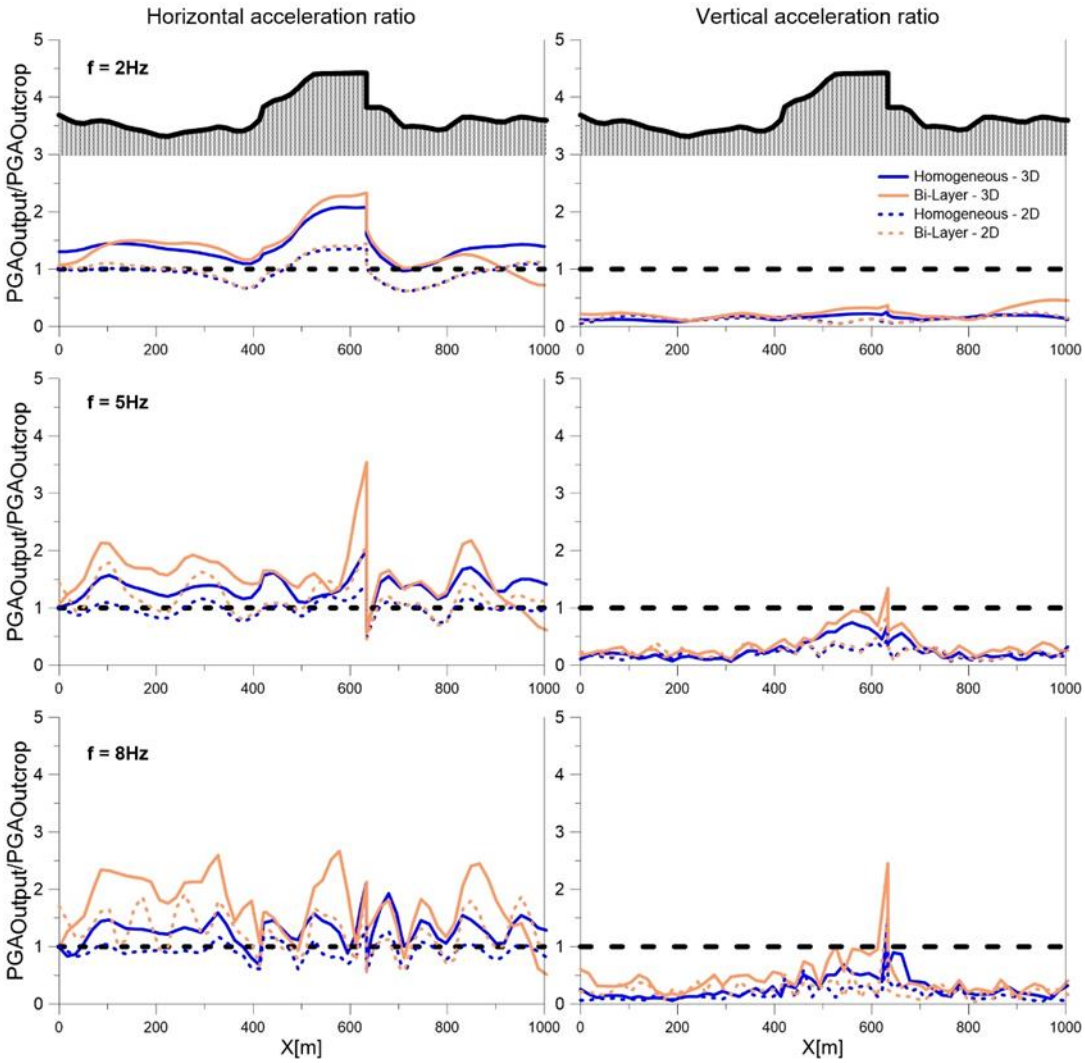

Figure 5.14: Comparison between Homogeneous model (blue lines) and Bi-Layer model (brown lines) for section B. Solid lines 3D numerical results and dashed lines 2D ones.

5.2.5 Bi-Layer + sediment-filled valleys model

In order to take into account the sediment-filled valleys on dynamic response of Palatino hill and surrounding area, another model was developed obtained by merging all units except the cover layer (RPI_AEL) and the sediment-filled valleys (SFTa) (Figure 5.15).

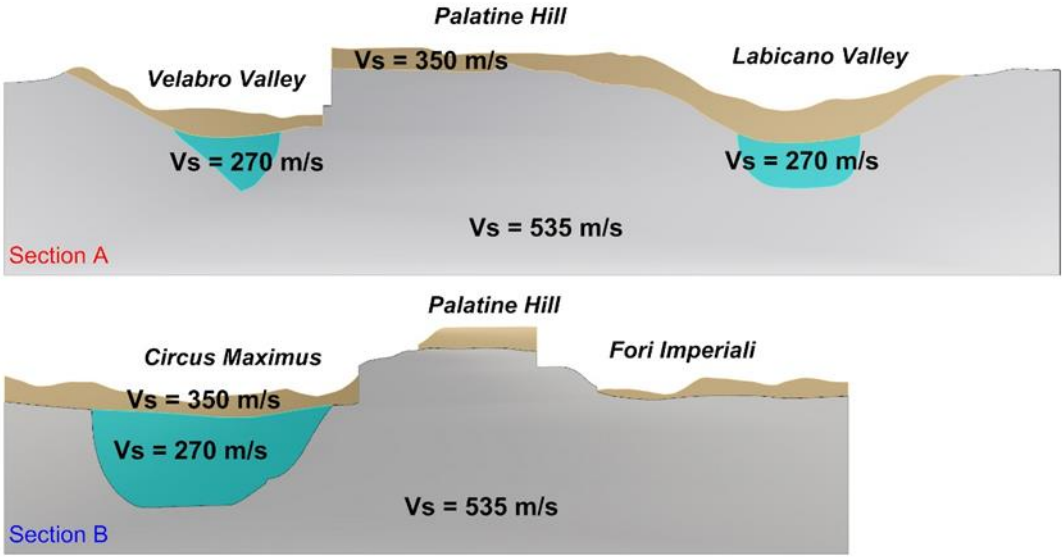

Figure 5.15: Bi-Layer + sediment filled valleys model, above: section A and below: section B.

The valleys are characterized by a semi-elliptical shape with variable depth and shear wave velocity Vs = 270 m/s. Along section A the depth and half-width are about 20 m and 65 m respectively while for section B the depth is about 40 m and the half-width 120 m. Therefore, along the two sections the valley has the same shape-ratio h/l ≈ 0.3. The velocity contrast between merged units and the valleys is 1.98. Therefore, 1D resonance + lateral propagation phenomena in according to Bard & Bouchon (1985) are expected (see Chapter 2)

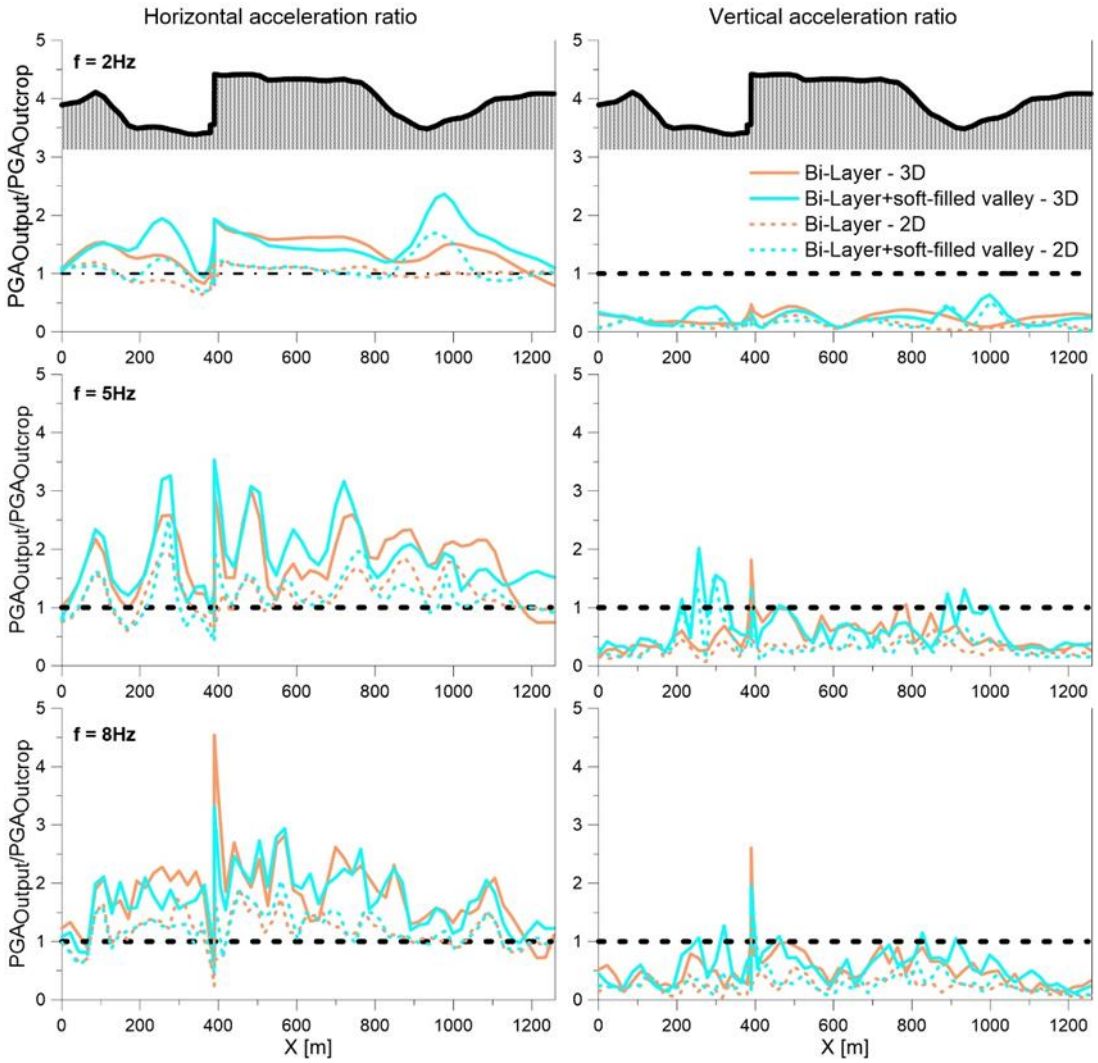

Figure 5.16: Comparison between Bi-Layer model (brown lines) and Bi-Layer+soft filled valley model (cyan lines) for section A. Solid lines three-dimensional numerical results and dashed lines bi-dimensional ones.

In Figure 5.16 and Figure 5.17 are shown the comparisons between the previous Bi-layer model and Bi-Layer+sediment-filled valley model for section A and B, respectively. The introduction of sediemnt-filled valley along cross section A and B provides no appreciable difference with bi-layer model except at low frequency (f=2Hz) in correspondence of the valleys both for 2D and 3D numerical results. This is presumably related to the resonance frequency of valley which is around 2.5-3.0 Hz.

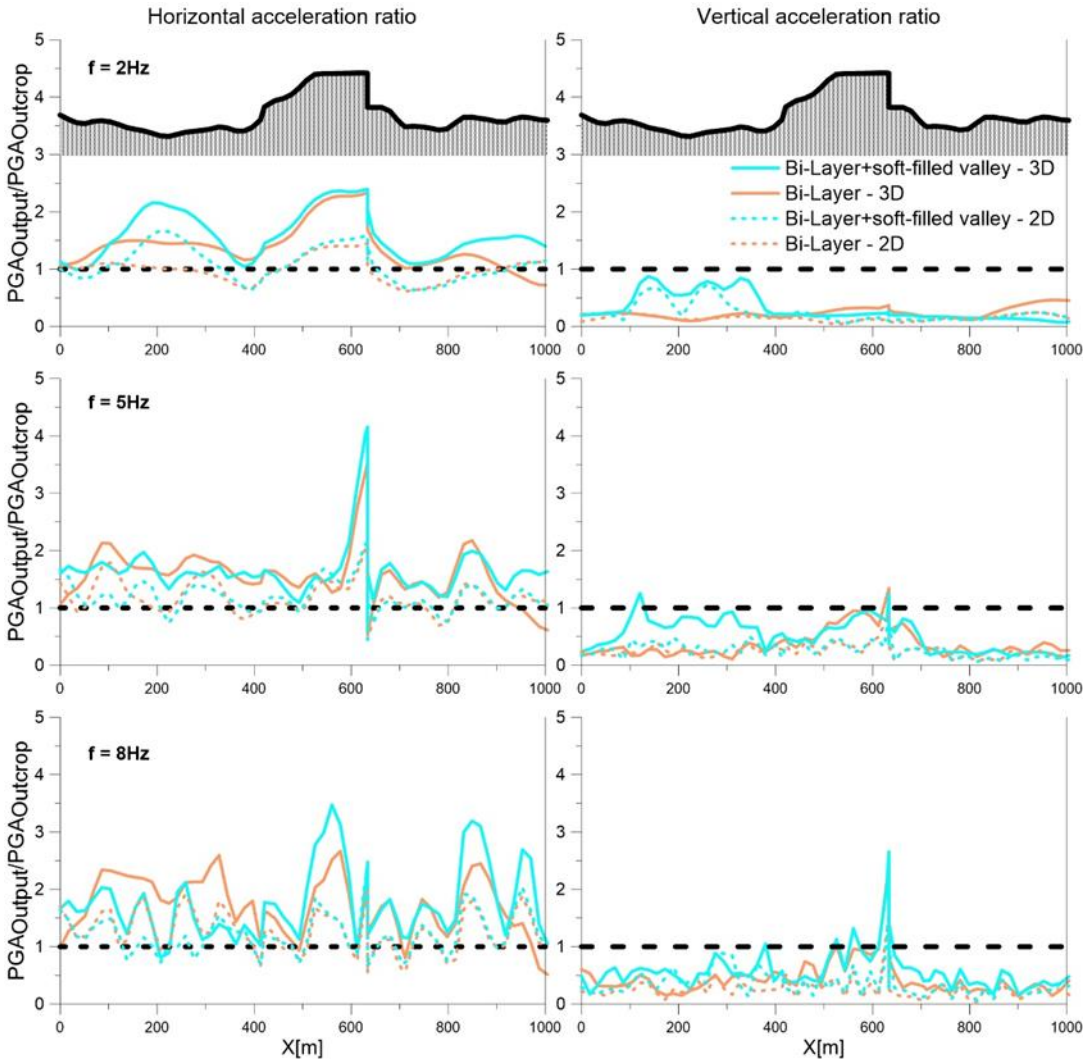

Figure 5.17: Comparison between Bi-Layer model (brown lines) and Bi-Layer+soft filled valley model (cyan lines) for section B. Solid lines three-dimensional numerical results and dashed lines bi-dimensional ones.

5.2.6 Complete model

The numerical results presented in the preceding paragraphs, obtained by applying only horizontal input motion, show that the topographic amplification ratios are 1.8-2.0 and 1.2-1.4 for 3D and 2D conditions, respectively. The introduction of cover layer (RPI-AEL) provides the greater amplifications ratio (up to 5.0), especially at medium and high frequencies, and the introduction of sediment-filled valleys does not provide appreciable difference except in correspondence of valley at its natural frequencies.

In this paragraph the comparisons between the Complete model, illustrated in Figure 5.18, and the simplified Bi-Layer + soft-filled valley model (which represents the simplified model with greater complexity among the studied simplified models). The seismic scenario 1 (only N-S and E-W input motion) and 2 (adding the vertical component) have been considered.

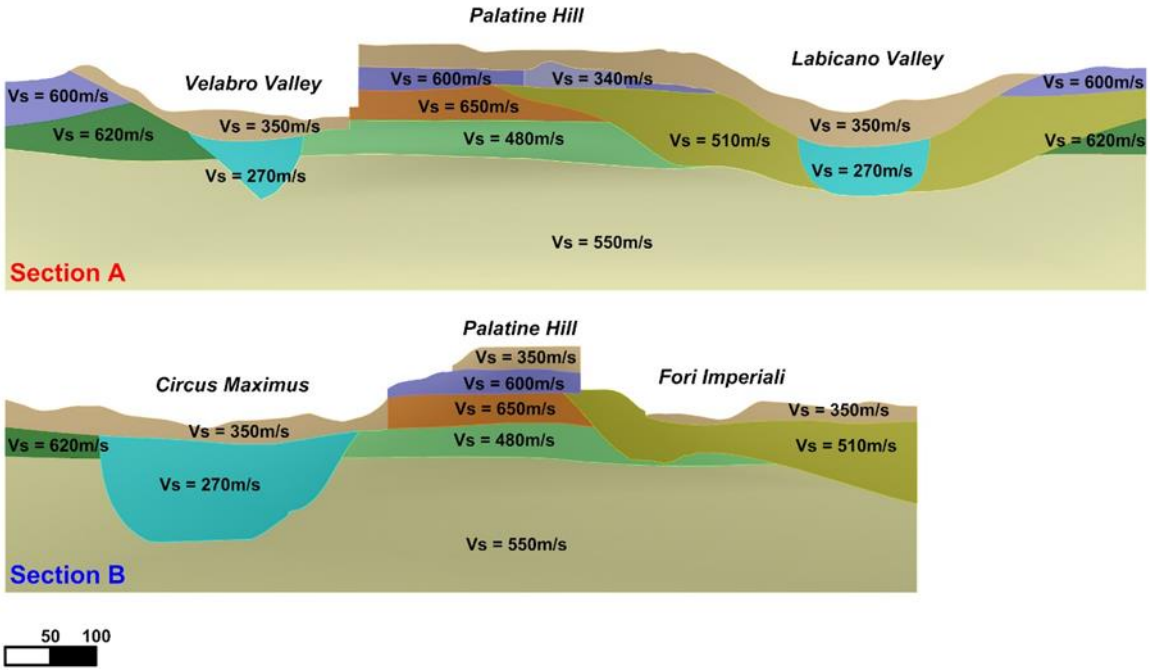

Figure 5.18: Complete model of Palatino hill and surrounding area model, above: section A and below: section B.

In Figure 5.19 and Figure 5.20 the comparisons between the Complete model and the Bi-Layer + sediment-filled valleys model are shown for section A and B respectively, for the seismic scenario 1. Both 2D and 3D numerical results of the complete model are slightly greater than those of the Bi-layer+sediment-filled valley model, regardless of frequency.

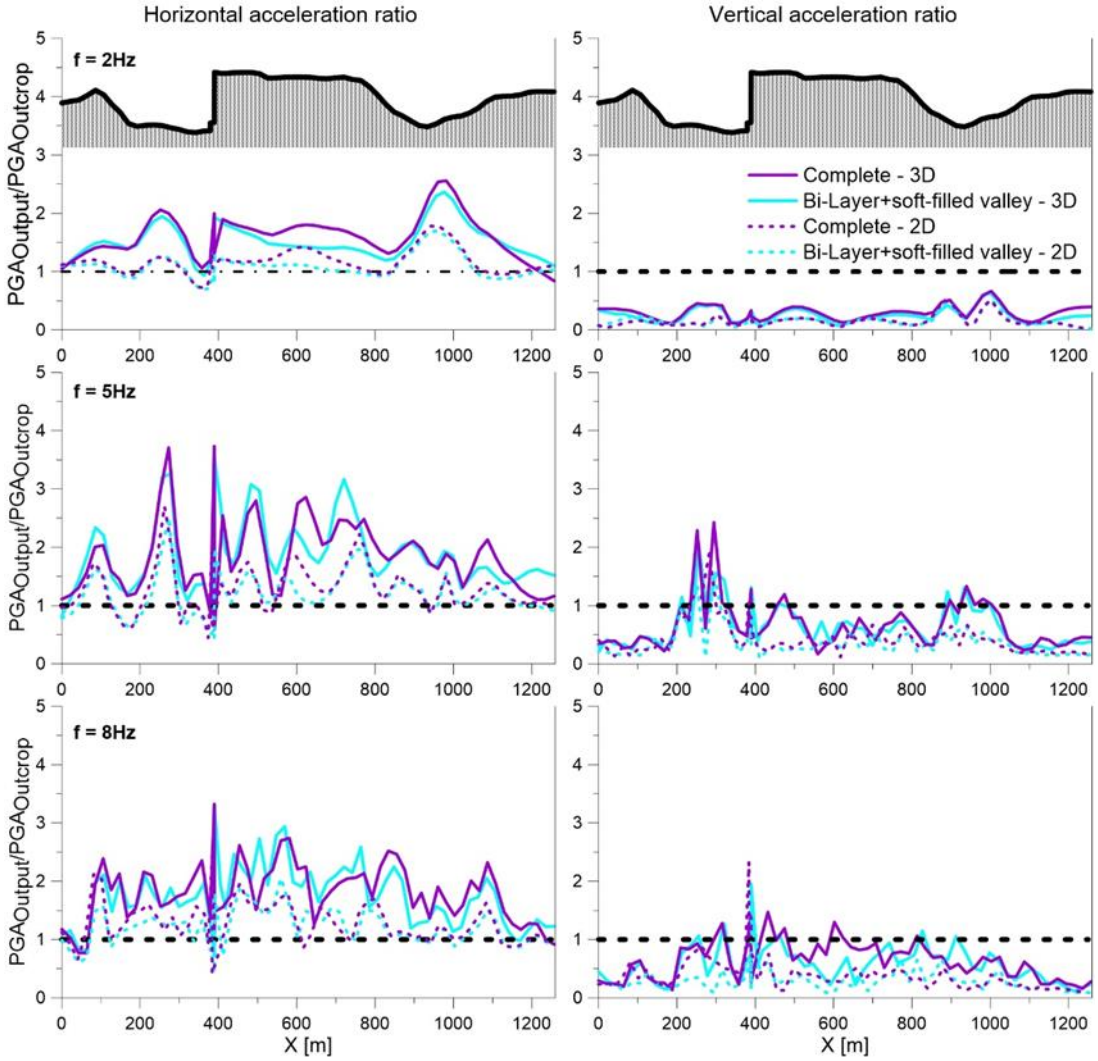

Figure 5.19: Comparison between Bi-Layer+soft filled valley model (cyan lines) and complete model (violet lines) for section A. Solid lines three-dimensional numerical results and dashed lines bi-dimensional ones.

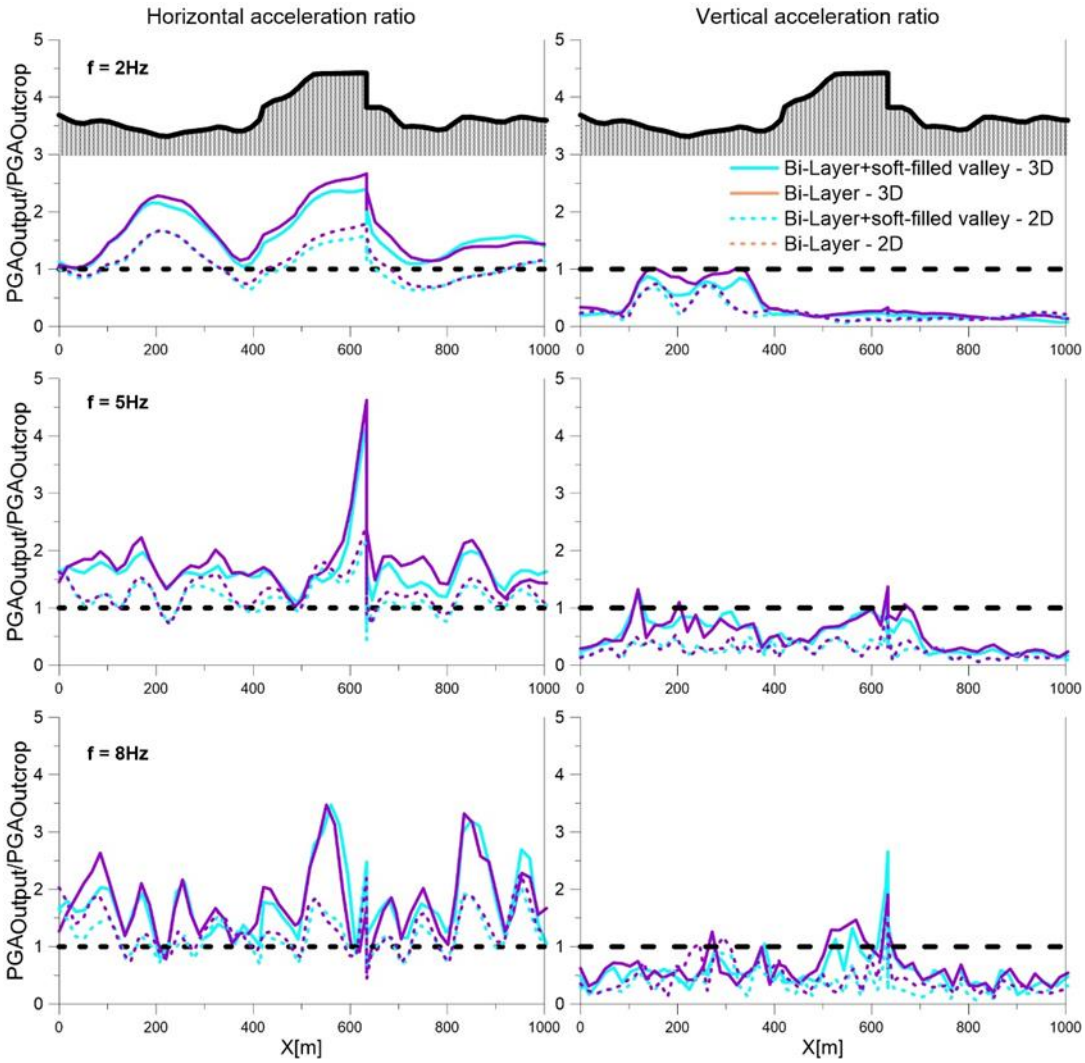

Figure 5.20: Comparison between Bi-Layer+soft filled valley model (cyan lines) and complete model (violet lines) for section B. Solid lines three-dimensional numerical results and dashed lines bi-dimensional ones.

In Figure 5.21 and Figure 5.22 are shown the comparisons for seismic scenario 2. The Complete model exhibits greater amplification as compared to the Bi-layer+ sediment-filled valley one in terms of vertical component both for 2D and 3D numerical results, especially at high frequency.

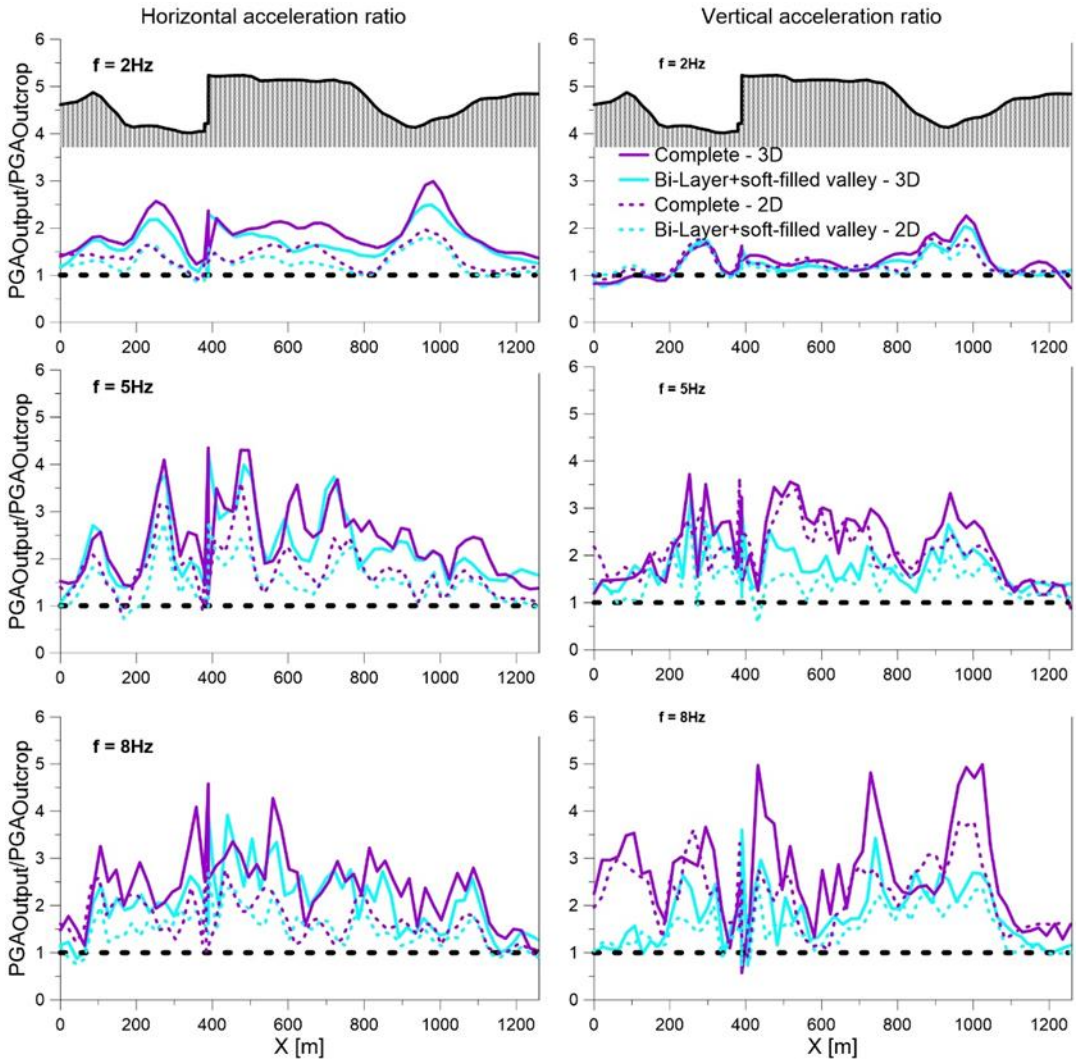

Figure 5.21: Comparison between Bi-Layer+soft filled valley model (cyan lines) and complete model (violet lines) for section A. Solid lines three-dimensional numerical results and dashed lines bi-dimensional ones.

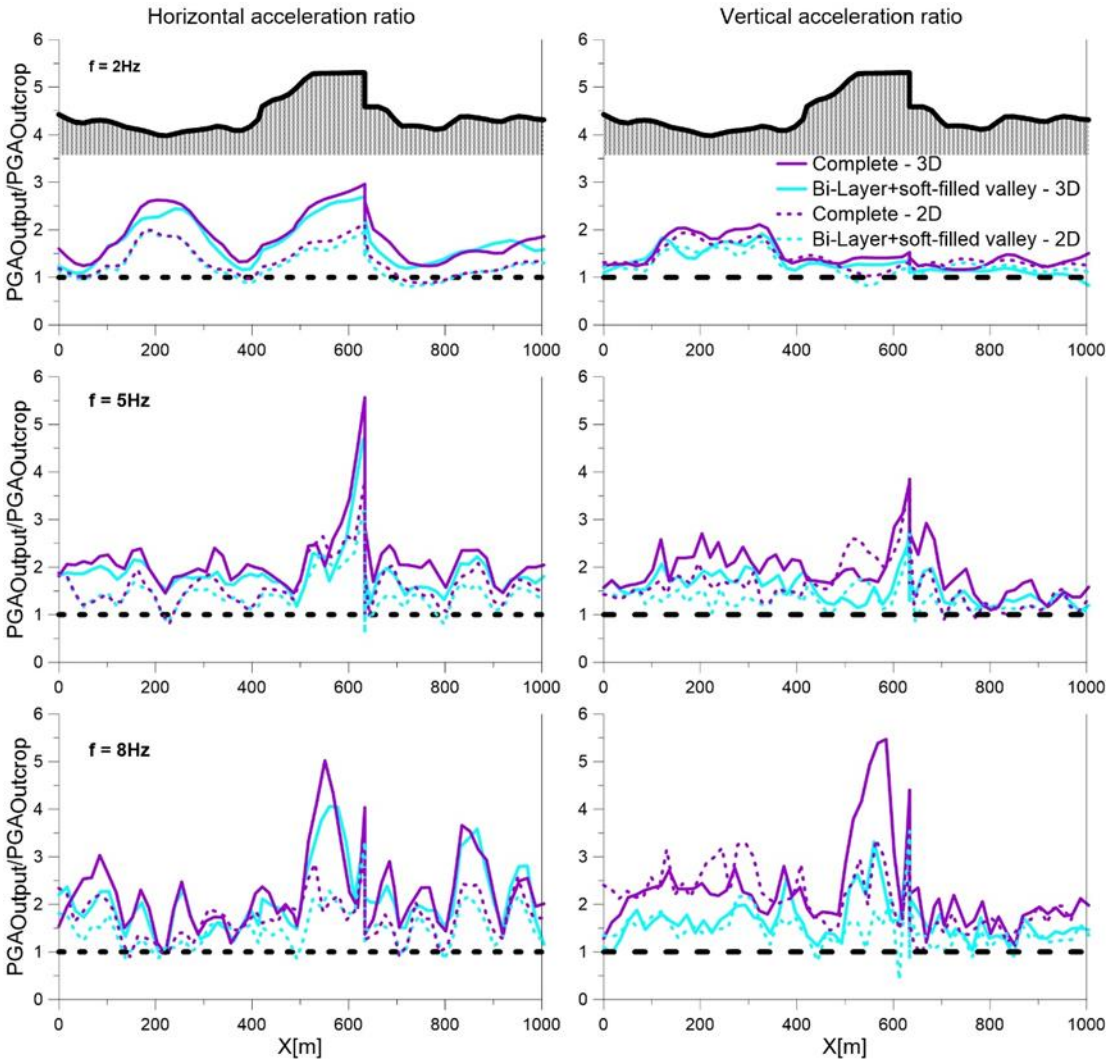

Figure 5.22: Comparison between Bi-Layer+soft filled valley model (cyan lines) and complete model (violet lines) for section B. Solid lines three-dimensional numerical results and dashed lines bi-dimensional ones.

In Figure 5.23 to Figure 5.25 the contours of amplitude of acceleration, defined as $mag(t) = \sqrt[2]{acc\_x(t)^2 + acc\_y(t)^2 + acc\_z(t)^2}$ (where acc_x, acc_y and acc_z are the acceleration components and t = 1.5s the time), are shown for seismic scenario 1 for f= 2, 5 and 8Hz, respectively. Similarly, from Figure 5.26 to Figure 5.28 the contours of vertical acceleration for seismic scenario 2 are plotted. At low frequency (f=2Hz) maximum accelerations occur in the sediment-filled valley bordering the Palatino hill, generally output accelerations increase and became more complex with frequency.

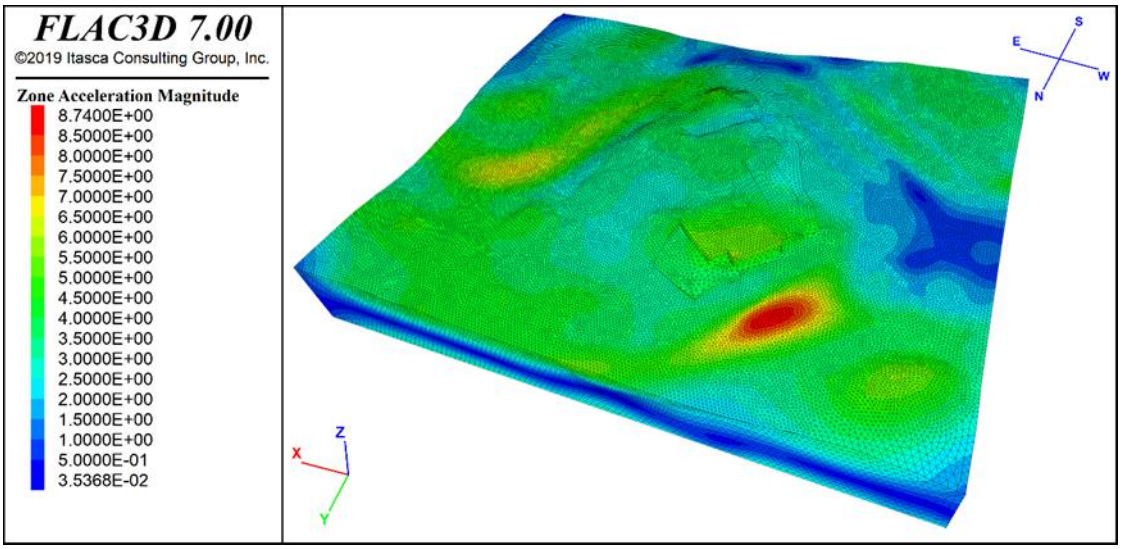

Figure 5.23: contours of magnitude acceleration for seismic scenario 1 with f = 2Hz.

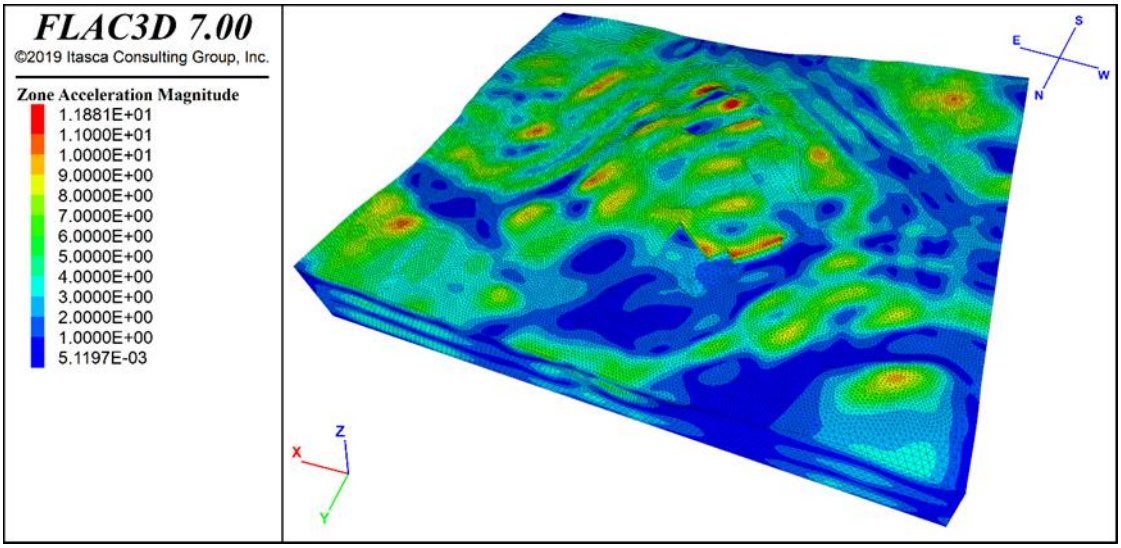

Figure 5.24: contours of magnitude acceleration for seismic scenario 1 with f = 5Hz.

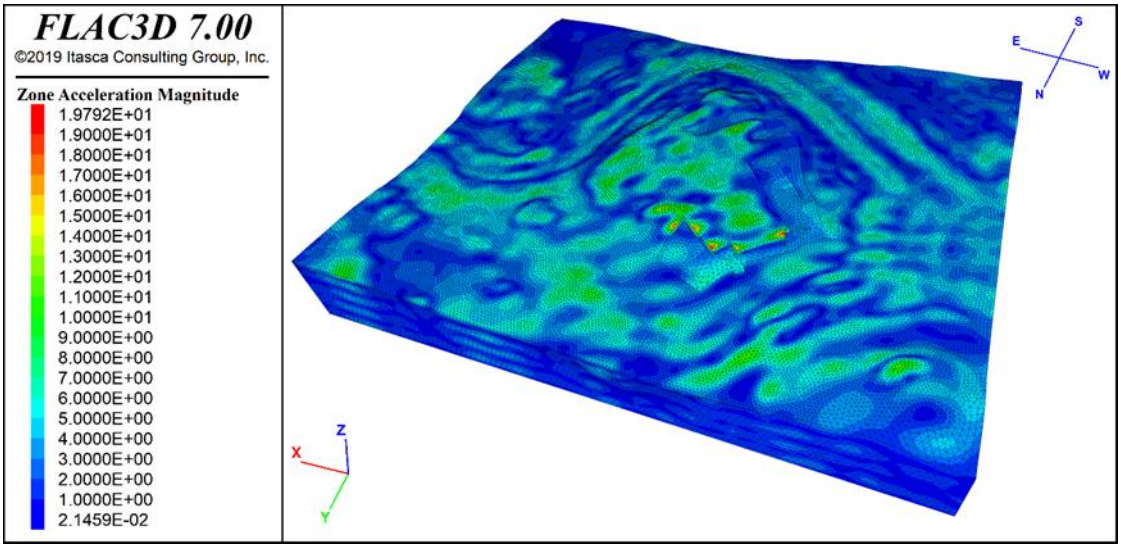

Figure 5.25: contours of magnitude acceleration for seismic scenario 1 with f = 8Hz.

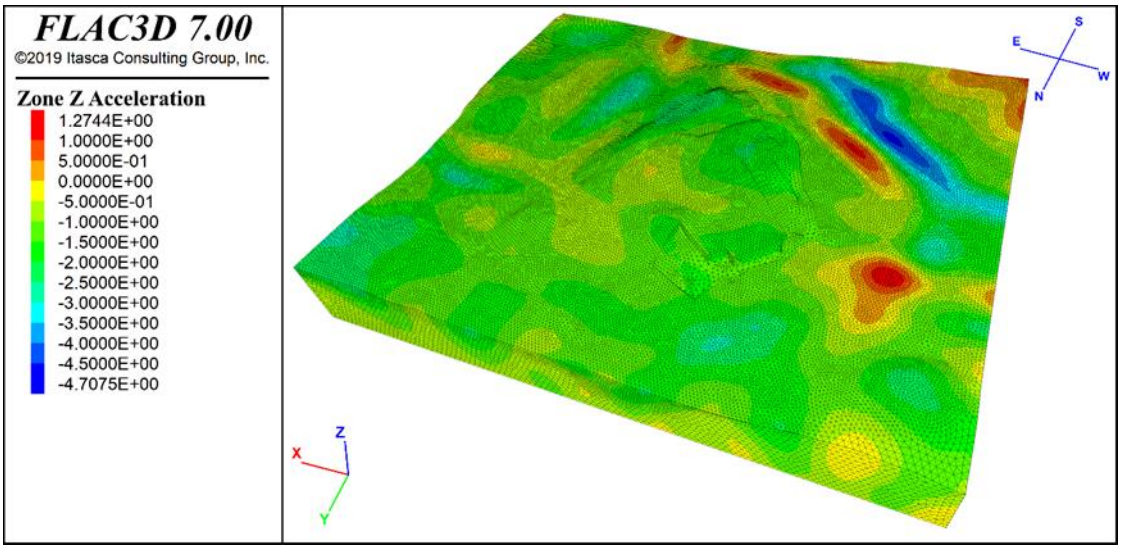

Figure 5.26: contours of vertical acceleration for seismic scenario 2 with f = 2Hz.

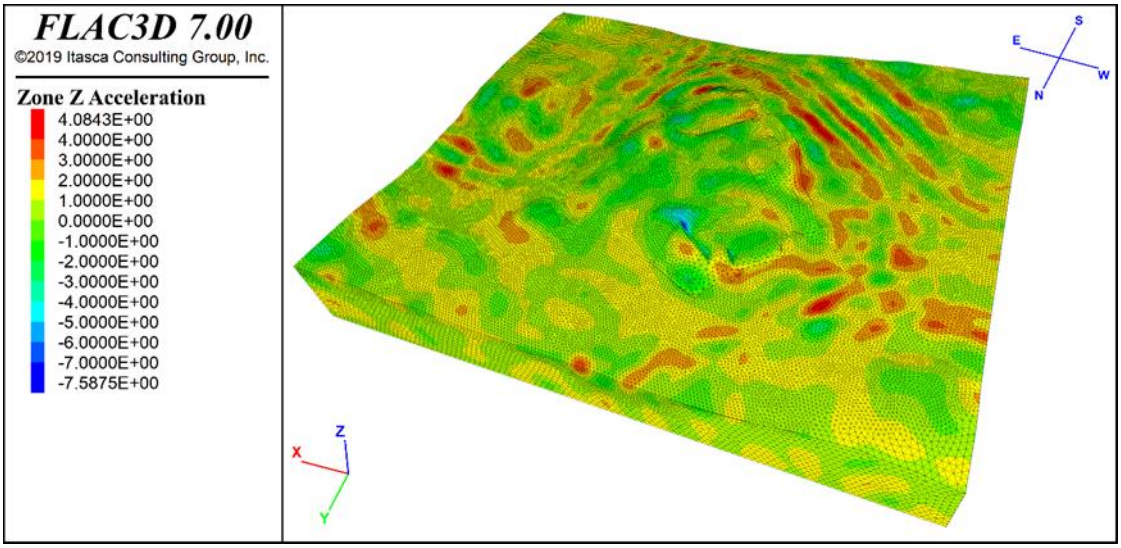

Figure 5.27: contours of vertical acceleration for seismic scenario 2 with f = 5Hz.

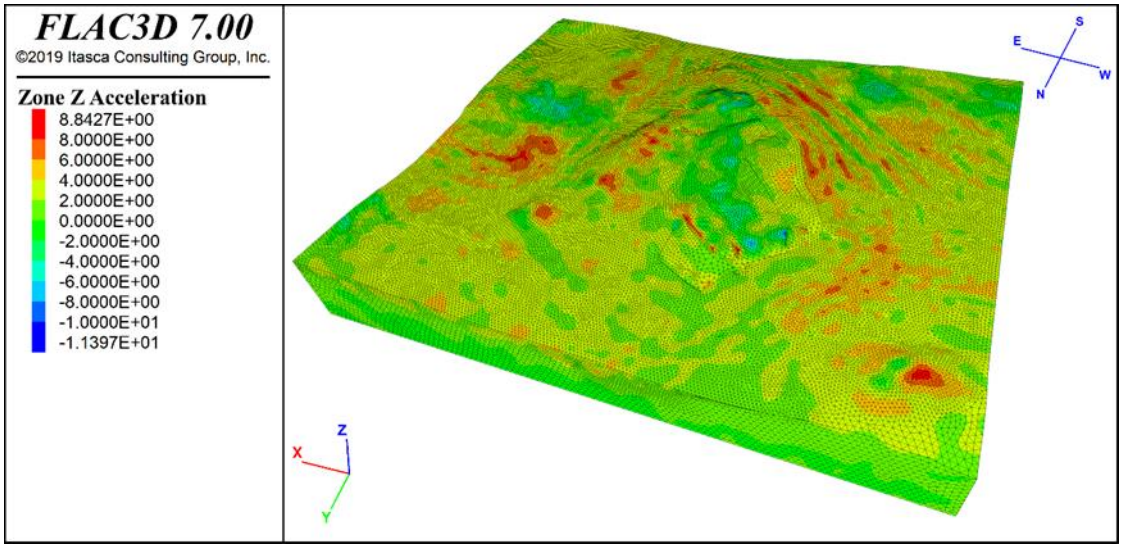

Figure 5.28: contours of vertical acceleration for seismic scenario 2 with f = 8Hz.

5.3 The Angitola earth dams in Southern Italy (Calabria)

5.3.1 Background

The Angitola reservoir (or *Monte Marello*) is located about 5 km from Sant'Eufemia Gulf in Calabria (Southern Italy), with capacity of $21 \cdot 10^6$ m3. The construction started in 1960 and was completed in 1967. The Angitola reservoir is composed of two zoned trapezoidal earth dams. The principal (or left dam) is 29.8 m high with shape-ratio L/H = 4.5 and the secondary (or right dam) is 24.1m with L/H = 3, the dams are separated by Monte Marello. The distance between the two dams is about 90 m (Figure 5.29). Both dams has the same crest elevation (48.3 m a.s.l.). The maximum water level elevation is 44.2 m a.s.l.

Figure 5.29: Aerial photo of Angitola reservoir in Calabria (Google Earth, 2019), Angitola lake; Monte Marello; Left and Right dams.

5.3.2 Geological setting and subsoil model

Ground investigations have been carried out at the Angitola site in different geotechnical campaigns in 1999, 2015 and 2017 involving continuous-coring boreholes, geophysical tests (e.g. MASW, Down-Hole), penetrations test (CPT, SCPTU, or SPT), ambient noise measurements, electrical resistivity tomographies performed both on dams body and in the surrounding areas. In particular down-hole were put down from the dam crest and from the downstream shoulder and were essential to assess the dynamic properties of the different geotechnical units; a SCPTU test was carried out from the crest of the left dam and investigated

all the dam body. In Figure 5.30 a plane view with the locations of some surveys is illustrated. Undisturbed samples were also taken from different depths in the body and in the foundations soils and have been used to assess standard physical and mechanical properties.

Both dams are zoned earth dams, composed of a dam core, filter layers and rockfill shoulder (shells) materials compacted in situ. The left dam is underlain by an alluvial layer formed by sands, approximately 23 m thick, where the bedrock is encountered; this is constituted by a gneiss formation, which is weathered in the surficial part. On the other hand, more complex subsoil conditions can be found below the right dam; in this case the weathered gneiss is covered by different layers of various thickness comprising, from bottom to top, gravelly sands, silty sands and silty clays. The thickness of the top of weathered gneiss is variable, it is maximum below the downstream toe (approximately 20-25 m) while it reduces below the upstream toe (about 10-15 m). Figure 5.31 show the plane views, transversal and longitudinal sections of both dams with the geometrical dimensions reported in Table 5.3 (for the symbols in the Table see § 2.4)

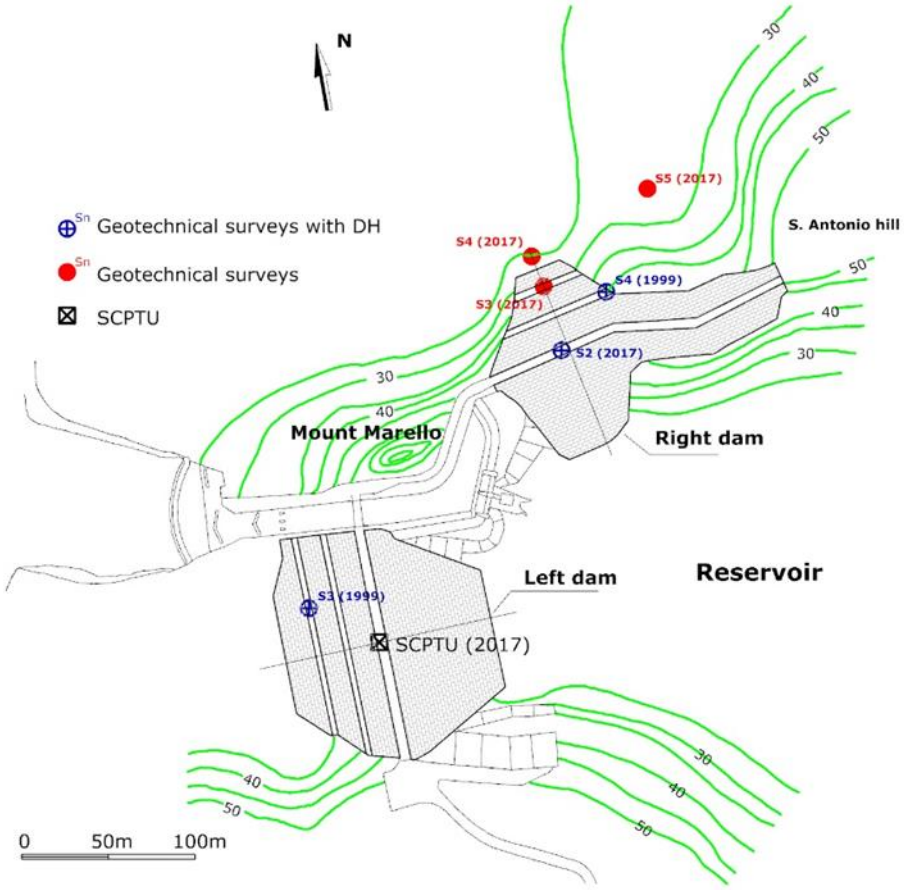

Figure 5.30: Plane view of Angitola dams and location of geotechnical surveys.

Table 5.3: Geometric dimensions of Angitola earth dams

Dam	L	H	L/H	B	λ
[-]	[m]	[m]	[-]	[m]	[%]
Principal (left)	136.0	29.8	4.5	135.1	4
Secondary (Right)	72.0	24.1	3.0	120.3	4

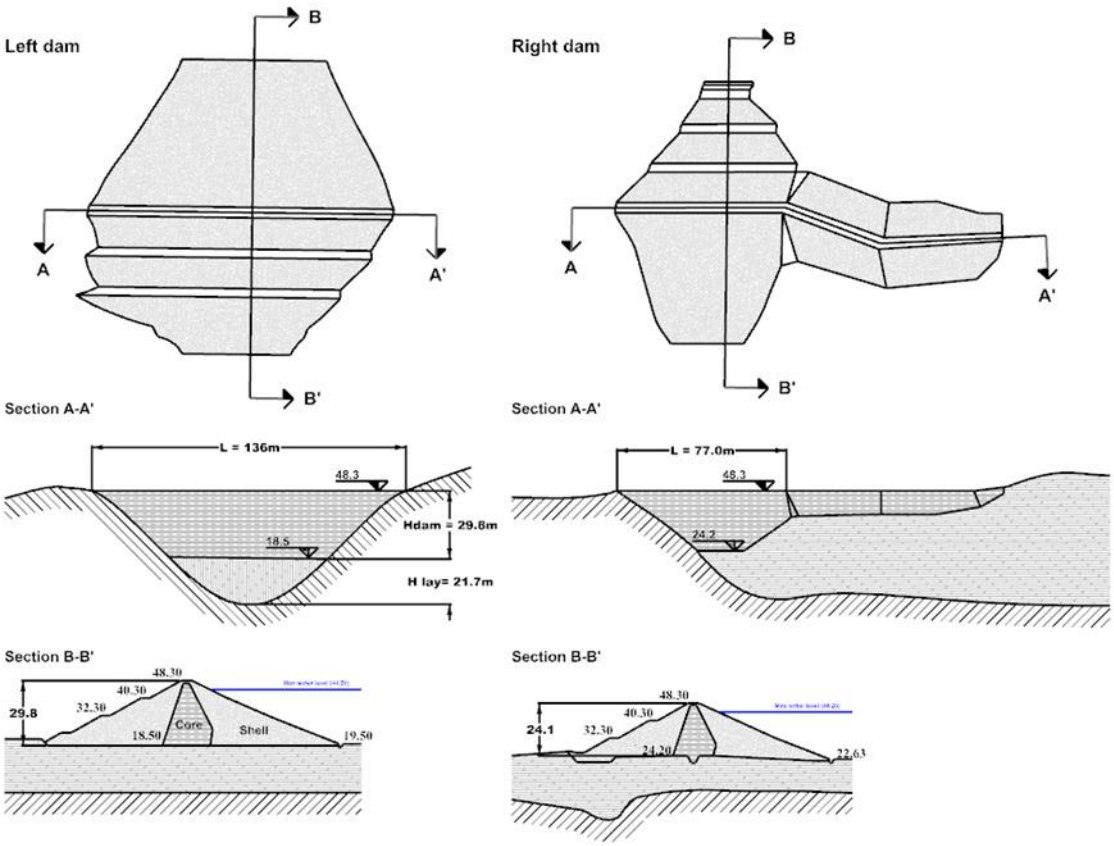

Figure 5.31: Plane view, cross- and longitudinal- sections with geometric of interest.

The shear wave velocity of the core material of both dams is about 140 m/s near the top of both dams, and about 340 m/s at 25 m depth. In Figure 5.32 the measured shear wave profiles carried out within the core from DH (right dam) and SCPTU (left dam) are shown. It can be seen a very good agreement of the measurements, even if are obtained from different geophysical techniques. The variation of G0 (or Vs) with depth can be described by the flowing power-law function:

$$G_0 = 43 \cdot z^{0.5262} \tag{5.1}$$

The shear wave velocity in the rockfill units for both dams was estimated based on the down-hole test performed in 1999 in the downstream shells (borehole S3 in left dam and S4 in right dam, Figure 5.33). The P wave velocity (Vp) values were derived from the seismic refraction tests performed in 2015. These tests have shown that in the materials of the shell Vp vary with depth, between 700-800 and 1200 m/s. For the Poisson's ratio, a value of ν = 0.33 was assumed, therefore Vs was taken variable in the range 350-600m/s. In terms of variation of G0 with the average effective stress p ' the following power law was adopted:

$$G_0 = 100kPa \qquad p' \leq 20MPa$$
$$G_0 = 214ln(p') - 214 \qquad p' \leq 20MPa \tag{5.2}$$

As far as the seismic bedrock is concerned, based on the results of geophysical tests the weathered bedrock was assigned a value of 800 m/s as while the intact gneiss was assigned Vs =1500 m/s. In Figure 5.34 the central cross-sections of both dams adopted for numerical analyses are shown. The physical and mechanical properties adopted for analyses are summarized in Table 5.4.

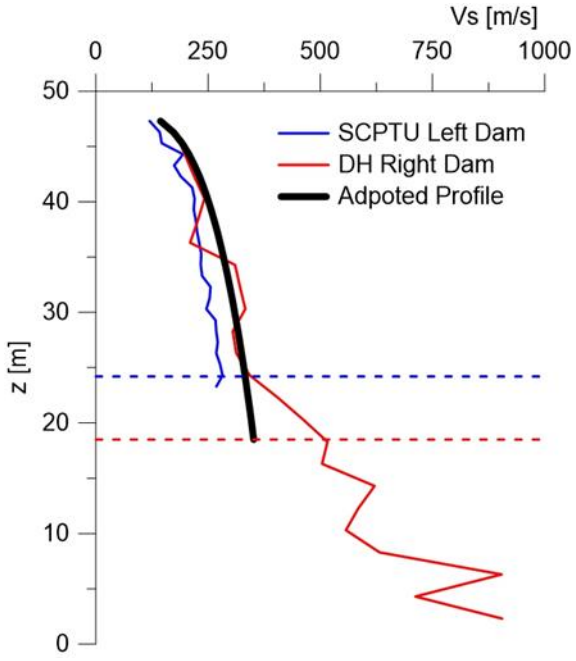

Figure 5.32: Shear waves profiles measured from the crest of both dams (48.3 m a.s.l.). Blue line: Left dam; Red line: Right dam; Black line: adopted profile.

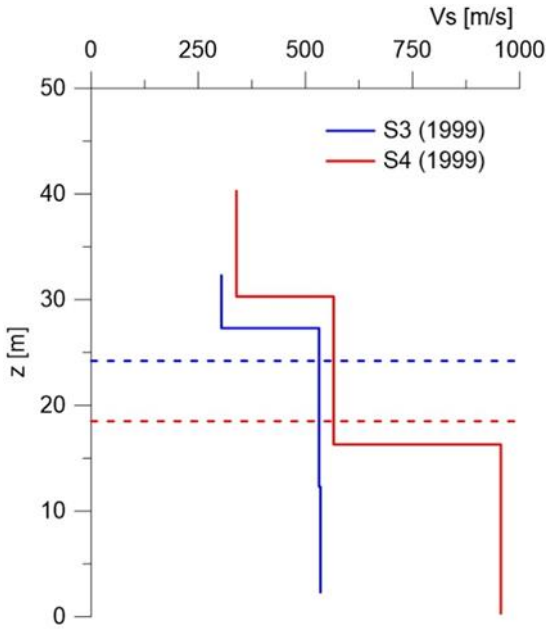

Figure 5.33: Shear waves profiles measured on body dams performed in 1999. S3 on left dam and S4 on right dam.

Table 5.4: Subsoil model for site response analyses

Material	**γ**	**Vs**	**ν**	**D**
[-]	**[kN/m3]**	**[m/s]**	**[-]**	**[%]**
Core	20.36	140 - 340	0.40	1.0
Shell	21.92	100 - 550	0.33	
Alluvial Sand	19.0	470 - 600	0.45	
Sandy silty	18.5	350	0.47	
Silty gravel	18.5	450	0.46	
Silty clay	18.25	480	0.44	
Gravelly Sand	19.5	600	0.45	
Weathered Gneiss	25.5	850	0.35	
Gneiss	25.5	1500	0.35	

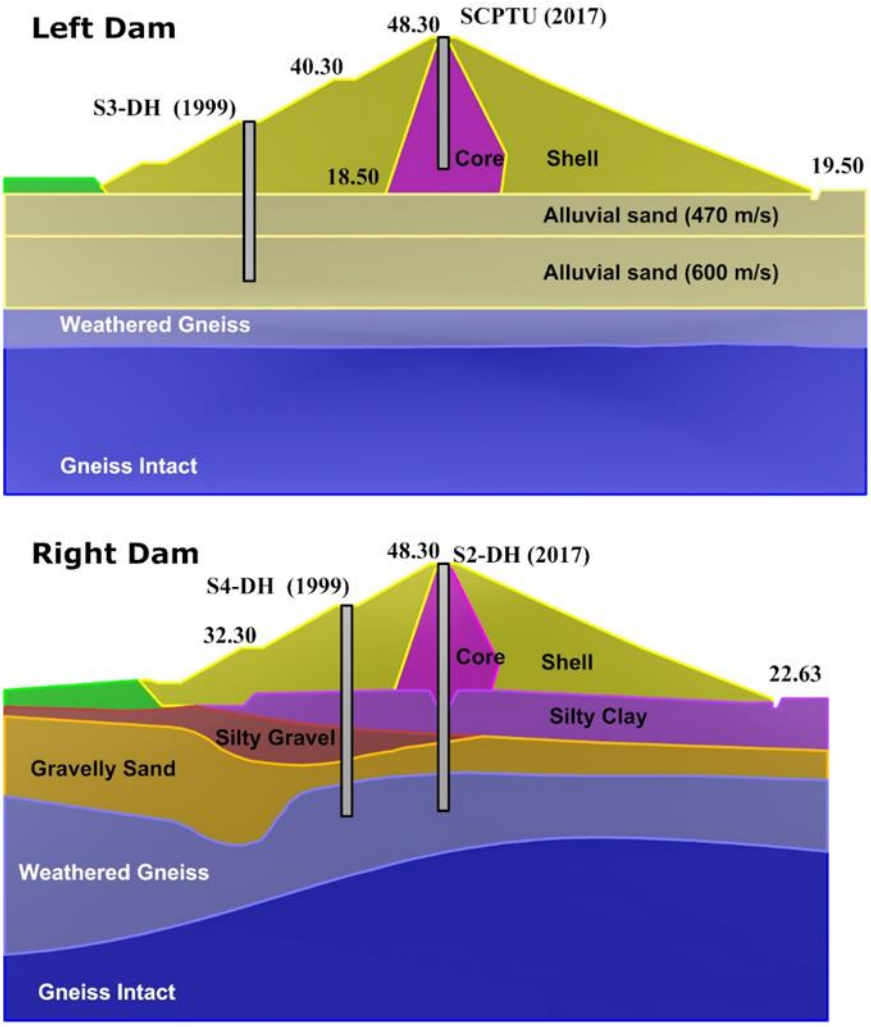

Figure 5.34: Central cross-section of left dam (above) and right one (below).

As mentioned earlier, the aims of this work are: i) to study some of parameters that affect seismic response; ii) the comparison between 3D and 2D conditions for both dams considered separately; iii) the interaction between both dams in 3D conditions. Two simplified models, for each dam, obtained by merging some geological-geotechnical units have been considered: 1) Homogeneous subsoil model, obtained by merging all units except the dam body, to study the effect of shape ratio (stiffening effect); 2) Foundation layer model, obtained by merging all units between the base of the dams and the top of gneiss units, to study the foundation layer effects (Dakoulas, 1991). The simplified models considered are shown in Figure 5.35. In Figure 5.36 FLAC3D numerical grid for the whole system (two dams + Monte Marello) is shown.

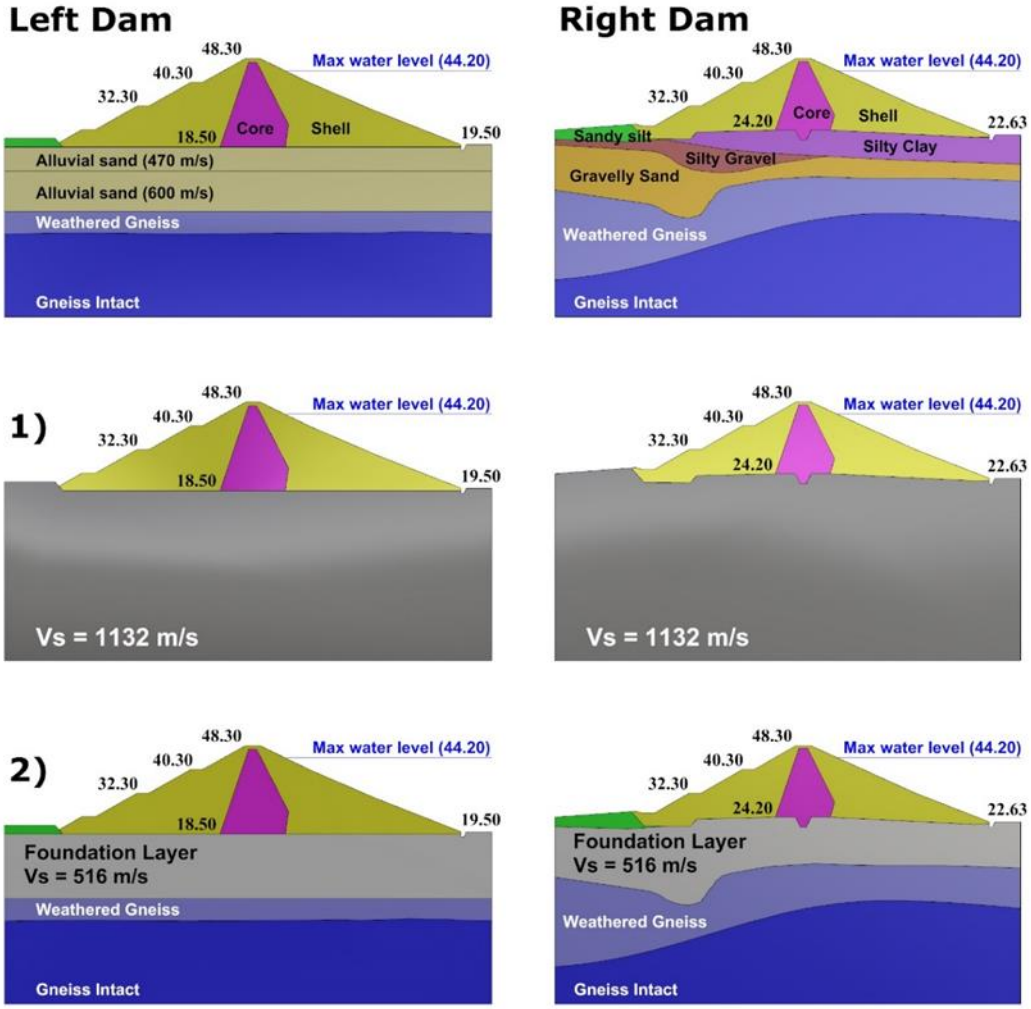

Figure 5.35: Central cross-sections of both dams with real subsoil conditions. Simplified models of left dam (left side) and right dam (right side); 1) Homogeneous subsoil model; 2) Foundations layer model.

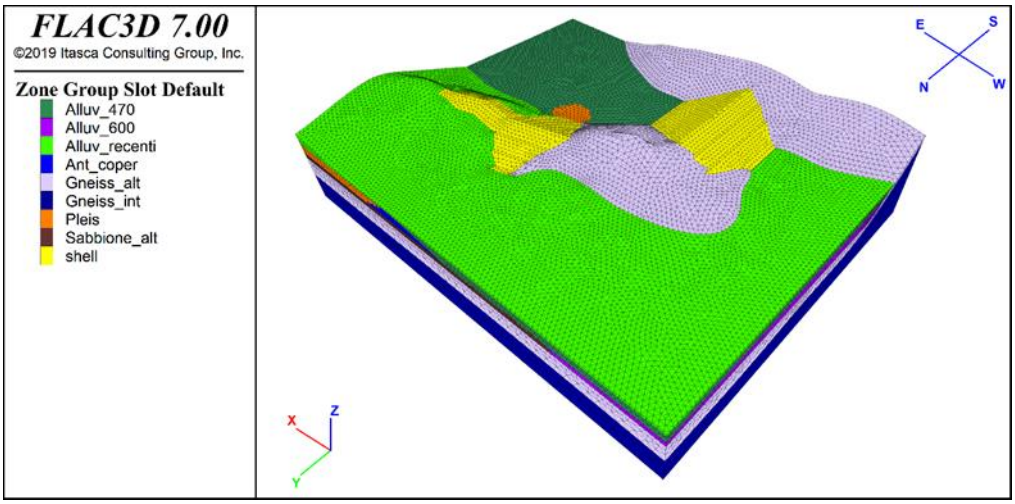

Figure 5.36: FLAC3D numerical grid for the Angitola reservoir

The comparison between single dams and whole system (two dams + Monte Marello) provide the interaction between dams. The 3D model for single dams and for the whole system are shown in Figure 5.37 and Figure 5.38 respectively. The numerical results were carried out along three horizontal axes: 1) central axis; left axis; right axis) in terms of displacement ratio ($disp_{output}/disp_{outcrop}$)

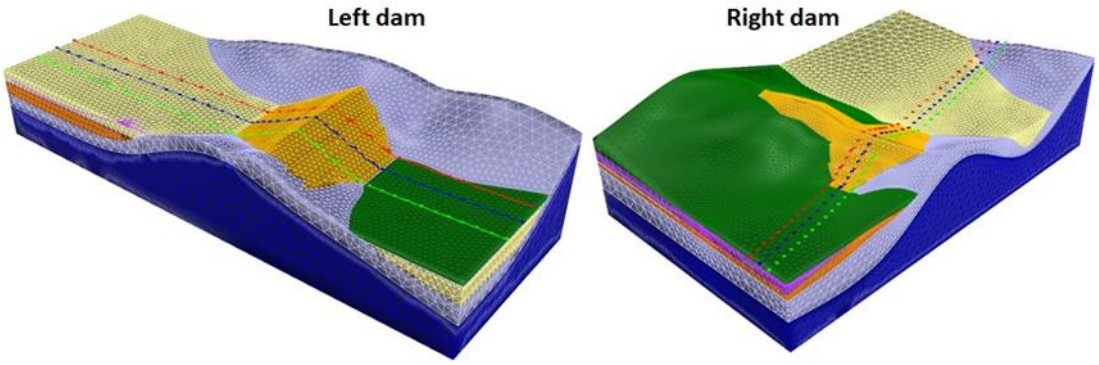

Figure 5.37: Three-dimensional model for the left and right dams considered separately.

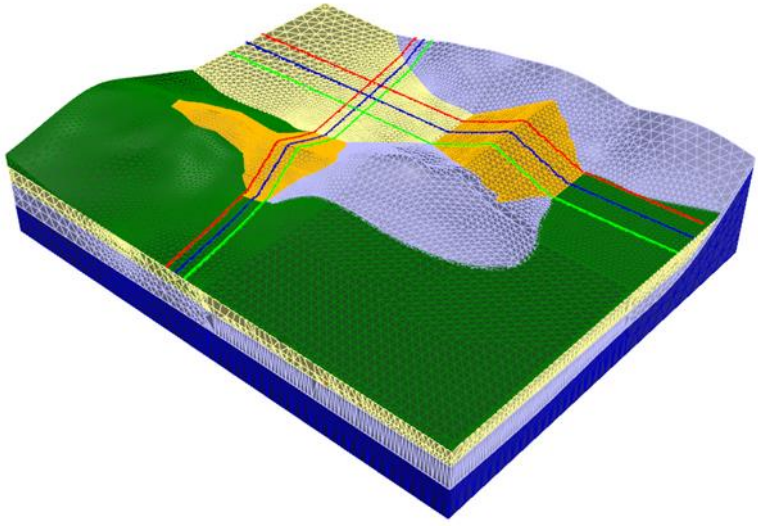

Figure 5.38: Three-dimensional model for the whole system considering both dams and Monte Marello.

5.3.3 Homogeneous subsoil model

In this paragraph the comparisons between 2D and 3D numerical results for Homogeneous subsoil model obtained by merging all subsoil units (Figure 5.39) is carried out. Average constant values of shear and compression waves velocity adopted for dynamic analyses are reported in Table 5.5 together with values of constant damping ratio. With these assumptions this model takes into account only the effect of shape-canyon (L/H = 4.5 for left dam and 3.0 for right one). Only horizontal input motion was applied in this case; therefore, the vertical output component is parasitic.

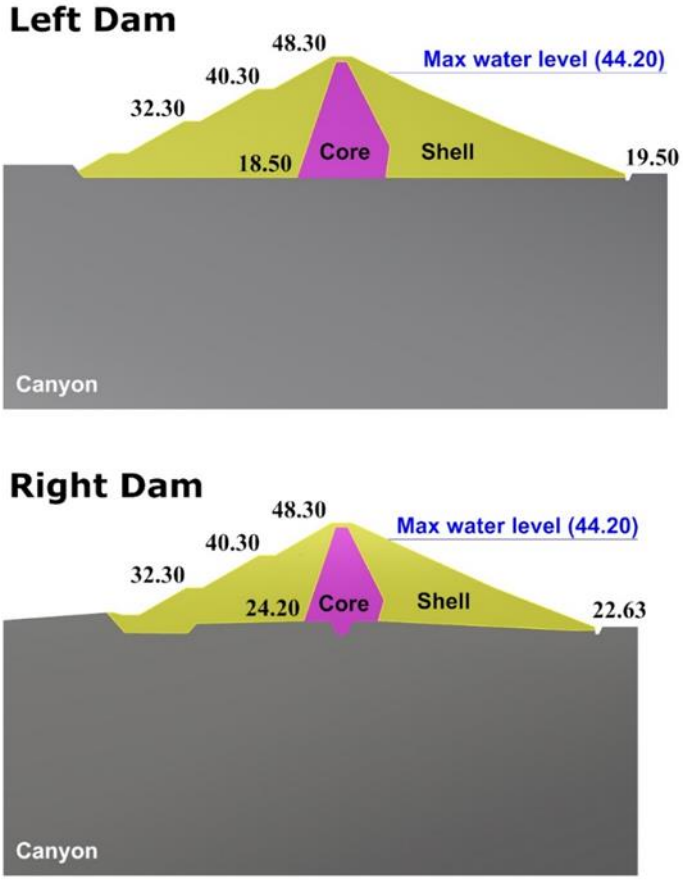

Figure 5.39: Homogeneous subsoil model cross-section. Left dam (above) and right dam (below).

Table 5.5: Linear properties adopted for the Homogeneous model

Material	γ	Vs	ν	D
[-]	[kN/m3]	[m/s]	[-]	[%]
core	20.36	278	0.40	1.0
shell	21.92	395	0.33	
canyon	23.73	1132	0.38	

The 2D and 3D numerical results (dashed and solid lines, respectively), are illustrated in Figure 5.40 and Figure 5.41 in terms of displacement ratio at the crest of profile, for left and right dams, respectively. Both dams exhibit greater 2D amplification at low frequency (f=2Hz) compared to 3D due to frequency shift (stiffening effect). At medium frequency (f=5Hz) greater 3D horizontal amplifications (especially for central axis) are present as compared to 2D. Right dam exhibits greater amplifications as compared to left one both in 2D and 3D conditions presumably due to the lower shape ratio. At high frequency (f=8Hz), left dam exhibits minor difference between 2D and 3D. The parasitic vertical component increases with input frequency especially for 3D; it is negligible at low frequency and of the same order of magnitude as horizontal at high frequencies. Generally central axis (blue lines) exhibits greater amplifications as compared to the right (red lines) and left (blue lines) ones, except at low frequencies.

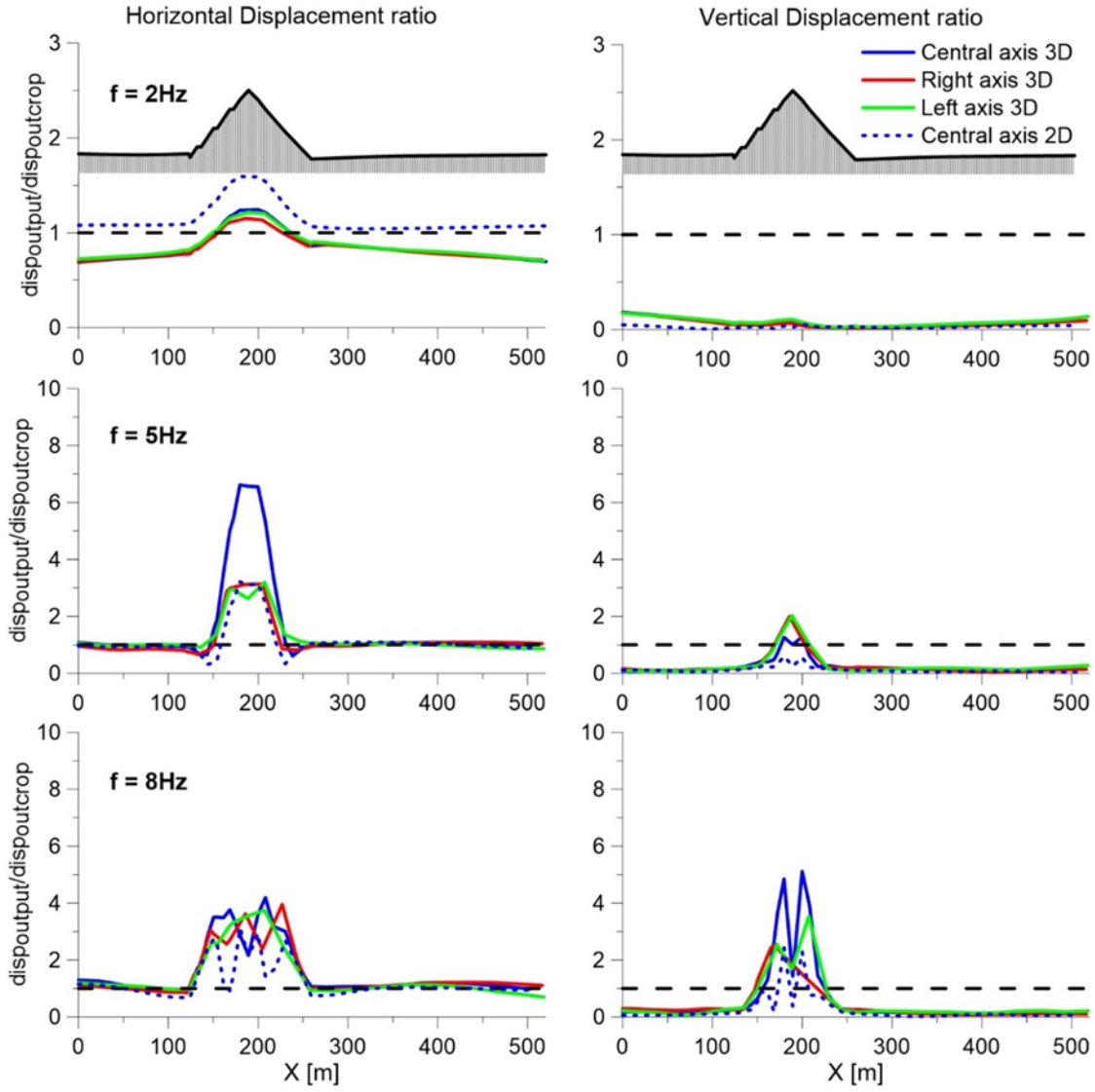

Figure 5.40: Comparison between 3D (solid lines) and 2D (dashed lines) for Homogeneous model for left dam. Blue lines: central axis; red lines: right axis; green lines: left axis

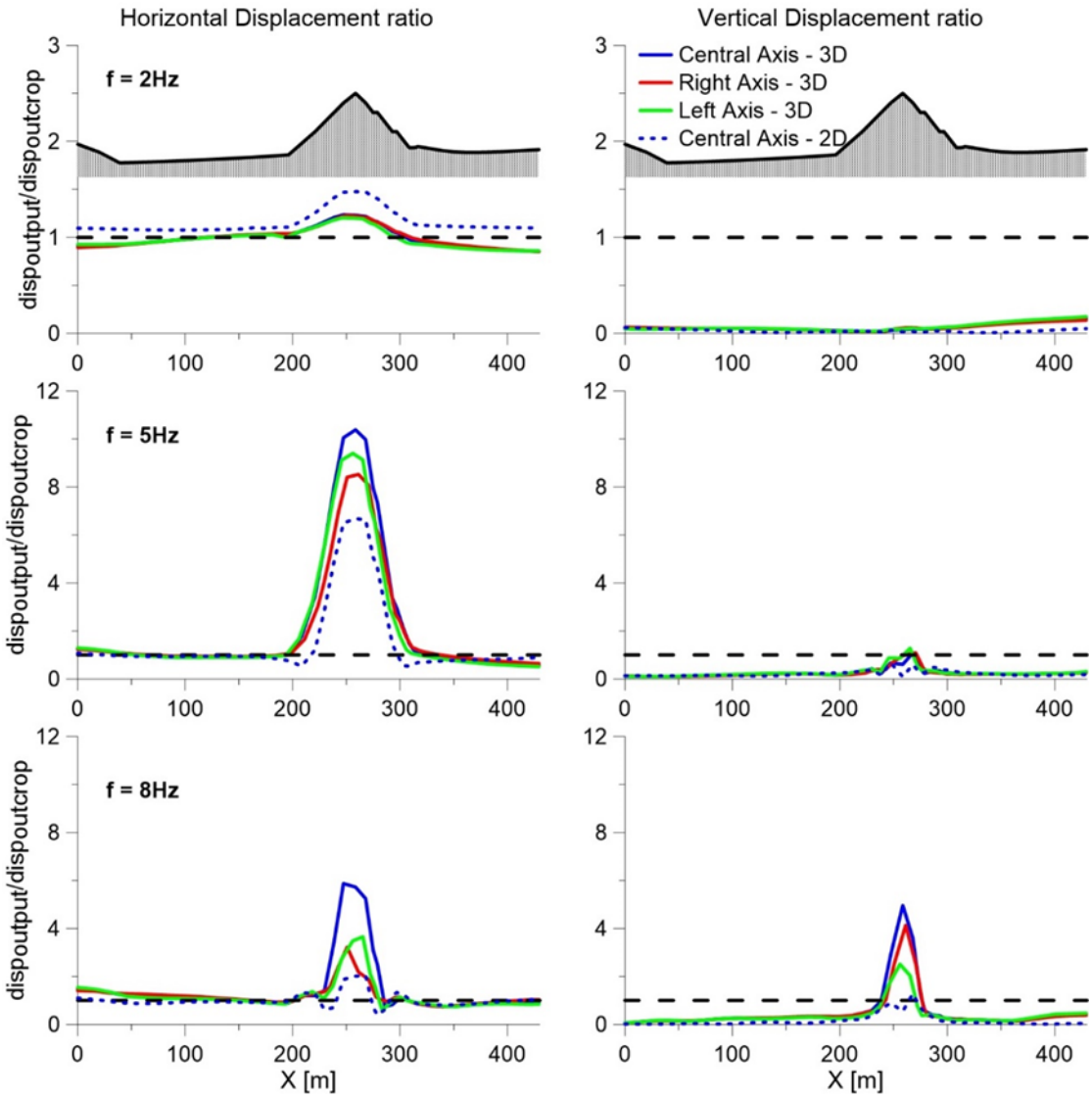

Figure 5.41: Comparison between 3D (solid lines) and 2D (dashed lines) for Homogeneous model for right dam. Blue lines: central axis; red lines: right axis; green lines: left axis.

5.3.4 Foundation layer model

The Foundation layer model was obtained by merging the geological units between the base of the dams and the weathered gneiss units. In Figure 5.42 the cross sections are shown: the right dam is characterized by a variable thickness of the foundation layer while for the left dam the subsoil is characterized by horizontal layers. The linear properties adopted are shown in Table 5.6. To study the effect of the foundation layer on dynamic response, the comparison with Homogeneous model for central axis, in terms of displacement ratios at the top of both dams, periods and transfer functions, has been carried out applying only horizontal motion.

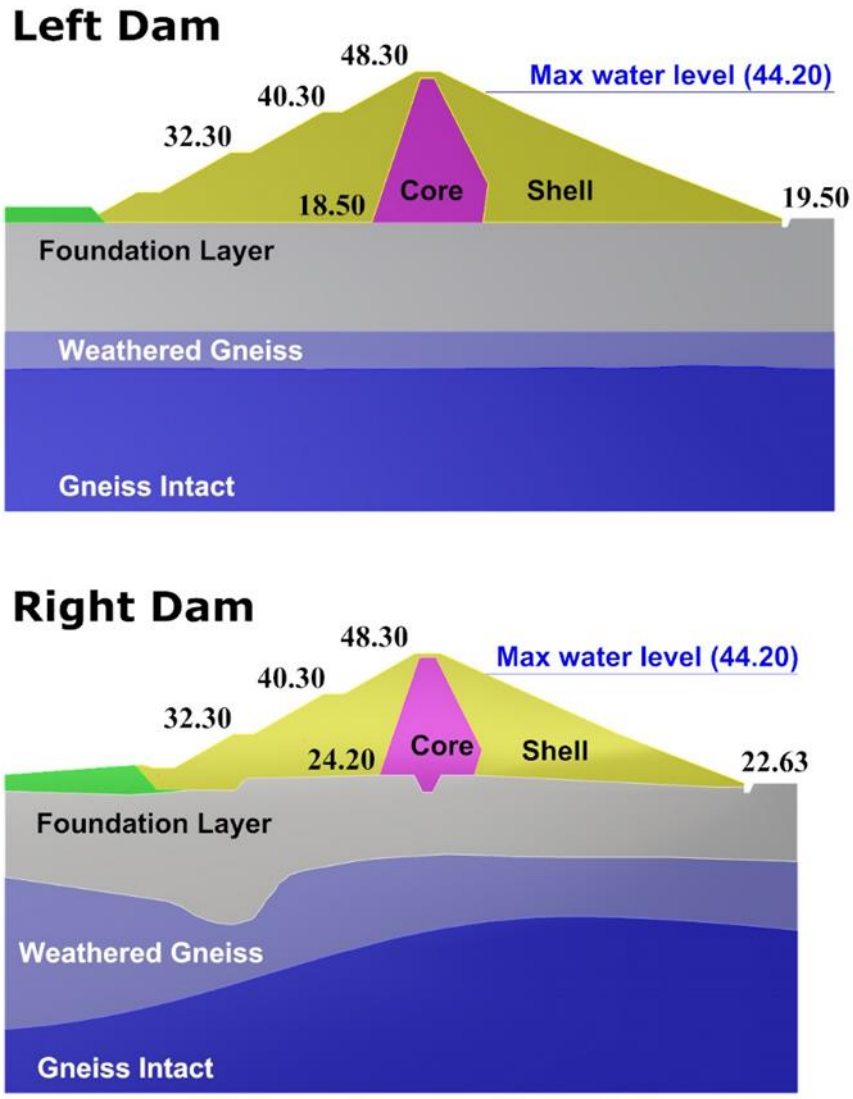

Figure 5.42: Foundation layer model cross-section. Left dam (above) and right dam (below).

Table 5.6: Linear properties adopted for Foundation layer model

material	γ	Vs	ν	D
[-]	[kN/m3]	[m/s]	[-]	[%]
Core	20.36	278	0.40	1
Shell	21.92	395	0.33	
Foundation Layer	18.98	543.6	0.45	
Weathered gneiss	25.5	850	0.35	
Gneiss	25.50	1500	0.35	

In Figure 5.43 and Figure 5.44, for left and right dam respectively, the 2D and 3D numerical results for Foundation layer model and the comparisons between Homogeneous model on central axis are shown. The following considerations can be made: i) at low frequency (f=2Hz) 3D horizontal amplification for both dams is larger for Foundation layer model as compared to the 3D Homogeneous model, while the reverse occurs at medium frequency (f=5 Hz) for right dam; negligible difference do exist between the models for both dams at the higher 8 Hz frequency; this is due to the lengthening period (Dakoulas, 1991) because of the presence of the foundation layer; ii) 3D horizontal amplification is larger than 2D one, especially at medium frequency; iii) the introduction of foundation layer provides drastic amplifications for vertical parasitic component especially at medium frequency both for 2D and 3D models for both dams. To evaluate the elongation of periods, due at foundation layer, the comparisons between periods of Foundation layer model (Tdam+layer) and Homogeneous model (Tdam) one was carried out. In Figure 5.45 the transfer functions, calculated at crest of dams, both in bi- and three-dimensional conditions for left dam (above) and right one (below) are portrayed. The comparison shown that: i) in 2D conditions (dashed lines) the elongations are 28% and 18% for left dam and right one respectively, due at greater thickness ratio of right dam (see Table 5.7); ii) instead in 3D condition right dam exhibits greater elongation (about 50%) as compared to left one.

As explained in Chapter 2, for the calculation of the elongation period due to the presence of layer foundation, Dakoulas (1991) provides closed-form solution for 3D dam in rectangular canyon. In Table 5.7 are shown the thickness ratio t = Hdam/HLayer and velocity ratio c =

Vs,dam/Vs,Layer for both dams. These results are confirmed for right dam but not for left one (Figure 5.46).

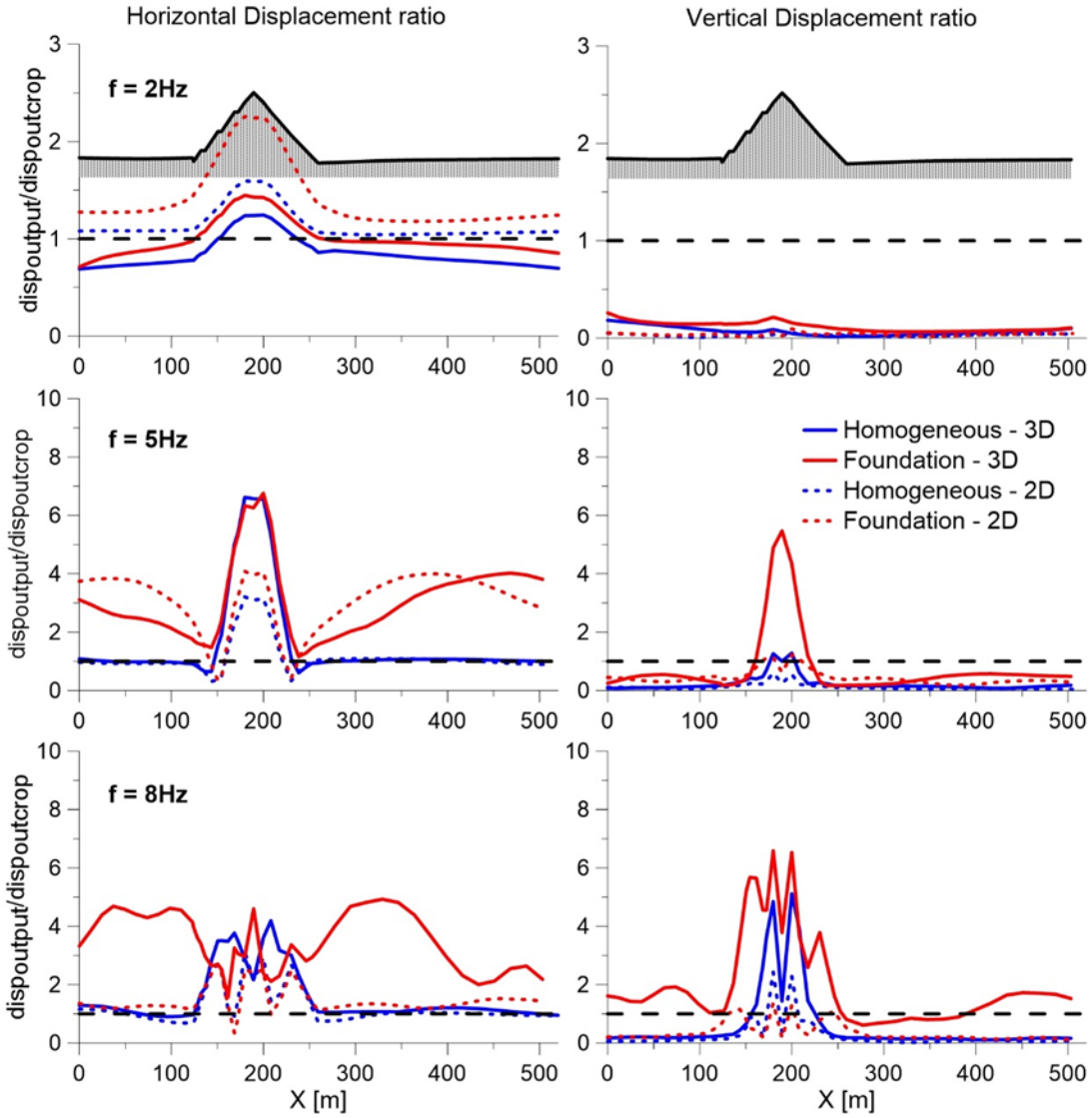

Figure 5.43: Comparison between Foundation layer model (red lines) and Homogeneous model (blue line) for left dam.

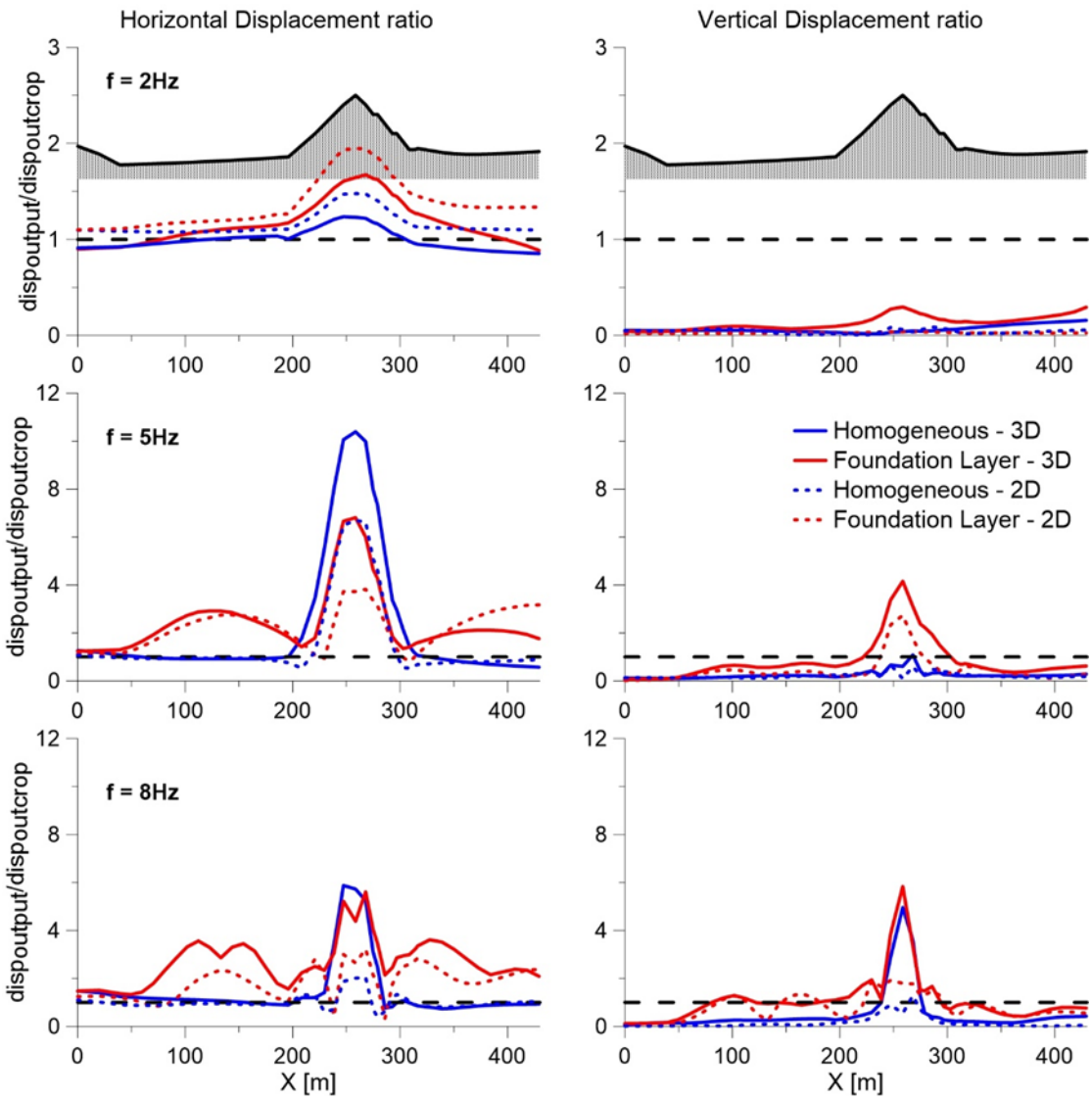

Figure 5.44: Comparison between Foundation layer model (red lines) and Homogeneous model (blue line) for right dam.

Table 5.7: Parameters for calculation of the elongation periods for earth dam on alluvial layer (Dakoulas,1991)

Dam	t (thickness ratio)	c (velocity ratio)
Left	0.70	0.73
Right	1.05	0.73

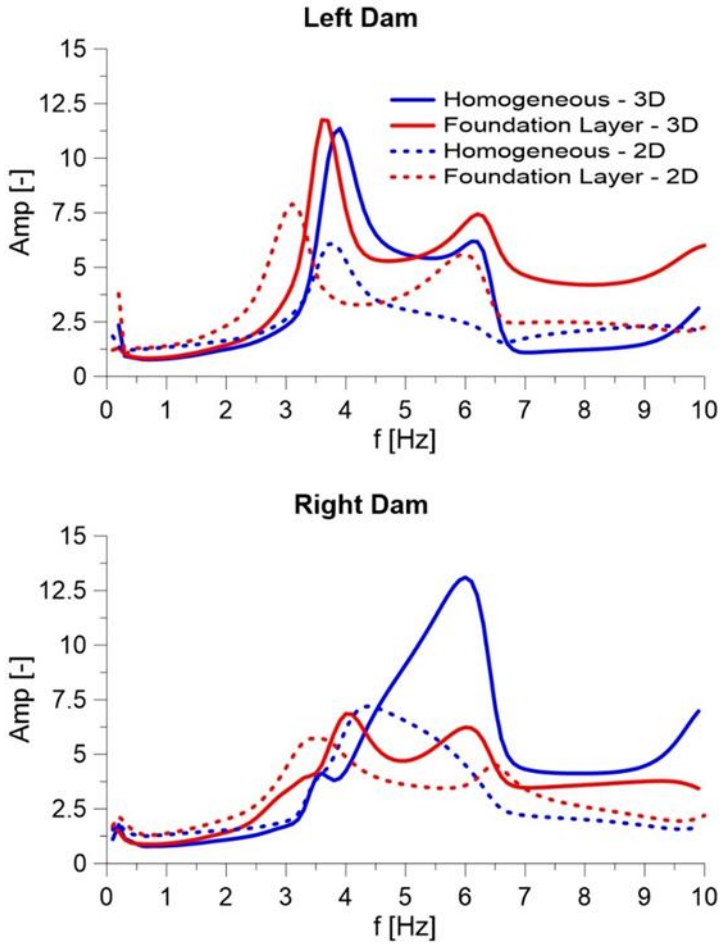

Figure 5.45: Comparison between Foundation Layer Model (red line) and Homogeneous Model (blue line) in terms of transfer functions at crest of dams.

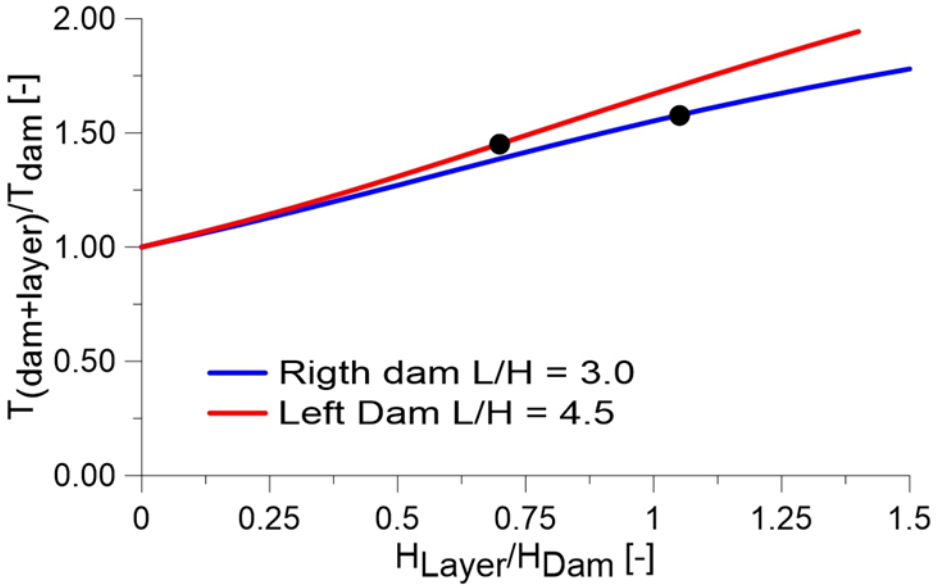

Figure 5.46: Elongation of periods due to Foundation Layer for left dam (red line) and right one (blue line)

5.3.5 Complete models

The 2D and 3D numerical results for Complete model (Figure 5.47) and the comparison with *Foundation Layer model* are shown in Figure 5.48 and Figure 5.49 for left and right dams, respectively. The linear properties adopted for analysis are summarized in Table 5.4.

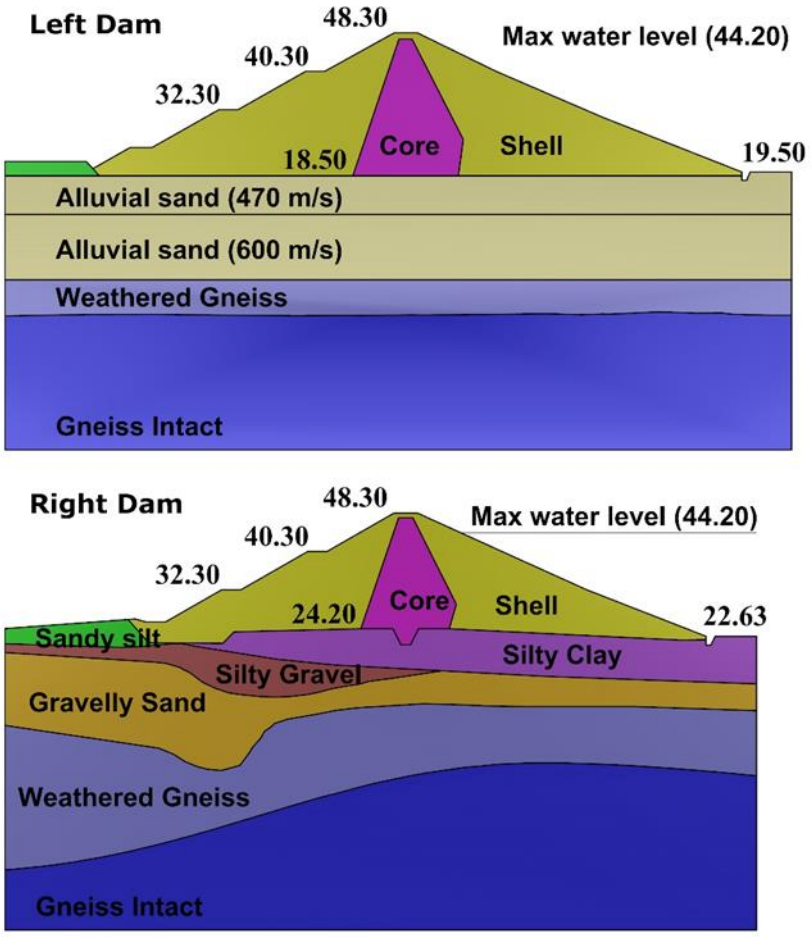

Figure 5.47: Complete models of the central cross-sections for left dam (above) and right dam (below).

Negligible differences between Foundation layer model and Complete model both for 2D and 3D numerical results for both dams do exist. This is expected for left dam because there are slight differences in terms of shear waves velocity between the two models. On the contrary, the subsoil of right dam is more heterogeneous as compared to the Foundation layer model both in terms of geometry and soil characteristics.

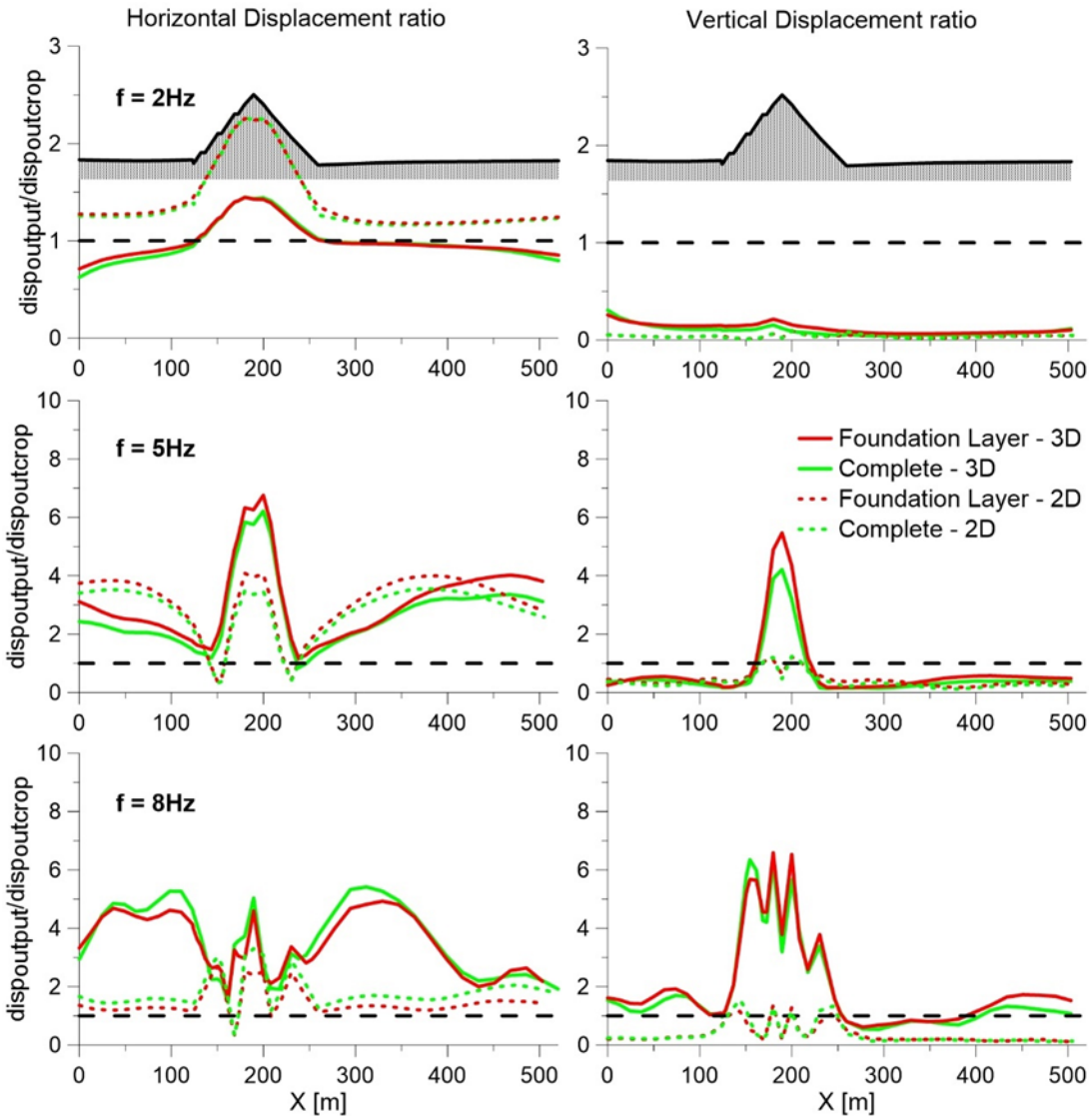

Figure 5.48: Comparison between Complete model (green lines) and Foundation layer model (red lines) for left dam.

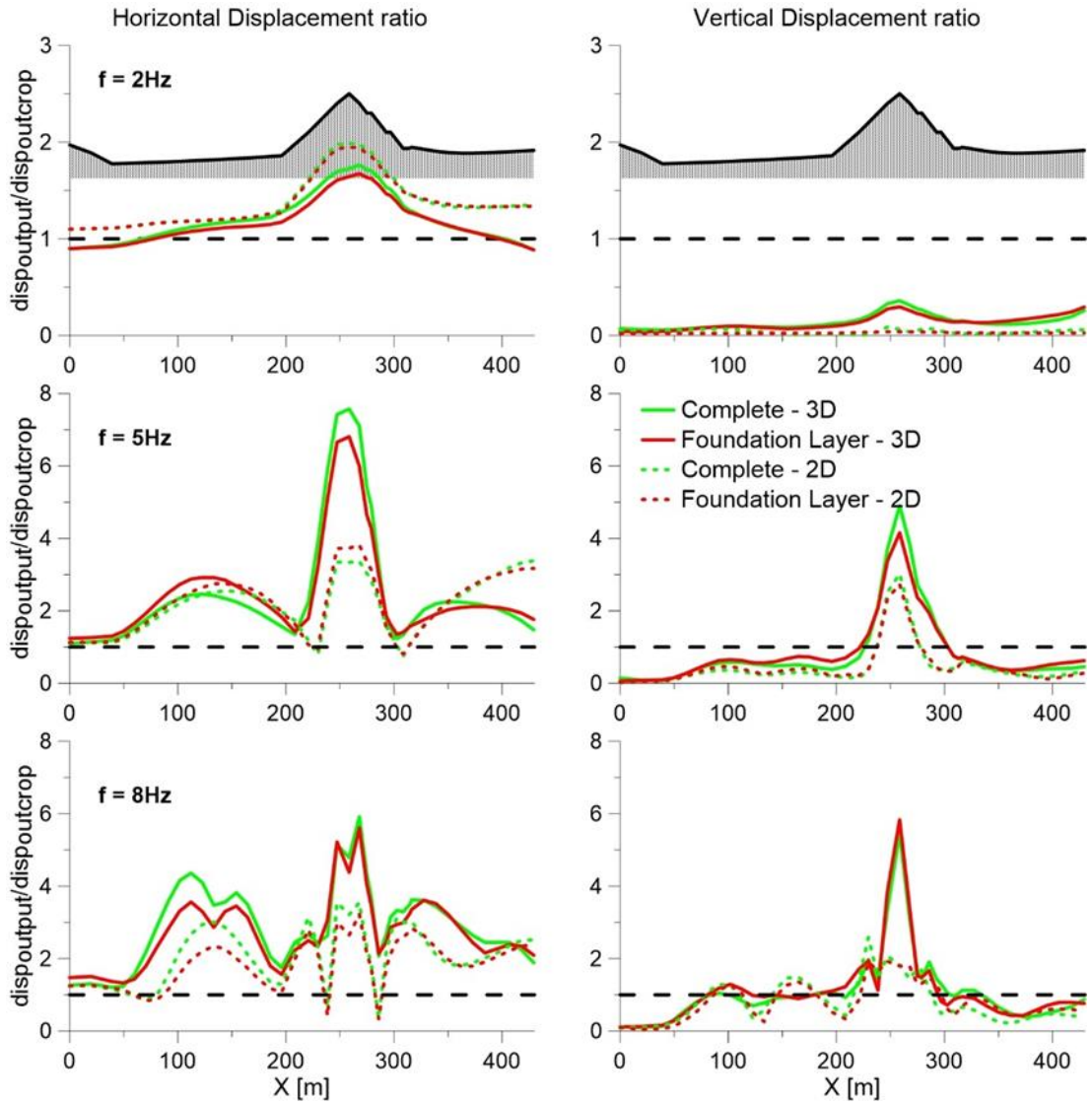

Figure 5.49: Comparison between Complete model (green lines) and Foundation layer model (red lines) for right dam.

5.3.6 The whole system

Previous results were obtained applying only horizontal motion on both dams taken separately (Figure 5.37). For the whole system, which include the two dams and *Monte Marello*, it was investigated: i) the dynamic interaction between dams; ii) the effects of vertical input motion considered the seismic scenario 2 (as defined in paragraph 5.1), both in 3D conditions. The numerical grid is shown in Figure 5.38, the central axes of both dams are orthogonal, the distance measured at center of dams is 200m. The dynamic interaction between the two dams depends on the ratio between the wavelength of input motion and a characteristic dimension (e.g. distance). In Table 5.8 the wavelength that corresponding at horizontal and vertical input motions frequencies for each unit of Angitola reservoir are shown.

Table 5.8: Wavelengths corresponding to horizontal and vertical input motions frequencies for each unit of Angitola dams

			f = (2-2.9) Hz		**f = (5-7.25) Hz**		**f = (8-11.6) Hz**	
material	**Vs**	**Vp**	**λs**	**λp**	**λs**	**λp**	**λs**	**λp**
	[m/s]	**[m/s]**	**[m]**	**[m]**	**[m]**	**[m]**	**[m]**	**[m]**
Core	240	587.88	120	203	48	81	30	51
Shell	325	645.20	163	222	65	89	41	56
Alluvial Sand	470	1558.8	235	538	94	215	59	134
Alluvial Sand	600	1990.0	300	686	120	274	75	172
Sandy silty	350	1471.1	175	507	70	203	44	127
Silty gravel	450	1653.4	225	570	90	228	56	143
Silty clay	480	1466.4	240	506	96	202	60	126
Gravely Sand	600	1990.0	300	686	120	274	75	172
Weathered Gneiss	850	1769.4	425	610	170	244	106	153
Gneiss	1500	3122.5	750	1077	300	431	188	269

Figure 5.50 presents the comparison, in terms of transfers functions calculated at the crest of the dams in East-West, North-South and Up-Down directions (obtained applied only the corresponding input component), between whole system (solid lines) and separate ones (dashed lines) for left dam (effect of right dam on left one) and right one (effect of left dam on right one). The comparison indicates generally negligible differences in horizontal directions for frequencies less than 4Hz that corresponds to wavelength of input motion greater than geometrical dimensions of dams and respective distance (200 m) for both dams. At high frequencies, right dam exhibits greater differences between whole system and separate one as compared to left one.

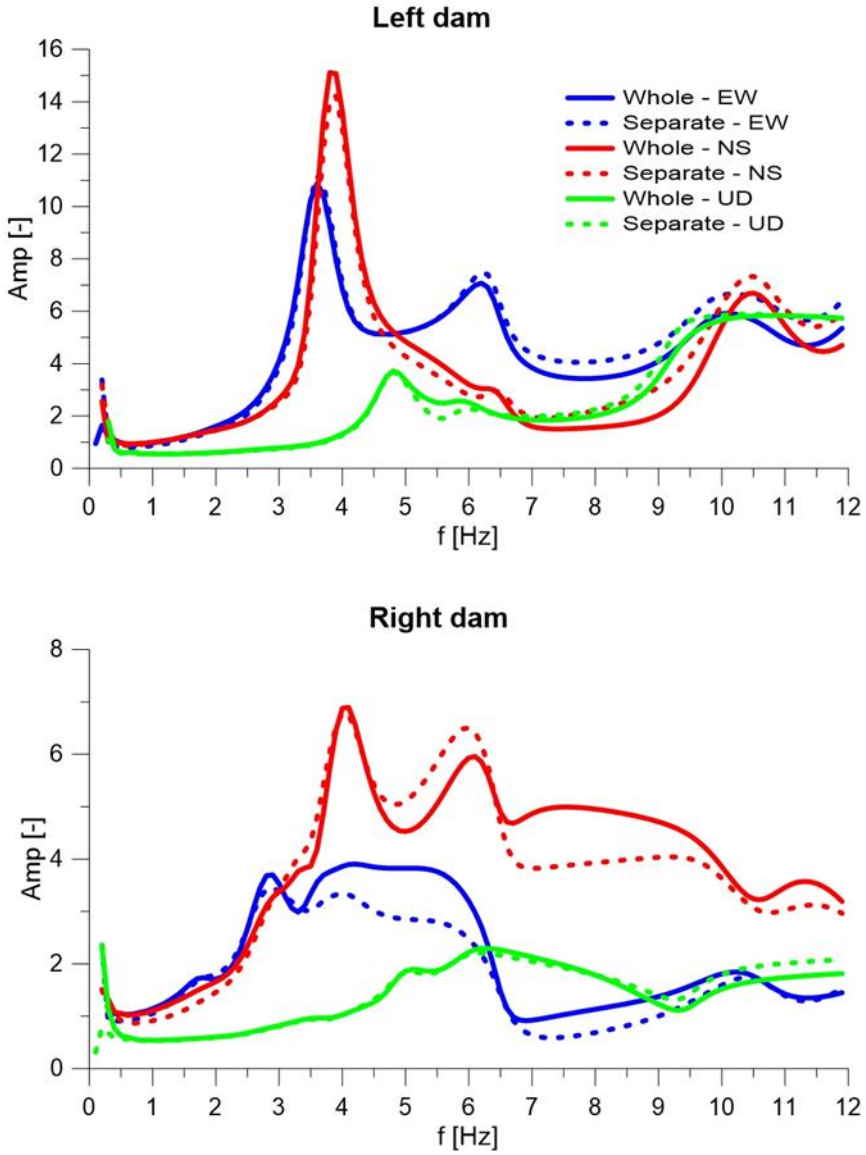

Figure 5.50: Transfer functions at the crest of both dams for the whole system (solid lines) and for the dams taken separately (dashed lines) in East-West (blue lines), North-South (red lines) and Up-Down (green lines) directions.

Figure 5.51 and Figure 5.52 present the same comparison, but in terms of horizontal and vertical displacement amplitude ratios, applying both horizontal and vertical input motion components. The same figures also show the effect of introduction of vertical motion that lead to significant amplifications of vertical displacements at medium and high frequencies.

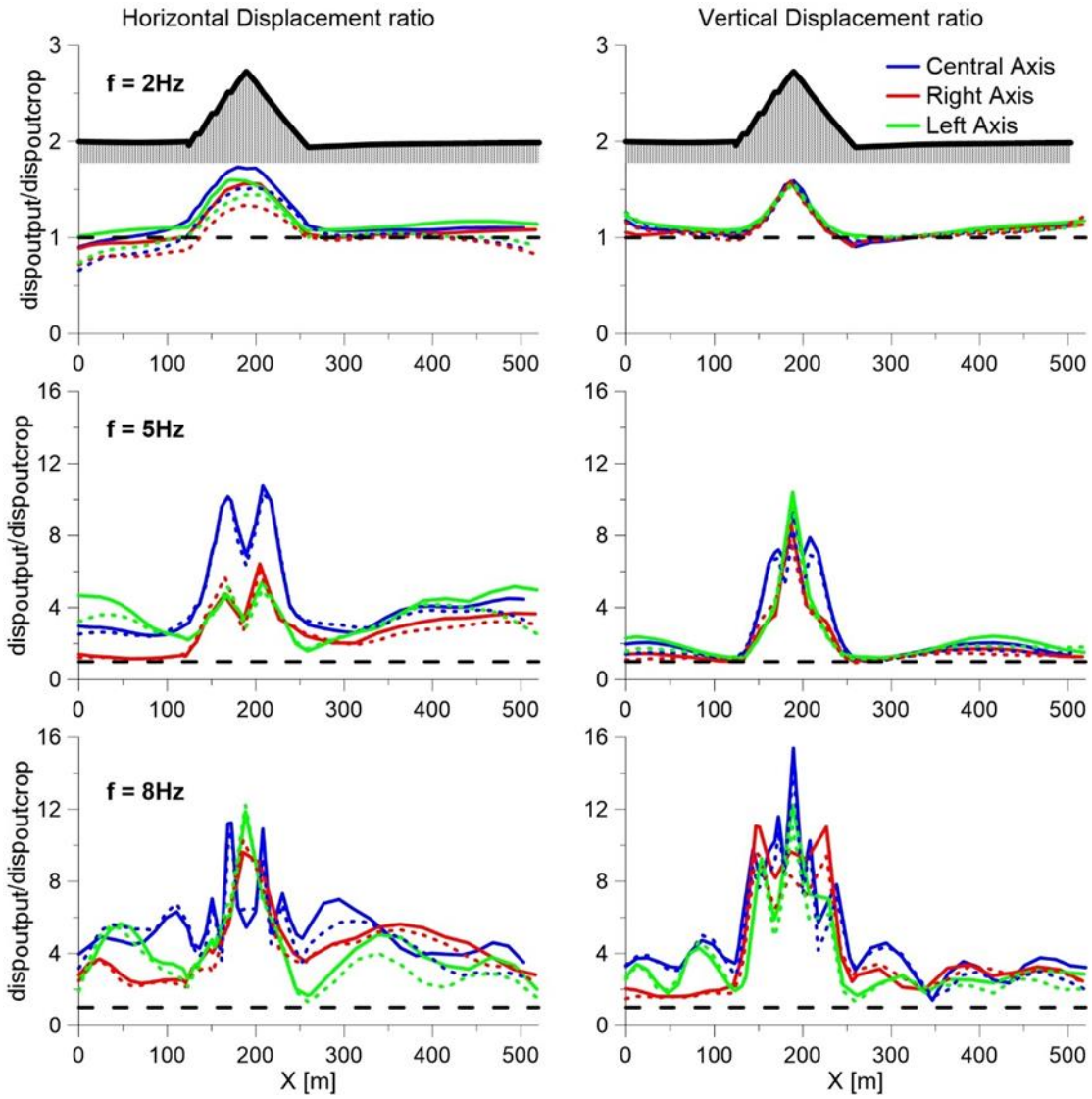

Figure 5.51: Comparison between 3D displacement ratios for whole system (solid lines) and separate ones (dashed lines) for left dam. Blue lines: central axis; red lines: right axis; green lines: left axis

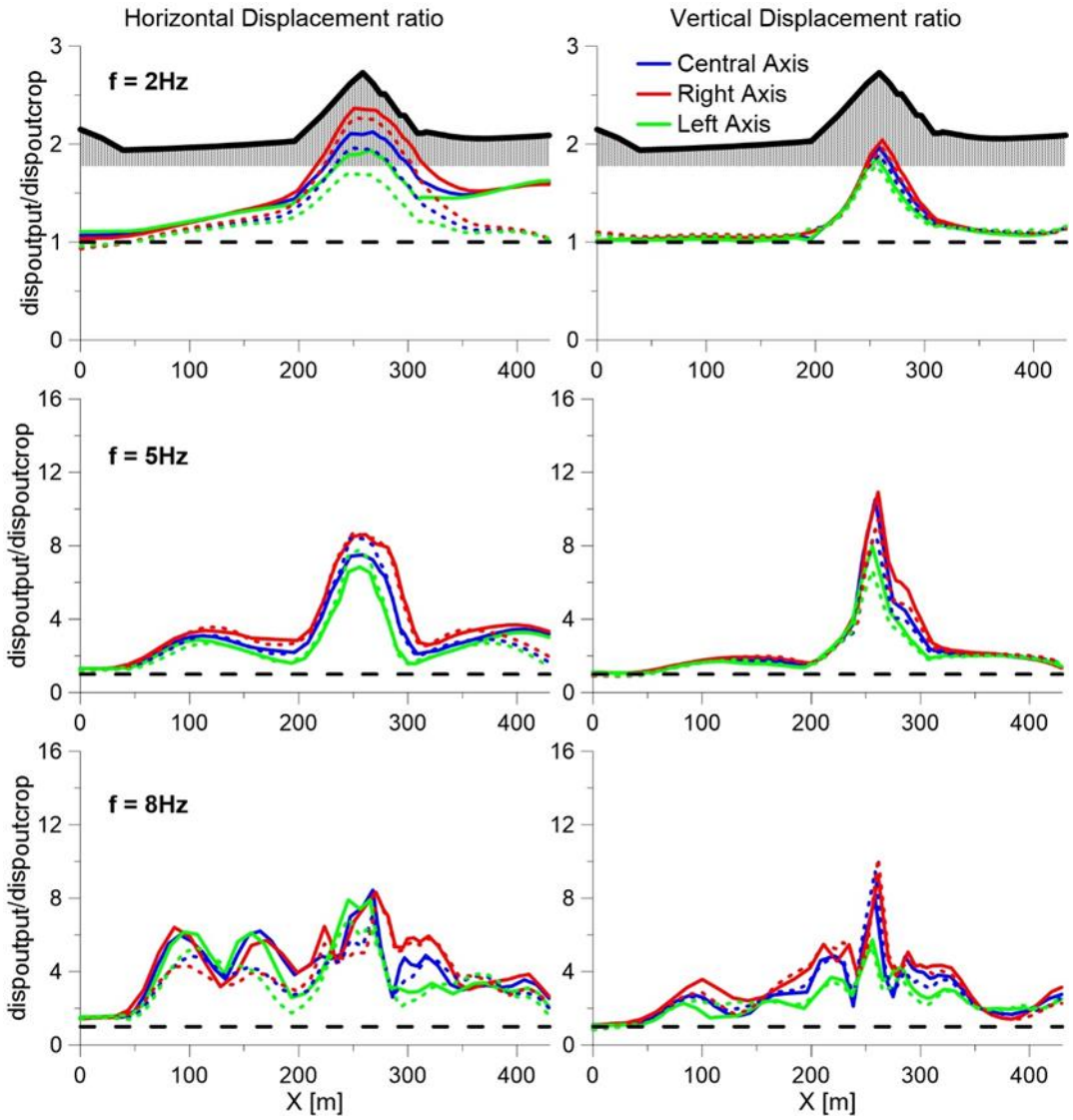

Figure 5.52: Comparison between 3D displacement ratios for whole system (solid lines) and separate ones (dashed lines) for left dam. Blue lines: central axis; red lines: right axis; green lines: left axis

The contours of acceleration amplitude, defined as $mag(t) = \sqrt[2]{acc\_x(t)^2 + acc\_y(t)^2 + acc\_z(t)^2}$ (where acc_x, acc_y and acc_z are the acceleration components and t = 1.5 s the time) for seismic scenario 1 for f= 2, 5 and 8Hz, are shown for Figure 5.53 to Figure 5.55, respectively. Similarly, from Figure 5.56 to Figure 5.58 the contours of vertical acceleration for seismic scenario 2 are presented. Generally, output accelerations increase and became more complex with frequency.

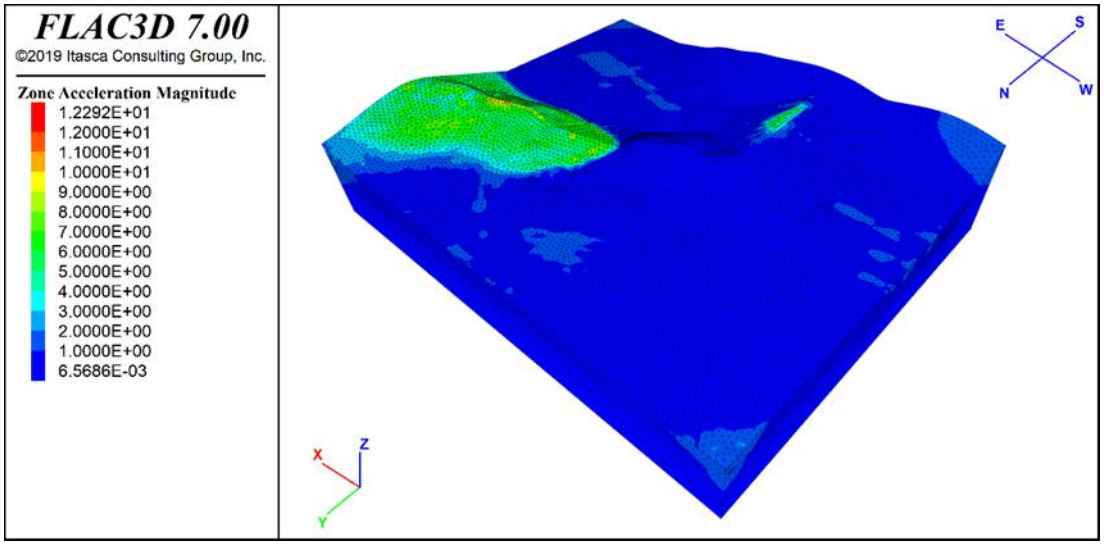

Figure 5.53: Contours of acceleration amplitude for seismic scenario 1 with f = 2Hz.

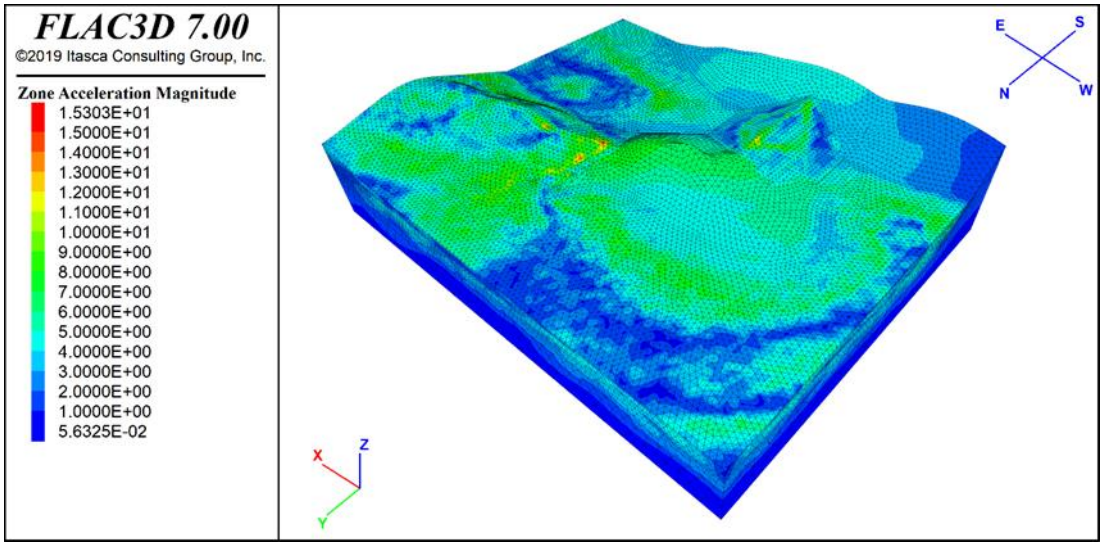

Figure 5.54: Contours of acceleration amplitude for seismic scenario 1 with f = 5Hz.

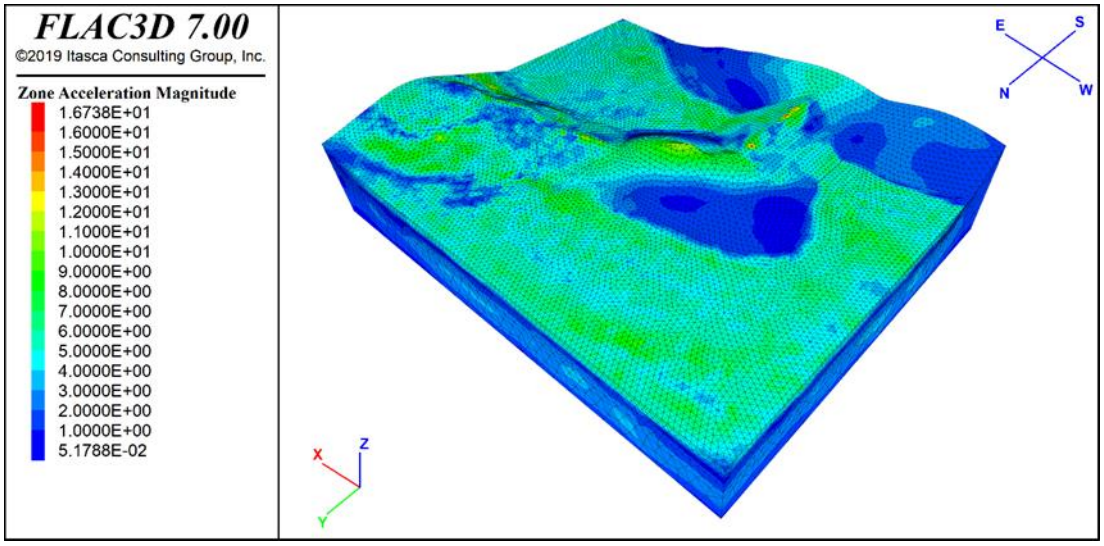

Figure 5.55: Contours of acceleration amplitude for seismic scenario 1 with f = 8Hz.

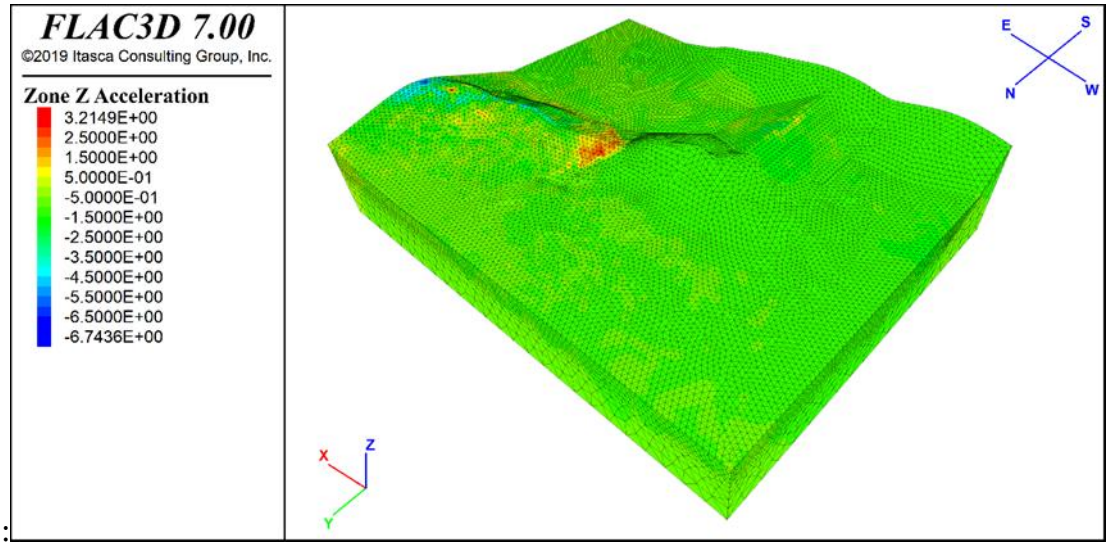

:

Figure 5.56: Contours of vertical acceleration for seismic scenario 2 with f = 2Hz.

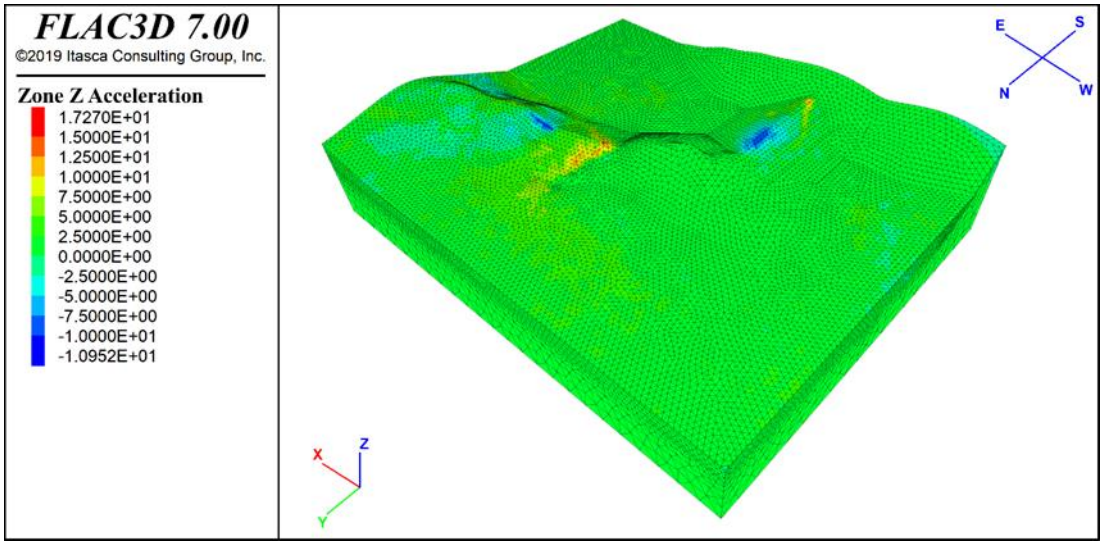

Figure 5.57: Contours of vertical acceleration for seismic scenario 2 with f = 5Hz.

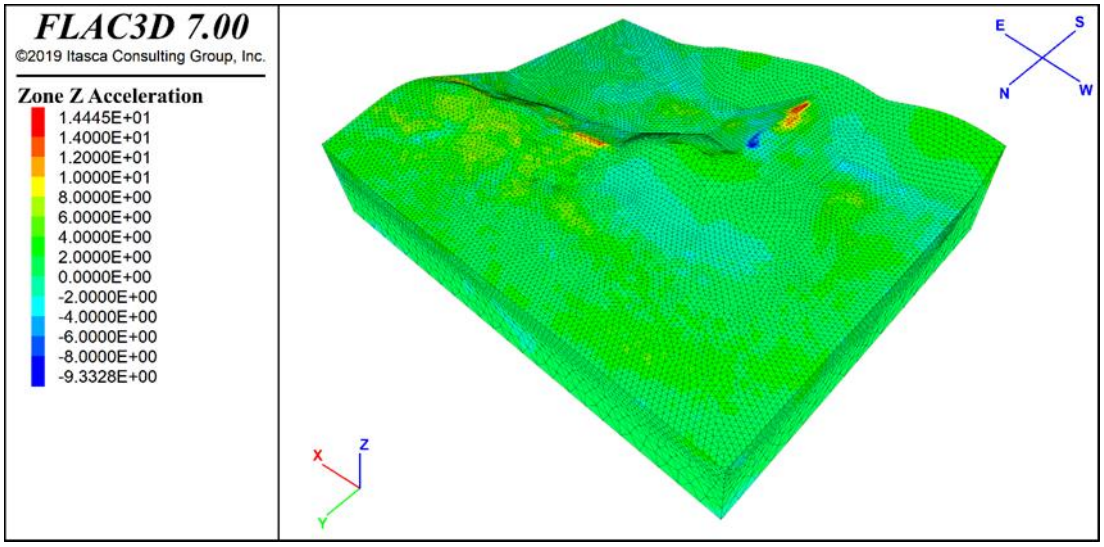

Figure 5.58: Contours of vertical acceleration for seismic scenario 2 with f = 8Hz.

6 Conclusions and future perspectives

Numerical simulations of waves propagation are increasingly used in seismic hazard studies because are fundamental tools for the assessment of surface motion for given seismic input scenarios. Since seventies, for many decades the one-dimensional (1D) vertical propagation of shear waves from bedrock to the ground surface of a soil deposit was the standard to obtain the characteristics of seismic motion. In fact, two-dimensional (2D) and, to a larger extent, three-dimensional (3D) simulations involve more complicated phenomena, absent in 1D models, such as focusing and defocusing of seismic energy, scattering and diffraction of seismic waves which can lead to mode conversion near surface and subsurface irregularities, generation of surface waves, constructive and destructive interference patterns giving rise to very complex wavefields. However, in the last decades, the increasing efficiency of computational tools has facilitated the use of 2D and 3D numerical methods for modelling the seismic behaviour under complex geomorphologic conditions. These numerical methods have in some way replaced the analytical ones which were developed since seventies, even if the closed-form solutions of the analytical methods are still widely used to check the accuracy of numerical simulations.

It is the aim of this research work to: 1) validating the finite difference code FLAC3D for assessing 2D and 3D seismic motion which takes into account the effect of surface and subsurface irregularities using closed-form solutions available in the literature; 2) comparing the results of 2D and 3D numerical simulations to identify the main parameters which affect the intensity of seismic motion, with particular attention to those resulting in major differences between 2D and 3D conditions. This latter aspect has been investigated first with numerical simulations of simple geometric features (ridges, sediment-filled valleys, earth dams). Further, two well-documented large-scale case studies, that is the Palatino Hill in Rome and the Angitola earth dams in Southern Italy, have been studied. In both cases, an analogous procedure was followed, which consisted in considering several models of increasing complexity, starting from the homogenous subsoil to the layered ones with various degree of in-homogeneity. All the dynamic analyses have been carried out with the assumption of linear visco-elastic soil behaviour.

As input motion a Chang wavelet was applied at base of the models as outcrop motion. Two seismic input have been considered: 1) motion was applied along the two horizontal components (EW and NS direction) by using three input motion frequencies (f = 2, 5 and 8

Hz); 2) as above, adding the vertical component; this latter was assumed of amplitude equal to half the horizontal one and frequency 40% larger than horizontal one.

6.1 Summary of the results for surface and subsurface irregularities

Several insights can be obtained from the results of analytical and numerical studies available in literature on the effects of the 2D and 3D scattering and diffraction of elastic waves by canyons, alluvial valleys and topographic irregularities.

These results show that the response of canyons to SH waves depend predominantly on the dimensionless frequency parameter η (defined as the ratio between a geometric characteristic and the wavelength of input motion) and the angle of incidence of arriving waves γ. Higher η (i.e., for wavelength of incident motion shorter than the radius of the canyon), leads to great complexity of the pattern of the surface displacement amplitudes, while γ determines the overall trends of displacement amplitudes: generally, an amplification of surface motion occurs in front of the canyon whereas a shadow zone is developed behind the canyon leading to a uniform de-amplification.

The presence of an alluvial deposit in a canyon can significantly modify the motion along the canyon surface. A comprehensive study by Bard and Bouchon (1985) identified the main physical parameters affecting the so-called valley effects. The study showed the generation at the edge of the valleys of surface waves (Love waves for incident SH waves and Rayleigh waves for incident P-SV waves) which may have much larger amplitude than the incident signal. These surface waves can propagate back and forth within the soil deposit and this can lead to an amplification of the surface motion, an elongation of duration and, finally, a significant differential motion. More specifically, in shallow valleys, the wavefield is dominated by laterally propagating surface waves generated at the valley edges. In deeper valleys, the interference of these surface waves with vertically propagating waves gives rise to a 2-D resonance pattern. The transition between the behaviour of shallow and deep valleys is governed by a critical shape ratio, which is defined as the ratio of the maximum sediment thickness to the valley half-width. The critical shape ratio depends on the velocity contrast between bedrock and fill material.

In the last two decades, a number of researchers have investigated the response of alluvial valleys by means of numerical parametric studies. They found that the most important dimensionless parameters governing the seismic response are λ/H and B/λ ratios, where B and

H are the width and the thickness of the valley, and λ is the predominant wavelength of S wave, and the soil-to-bedrock impedance ratio. In particular, aggravation of surface motion generally decreases with increasing of the dimensionless parameters λ/H, B/λ and impedance ratio. This means that amplification under 2D condition is larger for narrow and thick valleys, especially for soils much softer than the underlying bedrock. Other factors that have emerged are: i) soil nonlinearity which may result in a drastic reduction of the amplitude of ground motion amplification; ii) even when the valley is excited exclusively by horizontal waves, the generation of a "parasitic" vertical component which may be detrimental for overlying structures being of practically the same dominant period as the horizontal component.

As the surface irregularities (topographic effects) are concerned, the result of analytical/numerical simulations can be summarised as follows: (i) the irregularity has quite considerable effects on ground motions for both the points on the feature itself and its environs; (2) slope angle and normalized height (H/λ) of the slope have a significant effect on the horizontal and vertical amplification of motion, as well as the distance to the free-field in front and behind the slope; iii) topography effects become important for H/L values larger than 0.16 and slope inclinations larger than 17°; iv) attenuation near the toe of the slope indicates that topographic effects can be overestimated when comparing crest-toe ground motions, therefore an adequate free-field site has to be identified in order to reliable quantify site effects; v) topographic effects are frequency-dependent; vi) even purely horizontal accelerations (vertically propagating SV waves) generates significant parasitic vertical accelerations; vii) generally, numerical predictions always underestimate the field observations; in this respect, 3D numerical models could be more efficient than 1D and 2D ones for studying wave propagation for topographic features.

The Palatino hill and the surrounding archaeological area in the historical centre of Rome was studied to evaluate the parameter that affect the dynamic response of natural reliefs. The model is characterized by complex site conditions in terms of surficial and buried morphology, stratigraphy and small-strains dynamic properties. The 2D and 3D numerical results are compared in terms of acceleration ratio PGAoutput/PGAoutcrop, along two cross-sections (A and B) representative of the morphological and geological characteristics of the whole area. Cross-section A cuts the Palatino hill through its centre in a NW-SE direction while cross-section B is traced along the SW-NE direction. Three simplified models of increasing complexity have been defined to study the main parameters influencing the seismic response:

- ✓ Homogeneous model, obtained by merging all subsoil units, in order to study the effect of topography;
- ✓ Bi-layer model, obtained by merging all units except the anthropic cover (RPI_AEL);
- ✓ Bi-layer + sediment-filled valley model, obtained by merging all units except RPI_AEL and sediment-filled valleys (SFTba).

As mentioned, the Homogeneous model takes into account only topographic effects. The comparison between 2D and 3D numerical results, obtained by applying only horizontal motion (E-W and N-S directions) for both cross-sections, allows the following considerations:

- ✓ 2D analyses provide amplifications ratios of 1.2-1.4 (in agreement with EC8 indications) regardless of the frequency;
- ✓ 3D numerical results exhibit amplification ratio larger than 2D ones; these latter underestimate the amplification of about 50%;
- ✓ vertical (parasitic) component increases with frequency especially for 3D analyses;
- ✓ applying the motion parallel to the section, there are no appreciable differences with 2D numerical results.

In order to study the effect of cover layer (Vs = 350m/s and h ≈ 10m), Bi-Layer model was studied. The numerical results show:

- ✓ no appreciable difference with homogeneous model at low frequency (f = 2Hz);
- ✓ 3D model provides greater amplitudes as compared to 2D ones at medium and high frequencies (f = 5 and 8 Hz);
- ✓ the 3D amplitudes are about twice those of the homogeneous model.

The sediment-filled valleys bordering Palatino hill are characterized by variable depth. Along cross section A (that intersect two valleys) the valley is characterized by minor width and depth as compared to section B, but the shape-ratio h/l is actually similar. Numerical results show:

- ✓ no appreciable difference with bi-layer model except at low frequency (f=2Hz) in correspondence of the valleys both for 2D and 3D numerical results; this is related to the resonance frequencies of both valleys which is around 2.5-3.0 Hz;

The comparison between Complete model and Bi-layer+sediment-filled valley model, adding the vertical input motion show:

- ✓ 3D numerical results of the complete model are slightly greater than those of the Bi-layer+soft-filled valley model, regardless of frequency;

Complete model show greater amplification as compared to Bi-layer+sediment-filled valley in terms of vertical component both for 2D and 3D numerical results.

6.2 Summary of the results for earth dams

Several closed-form solutions are available in literature, both for 2D and 3D dynamic response of earth dams, based on the shear-beam approach. The limitations of these solutions are: 1) only transversal displacement are considered due at shear-beam approach; therefore no vertical, longitudinal input motion components and parasitic vertical are taken into account. The following points can be highlighted, as reported in Gazetas and Dakoulas (1992). The 2D approach is strictly valid for infinitely long dams. For dams built in narrow canyons, a number of analytical solutions have been developed for the seismic response analyses of 3D dam-canyon systems subjected to rigid-base excitation. It has been found that the fundamental natural period of a dam significantly depends on the canyon geometry and its aspect ratio (L/H) and it increases as L/H decreases. This restraining effect is called stiffening effect. The 3D "narrowness" effect was also highlighted in the amplification function. It was shown that, in addition to predict lower natural frequencies, the 2D model underpredicts both the amplification at the fundamental frequency and the higher mode resonances. Analogous differences between 2D and 3D results can be seen in the acceleration profiles. Peak accelerations near the crest of dams in narrow canyons (L/H=2) may exceed by a factor of 2 the corresponding 2D values. Moreover, 3D accelerations histories are much richer in high frequency components of motion since the fundamental frequency is shifted towards higher frequency and due to the importance of the higher harmonics, as compared to the 2D case. The analytical results have also shown that amplification at the crest would increase if the material inhomogeneity of dam body is taken into account. On the contrary, amplification effects would reduce for the assumption of deformable (elastic) canyon, as a considerable amount of energy would radiated back into the canyon half-space. The presence of a deformable foundation layer would increase the overall flexibility of the dam-foundation system, and hence this would result in a lengthening of the fundamental period of the dam. Finally, all the above considerations refer to linear soil behaviour. If soil nonlinearity that develop in case of strong seismic excitations is considered, this would lead to a reduction of peak crest accelerations. This would happen because of the increased hysteretic damping, which acts especially on the high-frequency motion, and possible destruction of resonances. Therefore, soil nonlinearity would potentially reduce some of the adverse effects of narrow canyon geometries on crest accelerations.

The Angitola reservoir located in Calabria (Southern Italy) was considered as case study for investigating the dynamic response of a complex 3D geotechnical system. In fact, the whole system is composed of two trapezoidal embankment dams separated by a rock spur (Monte

Marello). The principal (or left) dam is 29.8 m high with shape-ratio L/H = 4.5 and the secondary (or right) dam is 24.1 m with L/H = 3. The subsoil of right dam is more heterogeneous as compared to the subsoil of left dam. The seismic bedrock is constituted by a gneiss formation, which is weathered in its surficial portion. Two simplified models have been considered in order to study the main parameters affecting dynamic response:

- ✓ Homogeneous subsoil model, obtained by merging all geological/geotechnical units present in the foundation soil (therefore with the exception of the dam body), to study the effect of shape ratio (stiffening effect);
- ✓ Foundation layer model, obtained by merging all units between base of the dams and the top of gneiss formation.

The numerical analyses has been conducted first considering the two dams separately; then, the whole system (two dams + Monte Marello) was studied to evaluate the interaction between dams. The comparisons between 3D and 2D numerical results have been carried out in terms of surface displacement ratio (dispoutput/dispoutcrop) along three horizontal axes, that is central, left and right ones. The comparisons between 2D and 3D numerical results, obtained applying only the horizontal motion, for Homogeneous subsoil model for both dams shows:

- ✓ greater 2D amplification at low frequency compared to 3D (frequency shift due to stiffening effect);
- ✓ greater 3D amplification as compared to 2D, especially at medium frequency (f=5Hz) for central axis;
- ✓ the vertical parasitic component increases with input frequency, that is negligible values are exhibited at low frequency (f = 2Hz) both for 2D and 3D conditions while the same order of magnitude than horizontal can be recognized at high frequency (f = 8Hz);
- ✓ principal dam exhibits greater amplifications, especially at medium and high frequencies, than secondary one, probably due to the minor shape ratio L/H.

The Foundation layer model takes into account the effects of softer layers between the base of the dams and the seismic bedrock (foundation layer). Numerical results show that the introduction of the foundation layer leads to:

- ✓ at low frequency (2Hz), 3D amplification is larger for foundation layer system as compared to the 3D homogeneous model while the reverse occurs at medium frequency (5 Hz) for secondary dam; this is due to the period lengthening because of the presence of the foundation layer;

- ✓ 3D amplification is larger than 2D one, especially at medium frequency while negligible difference are present at low frequency;
- ✓ the vertical parasitic component increases with frequency; 3D component is larger than 2D one.

For the complete model, it was investigated: 1) the effect of interaction between dams, obtained comparing the seismic response of the dam considered separately with the whole system; 2) introduction of vertical input motion on whole system:

- ✓ the comparison between complete and separate models indicates generally slight differences;
- ✓ the introduction of vertical motion provides significant amplifications on vertical displacements, especially at high frequency.

6.3 Remarks on dynamic response of natural reliefs and earth dams

For Palatino Hill and surrounding areas, 3D numerical results indicate greater amplification of horizontal motion as compared to 2D results, regardless of the frequency of the input motion. 3D Homogeneous model, which that takes into account only topographic effects, provide amplification of 2. The increase of frequency leads to great complexity of the pattern of the surface amplification but negligible increase of amplitude. The Bi-Layer model, that considers the cover layer effects, provides larger amplifications up to 3 and 5 at medium and high frequency, respectively. The introduction of sediment-filled valley does not drastically change the pattern of amplification of the previous model, except in correspondence of the valleys where significant amplification can be observed for input frequencies near the natural frequency of the valleys. The Complete model provides greater amplification as compared to simplified ones.

For earth dams both closed-form solutions and numerical results show that the 2D models provide greater amplifications than 3D at low frequencies. For 3D models the parameters that provide the greater horizontal amplifications at the crest of the dams, are the canyon shape and its shape ratio (L/H). the Homogeneous models provide horizontal displacement ratio up to 7.0 and 10.0 for principal dam (L/H = 4.5) and secondary one (L/H = 3.0), respectively. The Foundation layer model provides a slight decrease of horizontal amplification as compared to the Homogenous model. It leads to similar displacement ratio (equal to 6.0) for both principal and secondary dams. Indeed, the introduction of foundation layer provides significant increase

of vertical parasitic component, especially at medium frequencies. Complete models and whole system do not provide significant increase of amplification as compared to the foundation layer model, both for horizontal and vertical components.

There are some common aspects on 2D and 3D dynamic response of natural reliefs and earth dams that need to be pointed up. The results of large-scale visco-elastic linear 3D numerical analyses carried out on different complex geological/geotechnical systems have shown that:

- ✓ 3D ground motion amplification of the horizontal components increases as the complexity of the system increases moving from homogeneous model (i.e. topographic amplification) to heterogeneous ones (topographic + stratigraphic/valley + buried morphology amplifications);
- ✓ 3D ground motion amplification is frequency-dependent (e.g., effect of cover layer or valleys in Palatino hill/ and lengthening period effect for foundation layer in Angitola dams);
- ✓ amplitude of vertical parasitic component increases with frequency of motion;
- ✓ generally, in the two case studies examined, 3D analyses provide higher ground motion amplification than 2D ones.

6.4 Future perspectives

Perspectives for further research on the topics addressed in this thesis may stem from some limitations or some issues that were covered within the present work. The thesis has analysed two well-documented case histories characterized by complex geomorphological/geotechnical conditions. However, it is evident that a single case history, one for topographic irregularity and the other for earth dam, is not enough to allow a generalization of the results on the 2D versus 3D differences in seismic ground motion amplification. Therefore, future work could focus on the definition of other cases histories, indicatively earth dams with different canyon shapes and shape ratio, and natural reliefs with different geometric configurations. Another topic which deserves attention is related to the soil nonlinearity, which has been not thoroughly investigated.

7 References

Alongkorn A. Lee V. W. (2013) Scattering of anti-plane (SH) waves by a semi-elliptical hill: II—deep hill, Soil Dynamics and Earthquake Engineering, Volume 52, Pages 126-137, ISSN 0267-7261,

Ambraseys N. N. (1960) On the shear response of a two-dimensional truncated wedge subjected to an arbitrary disturbance, Bull. Seism. Soc. Am. 50(1), 45-56

Aki K. & Larner K. L. Surface motion of a layered medium having an irregular interface due to incident plane SH waves. Journal of Geophysical Research Volume 75, Issue 5 10 February 1970 Pages 933-954

Ashford S. A. et al. (1997) Topographic effects on the seismic response of steep slopes. Bulletin of the Seismological Society of America (1997) 87 (3): 701–709.

Ashford S. A. & Sitar N. Analysis of topographic amplification of inclined shear waves in a steep coastal bluff. Bulletin of the Seismological Society of America (1997) 87 (3): 692–700.

Assimaki D. et al (2005) Effects of Local Soil Conditions on the Topographic Aggravation of Seismic Motion: Parametric Investigation and Recorded Field Evidence from the 1999 Athens Earthquake, Bulletin of the Seismological Society of America (2005) 95 (3): 1059–1089.

Assimaki D. & Jeong S. (2010) Ground-Motion Observations at Hotel Montana during the M 7.0 2010 Haiti Earthquake: Topography or Soil Amplification? Bulletin of the Seismological Society of America (2013) 103 (5): 2577–2590.

Bard P. & Bouchon M. (1980a) The seismic response of sediment-filled valleys. Part I. The case of incident SH waves, Bulletin of Seismol. Soc. of America, 70(4), 1263-1286.

Bard, P. & Bouchon, M. (1980b) The seismic response of sediment-filled valleys. Part 2. The case of incident P & SV waves, Bulletin of Seismol. Soc. of America, 70(5), 1921-1941.

Bard P. Y. (1982) Diffracted waves and displacement field over two-dimensional elevated topographies. Geophysical Journal International, Volume 71, Issue 3, December 1982, Pages 731–760.

Bard, P. & Bouchon, M. (1985) The two-dimensional resonance of sedimentary-filled valleys, Bulletin of the Seismological Society of America, 75, 519-541.

Bard P. Reipl-Thomas J. Wave propagation in complex geological structures and their effect on strong ground motion.

Bielak et al (2000). One- vs Two- or three-dimensional effects in sedimentary valleys 12WCEE 2000.

Bouchon M. (1973) Effect of topography on surface motion. Bulletin of the Seismological Society of America 63 (2): 615–632.

Bouckovalas G. & Papadimitriou G. (2004) Numerical evaluation of slope topography effects on seismic ground motion, Soil Dynamics and Earthquake Engineering 25 547–558.

Bouckovalas G. & Papadimitriou A. (2006) Aggravation of seismic ground motion due to slope Topography, First European Conference on Earthquake Engineering and Seismology (a joint event of the 13th ECEE & 30th General Assembly of the ESC) Geneva, Switzerland, 3-8 September 2006 Paper Number: 1171.

Chávez-García, F. J. (2003) Site effects in Parkway Basin: comparison between observations and 3-D modelling. Geophysical Journal International, 154, 633–646

Cao H. and Lee V. W. (1989) Scattering of plane SH waves by circular cylindrical canyons with variable depth-to-width ratio, European J. of Earthquake Engineering, 1989.

Cao H. and Lee V. W. (1990) Scattering and diffraction of plane P waves by circular cylindrical canyons with variable depth-to-width ratio, Soil Dynamics and Earthquake Engineering, 1990, Vol. 9, No.3.

Chávez-García F. J. (2003) Site effects in Parkway Basin: comparison between observations and 3-D modelling. Geophysical Journal International, Volume 154, Issue 3, September 2003, Pages 633–646, https://doi.org/10.1046/j.1365-246X.2003.02055.x

Dakoulas, P. & Gazetas, G. (1985) A class of inhomogeneous shear models for seismic response of dams and embankments, Soil Dynamic and Earthquake Engineering. Vol. 4, No. 4, 166 182.

Dakoulas, P. & Gazetas, G. (1986) Seismic lateral vibration of embankment dams in semi-cylindrical valleys, Earthquake Engineering. and Structural Dynamic. No. 14, 19-40

Dakoulas P. (1990) Nonlinear response of dams founded on alluvial deposits in narrow canyons, Soil Dynamics and Earthquake Engineering Volume 9, Issue 6, November 1990, Pages 301-312

Dakoulas P. Hashimi H. (1991) Response of Earth Dams in Canyons Subjected to Asynchronous Base Excitation. International Conferences on Recent Advances in Geotechnical Earthquake Engineering and Soil Dynamics. 23.

Dakoulas P & Gazetas G. (1992), Aspects of Seismic Analysis and Design of Rockfill Dams. International Conferences on Recent Advances in Geotechnical Earthquake Engineering and Soil Dynamics.

Dakoulas, P. (1993) Response of Earth Dams in Semicylindrical Canyons to Oblique SH Waves, January 1993 Journal of Engineering Mechanics 119(1)

Dakoulas, P. (1993) Earth Dam-Canyon Interaction Effects for Obliquely Incident SH Waves, November 1993 Journal of Geotechnical Engineering 119:11(11)

Dakoulas P. & Hsu C. H. (1993) Lateral response of dams in semi-elliptical rigid canyons. Soil Dynamics and Earthquake Engineering 12 (1993) 497-507.

Dakoulas P. & Hsu C. H. (1995) Response of dams in semielliptical canyons to oblique SH waves. Journal of Engineering Mechanics. Vol. 121, No.3, March, 1995.

Faccioli, E., Maggio, F., Paolucci, R. et al. (1997) 2d and 3D elastic wave propagation by a pseudo-spectral domain decomposition method. Journal of Seismology 1, 237–251. https://doi.org/10.1023/A:1009758820546

Faccioli E. (2002) Complex" site effects in earthquake ground motion, including topography, 12th European Conference on Earthquake Engineering Paper Reference: 844

Funiciello R. and Giordano G. (2008). Foglio e Note illustrative, Carta Geologica d'Italia alla scala 1:50.000, Foglio 374 ROMA, APAT - Servizio Geologico d'Italia, Roma.

Garini E. et al (2020) Soil, basin and soil–building–soil interaction effects on motions of Mexico City during seven earthquakes, Géotechnique Volume 70 Issue 7, July, 2020, pp. 581-607.

Gazetas, G. (1981) A new dynamic model for earth dams evaluated through case histories, Soils and Foundations 21(1), 67-68.

Gazetas, G. (1981) Vertical oscillation of earth and rockfill dams: analysis and field observation, Soils and Foundations 21 (4), 265-277

Gazetas, G. (1982) Shear vibrations of vertically inhomogeneous earth dams, Int. J. for Numerical and Analytical Methods in Geomechanics, 6[1], 219-241

Gazetas G. (1987) Seismic response of earth dams: some recent development. Soil Dynamics and Earthquake Engineering Volume 6, Issue 1, January 1987, Pages 2-47

Gazetas G & Dakoulas P. (1992) Seismic analysis and design of rockfill dams: state-of-the-art. Soil Dynamics and Earthquake Engineering Volume 11, Issue 1, 1992, Pages 27-61

Gelagoti F., Kourkoulis R., Anastasopoulos I., Tazoh T., Gazetas. G. (2010) Seismic Wave Propagation in a Very Soft Alluvial Valley: Sensitivity to Ground-Motion Details and Soil Nonlinearity, and Generation of a Parasitic Vertical Component Bulletin of the Seismological Society of America (2010) 100 (6): 3035–3054. https://doi.org/10.1785/0120100002

Geli et al. (1988) The effect of topography on earthquake ground motion: A review and new results, Bulletin of the Seismological Society of America 78 (1): 42–63, 1988.

Griffiths D. V. & Prevost J. H. (1988) Two- and three-dimensional dynamic finite element analyses of the Long Valley Dam. Géotechnique ISSN 0016-8505 | E-ISSN 1751-7656
Volume 38 Issue 3, September, pp. 367-388.

Hayir A. Todorovska M. Trufunac M.. Antiplane. (2001) Response of a dike with flexible soil-structure interface to incident SH waves. October 2001, Soil Dynamics and Earthquake Engineering 21(7):603-613 DOI: 10.1016/S0267-7261(01)00035-5.

Hashmi, H. (1989) Response of earth dams in canyons subjected to asynchronous base excitation, M.S. Thesis, Rice University, Houston, Texas.

Hatanaka, M. (1952) Fundamental consideration on the earthquake resistant properties of the earth dam, Bull. No. It, Disaster Prevention Research Inst., Kyoto Univ.

Kawase H. (1996) The Cause of the Damage Belt in Kobe: “The Basin-Edge Effect,” Constructive Interference of the Direct S-Wave with the Basin-Induced Diffracted/Rayleigh Waves. Seismological Research Letters (1996) 67 (5): 25–34.

Khanbabazadeh, H., Iyisan, R. (2014) A numerical study on the 2D behavior of the single and layered clayey basins. Bulletin Earthquake Engineering 12, 1515–1536 (2014). https://doi.org/10.1007/s10518-014-9590-4

Kramer, S. L. (1996) Geotechnical Earthquake Engineering. New Jersey: Prentice-Hall.

Kuhlemeyer R. L. Lysmer J. (1973) Finite element method accuracy for wave propagation problems. J Soil Mechanism & Foundation Div ASCE 99 (SM5):421–427.

Idriss I.M & Seed B. H. (1967) response of horizontal soil layers during earthquakes. Soil Mechanics and Foundations Division, Proceedings of the American Society of Civil Engineers, Vol. 94, No. SM4, July, 1968.

Itasca Consulting Group (2005). "FLAC, Fast Lagrangian Analysis of Continua, User's Guide, Dynamic Analysis". Minneapolis, Minnesota, USA.

Iyisan, R., Khanbabazadeh, H. (2013) A numerical study on the basin edge effect on soil amplification. Bulletin Earthquake Engineering 11, 1305–1323.

Lanzo G., Pagliaroli A. (2009). Numerical modeling of site effects at San Giuliano di Puglia (Southern Italy) during the 2002 Molise seismic sequence. ASCE, Journal of Geotechnical and Geoenvironmental Engineering, 135, 9, 1295-1313.

Lee V. W. and Cao H. (1989) Diffraction of SV waves by circular canyons of various depths, Journal of Engineering Mechanics, Vol. 115, No. 9, September 1989. Paper No. 23884.

Lee, V. W. (1977) On deformations near circular underground cavity subjected to incident plane SH-waves, Proc. of Symposium 011 Applications on Computer Methods in Engineering, Vol II, USC 951-962

Lee, V. W. (1978) Displacements near a three-dimensional hemispherical canyon subjected to incident plane waves, USC Report No. CE 78-16,

Lee V. W. (1984) Three-dimensional diffraction of plane P, SV & SH waves by a hemispherical alluvial valley, International Journal of Soil Dynamics and Earthquake Engineering, Volume 3, Issue 3, 1984, Pages 133-144.

Lee V. W. (2006) Antiplane (SH) Waves Diffraction by a Semicircular Cylindrical Hill Revisited: An Improved Analytic Wave Series Solution. Journal of engineering mechanics ASCE/ October 2006

Lee V. W. and Amornwongpaibun A. (2013) Scattering of anti-plane (SH) waves by a semi-elliptical hill: I—Shallow hill, Soil Dynamics and Earthquake Engineering, Volume 52, Pages 116-125, ISSN 0267-7261.

Lee V. W. and Sherif R.I. (1966) Diffraction around circular canyon in elastic wedge space by plane SH-waves- Journal of engineering mechanics,

Lee V. W. (1990) Scattering of Plane SH-Waves by a Semi-Parabolic Cylindrical Canyon in an Elastic Half-Space. Geophysical Journal International, Volume 100, Issue 1, January 1990, Pages 79–86.

Lysmer J. & Kuhlemeyer R. L. (1969) Finite Dynamic Model For Infinite Media. Journal of the Engineering Mechanics Division, 1969, Vol. 95, Issue 4, Pg. 859-878

Makdisi F. I., Kagawa T., Seed H. B. (1982) Seismic Response of Earth Dams in Triangular Canyons. Journal of the Geotechnical Engineering Division, Vol. 108, Issue 10, Pg. 1328-1337

Makra, K., Chávez-García, F.J. (2016) Site effects in 3D basins using 1D and 2D models: an evaluation of the differences based on simulations of the seismic response of Euroseistest. Bull Earthquake Eng 14, 1177–1194. https://doi.org/10.1007/s10518-015-9862-7

Mancini M., Marini M., Moscatelli M., Pagliaroli A., Stigliano F., Di Salvo C., Simionato M., Cavinato G.P., Corazza A. (2014). “A physical stratigraphy model for seismic microzonation of the Central Archaeological Area of Rome (Italy)”. Bull. Earthquake Eng., 12, 1339-1363. doi: 10.1007/s10518-014-9584-2

Mancini M, Marini M, Moscatelli M, Pagliaroli A, Cavinato GP, Corazza A, Di Salvo C, Simionato M, Stigliano F (2013). “Subsoil of the Central Archaeological Area of Rome: a physical stratigraphy approach to delineation of a geotechnical reference model for level 1

seismic microzonation". Bull Earthq Eng, Special issue on "Seismic Microzonation of Palatine hill, Roman Forum and Coliseum Archaeological Area".
Marra F. & Rosa C. (1995a). Stratigrafia e assetto geologico dell'area romana, in R. Funiciello (Ed.), La Geologia di Roma. Il centro storico, Memorie Descrittive della Carta Geologica d'Italia, Roma, Istituto Poligrafico e Zecca dello Stato, 49-112.

Marra F. & Rosa C. (1995b). Carta della superficie di letto delle alluvioni recenti in scala 1:10.000, in R. Funiciello (Ed.), La Geologia di Roma. Il centro storico, Memorie Descrittive della Carta Geologica d'Italia, Roma, Istituto Poligrafico e Zecca dello Stato.

Martinez, B. & Bielak, J. (1980) On the three-dimensional seismic response of earth structures, Proc. 7th World Conf. Earthq. Engrg., Instanbul, 8, 523-528

Mejia L. H. & Seed H. B. (1983) Comparison of 2-D and 3-D Dynamic Analyses of Earth Dams, Journal of Geotechnical Engineering/Volume 109 Issue 11 - November.

Mejia L. & Dawson E. (2010) "3D Analysis of the Seismic Response of Seven Oaks Dam" International Conferences on Recent Advances in Geotechnical Earthquake Engineering and Soil Dynamics. 2.

Moscatelli M., Piscitelli S., Piro S., Stigliano F., Giocoli A., Zamuner D., Marconi F. (2014) - Integrated geological and geophysical investigations to characterize the anthropic layer of the Palatine hill and Roman Forum (Rome, Italy). Bull. Earthquake Eng., 12:1319-1338. doi:10.1007/s10518-013-9460-5

Ohmachi, T. (1981) Analysis of dynamic shear strain distributed in 3-dimensional earth dam models, Proc. Int. Conf. on Recent advances in Geotech. Earthq. Engrg. and Soil Dyn., St. Louis, 1,459-464

Pagliaroli A., Lanzo G., Tommasi P., Di Fiore V. (2013). Dynamic characterization of soils and soft rocks of the Central Archeological Area of Rome. Bull. Earthquake Eng., DOI 10.1007/s10518-013-9452-5

Pagliaroli A. Quadrio B. Lanzo G. Sanò T. (2014) Numerical modelling of site effects in the Palatine Hill, Roman Forum, and Coliseum Archaeological Area, Bull Earthquake Eng 12:1383–1403, DOI 10.1007/s10518-013-9436-5.

Papadimitriou, Achilleas G. and Chaloulos, Yannis, (2010) "Aggravation of the Peak Seismic Acceleration in the Vicinity of 2D Hills, Canyons and Slopes". International Conferences on Recent Advances in Geotechnical Earthquake Engineering and Soil Dynamics. 3.

Papadimitriou A. (2019) An engineering perspective on topography and valley effects on seismic ground motion. VII International Conference on Earthquake Geotechnical Engineering Roma (Italy), 17-20 June.

Pitilakis K. (2004) Site Effects. In: Ansal A. (eds) Recent Advances in Earthquake Geotechnical Engineering and Microzonation. Geotechnical, Geological, and Earthquake Engineering, vol 1. Springer, Dordrecht. https://doi.org/10.1007/1-4020-2528-9_6

Psarropoulos, P. N. et al (2007) Linear and Nonlinear Valley Amplification Effects on Seismic Ground Motion, Soils and Foundations, Volume 47, Issue 5, 2007, Pages 857-871, ISSN 0038-0806,

Qiu F., Liu D. (2005) Antiplane response of isoceles triangular hill to incident SH waves. Earthq. Engin. Engin. Vib. 4, 37–46. https://doi.org/10.1007/s11803-005-0022-y

Riga E., Makra K., Pitilakis K., (2016) Aggravation factors for seismic response of sedimentary basins: A code-oriented parametric study, Soil Dynamics and Earthquake Engineering, Volume 91, Pages 116-132, ISSN 0267-7261, https://doi.org/10.1016/j.soildyn.2016.09.048.

Roten D. (2006) Two-dimensional resonances in Alpine valleys identified from ambient vibration wavefield. Geophysical Journal International, Volume 165, Issue 3, June 2006, Pages 889–905.

Sánchez-Sesma, F. J. (1982) A boundary method for elastic wave diffraction: Application to scattering of SH waves by surface irregularities. Bulletin of the Seismological Society of America (1982) 72 (2): 473–490.

Sánchez-Sesma, F. J. (1985), Diffraction of elastic SH waves by wedges, Bull. Seism. Soc. Am. 75, 1435-1446.

Sánchez-Sesma, F. J. (1987), Site effects on strong ground motion. Soil Dynamics and Earthquake Engineering Volume 6, Issue 2, April 1987, Pages 124-132

Schnabel P. et all (1972) Modification of seismograph records for effects of local soil condition. Bulletin of the Seismological Society of America (1972) 62 (6): 1649–1664.

Seed, H. B. (1973) "Stability of earth and rockfill dams during earthquakes, in Embankment-Dam" Engrg., Casagrande Vol., (EdsHirschfeld and Poulos), John Wiley.

Sherif R. I. Lee V. W. Diffraction around Circular Canyon in Elastic Wedge Space by Plane SH-Waves. Journal of Engineering Mechanics/Volume 122 Issue 6 - June 1996

Signorini R. (1939) Risultati geologici della perforazione eseguita dall'AGIP alla mostra autarchica del minerale nel Circo Massimo di Roma, Bollettino della Società Geologica Italiana, 58, 60-63

Smerzini, C., Paolucci, R. & Stupazzini, M. (2011). Comparison of 3D, 2D and 1D numerical approaches to predict long period earthquake ground motion in the Gubbio plain, Central Italy. Bull Earthquake Eng 9, 2007–2029 https://doi.org/10.1007/s10518-011-9289-8

Smerzini C. & Paolucci R. Comparison of 3D, 2D and 1D numerical approaches to predict long period earthquake ground motion in the Gubbio plain, Central Italy. Bull Earthquake Eng (2011) 9:2007–2029.

Stupazzini M., Paolucci R., Igel H. (2009) Near-Fault Earthquake Ground-Motion Simulation in the Grenoble Valley by a High-Performance Spectral Element Code. Bulletin of the Seismological Society of America 99 (1): 286–301. https:// doi.org/10.1785/0120080274.

Todorovska M. I. & Lee V. W. (1991) Surface motion of shallow circular alluvial valleys for incident plane SH waves-analytical solution. Soil Dynamics and Earthquake Engineering, 1991, Volume 10, Number 4, May

Trifunac, M.D. (1971) Surface motion of a semi-cylindrical alluvial valley for incident plane SH waves, Bulletin of the Seismol. Soc. of America, 61(6), 1755-1770.

Trifunac, M.D. (1972) Scattering of plane SH waves by a semicylindrical canyon, Int. J. of Earthquake Engineering Structural Dynamic, 1(3), 267-281.

Tsaur DH & Chang KH. (2008) An analytical approach for the scattering of SH waves by a symmetrical V-shaped canyon: Shallow case - Geophysical Journal International.

Tsaur D.H. et al. (2010) An analytical approach for the scattering of SH waves by a symmetrical V-shaped canyon: deep case - Geophysical Journal.

Wong H. L. & Trifunac M. D. (1974) Scattering of plane SH waves by a semi-elliptical canyon. Earthquake Engineering Structural Dynamic Volume 3, Issues 2.

Yegian M. K. (1994) Liquefaction and Embankment Failure Case Histories, 1988 Armenia Earthquake. Journal of Geotechnical Engineering/Volume 120 Issue 3 - March 1994

Yuan X. Men F. (1992) Scattering of plane sh waves by a semi-cylindrical hill - Earthquake Engineering and Structural Dynamics, vol. 21, 109-1098.